UNIVERSIDAD COMPLUTENSE DE MADRID

FACULTAD DE CIENCIAS QUÍMICAS

Departamento de Química Orgánica I

DEVELOPMENT OF NON-PEPTIDE INHIBTORS OF THE HER2-GRB2 INTERACTION USING MOLECULAR MODELING AND NMR SPECTROSCOPY

MEMORIA PARA OPTAR AL GRADO DE DOCTOR
PRESENTADA POR

Ángel Lorenzo Orcajo Rincón

Bajo la dirección de los doctores

María Luz López Rodríguez
Bellinda Benhamú Salama
Silvia Ortega Gutiérrez

Madrid, 2013

©Ángel Lorenzo Orcajo Rincón, 2012

UNIVERSIDAD COMPLUTENSE DE MADRID

FACULTAD DE CIENCIAS QUÍMICAS

Departamento de Química Orgánica I

Development of Non-peptide Inhibitors of the HER2-Grb2 Interaction Using Molecular Modeling and NMR Spectroscopy

Ph.D. candidate:

Ángel Lorenzo Orcajo Rincón

Advisors:

Prof. María Luz López Rodríguez, Ph.D.

Prof. Bellinda Benhamú Salama, Ph.D.

Prof. Silvia Ortega Gutiérrez, Ph.D.

MADRID, 2012

In a chemist research, three convictions perch.

First: the absolute certainty of doing it.

Second: it is a kind of fight between the man and his own despair. Even not knowing the names of those ancient wise masters, we will always follow them right after.

Third: the columns of his work are the table of elements and much of human empowerment.

Together with these three certainties, what remains is dark obscurity: brave discoverers plunge not knowing how far the ocean borders are going.

We are definitely some water alchemy and lots of fantasy!

-*Personal thoughts*, **AO**

De acuerdo con la Normativa de desarrollo del régimen relativo a elaboración, tribunal, defensa y evaluación de la Tesis Doctoral, del Real Decreto 1393/2007, de 29 de Octubre, (BOE 30 de Octubre de 2007) por el que se establece la ordenación de las enseñanzas universitarias oficiales de la Universidad Complutense de Madrid, y de acuerdo a lo dispuesto en sus artículos 4.1 y 4.2, la presente Tesis Doctoral se ha redactado en inglés previo visto bueno de los directores, autorización del Departamento así como autorización de la Comisión de Doctorado. Conforme a esta normativa se incluye adicionalmente un amplio resumen en español que consta de introducción, objetivos, resultados y discusión y conclusiones (véase sección S1-S43 al final de este manuscrito).

Este trabajo ha sido realizado en el Laboratorio de Química Médica del Departamento de Química Orgánica I de la Facultad de Ciencias Químicas de la Universidad Complutense de Madrid.

El tema ha sido propuesto y dirigido por la Catedrática Dra. Mª Luz López Rodríguez, la Dra. Bellinda Benhamú Salama y la Dra. Silvia Ortega Gutiérrez. A ellas, antes que a nadie, deseo expresar mi agradecimiento por su acogida, por sus continuas enseñanzas y por el aliento y confianza con que han promovido el desarrollo de este proyecto.

Asimismo quiero expresar mi agradecimiento:

Al Profesor Kurt Wüthrich y al Dr. Pedro Serrano del Scripps Research Institute (La Jolla, California, USA) por la realización de los experimentos de RMN-HSQC.

Al Profesor Ole Nørregaard Jensen y al Dr. Ivo Fierro Monti del Laboratorio de Bioquímica y Biología Molecular de la Universidad del Sur de Dinamarca (Odense, Dinamarca) por su acogida y guía en la realización de los estudios de proteómica y biología molecular.

Al Profesor Leonardo Pardo, a la Profesora Mercedes Campillo y al Dr. Iván R. Torrecillas, del Laboratorio de Medicina Computacional de la Facultad de Medicina de la Universidad Autónoma de Barcelona por su inestimable colaboración en la modelización y optimización de las series estructurales presentadas en este trabajo.

Al profesorado y personal del Departamento de Química Orgánica I de la Universidad Complutense de Madrid por el constante apoyo brindado durante la realización de este proyecto.

A la Consejería de Educación de la Comunidad de Madrid y a su eficiente personal de apoyo al estudiante de tercer ciclo que, mediante su programa de Becas de Formación del Personal Investigador, ha hecho posible esta Tesis Doctoral.

A mis compañeros de laboratorio, con los que he compartido experiencias más allá del lugar de trabajo y que han hecho del Medicinal Chemistry Lab uno de los mejores sitios para aprender y reir a la vez. A los que compartieron mis años de bata blanca: Isabel, Tania, Rocío, Carlos, Marga, Jose, Marisa, David, Mar, Lidia, Dulce, Inés, Moisés, Henar, Jorge, Laura, Javi y a todos aquéllos que de alguna manera han tocado mi vida con su paso por nuestro laboratorio, mi eterno agradecimiento. A mis amigos de siempre, gracias!

Por último, a mi familia, mi mayor fuerza vital: mis padres Mery y Ángel, mis hermanos Javier y Gisela, mis cuñados Verónica y Miguel, y por supuesto, mis pequeños sobrinos: gracias desde la primera hasta la última letra de esta tesis. Sois mi mayor valor y apoyo.

Table of Contents

References, Abbreviations and Acronyms

All references have been placed at the bottom of each page in which they are first cited.

Abbreviations and acronyms used in this manuscript are in accordance with the guidelines for authors provided by the American Chemical Society in its *Journal of Organic Chemistry* (http://pubs.acs.org/page/joceah/submission/authors.html) and its *Journal of Medicinal Chemistry* (http://pubs.acs.org/page/jmcmar/submission/authors.html), together with the following entries incorporated in strict order of appearance:

2-Abz: *2-Aminobenzoyl.*

Ac_6c: 1-*Aminocyclohexanecarboxylic acid.*

Achec: *2-Amino-3-cyclohexenecarboxylic acid.*

ADCC: *Antibody-dependent cell-mediated cytoxicity.*

AP: *Affinity Purification.*

AR: *Amphiregulin.*

BTC: *Betacellulin.*

CREB: *cAMP response element-binding*.

EDC: *1-Ethyl-3-(3-dimethylaminopropyl)carbodiimide*.

EPR: *Epiregulin.*

GEFs: *Guanine nucleotide exchange factors.*

GO: *Gene Ontology Consortium.*

HB-EGF: *Heparin-binding EGF.*

HER: *Human EGF receptor.*

HRP: *Horseradish peroxidase.*

m^7GTP: : *7-Methylguanosine triphosphate*.

mAbs: *Monoclonal antibodies.*

MEK: *MAPK/ERK kinase (MAPKK).*

MM-GBSA: *Molecular Mechanics - Generalized Born Surface Area*.

NRGs: *Neuregulins.*

pre-mRNAs: *Precursor messenger RNAs.*

pTyr: *Phosphotyrosine*.

SH2: *Src homology 2.*

TGF-α: *Transforming growth factor α.*

TKRs: *Tyrosine kinase receptors.*

TMB: *3,3',5,5'-Tetramethylbenzidine*.

UCM: *Universidad Complutense de Madrid.*

General Introduction

1. General Introduction

Cancer is the generic term used to describe a group of more than a hundred different diseases with one common defining feature: the rapid generation of abnormal cells that grow beyond their usual boundaries and can then invade adjoining tissues or, in many cases, migrate to other parts of the body. The final outcome is mostly the same in all situations: progressive multiple organ dysfunction and death.

Recent studies conducted by the World Health Organization[1] have identified cancer as a leading cause of death worldwide. The disease accounted for 7.9 million demises (or around 13% of all deaths worldwide) in 2008, with estimations to continue rising with a projected 13.1 million deaths in 2030.

Cancer is a multistage process. In its most classical view, the transformation of a normal cell into a tumour cell starts when a specific damage to its DNA occurs as a consequence of mutations in one or many different genes due to the action of external agents, including physical carcinogens (such as X rays or ultraviolet and ionizing radiation); chemical carcinogens (such as asbestos, components of tobacco smoke; aflatoxin, a food contaminant; or arsenic, a drinking water contaminant); and biological carcinogens (such as some viral, bacterial, or parasitic infections).

Important processes such as cell proliferation, growth, differentiation and apoptosis can be severely altered by these mutations. When the outcome of such modifications is the start of a carcinogenic progression, those genes involved are called proto-oncogenes. Their mutation unleashes a rapid and abnormally permanent clonal expansion independent of external stimulation (*i.e.* growth factors, hormones, etc), carrying built-in proliferative advantages that will help them prevail over their normal peers. This unnaturally sped up process, together with an accumulated genetic instability and the consequent selective pressure from the surroundings upon this group of cells, increases the chances for future mutations possibly affecting a second group of genes called tumour suppressor genes. These are in charge of controlling the progression of the cell cycle whenever a repairable damage to the DNA is found, and also responsible for the initiation of the apoptotic signal as far as the damage is reckoned irreversible. The loss of function of these genes follows a recessive pattern, meaning it only happens after the two alleles are damaged. This is a gradual process during which an individual can perfectly live for many years without presenting any symptom, as the amount and efficacy of the protein encoded by the healthy allele can entirely suffice for its requirements in the specific cell. Complete loss of function of these genes happens via a degenerative process known as loss of heterozygosity, an event immediately followed by the appearance of the disease phenotype.[2]

---

[1] http://www.who.int/mediacentre/factsheets/fs297/en/index.html.

[2] (a) Fukasawa, K. *Nat. Rev. Cancer* **2007**, *7*, 911-924. (b) Haber, D. A.; Gray, N. S.; Baselga, J. *Cell* **2011**, *145*, 19-24.

Up to this stage the cellular mass has become a malignant neoplasm growing even more but in a less differentiated fashion and out of control. At a certain point, survival signals override the cell own apoptotic mechanisms and the tumour is then able to elicit the generation of new blood vessels to its periphery (angiogenesis), to help supply for the shortage of nutrients and oxygen of its ever-growing cell population. To reach the maximum level of propagation, this primary tumour has yet to start a spreading process, but as soon as it kicks off the proteolytic digestion of the cell lining or endothelium that deters it from overtaking the blood flow, colonization of new tissues (metastasis)[3] takes no long.

Upon mutation, a proto-oncogene (or its product) can become a tumour-inducing agent, an oncogene. Among these are found many genes coding for membrane receptors comprised in processes like cell division and growth. Therefore, if it were possible to ascertain which of these components are entangled in most tumour processes, as well as their activation mechanisms, developing new therapeutic strategies would seem straightforward.

Cell division takes place when certain membrane receptors are activated by their endogenous ligands. These can be released by neighbouring cells (paracrine signalling), or by the target cell on its own (autocrine signalling). Most receptors implicated in processes like cell division and differentiation are tyrosine kinase receptors (TKRs), namely those capable of transferring phosphate groups from the donor molecule adenosine triphosphate (ATP), to serine, threonine or tyrosine residues on the substrate protein.[4] Protein phosphorylation has two fundamental goals: (i) to change a temporary conformation of a protein, modifying its enzymatic activity, and (ii) to generate recognition sites for other proteins intervening in the same signalling pathway. In general, it is assumed that protein phosphorylation controls the transmission and amplification of the mitogenic signal. Usually, these two complex processes result in the sequential activation of the Ras protein and the mitogen-activated protein kinases (MAPKs) pathway.[5] These latter are ultimately responsible of activating those genes involved in cell division.[6]

1.1. Tyrosine kinase receptors (TKRs)

TKRs are classified into four main families according to their structural similarity. In particular, subclass I, absolutely vital in tumour processes, comprises all sorts of epidermal growth factor receptors (EGFRs). This group is further divided into four well differentiated

---

[3] (a) McSherry, E. A.; Donatello, S.; Hopkins, A. M.; McDonnell, S. *Cell. Mol. Life Sci.* **2007**, *64*, 3201-3218. (b) Brennan, K.; Offiah, G.; McSherry, E. A.; Hopkins, A. M. *J. Biomed. Biotechnol.,* Hindawi Publishing Corporation, doi:10.1155/2010/460607 **2010**. (c) Arteaga, C. L.; Baselga, J. *Clin. Cancer Res.* **2012**, *18*, 612-618.

[4] (a) Alberts, B.; Johnson, A.; Lewis, J.; Raff, M.; Roberts, K.; Walter, P. *Molecular Biology of the Cell*, Taylor & Francis Inc., 5th Ed., **2007**. (b) DeVita Jr., V. T.; Lawrence T. S.; Rosenberg, S. A.; DePinho, R. A.; Weinberg, R. A. *Cancer: Principles and Practice of Oncology*, Wolters Kluwer - Lippincott Williams & Wilkins, 9th Ed., **2011**.

[5] (a) Sebolt-Leopold, J. S. *Oncogene* **2000**, *19*, 6594-6599. (b) Chapman, M. S.; Miner, J. N. *Expert Opin. Investig. Drugs* **2011**, *20*, 209-220.

[6] (a) Barbacid, M. *Ann. Rev. Biochem.* **1987**, *56*, 779-827. (b) Young, A.; Lyons, J.; Miller, A. L.; Phan, V. T.; Alarcón, I. R.; McCormick, F. *Adv. Cancer Res.* **2009**, *102*, 1-17.

members: HER1 (also called EGFR or ErbB1), HER2 (neu or ErbB2), HER3 (ErbB3) and HER4 (ErbB4).[7] All HERs are expressed in many tissue types, though primarily found in epithelial, mesenchymal, and neuronal tissues. The four receptors consist of an extracellular domain, further composed of four (I-IV) regions or sub-domains, at which the ligand binding occurs, a hydrophobic α-helical transmembrane segment, and an intracellular tyrosine kinase domain that contains motifs and residues that mediate interactions with intracellular signalling molecules (Figure 1a).[8]

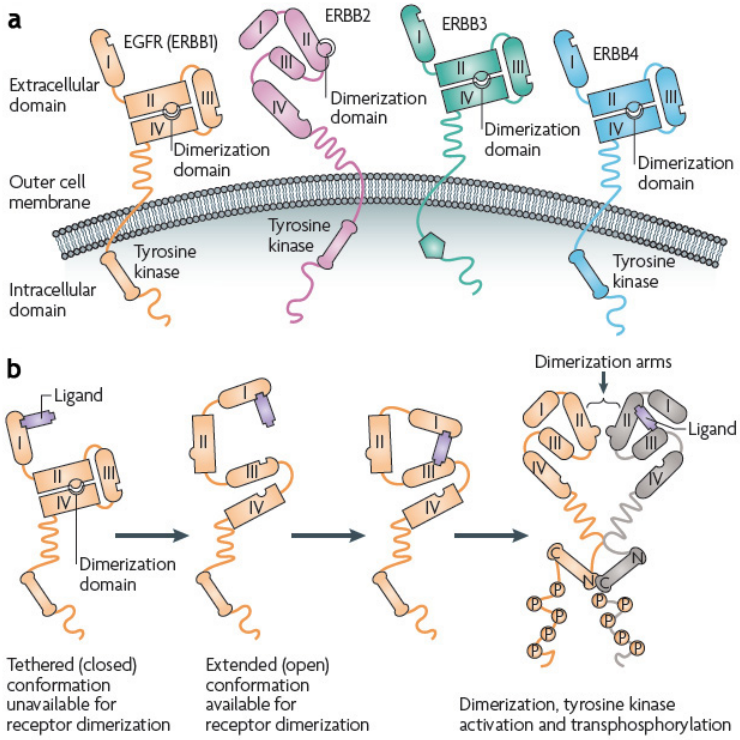

Figure 1. a. Details on the structural features of the four members of the ErbB family (ErbB1-4). **b.** Schematic analysis of ligand-mediated receptor rearrangement to gain extended conformation necessary for receptor dimerization. (Source: See citation 7)

The intracellular tyrosine kinase domain of these HERs is highly conserved among the family excepting HER3 which apparently lacks kinase activity (Figure 1a). On the other hand, extracellular domains do not have the same degree of structural conservation, which suggests high level of specialization in ligand recognition,[9] except for HER2, whose endogenous ligand has not yet been identified. This receptor exists in the extended (open) 'active' conformation state, being constitutively available for dimerization. There are two main reasons for this. The

[7] Baselga, J.; Swain, S. M. *Nat. Rev. Cancer* **2009**, *9*, 463-475.

[8] (a) Olayioye, M. A.; Neve, R. M.; Lane, H. A.; Hynes, N. E. *EMBO J.* **2000**, *19*, 3159-3167. (b) Ferguson, K. M.; Berger, M. B.; Mendrola, J. M.; Cho, H. S.; Leahy, D. J.; Lemmon, M. A. *Mol. Cell* **2003**, *11*, 507-517. (c) Lurje, G.; Lenz, H. J. *Oncology* **2009**, *77*, 400-410.

[9] (a) Yarden, Y.; Sliwkowski, M. X. *Nat. Rev. Mol. Cell Biol.* **2001**, *2*, 127-137. (b) Burgess, A. W. *Growth Factors* **2008**, *26*, 263-274.

first one has do to with the absolute absence of interaction, the so-called 'tether', between sub-domains II and IV; a normal situation in any inactive (not ligand-bound) representative of the HER family of receptors. The second reason deals with sub-domains I and III, those involved in ligand recognition by HER1, 3, and 4. When a ligand recognizes its receptor, these two sub-domains are bridged together (Figure 2b) by the ligand. This induces a dramatic conformational change that leaves their dimerization arm (located in region II) exposed and ready to interact with a second, same or different, receptor (Figure 1b). The extensive and highly complementary nature of the I-III interface on HER2 buries much of this receptor's surface that corresponds to the equivalent EGFR ligand binding sites, keeping the receptor extracellular domain in continuous 'autoactivated' conformation ready to dimerize (Figure 2a).[10] This might explain the unique ability of HER2 to transform cells (and to cause cancer) when overexpressed.

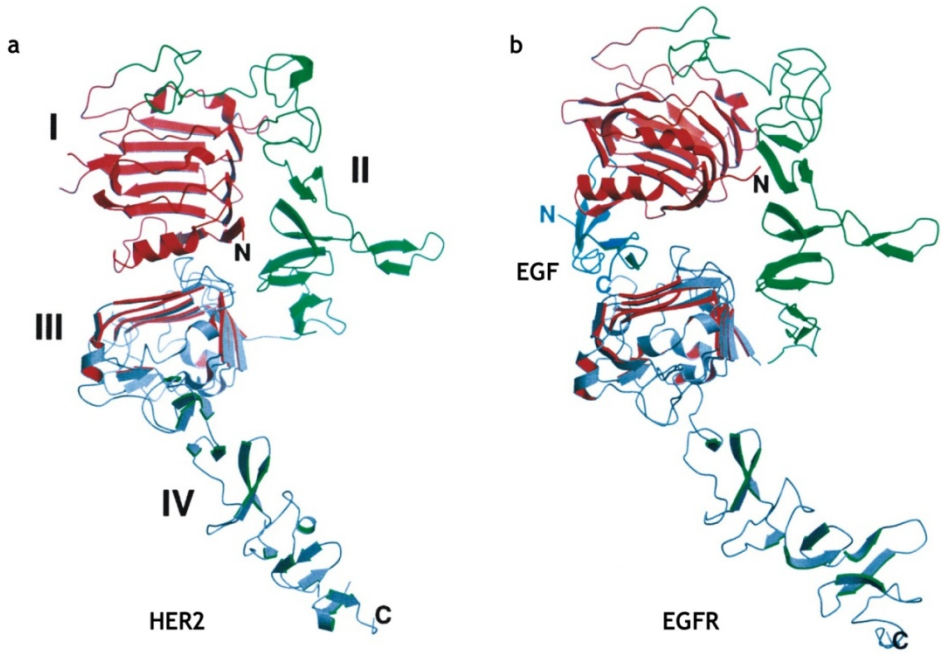

Figure 2. a. Ribbon representation of the human extracellular domain of the HER2 receptor (PDB code 1n8z). Individual sub-domains are labelled, same as other structures (red for sub-domains I and III, green for sub-domains II and IV). The close proximity of domains I and III is notable, as discussed in the text. The HER2 dimerization loop is also clearly exposed. **b.** One-half of the EGFR dimer model is shown for comparison. (Source: See citation 9)

Under physiological conditions, HER activation is mostly controlled by both spatial and temporal expression of their endogenous ligands. These are proteins that belong to the epidermal growth factors (EGFs) family, which upon binding to their target receptors, cause them to stabilize in a conformation that allows dimerization with another vicinal receptor of the same (homodimerization) or different class (heterodimerization), and thus setting off the

[10] (a) Burgess, A. W.; Cho, H. S.; Eigenbrot, C; Ferguson, K. M.; Garrett, T. P. J.; Leahy, D. J.; Lemmon M. A.; Sliwkowski, M. X.; Ward, C. W.; Yokoyama, S. *Mol. Cell* **2003**, *12*, 541-552. (b) Lemmon, M. A. *Exp. Cell Res.* **2009**, *315*, 638-648.

complete signalling pathway.[11] The EGF family of ligands consists of thirteen members sharing in many cases structural features which bias them to overlap their action on the same receptor.[12] They are generally assorted into three main subgroups. The first one comprises the actual EGF, transforming growth factor-α (TGF-α), and amphiregulin (AR), all of which show exclusive preference for the HER1. The second group contains betacellulin (BTC), heparin-binding EGF (HB-EGF) and epiregulin (EPR), which show dual specificity, binding both HER1 and HER4. The third group is composed of neuregulins (NRGs), which further subdivide into NRG1 and NRG2 showing dual capacity to bind HER3 and HER4, plus NRG3 and NRG4 which only bind HER4. In such a way, each receptor can be activated by more than one ligand, except for HER2, which, as previously explained, has been found not to bind any endogenous ligand. In spite of this, it is the most appealing receptor in today's molecular and clinical oncology, as it has demonstrated to be the preferred heterodimerization partner within the members of the HER family (Figure 3a).[13]

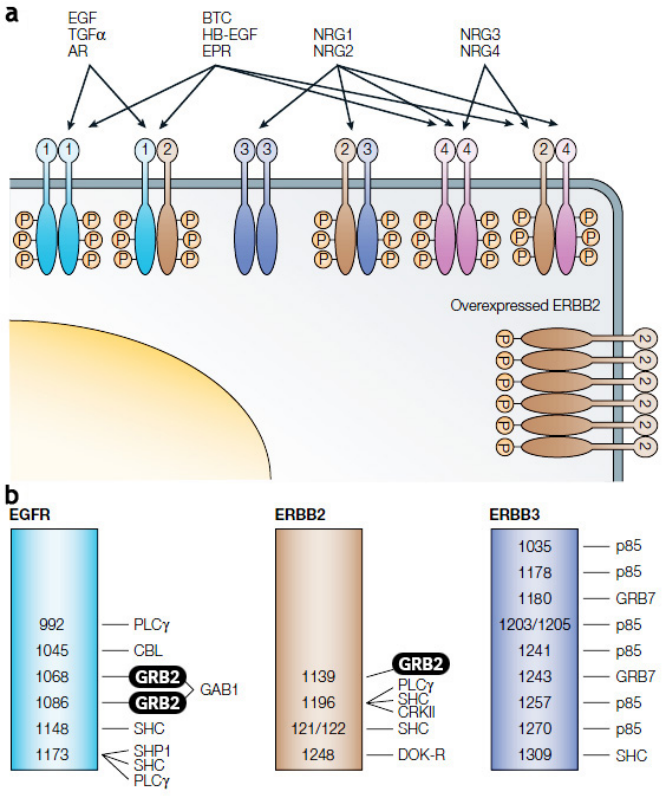

Figure 3. a. Members of the EGF family and their respective receptors. **b.** Schematic representation of the main autophosphorylation sites on HER1-3, as well as their corresponding associated adapter proteins. (Source: See citation 13a)

[11] Wieduwilt, M. J.; Moasser, M. M. *Cell. Mol. Life Sci.* **2008**, *65*, 1566-1584.

[12] (a) Citri, A.; Yarden, Y. *Nat. Rev. Mol. Cell Biol.* **2006**, *7*, 505-516. (b) Avraham, R.; Yarden, Y. *Nat. Rev. Mol. Cell Biol.* **2011**, *12*, 104-117.

[13] (a) Hynes, N. E.; Lane, H. A. *Nat. Rev. Cancer* **2005**, *5*, 341-354. (b) Zhang, H.; Berezov, A.; Wang, Q.; Zhang, G.; Drebin, J.; Murali, R.; Greene, M. I. *J. Clin. Invest.* **2007**, *117*, 2051-2058. (c) Hynes, N. E.; MacDonald, G. *Curr. Opin. Cell Biol.* **2009**, *21*,177-184.

The specific binding of one ligand to its receptor brings about the formation of homo and/or heterodimers over the cell surface, which immediately entails the activation of the tyrosine kinase portion of them. This results in a series of trans and autophosphorylations of many tyrosine residues all along the receptor intracellular domain.[14] The phosphorylated residues serve as recognition sites for a great variety of adapter proteins (*e.g.* Shc, Grb7, Grb2, Nck, PLCγ, Figure 3b) which once bound initiate a cascade of sequential phosphorylations involving the proteins intervening in the transmission of the mitogenic signal, typically those of the MAPKs.[15] The activation of the MAPKs[16,17] takes place mainly through the adapter protein Grb2,[18] which is capable of recognizing phosphorylated tyrosine residues on HER2 by means of its Src homology 2 domain (SH2). Once bound to HER2, it couples with the proline-rich C-terminus of the Sos protein, via its two SH3 domains (Figure 4). Sos belongs to a broad family of molecules generically known as guanine nucleotide exchange factors (GEFs), components of intracellular signalling networks. They function as activators of small GTPases like Ras, exchanging guanosine diphosphate (GDP) for guanosine triphosphate (GTP). This single step promotes the recruitment of downstream-to-Ras signalling molecules to the cell membrane.[19]

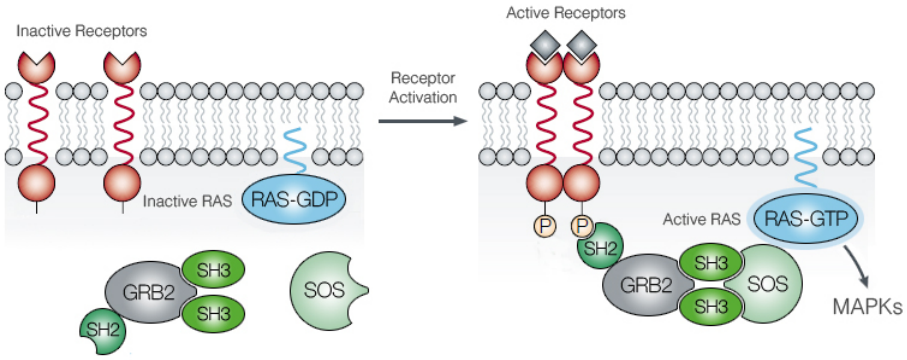

Figure 4. Schematic representation of ligand-mediated Ras-MAPKs activation via Grb2.

GEF-dependent signalling is antagonized by GTPase activating proteins (GAPs), which promote hydrolysis of GTP to GDP on Ras, rendering it inactive. Therefore, the normal activity of Ras is controlled by a delicate equilibrium of its GTP- over its GDP-bound state (Figure 5).[20]

---

[14] (a) Zhang, X.; Gureasko, J.; Shen, K.; Cole, P. A.; Kuriyan, J. *Cell* **2006**, *125*, 1137-1149. (b) Bose, R.; Zhang, X. *Exp. Cell Res.* **2009**, *315*, 649-658.

[15] (a) Mendelsohn, J.; Baselga, J. *J. Clin. Oncol.* **2003**, *21*, 2787-2799. (b) Cargnello, M.; Roux, P. P. *Microbiol. Mol. Biol. Rev.* **2011**, *75*, 50-83.

[16] Kolch, W. *Biochem. J.* **2000**, *351*, 289-305.

[17] Sebolt-Leopold, J. S.; Herrera, R. *Nat. Rev. Cancer* **2004**, *4*, 937-947.

[18] (a) Gale, N. W.; Kaplan, S.; Lowenstein, E. J.; Schlessinger, J.; Bar-Sagi, D. *Nature* **1993**, *363*, 88-92. (b) Tari, A. M.; Lopez-Berestein, G. *Semin. Oncol.* **2001**, *28*, 142-147. (c) Giubellino, A.; Burke, T. R. Jr.; Bottaro, D. P. *Expert Opin. Ther. Targets* **2008**, *12*, 1021-1033.

[19] McCormick, F. *Nature* **1993**, *363*, 15-16.

[20] (a) Downward, J. *Nat. Rev. Cancer* **2003**, *3*, 11-22. (b) Matallanas, D.; Crespo, P. *Curr. Opin. Mol. Ther.* **2010**, *12*, 674-683.

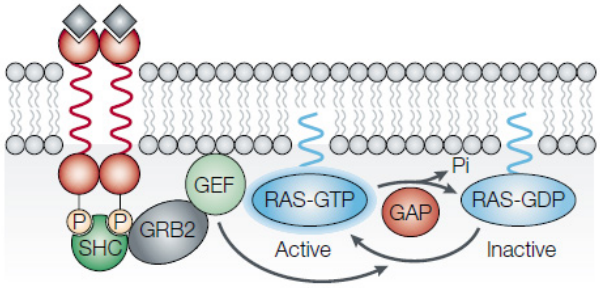

Figure 5. The active – inactive Ras state is controlled by a cycle of hydrolyses: Ras-GDP to Ras-GTP catalysed by GEFs (Sos) and from Ras-GTP to Ras-GDP catalysed by GAPs. (Source: See citation 20)

The MAPK signalling cascade consists of a network of messenger proteins, with the Ras family as the upstream elements (Figure 6). This is formed by three members: HRas, KRas, and NRas, generically called Ras. Once activated, Ras phosphorylates the next downstream enzyme Raf, which is actually a family of three serine/threonine kinases: c-Raf1, A-Raf and B-Raf, generically known as Raf or MAPKKK, a very important crossroad of complex interactions with other proteins besides MAPKs themselves. Raf amplifies the signal transmission by phosphorylating the third level down kinases MEK1 and MEK2 (MAPK/ERK Kinase), also named MAPKK. The signal travels further down to a fourth level with phosphorylation of ERK1 and ERK2 (extracellular signal regulated kinase), or simply MAPK. Translocation of ERK to the nucleus is followed by phosphorylation and activation of a variety of families of transcription factors such as: Ets-1, AP-1, c-Myc, NF-κB, or CREB. They promote translation of many genes (proto-oncogenes) that code for proteins involved in cell vital processes,[21] including cell cycle progression, cell growth, inflammation, proliferation, migration, cell repair mechanisms, and angiogenesis. Figure 6 shows a summary of the entire signalling pathway mediated by ligand-induced formation of the HER2-HER3 dimer.

[21] Chang, F.; Steelman, L. S.; Lee, J. T.; Shelton, J. G.; Navalonic, P. M.; Blalock, W. L.; Franklin, R. A.; McCubrey, J. A. *Leukemia* **2003**, *17*, 1263-1293.

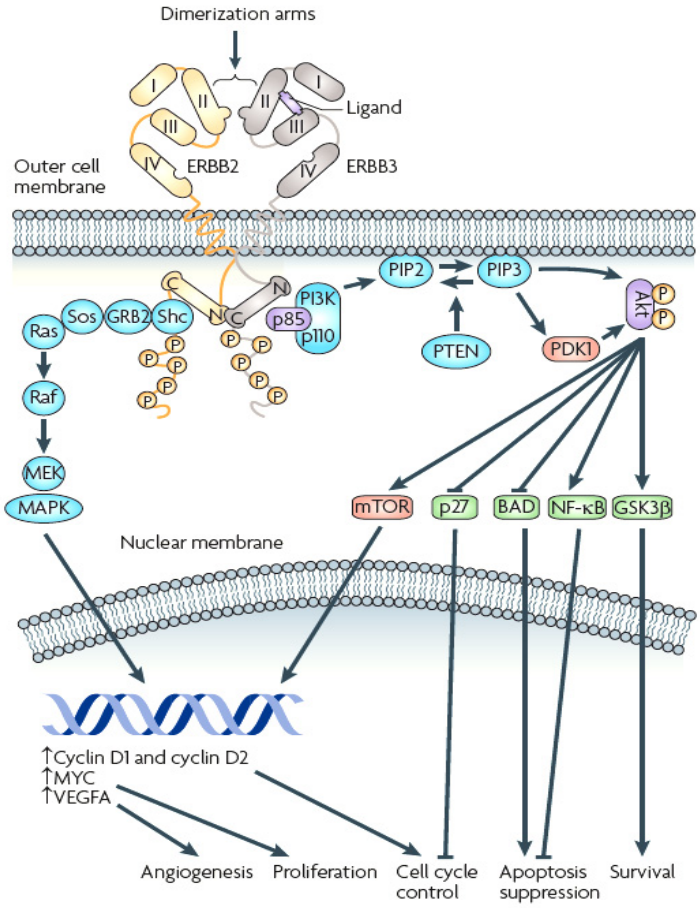

Figure 6. Schematic representation of ligand-induced HER2-HER3 dimerization and its downstream signalling pathway which entails the activation of genes coding for proteins involved in cell vital processes. (Source: See citation 7)

1.2. The HER2 receptor

All this complex network of events can be blocked by inhibition of HER2 signalling pathway. Therefore, the development of such inhibitors may constitute a new alternative therapeutic approach to the treatment of cancer,[22] mainly those types of tumours characterized by HER2 overexpression. Approximately 30% of all known invasive breast cancers overexpress this receptor, a situation also shown in other types of neoplasms like ovary,[23] lung, pancreas, colon, stomach, oesophagus, endometrium, cervix, and salivary glands.[24] Tumours presenting high levels of HER2 are, in general, extremely invasive over nearby tissues and the lymphatic

[22] (a) Schubbert, S.; Shannon, K.; Bollag, G. *Nat. Rev. Cancer* **2007**, *7*, 295-308. (b) Lee-Hoeflich, S. T.; Crocker, L.; Yao, E.; Pham, T.; Munroe, X.; Hoeflich, K. P.; Sliwkowski, M. X.; Stern, H. M. *Cancer Res.* **2008**, *68*, 5878-5887. (c) Baselga, J. *Ann. Oncol.* **2010**, *21*, Suppl. 7:vii36-40.

[23] Vermeij, J.; Teugels, E.; Bourgain, C.; Xiangming, J.; in 't Veld, P.; Ghislain, V.; Neyns, B.; De Grève, J. *BMC Cancer* **2008**, *8*, 1-9.

[24] (a) Slamon, D. J.; Clark, G. M.; Wong, S. G.; Levin, W. J.; Ullrich, A.; McGuire, W. L. *Science* **1987**, *235*, 177-182. (b) Holbro, T.; Hynes, N. E. *Annu. Rev. Pharmacol. Toxicol.* **2004**, *44*, 195-217. (c) Higgins, M. J.; Baselga, J. *J. Clin. Invest.* **2011**, *121*, 3797-3803.

system (Figure 7). Its presence is associated with poor disease-free survival and resistance to chemotherapeutic drugs, especially in breast cancer where it is used as a tumour marker.[25]

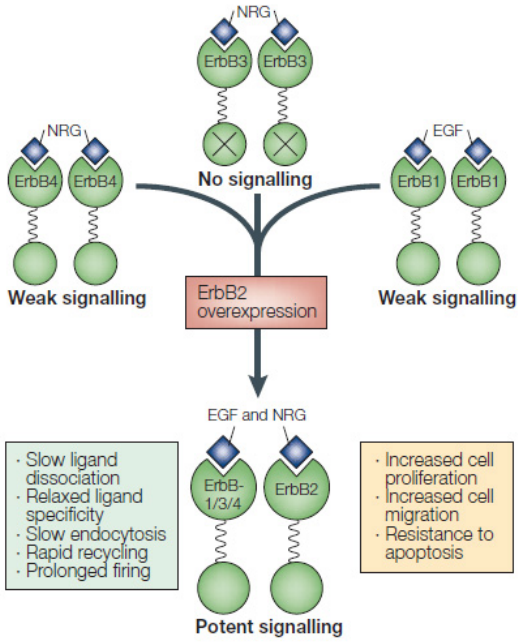

Figure 7. Overexpression and special structural characteristics of HER2 favour its presence in heterodimers with HER1, 3, and 4. Causes for the potent signalling capacity of the dimers are summarized in the green square, while its consequences, in the yellow one. (Source: See citation 9a)

Supported by the current wealth of information on the mechanisms of activation involved in the HER family of receptors, some therapeutic approaches have seen light successfully. Drugs targeting these receptors, and in particular HER2, have two major sites of action: (i) the extracellular and (ii) the intracellular kinase domains of the HER receptors. As implicated in the recognition of activating ligands and subsequent dimerization with a partner, the extracellular domain of these proteins constitute the first line of treatment and an excellent target accessible to monoclonal antibodies (mAbs). One humanized mAb targeting the HER2 has been approved for clinical use, and many others are under advanced phase clinical trials. The first mAb to enter clinical use was the HER2-targeting mAb trastuzumab (Herceptin®; Roche Registration Ltd.) derived from the first ever murine monoclonal antibody, 4D5, which inhibited the growth of human tumour xenografts overexpressing the receptor in athymic mice.[26] Trastuzumab binds to the extracellular juxtamembrane portion of HER2 (sub-domain IV, shown in Figure 8a). By doing so, it is not just able of disrupting the further intracellular modifications necessary for the internal kinase to become phosphorylated, but actually elicits an immune response (antibody-dependent

[25] (a) Nahta, R.; Yu, D.; Hung, M. C.; Hortobagyi, G. N.; Esteva, F. J. *Nat. Clin. Pract. Oncol.* **2006**, *3*, 269-280. (b) Di Cosimo, S.; Baselga, J. *Nat. Rev. Clin. Oncol*. **2010**, *7*, 139-147.

[26] Hudziak, R. M.; Lewis, G. D.; Winget, M.; Fendly, B. M.; Shepard, H. M.; Ullrich, A. *Mol. Cell. Biol.* **1989**, *9*, 1165-1172.

cell-mediated cytoxicity, ADCC)[27] and prevents cleavage of the HER2 extracellular domain, which is an additional mechanism for HER2 activation. It is the current standard of care for the treatment of HER2-amplified breast cancer where it causes tumour regression in 11-26% of patients with metastatic disease and increases disease-free survival (33-52%) and overall survival (34-41%) despite tumour size, nodal or hormone receptor status, and age when used with traditional chemotherapy in early stage disease.[28]

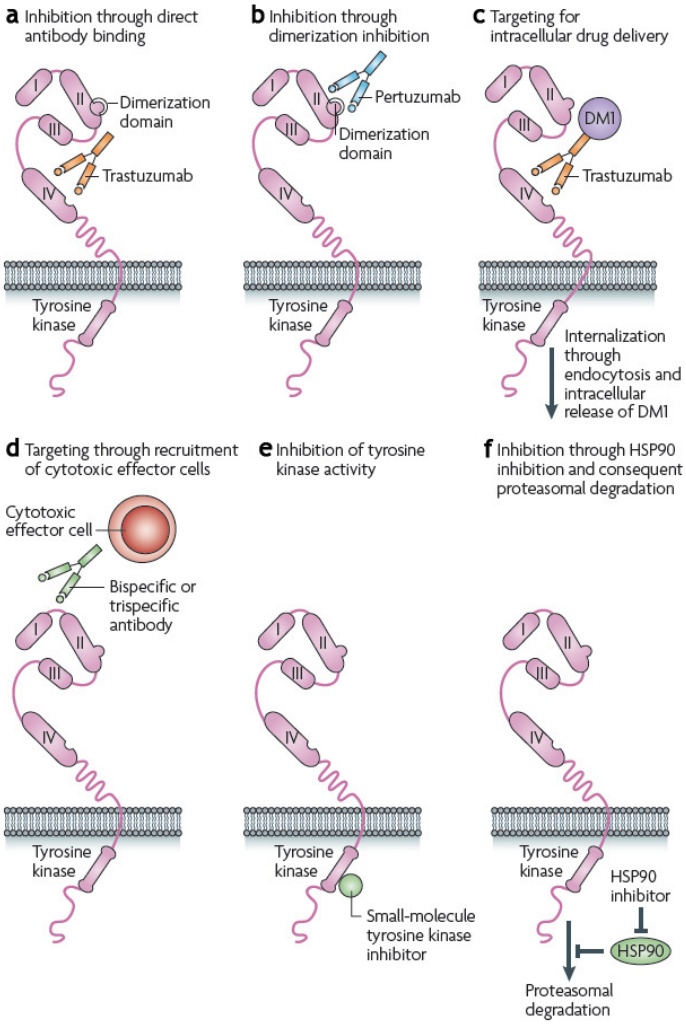

Figure 8. Current methodologies used to block signalling through HER2. **a.** mAb trastuzumab binds directly to domain IV of the extracellular region of HER2 suppressing its signalling and inducing ADCC. **b.** mAb pertuzumab binds directly to domain II of the extracellular region of HER2 preventing its dimerization with another ErbB receptor. **c.** The antibody–drug conjugate trastuzumab–DM1. **d.** HER2-specific binding by antibodies with bispecific or trispecific selectivity for cytotoxic effector cells can mark tumour cells that overexpress HER2 for immunological destruction. **e.** Inhibition of the activity of the HER2 tyrosine kinase domain with TKIs such as lapatinib. **f.** Inhibition of HSP90 activity results in ubiquitylation and proteasomal degradation of both HER2 and its downstream signalling partners. (Source: See citation 7)

[27] Musolino, A.; Naldi, N.; Bortesi, B.; Pezzuolo, D.; Capelletti, M.; Missale, G.; Laccabue, D.; Zerbini, A.; Camisa, R.; Bisagni, G.; Neri, T. M.; Ardizzoni, A. *J. Clin. Oncol.* **2008**, *26*, 1789–1796.

[28] (a) Hudis, C. A. *N. Engl. J. Med.* **2007**, *357*, 39-51. (b) Garnock-Jones, K. P.; Keating, G. M.; Scott, L. J. *Drugs* **2010**, *70*, 215-239. (c) Brufsky, A. *Am. J. Clin. Oncol.* **2010**, *33*, 186-195.

Since the structural basis for the HERs dimerization have been elucidated, a second HER2-targeting mAb, pertuzumab (Genentech/Hoffman-La Roche) has been developed and is currently under phase III clinical trials in combination with other mAbs and/or chemotherapeutic agents.[29] This antibody binds to the dimerization interface (domain II)[30] of HER2 extracellular region (Figure 8b). Pertuzumab potentially interferes with the formation of HER2 heterodimers interrupting MAPK and PI3K-Akt oncogenic pathways. The activation of immune effector functions such as ADCC might also contribute to the efficacy of pertuzumab. In combination with trastuzumab and no chemotherapy, clinical results show an efficacy of around 50% in clinical benefit, and an overall response rate of 24%.[31]

A variant to the use of "naked" antibody could be its association with a potent chemotherapeutic bullet. In this sense, trastuzumab-DM1 (T-DM1; Genentech/Hoffman-La Roche), consisting of the mAb conjugated to the potent anti-microtubule agent DM1, works as an excellent vehicle to deliver the drug inside the cell once trastuzumab has recognized and bound to HER2 (Figure 8c). Encouraging preclinical and early clinical anti-tumour activity with limited toxicity has been observed.[32]

One last approach in the field of HER2-targeting mAbs includes the investigation on bispecific and trispecific antibodies that contain within their structure, recognition sites for HER2 extracellular domain and for antigens on the surface of killer mature T cells. This dual capacity brings the two cells in close proximity, maximizing the immunological destruction of the tumour cell. This is the action mechanism of ertumaxomab (Fresenius Biotech GmbH), as shown in Figure 8d.[33]

The tyrosine kinase function of the HER members is essential for intracellular signalling and cell transformation. As such, inhibition of this enzymatic function provides a rational basis for another class of targeted therapies based on the development of tyrosine kinase inhibitors (TKIs). The only currently commercialized reversible anti-HER2 TKI is lapatinib (Tyverb®/Tykerb®; Glaxo Group Ltd.), a compound based on the quinazoline scaffold which is equally active against HER1 and HER2 (Figure 9). It binds to the ATP binding region of the

---

[29] (a) Agus, D. B.; Akita, R. W.; Fox, W. D.; Lewis, G. D.; Higgins, B.; Pisacane, P. I.; Lofgren, J. A.; Tindell, C.; Evans, D. P.; Maiese, K.; Scher, H. I.; Sliwkowski, M. X. *Cancer Cell* **2002**, *2*, 127-137. (b) Franklin, M. C.; Carey, K. D.; Vajdos, F. F.; Leahy, D. J.; de Vos, A. M.; Sliwkowski, M. X. *Cancer Cell* **2004**, *5*, 317-328. (c) Baselga, J.; Swain, S. M. *Clin. Breast Cancer* **2010**, *10*, 489-491.

[30] Spiridon, C. I.; Ghetie, M. A.; Uhr, J.; Marches, R.; Li, J. L.; Shen, G. L.; Vitetta, E. S. *Clin. Cancer Res.* **2002**, *8*, 1720-1730.

[31] Baselga, J.; Gelmon, K. A.; Verma, S.; Wardley, A.; Conte, P.; Miles, D.; Bianchi, G.; Cortes, J.; McNally, V. A.; Ross, G. A.; Fumoleau, P.; Gianni, L. *J. Clin. Oncol.* **2010**, *28*, 1138-1144.

[32] (a) Lewis Phillips, G. D.; Li, G.; Dugger, D. L.; Crocker, L. M.; Parsons, K. L.; Mai, E; Blättler, W. A.; Lambert, J. M.; Chari, R. V.; Lutz, R. J.; Wong, W. L.; Jacobson, F. S.; Koeppen, H.; Schwall, R. H.; Kenkare-Mitra, S. R.; Spencer, S. D.; Sliwkowski, M. X. *Cancer Res.* **2008**, *68*, 9280-9290. (b) Lorusso, P. M.; Weiss, D.; Guardino, E.; Girish, S.; Sliwkowski, M. X. *Clin. Cancer Res.* **2011**, *17*, 6437-6447.

[33] (a) Kiewe, P.; Hasmüller, S.; Kahlert, S.; Heinrigs, M.; Rack, B.; Marmé, A.; Korfel, A.; Jäger, M.; Lindhofer, H.; Sommer, H.; Thiel, E.; Untch, M. *Clin. Cancer Res.* **2006**, *12*, 3085-3091. (b) Jäger, M.; Schoberth, A.; Ruf, P.; Hess, J.; Lindhofer, H. *Cancer Res.* **2009**, *69*, 4270-4276.

kinase domain of these receptors blocking their downstream signalling (Figure 8e).[34] Though it has been trialled for other types of neoplasias, in a pivotal phase III study, lapatinib increased progression-free survival in patients with advanced HER2-positive breast cancer when given in combination with the DNA-synthesis inhibitor capecitabine (Xeloda®; Roche Registration Ltd.) (Figure 9). In patients who had failed therapy or become resistant to standard anthracyclines and taxanes chemotherapy even those including trastuzumab, lapatinib has turned out a promising alternative, therefrom it was granted marketing authorization in combination with capecitabine for second line treatment of refractory HER2-positive breast cancer. In addition to its ability to disrupt phosphorylation of wild-type HER2, this TKI is apparently capable of inhibiting the truncated form of HER2 (p95-HER2, whose extracellular domain has been lost), which is present in approximately 20% of all human breast cancers and could be held accountable for most of the observed resistance to trastuzumab. Lapatinib also induces accumulation of inactive HER2 dimers on the cell surface, resulting in increased trastuzumab binding and rendering the cell susceptible to its immune-mediated action. All the above has made this pair a neat synergistic team in preclinical models, suggesting that these agents could be combined in the clinic with impressive results.[35]

Among the last generation of irreversible TKIs, those that permanently modify the ATP binding region of HER receptors, is neratinib (Pfizer Ltd.) (Figure 9). This drug, slightly similar in structure to lapatinib, is highly selective against HER1 and HER2, and in recent phase II trials showed responses in 24% patients previously treated with trastuzumab and in 56% of those not pretreated.[36]

The most recent approach in the therapeutics of HER2-driven cancer is based on targeting heat-shock proteins (HSPs). These proteins facilitate the correct conformational maturation and folding of a range of signalling proteins like HER2. In particular, HSP90 controls the stability of nascent and mature HER2 and various components of the MAPKs. The disruption of HSP90 function results in ubiquitylation and proteasomal degradation of both HER2 and its downstream signalling partners, thereby abrogating their oncogenic activity (Figure 8f). Among a few promising candidates, tanespimycin (Bristol-Myers Squibb Pharma) (Figure 9) has shown important activity in combination with trastuzumab during phase II clinical trials.[37]

---

[34] Wood, E. R.; Truesdale, A. T.; McDonald, O. B.; Yuan, D.; Hassell, A.; Dickerson, S. H.; Ellis, B.; Pennisi, C.; Horne, E.; Lackey, K.; Alligood, K. J.; Rusnak, D. W.; Gilmer, T. M.; Shewchuk, L. *Cancer Res.* **2004**, *64*, 6652-6659.

[35] (a) Brandes, A. A.; Franceschi, E.; Tosoni, A.; Degli-Esposti, R. *Expert Rev. Anticancer Ther.* **2010**, *10*, 179-184. (b) Cameron, D.; Casey, M.; Press, M.; Lindquist, D.; Pienkowski, T.; Romieu, C. G.; Chan, S.; Jagiello-Gruszfeld, A.; Kaufman, B.; Crown, J.; Chan, A.; Campone, M.; Viens, P.; Davidson, N.; Gorbounova, V.; Raats, J. I.; Skarlos, D.; Newstat, B.; Roychowdhury, D.; Paoletti, P.; Oliva, C.; Rubin, S.; Stein, S.; Geyer, C. E. *Breast Cancer Res. Treat.* **2008**, *112*, 533-543.

[36] Burstein, H. J.; Sun, Y.; Dirix, L. Y.; Jiang, Z.; Paridaens, R.; Tan, A. R.; Awada, A.; Ranade, A.; Jiao, S.; Schwartz, G.; Abbas, R.; Powell, C.; Turnbull, K.; Vermette, J.; Zacharchuk, C.; Badwe, R. *J. Clin. Oncol.* **2010**, *28*, 1301-1307.

[37] Erlichman, C. *Expert Opin. Investig. Drugs* **2009**,*18*, 861-868.

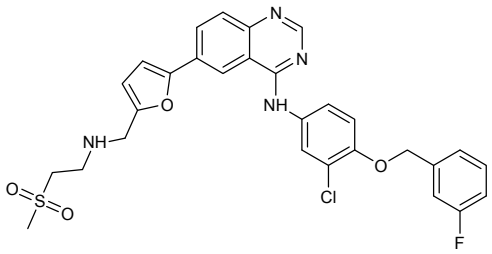

Lapatinib (Tykerb®; Glaxo Group Ltd.)

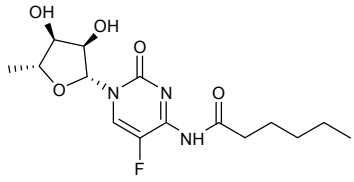

Capecitabine (Xeloda®; Roche Registration Ltd.)

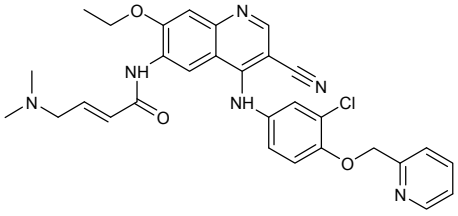

Neratinib (Pfizer Ltd.)

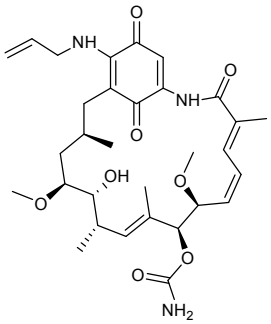

Tanespimycin (Bristol-Myers Squibb Pharma)

Figure 9. HER2-targeting chemotherapeutic agents.

1.3. HER2-Grb2 interaction

Besides the well understood interaction between HER2 and Grb2, this latter has also been found to recognize phosphorylated residues on HER1[38] and HER4[39] though with an overall different outcome. Mutations in HER1 lead up to its constitutive activation in numerous human cancers (including gliomas,[40] oesophagus carcinomas,[41] lung,[42] colorectal[43] and breast cancers[44]). This transformation makes them resistant to certain approved mAbs and TKIs. The role of HER4 in tumorigenesis is less known and sometimes contradictory. There is, for instance, evidence suggesting that HER4 signalling promotes differentiation and growth inhibition of breast cancer cells, consistent with a more favourable prognosis for this disease.[45]

Taken into account all these considerations, it turns out clear that hindering the interaction of Grb2 with HER1 and HER2 can offer a suitable pharmacological approach to the

---

[38] Voldborg, B. R.; Damstrup, L.; Spang-Thomsen, M.; Poulsen, H. S. *Ann. Oncol.* **1997**, *8*, 1197-1206.

[39] Schulze, W. X.; Deng, L.; Mann, M. *Mol. Syst. Biol.* **2005**, *1*, 1-13.

[40] (a) Moscatello, D. K.; Holgado-Madruga, M.; Godwin, A. K.; Ramirez, G.; Gunn, G.; Zoltick, P. W.; Biegel, J. A.; Hayes, R. L.; Wong, A. J. *Cancer Res.* **1995**, *55*, 5536-5539. (b) Lo, H. W. *Curr. Mol. Pharmacol.* **2010**, *3*, 37-52.

[41] Sunpaweravong, P.; Sunpaweravong, S.; Puttawibul, P.; Mitarnun, W.; Zeng, C.; Barón, A. E.; Franklin, W.; Said, S.; Varella-García, M. *J. Cancer Res. Clin. Oncol.* **2005**, *131*, 111-119.

[42] (a) Rosell, R.; Morán, T.; Carcereny, E.; Quiroga, V.; Molina, M. A.; Costa, C.; Benlloch, S.; Tarón, M. *Clin. Transl. Oncol.* **2010**, *12,* 75-80. (b) Burns, T. F.; Rudin, C. M. *Oncology (Williston Park)* **2010**, *24*, 48-49.

[43] Saif, M. W. *Expert Opin. Investig. Drugs* **2010**, *19*, 357-369.

[44] (a) Corzo, C.; Tusquets, I.; Salido, M.; Corominas, J. M.; Bellet, M.; Suarez, M.; Baró, T.; Fabregat, X.; Serrano, S.; Solé, F. *Tumour Biol.* **2005**, *26*, 25-30. (b) Guiu, S.; Coudert, B.; Favier, L.; Arnould, L.; Fumoleau, P. *Bull. Cancer* **2010**, *97*, 365-383.

[45] Koutras, A. K.; Fountzilas, G.; Kalogeras, K. T.; Starakis, I.; Iconomou, G.; Kalofonos, H. P. *Crit. Rev. Oncol. Hematol.* **2010**, *74*, 73-78.

treatment of many tumour processes characterized by the overexpression and/or kinase hyperactivity of these receptors.[46] In addition, it could represent an alternative strategy to overcome acquired resistance to mAbs or TKIs targeting HER2. The development of compounds capable of inhibiting the interaction between the HER2 receptor and its adapter protein Grb2 by binding its SH2 domain has received a great deal of attention in the late times.[47] Such molecules will aid to validate the applicability of this therapeutic approach for cancer treatment. This goal has been favoured by the elucidation of the tridimensional (3D) structure of many SH2 domains found in different proteins, and in particular, the Grb2-SH2 domain.

1.4. The Grb2-SH2 domain

The SH2 domain is an adapter module that recognizes peptide sequences containing one residue of phosphotyrosine (pTyr). It has been widely studied because of its frequent occurrence in a large number of physiologically relevant proteins (Figure 10). Nowadays more than 100 SH2 domains, belonging to 110 different proteins coded in the human genome, are known.[48]

The SH2 domain is made up of approximately 100 amino acids distributed all along a central region of β sheets flanked by two α helices. Peptides carrying a pTyr residue bind this domain perpendicularly to one of the sides of the β sheets. The most conserved residues are found in the pTyr recognizing pocket. Additionally, the invariable presence of an arginine residue (Arg 86) imposes the known great affinity for these phosphopeptides.[49]

In order to effectively design inhibitors of the SH2-pTyr interaction, it is key to know the SH2 domain as well as the SH2 domain-ligand complex X ray structures.

[46] Dharmawardana, P. G.; Peruzzi, B.; Giubellino, A.; Burke, T. R. Jr.; Bottaro, D. P. *Anticancer Drugs* **2006**, *17*, 13-20.

[47] See citation 18c.

[48] (a) Kasembeli, M. M.; Xu, X.; Tweardy, D. J. *Front. Biosci.* **2009**,*14*,1010-1022. (b) Pawson, T.; Kofler, M. *Curr. Opin. Cell. Biol.* **2009**, *21*, 147-153.

[49] Eck, M. J.; Shoelson, S. E.; Harrison, S. C. *Nature* **1993**, *362*, 87-91.

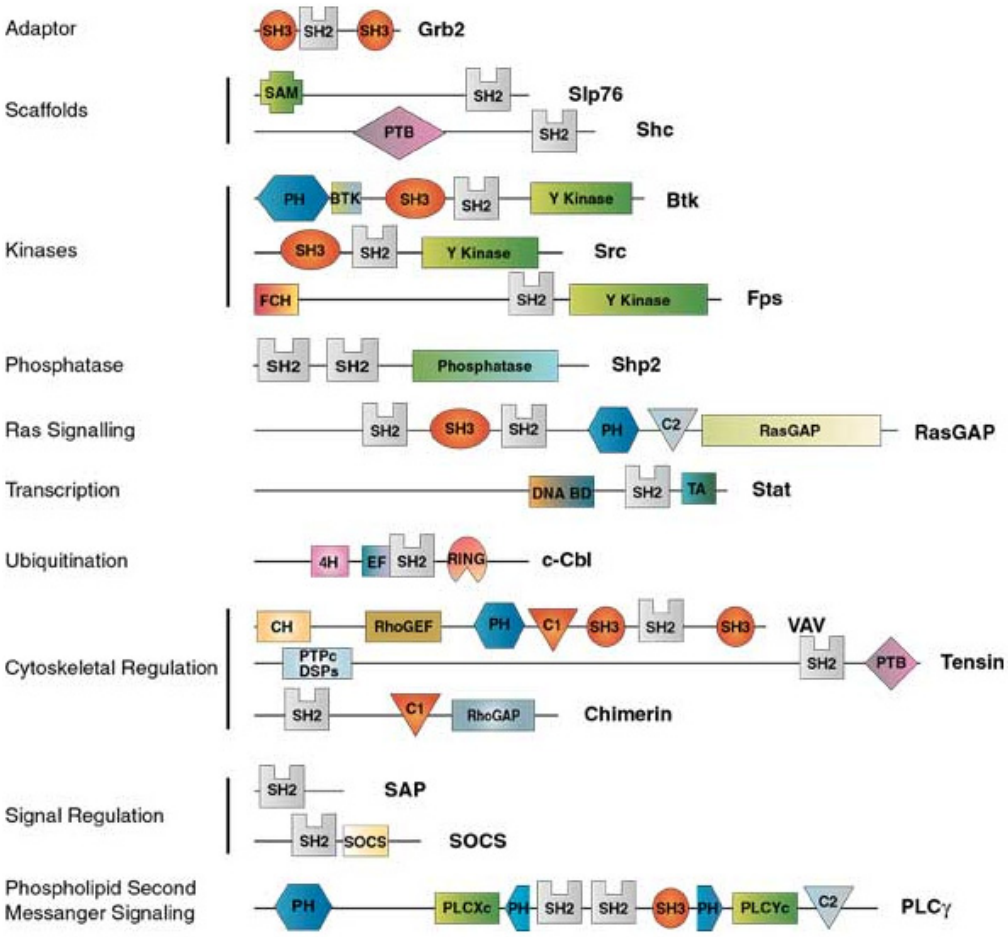

Figure 10. Representative protein families that contain at least one SH2  domain. The specific recognition function of this domain is constant, whereas the overall biological function of the protein may vary greatly according to the presence of other effector modules. (Source: Liu, B. A. et al. *Mol. Cell* **2006**, *22*, 851-868.)

Grb2 is a 25 KDa protein made up of one SH2 domain and two SH3 domains (Figure 11).[50] The SH3 domains specifically bind proline-rich regions on other proteins,[51] whereas the Grb2-SH2 domain recognizes pTyr-containing peptide sequences (such as Glu-pTyr-Ile-Asn-Gln).[52] The 3D structure of the Grb2-SH2 domain was firstly elucidated in 1996 by means of heteronuclear multidimensional NMR, being very similar to other known SH2 domains.[53]

[50] Maignan, S.; Guilloteau, J. P.; Fromage, N.; Arnoux, B.; Becquart, J.; Ducruix, A. *Science* **1995**, *268*, 291-293.

[51] See citation 18a.

[52] Rahuel, J.; García-Echeverría, C.; Furet, P.; Strauss, A.; Caravatti, G.; Fretz, H.; Schoepfer, J.; Gay, B. *J. Mol. Biol.* **1998**, *279*, 1013-1022.

[53] Thornton, K. H.; Mueller, W. T.; McConnell, P.; Zhu, G.; Saltiel, A. R.; Thanabal, V. *Biochemistry* **1996**, *35*, 11852-11864.

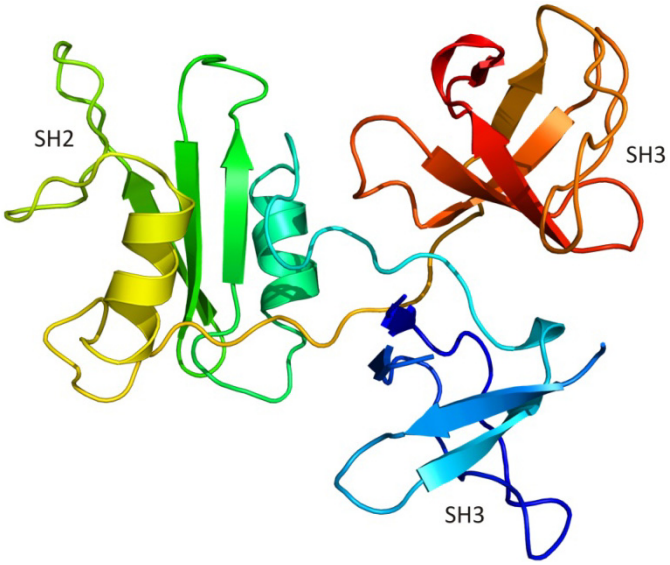

Figure 11. X ray structure of the human Grb2 protein obtained at a resolution of 3.1 Å (PDB code: 1gri).

Grb2-SH2 is composed of two α helices and eight β strands. According to Eck[54] notation, the whole structure can be described as a short fragment of a β strand (βA) followed by an α helix (αA) to which three antiparallel β strands (βB-βD) are directly connected. These are continued into another set of three shorter antiparallel β strands (βD'-βF), which finally coils in the second α helix (αB), leaving this latter perfectly opposite to the αA (Figure 12).

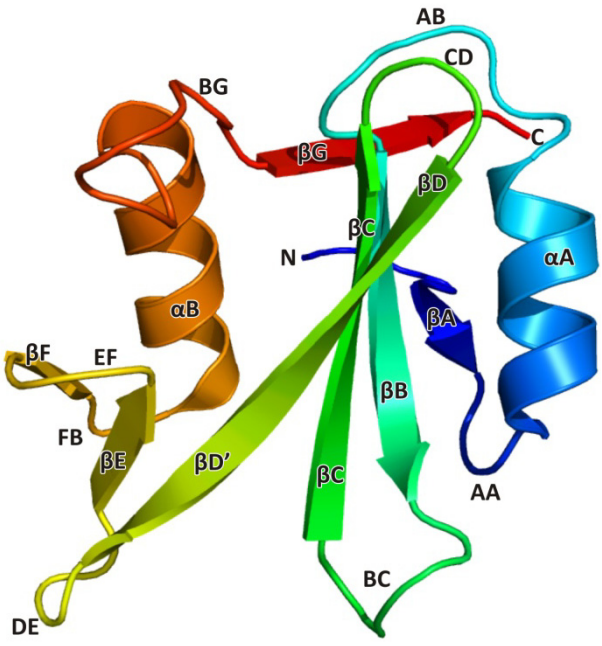

Figure 12. X ray structure of the SH2 domain of the human Grb2 protein obtained at a resolution of 1.8 Å (PDB code: 1zfp).

[54] See citation 49.

In general, SH2 domains possess two important regions devoted to the substrate docking. The first one specifically binds the pTyr residue, while the second one recognizes the peptide sequence surrounding the pTyr residue. Actually, pTyr alone does not confer specificity to the interaction of these compounds with the protein.[55]

The structural elucidation of the Grb2-SH2-ligand complex carried out through X ray crystallography[56] and NMR[57] indicates that the ligand adopts a U shape when bound to Grb2-SH2; contrary to what has been found in other SH2-containing proteins, in which the peptide bearing the pTyr residue lies perfectly extended along the domain.

1.5. Peptide inhibitors of the Grb2-SH2 domain

To start off the rational design of inhibitors to the HER2-Grb2 interaction, many peptide libraries containing pTyr were assayed in order to determine the minimal amino acid sequence necessary to selectively dock onto this domain. These studies have led to determine pTyr-X_{+1}-Asn-X_{+3} as the minimal peptide necessary for selective recognition of the SH2 domain, being the Asn absolutely required for affinity.[58] At the beginning, it was proposed the tetrapeptide pTyr-Val-Asn-Val as the minimal sequence capable of binding the SH2 domain of Grb2; but soon after, further studies revealed that the former tetrapeptide could be reduced in one amino acid to the tripeptide pTyr-X_{+1}-Asn, and still maintained its affinity for the SH2 domain. Its docking enabled confirmation of two important binding pockets in Grb2-SH2, as it has been observed in other SH2-bearing proteins. The first one, being of polar nature, accommodates the phosphate group; whereas the second one, mostly non-polar in nature, hosts the X_{+2} hydrophobic residue (Figure 13).

Once the structure of the SH2 domain was elucidated, and the requirements of ligands important for interaction were identified, all synthetic efforts were aimed at optimizing these compounds in order to obtain potent inhibitors able to block HER2-Grb2 interaction.

The most relevant modifications made on the structure of the tripeptide pTyr-X_{+1}-Asn-NH_2 are summarized in the following sections.

---

[55] Machida, K.; Mayer, B. J. *Biochim. Biophys. Acta* **2005**, *1747*, 1-25.

[56] Rahuel, J.; Gay, B.; Erdmann, D.; Strauss, A.; García-Echeverría, C.; Furet, P.; Caravatti, G.; Fretz, H.; Schoepfer, J.; Grütter, M. G. *Nat. Struct. Biol.* **1996**, *3*, 586-589.

[57] Ogura, K.; Tsuchiya, S.; Terasawa, H.; Yuzawa, S.; Hatanaka, H.; Mandiyan, V.; Schlessinger, J.; Inagaki, F. *J. Mol. Biol.* **1999**, *289*, 439-445.

[58] Songyang, Z.; Shoelson, S. E.; McGlade, J.; Olivier, P.; Pawson, T.; Bustelo, X. R.; Barbacid, M.; Sabe, H.; Hanafusa, H.; Yi, T.; Ren, R.; Baltimore, D.; Ratnofsky, S.; Feldman, R. A.; Cantley, L. C. *Mol. Cell. Biol.* **1994**, *14*, 2777-2785.

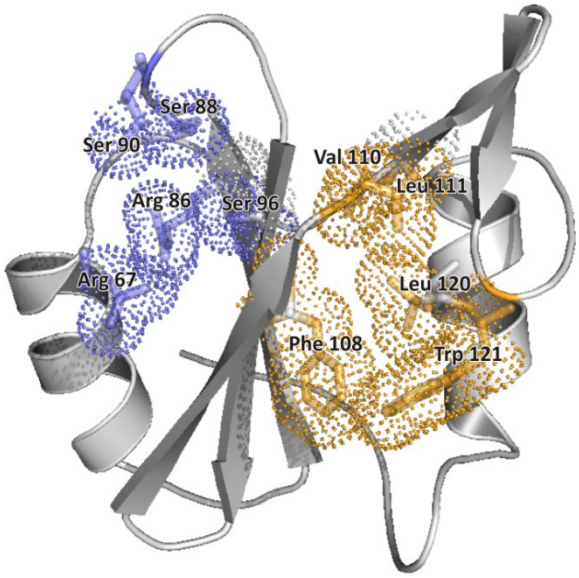

Figure 13. X ray structure of the SH2 domain of the human Grb2 protein obtained at a resolution of 1.8 Å (PDB code: 1zfp) in which the polar (blue) and the non-polar (orange) pockets are highlighted by the side chains of the amino acids comprised in them.

1.5.1. Modifications of the N-terminus (N_t)

The N-terminus, N_t, is the pTyr residue in the pTyr-Ile-Asn-NH_2 sequence. Different modifications, like *N*-alkylation of the pTyr or the formation of another peptide bond on this position, have been proposed. Results have shown a direct relationship between the increase in the substituent volume and the affinity for the SH2 domain, being the incorporation of an *N*-(2-aminobenzoyl)-α-glutamyl (2-Abz-Glu, Figure 14) the modification yielding the best affinity (inhibitory concentration 50, IC_{50}, of 22 nM).[59]

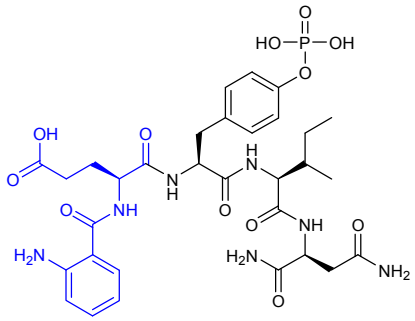

Figure 14. Tetrapeptide Abz-Glu-pTyr-Ile-Asn-NH_2.

Subsequent X ray studies of the complex formed by the peptide Abz-Glu-pTyr-Ile-Asn-Gln-NH_2 (IC_{50} = 26 nM), analogous to the former one, and the Grb2-SH2 domain, have confirmed the existence of stabilizing interactions between the pTyr phosphate group and the amino substituent of the Abz moiety. These interactions altogether with an extra overlapping

[59] Fretz, H.; Furet, P.; García-Echeverría, C.; Schoepfer, J.; Rahuel, J. *Curr. Pharm. Des.* **2000**, *6*, 1777-1796.

increase between the Abz aromatic ring and the Arg 67 guanidinium group are responsible for the high affinities observed.[60]

1.5.2. Modifications of the X_{+1} position

Variations of the X_{+1} position were examined on the (3-amino)-Z-pTyr-X_{+1}-Asn-NH_2 tripeptide (Z = bencyloxycarbonyl) studying the influence of different side chains. For instance, *gem*-dimethyl, cyclopropyl, indanyl, *sec*-butyl, and cyclohexyl substituents were introduced. Among them, the derivative (3-amino)-Z-pTyr-Ac_6c-Asn-NH_2, bearing the non-natural amino acid 1-aminocyclohexanecarboxylic acid (Ac_6c), showed the highest affinity (IC_{50} = 1 nM,[61] Figure 15).

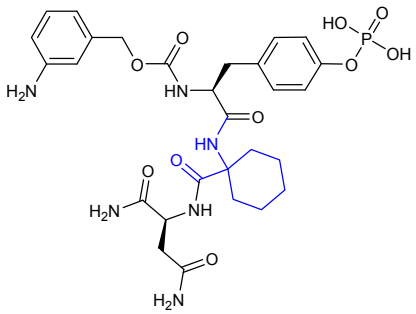

Figure 15. Tripeptide (3-amino)-Z-pTyr-X_{+1}-Asn-NH_2 (X_{+1} = 1-aminocyclohexanecarboxylic acid, Ac_6c).

1.5.3. Modifications of the X_{+2} position

It has been previously indicated the importance of the amino acid Asn for the specific binding to the Grb2-SH2 domain. The X ray structure of the SH2 domain complexed with the peptide H-Lys-Pro-Phe-pTyr-Val-Asn-Val-NH_2 reveals the presence of two H bonds between the side chain of the Asn and the peptide backbone of Lys 109 (located in the βD sheet), and a third one with the carbonyl group of Leu 120 of the βE sheet.[62]

Using the peptide (3-amino)-Z-pTyr-Ac_6c-X_{+2}-NH_2 with its optimized Ac_6c and 3-amino-Z subunits as the trial scaffold, several Asn surrogates (2-pentanone and the (*1S,2R*) and (*1R,2S*) enantiomers of the *cis*-2-amino-3-cyclohexenecarboxylic acid, *cis*-Achec) were tested. Among them, the derivative with X_{+2} = (*1S,2R*)-Achec (Figure 16) showed almost the same affinity for the protein (IC_{50} = 1.6 nM) as the original Asn-containing peptide (IC_{50} = 1 nM). The new amino acid perfectly mimics the three H bonds formed by the Asn. It is worth pointing out the

[60] See citation 52.

[61] García-Echeverría, C.; Furet, P.; Gay, B.; Fretz, H.; Rahuel, J.; Schoepfer, J.; Caravatti, G. *J. Med. Chem.* **1998**, *41*, 1741-1744.

[62] (a) Furet, P.; García-Echeverría, C.; Gay, B.; Schoepfer, J.; Zeller, M.; Rahuel, J. *J. Med. Chem.* **1999**, *42*, 2358-2363. (b) See citation 56.

significance of the peptide stereochemistry for its effective interaction with the SH2 domain, as its enantiomer (*1R,2S*) shows no affinity (IC_{50} > 5000 nM).[63]

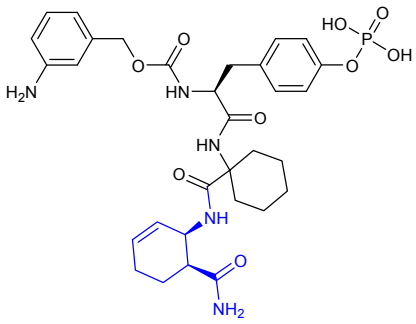

Figure 16. Tripeptide (3-amino)-Z-pTyr-Ac_6c-X_{+2}-NH_2 (X_{+2} = (*1S,2R*)-Achec).

1.5.4. Modifications of the C-terminus (C_t)

X ray studies[64] have demonstrated the existence of a hydrophobic region in Grb2-SH2 close to the C_t bound phosphopeptide. This region comprises the side chains of the residues Lys 109 (βD6), Leu 111 (βD'1) and Phe 119 (βE3). Employing the peptide Ac-pTyr-Ile-Asn-NH-R (R = H, IC_{50} = 890 nM) as the trial scaffold, a variety of substituents were attached to the C_t in order to increase the interactions in this hydrophobic pocket. The best two compounds contained the (naphth-1-yl)propyl and (2-hydroxynaphth-1-yl)propyl groups (Figure 17), which improved the affinity of the initial tripeptide in two orders of magnitude (IC_{50} values of 47[65] and 11[66] nM, respectively).

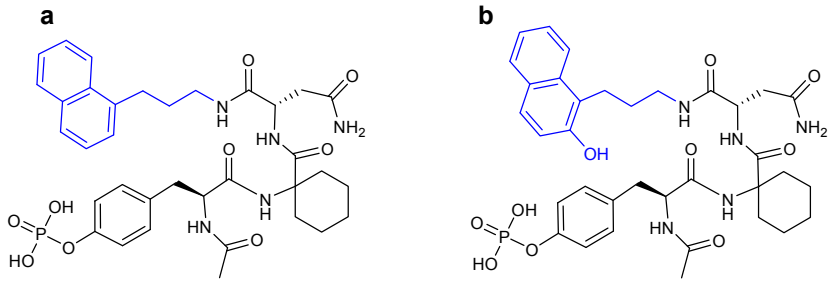

Figure 17. Tripeptides Ac-pTyr-Ac_6c-Asn-NH-X **a.** X = (naphth-1-yl)propyl. **b.** X = (2-hydroxynaphth-1-yl)propyl.

[63] See citation 62a.

[64] See citation 56.

[65] Furet, P.; Gay, B.; Caravatti, G.; García-Echeverría, C.; Rahuel, J.; Schoepfer, J.; Fretz, H. *J. Med. Chem.* **1998**, *41*, 3442-3449.

[66] See citation 59.

1.5.5. Replacement of the pTyr

Although the X ray data set clear that the presence of a phosphate group is key for binding, phosphate-containing inhibitors may have bioavailability and stability problems under physiological conditions. Therefore, several phosphotyrosyl mimetics (Table 1)[67,68] were tested, resulting in some cases in excellent affinities, although none of the variants reached the potency of the parent peptide.

Table 1. Substitution of the pTyr in the peptide Ac-pTyr-Ac$_6$c-Asn-NH-3(napht-1-yl)propyl

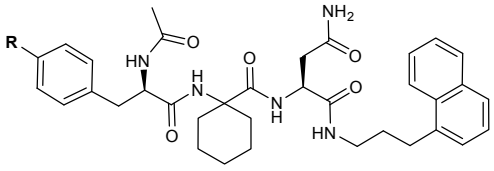

R	IC_{50} (μM)	R	IC50 (μM)
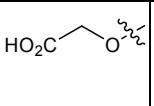	68	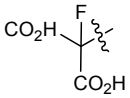	0.68
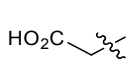	6.4	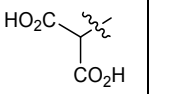	0.16
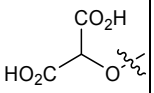	2.75	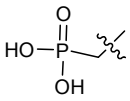	0.02

1.5.6. Conformational restrictions

Given the intrinsic flexibility of the Grb2-SH2 ligands described so far, it was hypothesized that affinity could be increased by introducing conformational restrictions in the molecule that would decrease the entropic penalization associated to the acquisition of the bioactive conformation. Conformational restrictions can be sorted out into two main groups: local (on the pTyr residue) or global.[69]

1.5.6.1. Local restrictions affecting the pTyr residue

The incorporation of rigid rings on the pTyr residue in peptides known for their high affinity for the Grb2-SH2 domain, like Ac-pTyr-Ac$_6$c-Asn-NH-X [X = (naphth-1-yl)propyl, IC_{50} =

[67] Yao, Z. J.; King, C. R.; Cao, T.; Kelley, J.; Milne, G. W.; Voigt, J. H.; Burke, T. R. Jr. *J. Med. Chem.* **1999**, *42*, 25-35.

[68] Gao, Y.; Luo, J.; Yao, Z. J.; Guo, R.; Zou, H.; Kelley, J.; Voigt, J. H.; Yang, D.; Burke, T. R. Jr. *J. Med. Chem.* **2000**, *43*, 911-920.

[69] Burke, T. R. Jr. *Int. J. Pept. Res. Ther.* **2006**, *12*, 33-48.

47 nM, Figure 17a], led to a new generation of cyclic systems (Figure 18a,b) with low ability to bind the SH2 domain (IC_{50} values of 5.5 μM and > 10 μM, respectively).[70,71]

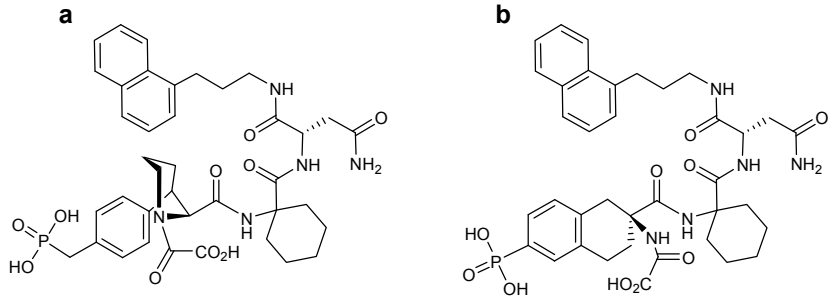

Figure 18. Local restrictions on the pTyr residue.

1.5.6.2. Global conformational restrictions

Global conformational restrictions are those affecting the entire peptide structure. These have been accomplished by means of ring-closing disulfide or thioether bridges in a head-to-tail fashion. In several examples, pTyr has been replaced by phosphomimetics[72] like (phosphonomethyl)phenylalanine (Figure 19a),[73] resulting in a very good IC_{50} value (2.4 nM). Notwithstanding, substitution of pTyr for Tyr together with a glutamic acid in position X_{+2} (Figure 19b), originally introduced to compensate for the lack of the phosphate group interactions with the Arg 86, carried along a significant affinity loss (IC_{50} = 20 μM).[74]

Application of metathesis reactions to close the ring[75] has brought a new family of macrocyclic inhibitors with very good affinity values, although with limited bioavailability indicators as main drawback. Among the best derivatives of this family,[76] Figure 19c shows the most active one with an IC_{50} value of 2 nM.[77]

---

[70] (a) See citation 68. (b) Wang, X. Z.; Yao, Z. J.; Liu, H.; Zhang, M.; Yang, D.; George, C.; Burke, T. R. Jr. *Tetrahedron* **2003**, *59*, 6087-6093.

[71] (a) Liu, D. G.; Wang, X. Z.; Gao, Y.; Li, B.; Yang, D.; Burke, T. R. Jr. *Tetrahedron* **2002**, *58*, 10423–10428. (b) Oishi, S.; Kang, S. U.; Liu, H.; Zhang, M.; Yang, D.; Deschamps, J. R.; Burke, T. R. Jr. *Tetrahedron* **2004**, *60*, 2971-2977.

[72] Song, Y. L.; Peach, M. L.; Roller, P. P.; Qiu, S.; Wang, S.; Long, Y. Q. *J. Med. Chem.* **2006**, *49*, 1585-1596.

[73] Song, Y. L.; Roller, P. P.; Long, Y. Q. *Bioorg. Med. Chem. Lett.* **2004**, *14*, 3205-3208.

[74] Li, P.; Zhang, M.; Long, Y. Q.; Peach, M. L.; Liu, H.; Yang, D.; Nicklaus, M.; Roller, P. P. *Bioorg. Med. Chem. Lett.* **2003**, *13*, 2173-2177.

[75] (a) Gao, Y.; Voigt, J.; Wu, J. X.; Yang, D.; Burke T. R. Jr. *Bioorg. Med. Chem. Lett.* **2001**, *11*, 1889-1892. (b) Oishi, S.; Karki, R. G.; Kang, S. U.; Wang, X.; Worthy, K. M.; Bindu, L. K.; Nicklaus, M. C.; Fisher, R. J.; Burke, T. R. Jr. *J. Med. Chem.* **2005**, *48,* 764-772. (c) Liu, F.; Worthy, K. M.; Bindu, L. K.; Fisher, R. J.; Burke, T. R. Jr. *J. Org. Chem.* **2007**, *72*, 9635-9642.

[76] (a) Schoepfer, J.; Gay, B.; End, N.; Muller, E.; Scheffel, G.; Caravatti, G.; Furet, P. *Bioorg. Med. Chem. Lett.* **2001**, *11*, 1201-1203. (b) Shi, Z. D.; Liu, H.; Zhang, M.; Worthy, K. M.; Bindu, L.; Yang, D.; Fisher, R. J.; Burke, T. R. Jr. *Bioorg. Med. Chem.* **2005**, *13*, 4200-4208. (c) Kang, S. U.; Shi, Z. D.; Worthy, K. M.; Bindu, L. K.; Dharmawardana, P. G.; Choyke, S. J.; Bottaro, D. P.; Fisher, R. J.; Burke, T. R. Jr. *J. Med. Chem.* **2005**, *48*, 3945-3948. (d) Phan, J.; Shi, Z. D.; Burke, T. R. Jr.; Waugh, D. S. *J. Mol. Biol.* **2005**, *353*, 104-115.

[77] Shi, Z. D.; Lee, K.; Wei, C. Q.; Roberts, L. R.; Worthy, K. M.; Fisher, R. J.; Burke, T. R. Jr. *J. Med. Chem.* **2004**, *47*, 788-791.

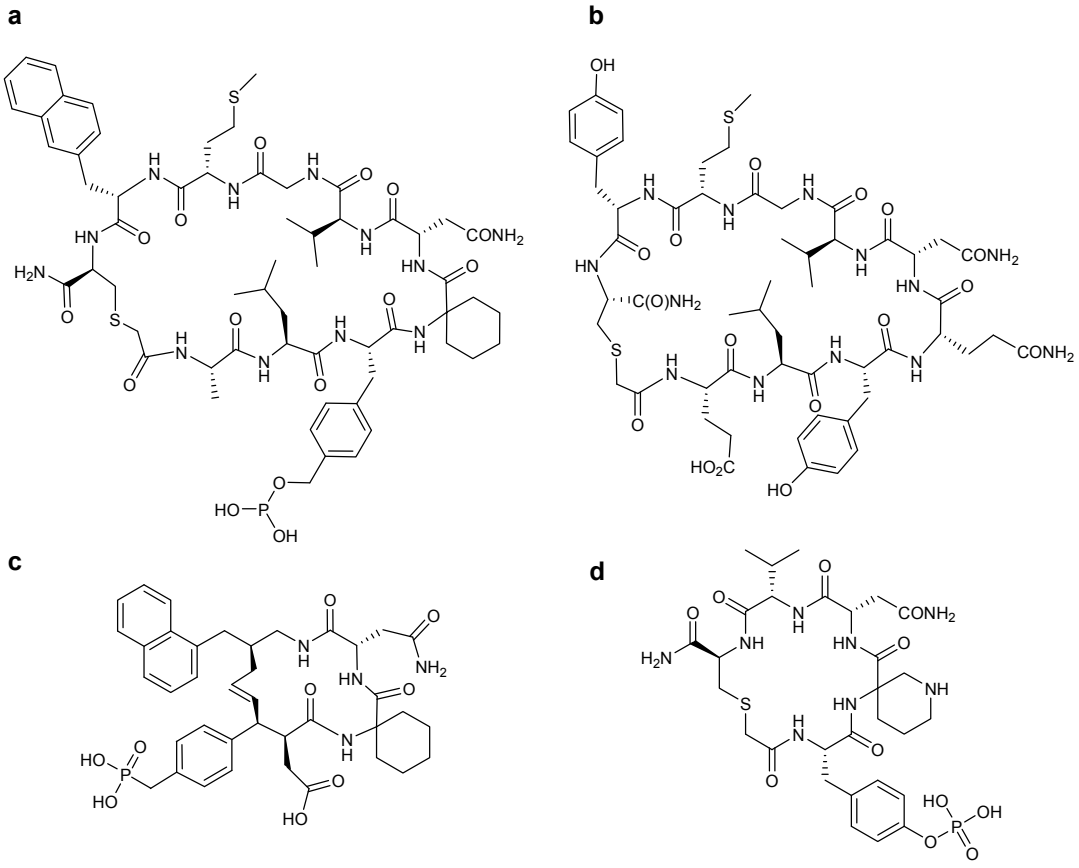

Figure 19. Global conformational restrictions: development of oligopeptide macrocycles.

Finally, a second generation of phosphotyrosine-containing cyclic pentapeptides, all reduced versions of the macrocycle of Figure 19b, have been prepared. In these structures, unnecessary amino acids have been removed, while the thioether linkage has been maintained and a β-turn inducing residue has been intentionally incorporated in order to gain affinity. Out of this new series, the derivative carrying 3-aminopiperidine-3-carboxylic acid as the β-turn inducer came out the best inhibitor with an IC_{50} of 0.4 μM (Figure 19d).[78]

1.6. Non-peptide inhibitors of the Grb2-SH2 domain

In spite of the high affinity values exhibited by many of the peptide inhibitors developed up to date, their validation as suitable drug-like agents for the treatment of cancer is still lacking mainly due to bioavailability drawbacks. In this context, there is need for a transition into new small non-peptide structures of lower molecular weight.

In the very first instance, the aim was to suppress the greatest possible number of peptide bonds within the molecule, while keeping with pTyr as the only amino acid and mimicking the rest of the original tripeptide employing non-amino acid structures. Compounds

[78] Jian, S.; Liao, C.; Bindu, L.; Yin, B.; Worthy, K. W.; Fisher, R. J.; Burke, T. R. Jr.; Nicklaus, M. C.; Roller, P. P. *Bioorg. Med. Chem. Lett.* **2009**, *19*, 2693-2698.

which incorporate a (3-aminomethylphenyl)urea were found to suit this requirement (Figure 20). These derivatives showed IC_{50} values ranging from 5 to 50 μM.[79]

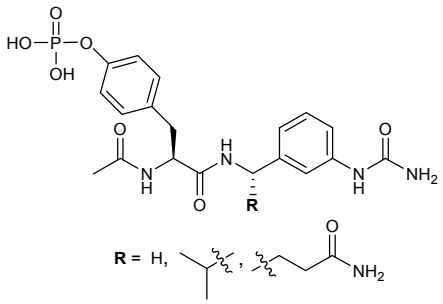

Figure 20. Small-molecule Grb2 ligands containing pTyr.

With regard to non-peptide compounds in which the pTyr residue is completely removed, there are just a few examples in the current literature. The only known structures came out of high-throughput screening (HTS) assays fed with huge libraries of exceptionally diverse entities. Among the most interesting outcomes are the molecules depicted in Figure 21, with IC_{50} values between 1 and 26 μM.[80]

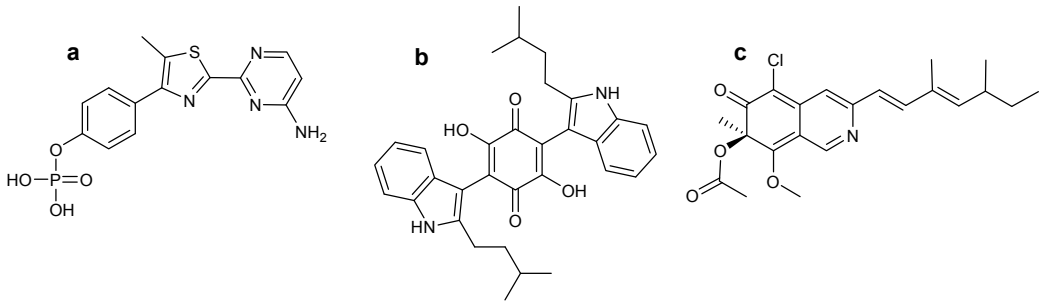

Figure 21. Grb2-SH2 non-peptide ligands devoid of pTyr in their structure.

In view of these facts, rational design of small molecules capable of efficiently interrupting HER2 downstream signalling by blocking its interaction with the adapter protein Grb2 seems a promising approach to definitely validate this protein as a target of interest in oncology.

However, most ligands of the SH2 domain of Grb2 (Grb2-SH2) that inhibit the HER2-Grb2 interaction described so far are of peptide nature and show important bioavailability limitations that preclude their development as drugs. In this regard, and in terms of finding non-peptide molecules as Grb2-SH2 ligands, very little progress has been reported. Therefore, the development of small molecules capable of disrupting binding between HER2 and Grb2 might bolster research in this field. These assumptions have led us to start a project aimed at

[79] Schoepfer, J.; Gay, B.; Caravatti, G.; García-Echeverría, C.; Fretz, H.; Rahuel, J.; Furet, P. *Bioorg. Med. Chem. Lett.* **1998**, *8*, 2865-2870.

[80] (a) Nam, J. Y.; Kim, H. K.; Kwon, J. Y.; Han, M. Y.; Son, K. H.; Lee, U. C.; Choi, J. D.; Kwon, B. M. *J. Nat. Prod.* **2000**, *63*, 1303-1305. (b) Harris, G. D.; Nguyen, A.; App, H.; Hirth, P.; McMahon, G.; Tang, C. *Org. Lett.* **1999**, *1*, 431-433. (c) Caravatti, G.; Rahuel, J.; Gay, B.; Furet, P. *Bioorg. Med. Chem. Lett.* **1999**, *9*, 1973-1978.

developing small-molecule inhibitors that bind Grb2-SH2 and so block its signalling pathway. Such molecules could overcome the limitations of the above mentioned peptides and thus be useful to validate this therapeutic approach.

Objectives and Work Plan

2. Objectives and work plan

The main goal of this project is to develop non-peptide small molecules capable of selectively binding the Grb2-SH2 domain. This overall objective will be addressed through the following steps:

1. Computer-assisted design of compounds based on the crystal structure of the Grb2-SH2 domain in complex with the potent pentapeptide ligand 2-Abz-Glu-pTyr-Ile-Asn-Gln-NH_2.

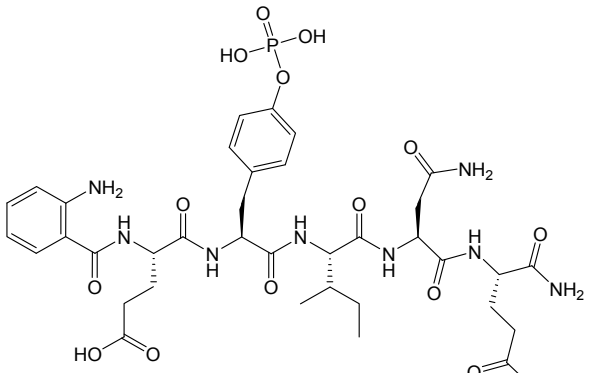

2-Abz-Glu-pTyr-Ile-Asn-Gln-NH_2

2. Synthesis and determination of the capacity of all compounds to bind the Grb2-SH2 domain.

3. Optimization process.

4. Validation of the biological potential of the optimized compound(s).

Results and Discussion

3. Results and Discussion

3.1. Design of Grb2-SH2 ligands

In search of Grb2-SH2 ligands with a structural novel core, we first identified the residues involved in key interactions with the protein from the crystal structure of the Grb2-SH2 domain in complex with the high-affinity 2-Abz-Glu-pTyr-Ile-Asn-Gln-NH_2 pentapeptide.[81] This structure reveals the pivotal roles of two protein sites in the interaction with the inhibitor. The first site is a highly conserved hydrophilic pocket among SH2 domains, which is responsible for pTyr binding and is defined by a cluster of serine residues, Ser88 (βB7), Ser90 (βC2) and Ser96 (βC3) (the positions in parentheses indicate the topology of the Grb2–SH2 domain, following the commonly used notation of Eck and collaborators[82]), and the positively charged amino acids Arg67 (αA2) and Arg86 (αB5) (Figure 22). Residue Arg67 (αA2) is especially important since it is involved in the interactions with the N-terminal domain of the peptide and forms a hydrogen bond with the backbone carbonyl group of the pY-1 amino acid ($NH_2^{R67}\cdots O=C^{pY-1}$). The second site includes the backbone atoms of the amino acids His107 (βD4), Lys109 (βD6), Leu120 (βE4), and the side chain of Trp121 (EF1). The backbone carbonyl group of His107 (βD4) interacts with the backbone N–H group of the pY+1 amino acid ($C=O^{H107}\cdots H–N^{pY+1}$) of the inhibitor, while both the backbone N–H ($N–H^{K109}\cdots O=C^{pY+2}$) and carbonyl ($C=O^{K109}\cdots H_2N^{pY+2}$) groups of Lys109 (βD6) form hydrogen bonds with the side chain of Asn at the position pY+2 (Figure 22).[83] In addition, the NH_2 group of this Asn side chain forms a hydrogen bond with the backbone carbonyl group of Leu120 (βE4) ($C=O^{L120}\cdots H_2N^{pY+2}$, Figure 22).

[81] See citation 52.

[82] See citation 49.

[83] See citations 52 and 57.

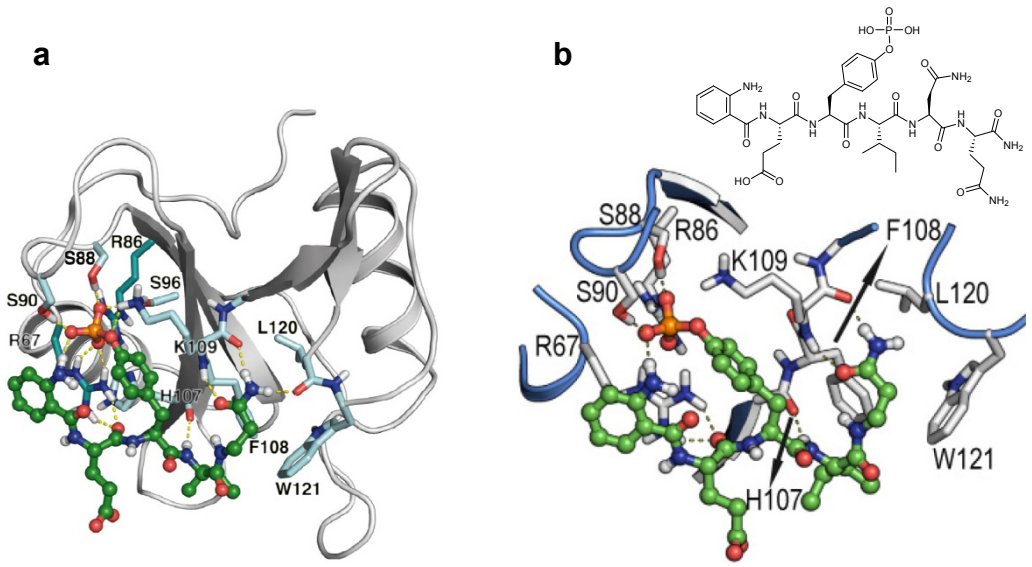

Figure 22. a. Representative structures obtained in the MD simulations of Grb2-SH2 in complex with the 2-Abz-Glu-pTyr-Ile-Asn-Gln-NH_2 pentapeptide (PDB code:1zfp). **a.** Entire SH2 domain shown **b.** Zoom-in detail of interacting amino acids.

According to these observations, we have designed two series of compounds with novel structural cores (Figure 23) that maintain all (series **I**) or some (series **II**) of the key interactions with the Grb2-SH2 domain. These compounds should shed light on the identification of the minimal key interactions needed for binding the Grb2-SH2 domain.[84] This work was carried out in collaboration with Prof. Leonardo Pardo group at Laboratori de Medicina Computacional, Unitat de Bioestadistica, Universitat Autonoma de Barcelona.

In series **I**, interactions with the hydrophilic pocket (responsible for the pTyr binding) and residues Arg67, His107, and Lys109 are kept. The W substituent mimics the backbone carbonyl group of the amino acid in position pY-1 that interacts with Arg67 (αA2) resembling the $NH_2^{R67}\cdots O{=}C^{pY-1}$ hydrogen bond with the pentapeptide 2-Abz-Glu-pTyr-Ile-Asn-Gln-NH_2; the pTyr is linked to the spacer by an amide group, which preserves the hydrogen bond with the backbone carbonyl group of His107 (βD4) observed for the N–H group of the pY+1 residue ($C{=}O^{H107}\cdots H{-}N^{pY+1}$). The terminal group is designed to contact both the backbone carbonyl and the N–H groups of Lys109 (βD6), mimicking the role of Asn in position pY+2 ($N{-}H^{K109}\cdots O{=}C^{pY+2}$ and $C{=}O^{K109}\cdots H_2N^{pY+2}$); and spacers of two and three methylene units were chosen to provide enough distance and flexibility to enable concerted interactions with the two binding sites of the protein domain (Figure 23).

[84] Orcajo-Rincón, Á. L.; Ortega-Gutiérrez, S.; Serrano, P.; Torrecillas, I. R.; Wüthrich, K.; Campillo, M.; Pardo, L.; Viso, A.; Benhamú, B.; López-Rodríguez, M. L. *J. Med. Chem.* **2011**, *54*, 1096-1100.

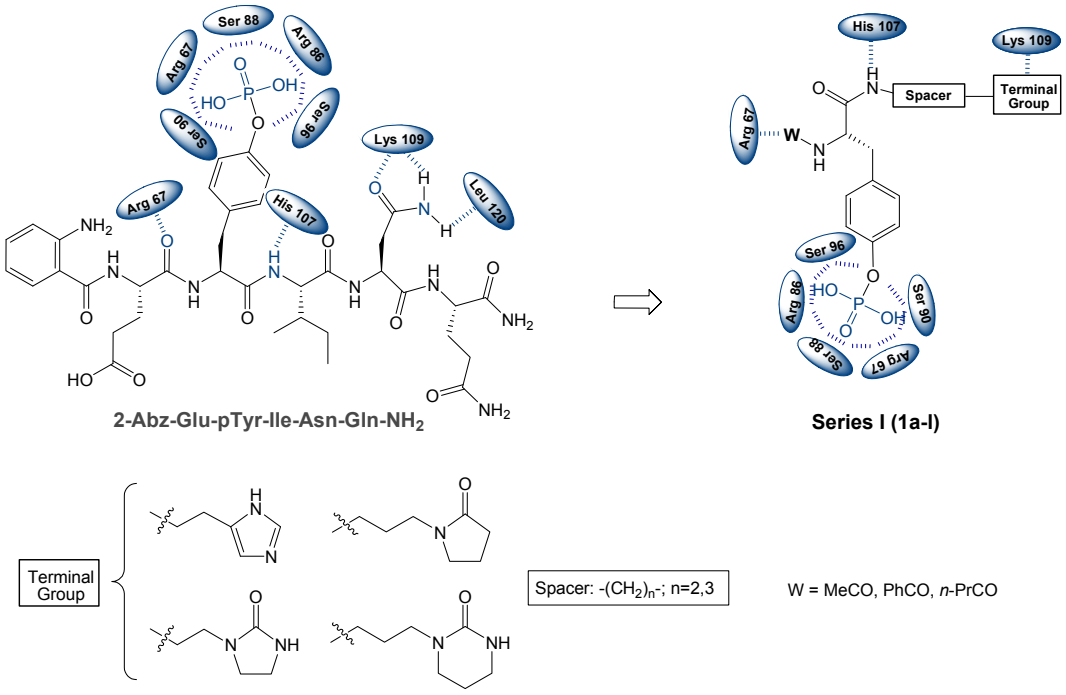

Figure 23. Design of general structures **I**.

The interactions of one of the designed compounds (**(*S*)-1k**) relative to the 2-Abz-Glu-pTyr-Ile-Asn-Gln-NH_2 pentapeptide were evaluated by comparing MD simulations for the two complexes performed with the Molecular Mechanics - Generalized Born Surface Area (MM-GBSA) methodology[85] (Figure 24). In both cases equilibration was achieved during the first 5 ns of simulation, as monitored by the all-atoms root-mean square deviation (rmsd) and from key interatomic ionic and hydrogen bond distances between Grb2-SH2 and either 2-Abz-Glu-pTyr-Ile-Asn-Gln-NH_2 or **(*S*)-1k** as a function of time. It is worth mentioning that for **(*S*)-1k** the key interactions with Arg67 (αA2), His107 (βD4), and Lys109 (βD6) were maintained during the full simulation time, similar to what was observed for 2-Abz-Glu-pTyr-Ile-Asn-Gln-NH_2 (Figure 22).

[85] Kollman, P. A.; Massova, I.; Reyes, C.; Kuhn, B.; Huo, S.; Chong, L.; Lee, M.; Lee, T.; Duan, Y.; Wang, W.; Donini, O.; Cieplak, P.; Srinivasan, J.; Case, D. A.; Cheatham, T. E. *Acc. Chem. Res.* **2000**, *33*, 889-897.

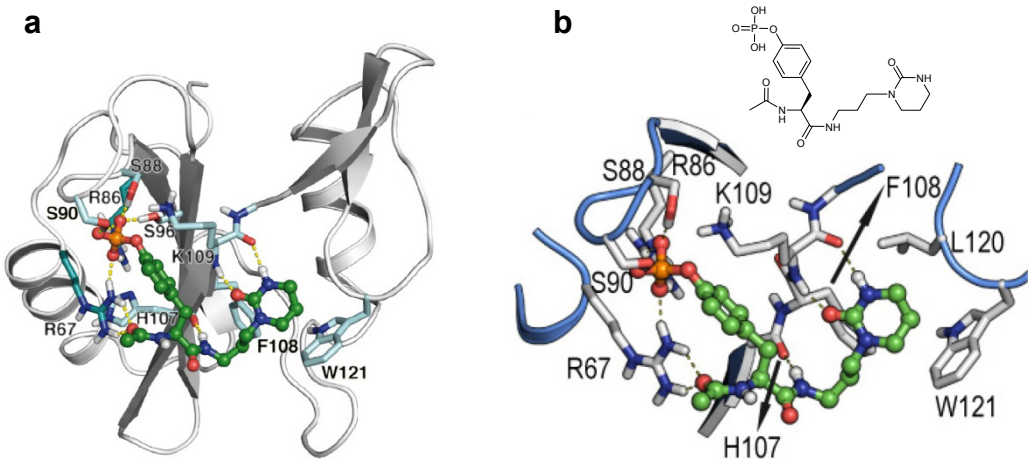

Figure 24. a. Representative structures obtained in the MD simulations of Grb2-SH2 in complex with one of the designed compounds of series **I** (**(*S*)-1k**). **a.** Entire SH2 domain shown. **b.** Zoom-in detail of interacting amino acids.

With respect to series **II**, it was designed without any amino acid in its structure and a reduced number of interactions with Grb2-SH2. The interactions with Arg67 ($NH_2^{R67}\cdots O{=}C^{pY-1}$) and His107 ($C{=}O^{H107}\cdots H{-}N^{pY+1}$) were eliminated. Compounds of series **II** contain an acidic phosphate group attached to a phenyl ring mimicking the pTyr residue of the pentapeptide, and an amide bond designed to interact with the backbone N–H group of Lys109 resembling the $N{-}H^{K109}\cdots O{=}C^{pY+2}$ interaction. The spacer between the phenylphosphate and amide groups is formed by an alkoxymethylene chain with the appropriate distance and flexibility so that the terminal group can fit into a hydrophobic pocket observed in the crystal structure. The aliphatic and aromatic moieties represented in Figure 25 were selected as hydrophobic terminal groups.

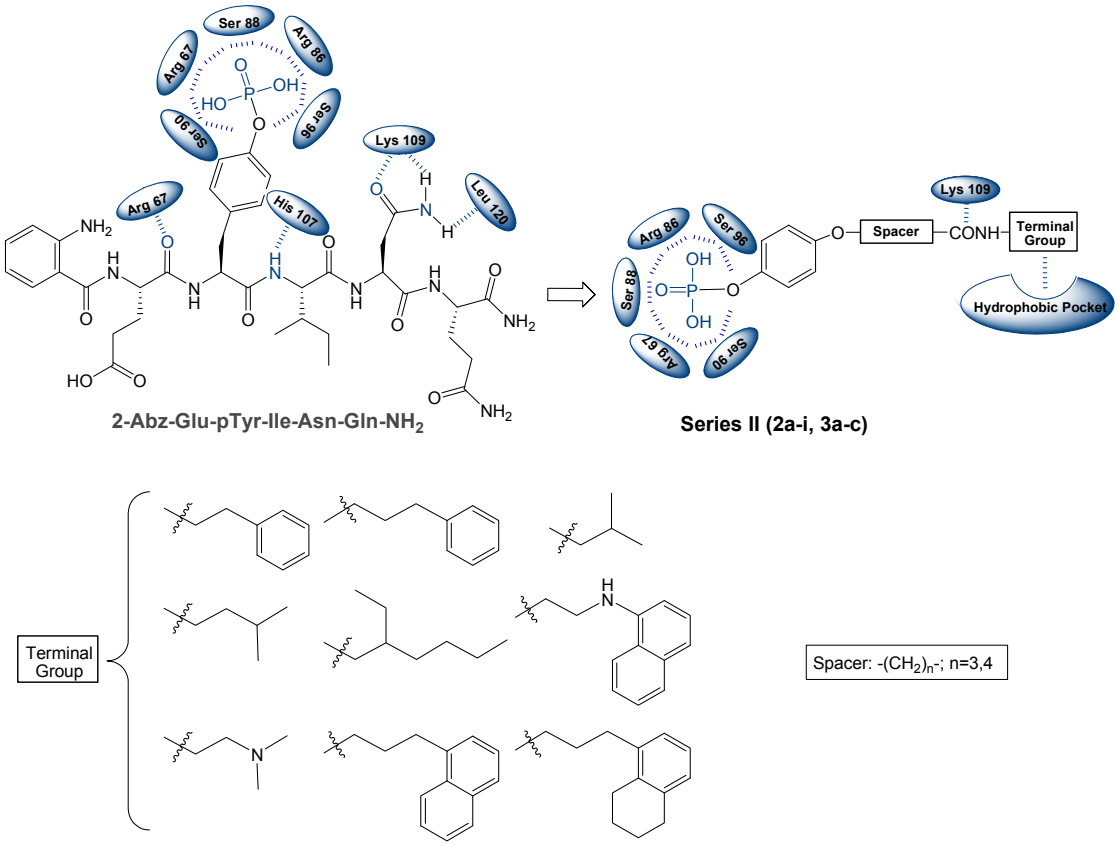

Figure 25. Design of general structures **II**.

Figure 26 shows the docking structures for two compounds of series **II** (**2f** and **3a**, respectively) in complex with the Grb2-SH2 domain obtained using the same MD simulations technique as for **(*S*)-1k**. The images show both compounds maintain the key interaction with Lys109 (βD6) and Leu120 (βE4) (only present in compound **2f**), but have lost those with Arg67 (αA2) and His107 (βD4), as such observed in the pentapeptide 2-Abz-Glu-pTyr-Ile-Asn-Gln-NH_2 (Figure 22).

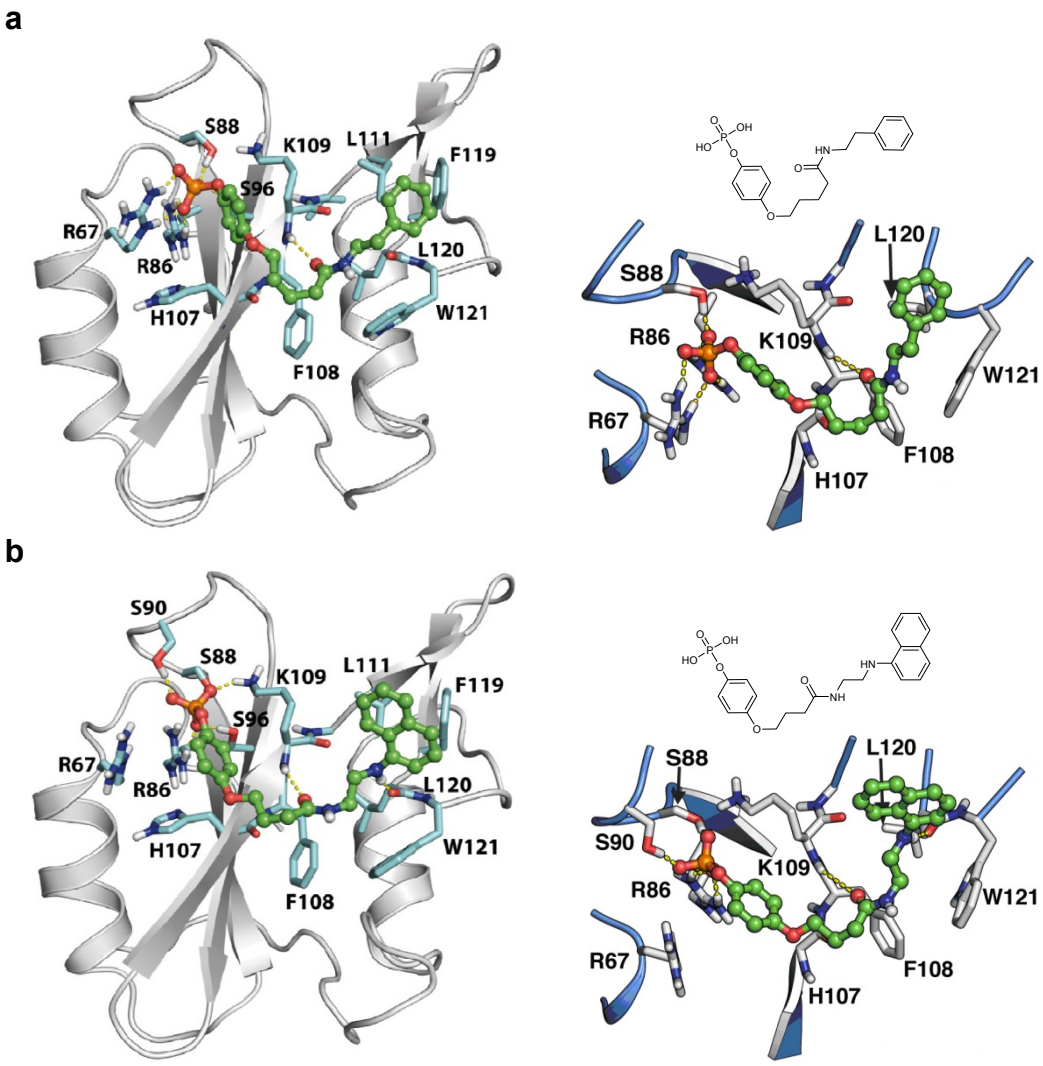

Figure 26. Representative structures obtained in the MD simulations of Grb2-SH2 in complex with compounds **3a** (panel **a**) and **2f** (panel **b**). Both images show the entire SH2 domain (left panels) as well as their corresponding zoom-in detail (right panels).

3.2. Synthesis and biological evaluation of compounds of series I and II

Considering that our objective was to design different structural cores that helped us to outline the key interactions at the Grb2-SH2 domain and, optimally, could led to the identification of one (or several) initial hit compound(s) for each series, synthesis and biological evaluation of the compounds were carried out in parallel and in an iterative manner.

3.2.1. Series I

The synthesis of compounds **1a**-**j** was accomplished by phosphorylation of commercial *N*-acetyl- or *N*-benzoyl-L-tyrosine, or of synthesized *N*-butyryl-L-tyrosine **4**,[86] which was followed by condensation with the appropriate amine and subsequent deprotection of the phosphate

[86] Moya, E.; Blagbrough, I. S. *Tetrahedron Lett.* **1995**, *36*, 9401-9404.

group (Scheme 1). Intermediates **5a**-**c** were prepared by a one-pot procedure, which involved the temporary protection of the carboxyl group of *N*-acyl-L-tyrosine as a silyl ester followed by *in situ* phosphitylation of the tyrosyl hydroxyl group and oxidation of the resultant phosphite triester. Derivatives **6a**-**j** were obtained by condensation of **5a**-**c** with the corresponding amine in the presence of 1-ethyl-3-(3-dimethylaminopropyl) carbodiimide (EDC) as a coupling reagent and 1-hydroxybenzotriazole (HOBt) as an additive to minimize racemization.[87] Final removal of the benzyl groups by catalytic hydrogenation of protected amides **6a**-**j** yielded the target compounds **1a**-**j**.

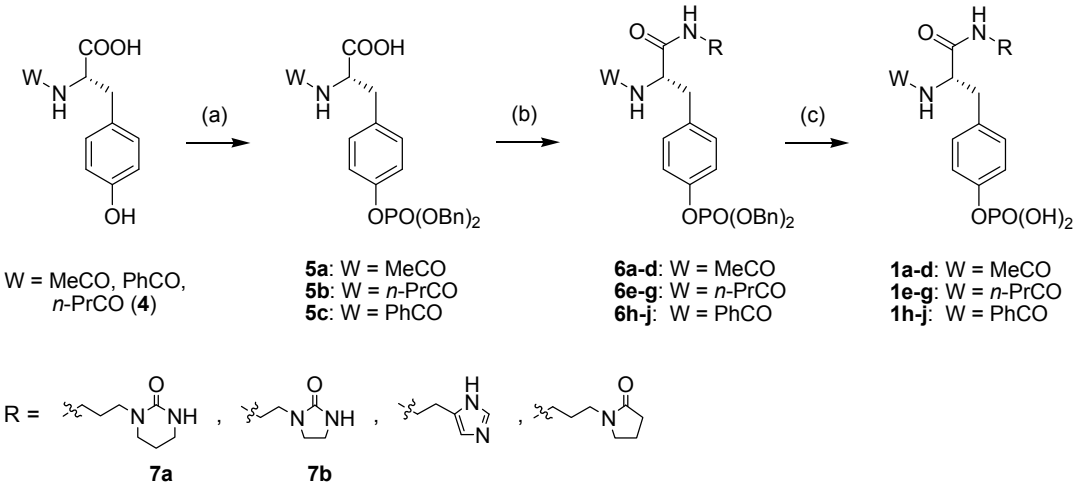

Reagents: (a) (i) NMM, $^{t}BuMe_2SiCl$, CH_3CN, rt; (ii) 1*H*-tetrazole, $^{i}Pr_2NP(OBn)_2$, rt; (iii) $^{t}BuOOH$ aq., -20 ºC; (b) EDC, HOBt, CH_2Cl_2, R-NH_2, rt; (c) H_2/Pd(C)/ethanol, rt.

Scheme 1. Synthesis of compounds **1a**-**j**.

Non-commercial 1-(3-aminopropyl)tetrahydropyrimidin-2(1*H*)-one (**7a**) and 1-(2-aminoethyl)imidazolin-2-one (**7b**) were obtained by treatment of *N*-(3-aminopropyl)propane-1,3-diamine or *N*-(2-aminoethyl)ethane-1,2-diamine, respectively, with urea (Scheme 2) in a reaction that involves two consecutive inter and intramolecular acylations.[88]

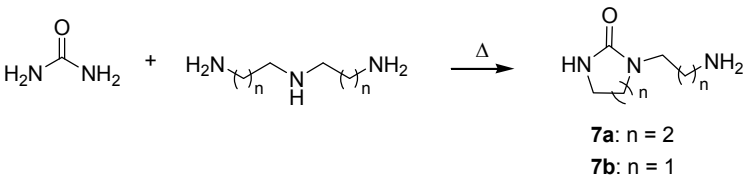

Scheme 2. Synthesis of amines **7a**,**b**.

[87] McNamara, J. F.; Lombardo, H.; Pillai, S. K.; Jensen, I.; Albericio, F.; Kates, S. A. *J. Pept. Sci.* **2000**, *6*, 512-518.

[88] Hurwitz, M. D.; Auten, J. P. US2613212, **1952**.

Although the conditions of the condensation to obtain the intermediates **6a**-**j** were chosen to avoid racemization of the chiral centre, we determined whether this was indeed the case. The extent of racemization associated to this synthetic procedure was estimated by coupling acid **(*S*)-5a** with (1*S*)-1-phenylethylamine and determination of the area of the peaks of methyl groups in the ^{1}H-NMR spectrum (Figures 27 and 28). The difference in the chemical shifts of both methyl groups was confirmed in the spectrum of the 1:1 diastereomeric mixture resulting from the coupling of **(*S*)-5a** with racemic 1-phenylethylamine (Figure 27). The ratio between the two diastereomers [*S*,*S* (1.38 ppm) and *S*,*R* (1.49 ppm)] was 5:1 (Figure 28). This result indicates a 20% of racemization and means that in the cases where the two enantiomers have different biological activities, we could be under-estimating the affinity, making it necessary to synthesize the pure enantiomer of the compound(s) with the highest affinity.

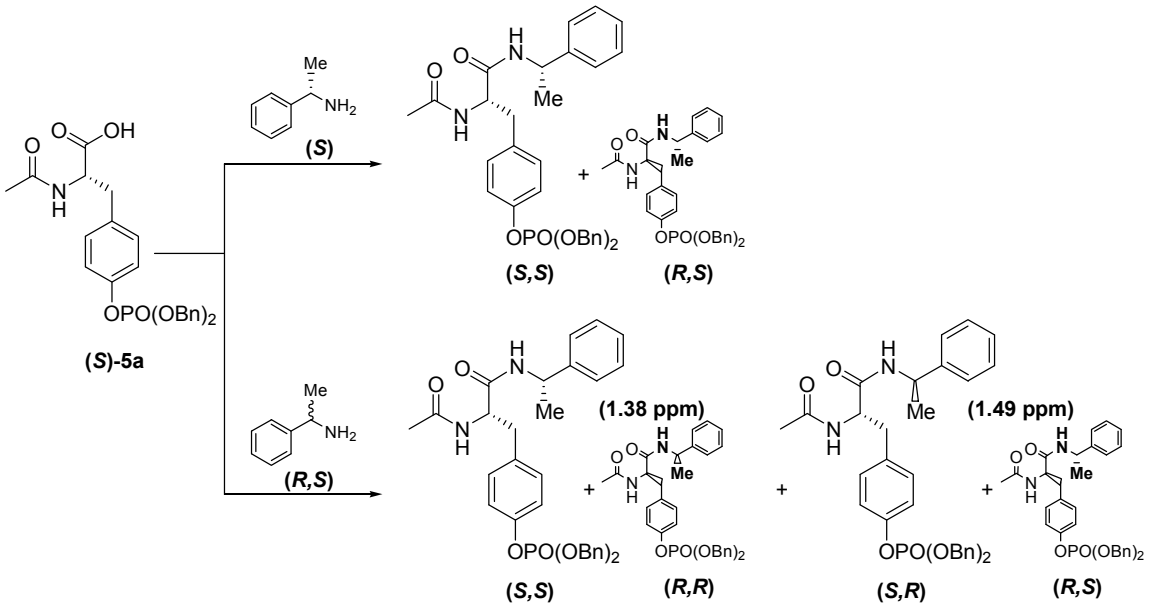

Figure 27. Evaluation of the racemization extent associated to the synthesis of derivatives **1a**-**j**.

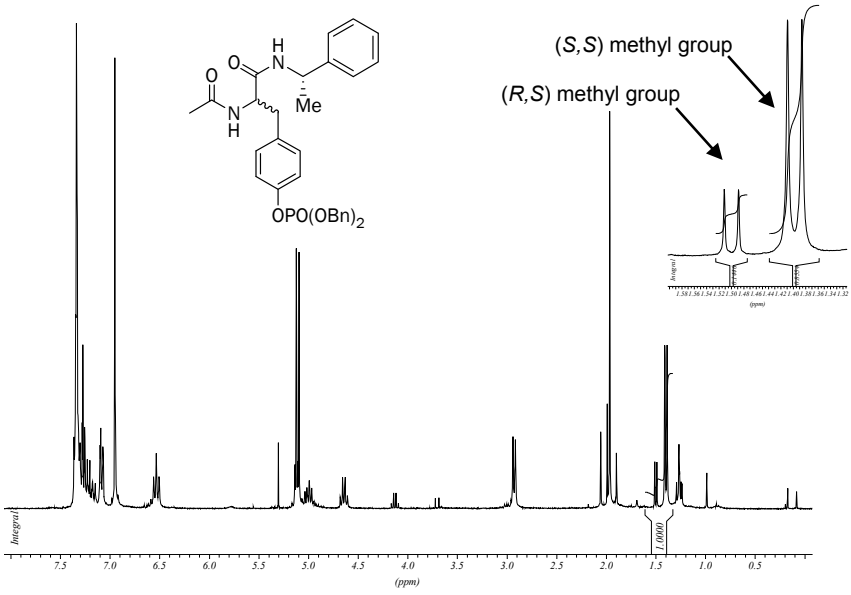

Figure 28. ^{1}H-NMR spectrum of the diasteriomeric mixture resulting from the condensation of acid **(*S*)-5a** with (1*S*)-1-phenylethylamine.

Considering this maximum grade of racemization was not too high for a preliminary screening of series **I** of compounds, their capacity to bind Grb2-SH2 was evaluated by means of an enzyme-linked immunosorbent assay (ELISA) procedure using a glutathione S-transferase (GST) -Grb2-SH2 conjugate and the phosphopeptide biotin-Ahx-PSpYVNVQN[89] as its partner ligand. Then, the extent of the Grb2-SH2-phosphopeptide interaction still observable in the presence of the compound could be measured by sequentially incubating with a mouse anti-GST and a horseradish peroxidase (HRP) -conjugated goat anti-mouse antibodies. Finally, addition of 3,3′,5,5′-tetramethylbenzidine (TMB), substrate of HRP, yielded a blue-coloured solution that becomes yellow after acidification to stop the reaction. Determination of the absorbance at 450 nm at different concentrations of the compound under study gave a sigmoidal dose-response curve, from which IC_{50} values were calculated. The results obtained for compounds **1a**-**j** are shown in Table 2.

[89] See citation 90.

Table 2. Affinities of compounds **1a-j** for the Grb2-SH2 domain.

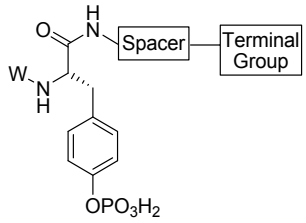

Compound	W	Spacer	Terminal G.	IC_{50} (μM)[a,b]
1a	Me-CO-	-$(CH_2)_3$-		190±25
1b	Me-CO-	-$(CH_2)_2$-		Inactive[c]
1c	Me-CO-	-$(CH_2)_2$-		Inactive[c]
1d	Me-CO-	-$(CH_2)_3$-		Inactive[c]
1e	*n*Pr-CO-	-$(CH_2)_3$-		314±5
1f	*n*Pr-CO-	-$(CH_2)_2$-		1330±98
1g	*n*Pr-CO-	-$(CH_2)_3$-		Inactive[c]
1h	Ph-CO-	-$(CH_2)_3$-		Inactive[c]
1i	Ph-CO-	-$(CH_2)_2$-		Inactive[c]
1j	Ph-CO-	-$(CH_2)_3$-		Inactive[c]

[a]Competition binding assays with the recombinant SH2 domain of Grb2 expressed as a GST fusion protein and the phosphopeptide biotin-Ahx-PSpYVNVQN were conducted as detailed in the Experimental Section. Dose-response relationships were generated by nonlinear regression fits of the competition curves with the software Prism. Data are expressed as mean±SEM of at least three independent experiments carried out in duplicate. [b]For the compound 1224-130, kindly donated by Prof. T. R. Burke, which was used as a control of the ELISA test, we obtained comparable IC_{50} values to those previously reported.[90] [c]Inactive compounds displace less than 10% of the phosphopeptide at the maximal concentration used (5 mM).

[90] Wei, C.-Q.; Li, B.; Guo, R.; Yang, D.; Burke, T. R. Jr. *Bioorg. Med. Chem. Lett.* **2002**, *12*, 2781-2784.

A structure-affinity relationship (SAR) study of the obtained data for this series of compounds enabled us to rationalize the influence of the different parts of the molecules, i.e., the terminal group, the spacer and the tyrosine *N*-acyl group (W substituent). Compound **1a** exhibits the highest affinity for the Grb2-SH2 domain, with an IC_{50} value of 190 μM. Modifications in **1a**, such as replacement of the six-membered ring of the terminal group for a five-membered ring, or shortening the spacer to two methylene units resulted, in all cases, in complete loss of affinity for the Grb2-SH2 domain (compounds **1b** to **1d**). In general, substitution of the W acetyl group with a longer butyryl chain led to inactive compounds. Increase of the volume of the W group by replacement of the acetyl *N*-terminal tyrosine-capping group with the bulkier benzoyl group also led in all cases to inactive compounds (**1h** to **1j**).

Given the partial racemization implicated in the synthesis of **1a**, the most potent compound within the series (IC_{50} = 190 ± 25 μM), we prepared its enantiopure isomers **(*R*)-1k** and **(*S*)-1k**. These were obtained using the 9-fluorenylmethyloxycarbonyl (Fmoc) protecting group in order to prevent racemization (Scheme 3). After phosphorylation, Fmoc derivatives **8a** and **8b** were condensed with amine **7a**. The acetyl group was introduced after Fmoc removal, and amides **10a**,**b** were finally debenzylated to yield the (*R*)- and (*S*)-*N*-acetyl-*N'*-[3-(2-oxoperhydropyrimidin-1-yl)propyl]-*O*-phosphonotyrosinamides, **(*R*)-** and **(*S*)-1k** (Scheme 3). Racemic **(*R*,*S*)-1k** was obtained from *N*-acetyl-D,L-tyrosine following the procedure in Scheme 1.

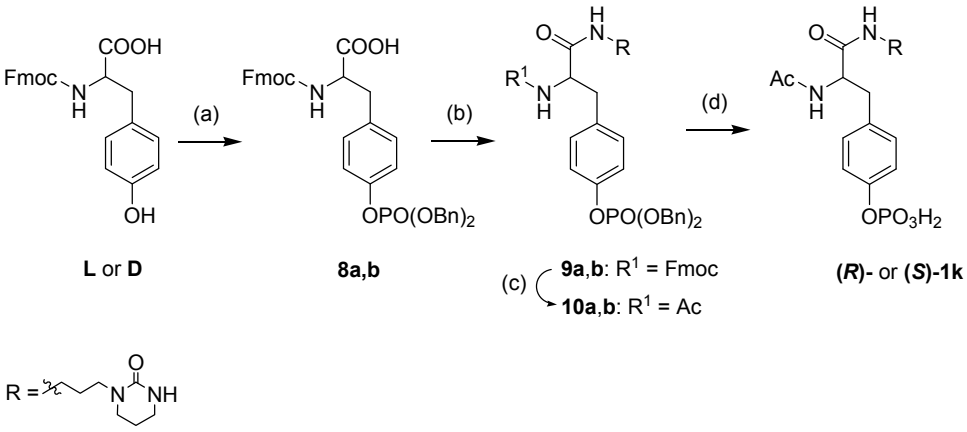

Reagents: (a) (i) NMM, $^{t}BuMe_2SiCl$, CH_3CN, rt; (ii) 1*H*-tetrazole, $^{i}Pr_2NP(OBn)_2$, rt; (iii) $^{t}BuOOH$ aq., -20 ºC; (b) EDC, HOBt, CH_2Cl_2, **7a**, rt; (c) piperidine, CH_3CN, 0 ºC; (ii) $^{i}Pr_2NEt$, Ac_2O, DMF, rt; (d) H_2/Pd(C), ethanol, rt.

Scheme 3. Synthesis of enantiopure derivatives **(*R*)-** and **(*S*)-1k**.

The ability of **(*R*)-**, **(*S*)-**, and **(*R*,*S*)-1k** to bind the Grb2-SH2 domain was determined as described previously and the results are shown in Table 3.

Table 3. Affinities of compounds **(*R*)-**, **(*S*)-**, and **(*R*,*S*)-1k** for the Grb2-SH2 domain.

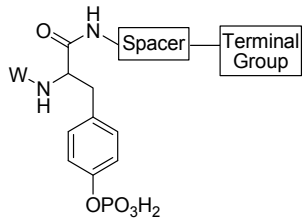

Compound	W	Spacer	Terminal G.	IC_{50} (μM)[a,b]
1a	Me-CO-	-$(CH_2)_3$-	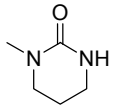	190±25
(*S*)-1k				174±22
(*R*)-1k				Inactive[c]
(*R,S*)-1k				2307±644

[a-c] See footnote of Table 2 for detailed explanation.

Among all compounds of series **I**, **(*S*)-1k** showed the highest affinity and was therefore selected as an initial hit for future optimization. From these results it stands out clearly the importance of the *S* configuration in the only chiral tyrosine carbon of the molecule for it to bind the Grb2-SH2 domain in a significant manner.

3.2.2. Series II

The synthesis of compounds **2a**-**i** and **3a**-**c** is outlined in Scheme 4. *O*-alkylation of 4-benzyloxyphenol with the adequate ethyl ω-bromoalkanoate in presence of potassium carbonate yielded intermediates **11a**,**b** which were subsequently deprotected by catalytic hydrogenation. Treatment of esters **12a**,**b** with the corresponding amines in presence of trimethylaluminium yielded amides **13a**-**h** and **14a**-**c**, which were phosphorylated in a two-step procedure that involved the preparation of the benzylated phosphate precursors **15a**-**h** and **16a**-**c** followed by their deprotection, to yield designed compounds **2a**-**i**, **3a**-**c**.

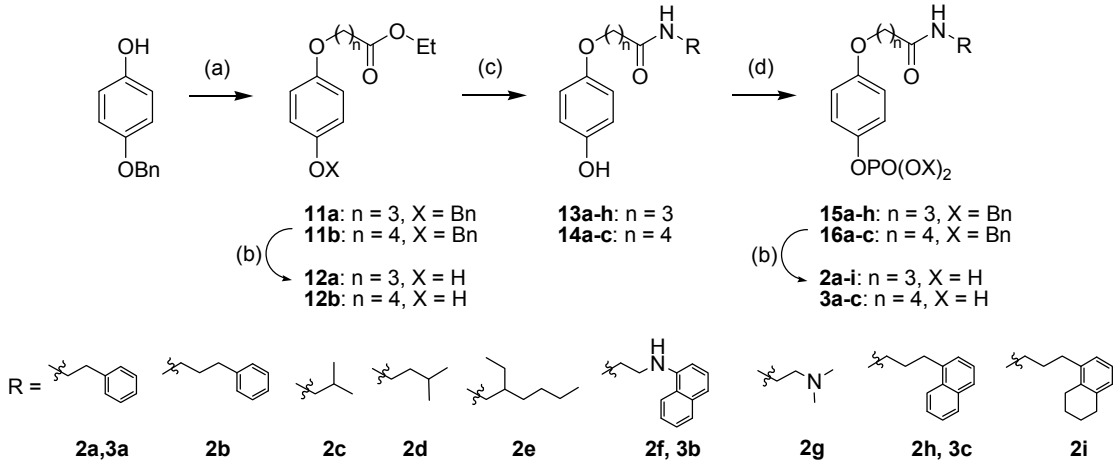

Reagents: (a) $Br(CH_2)_nCOOEt$, K_2CO_3, crown ether, acetone, 60 ºC; (b) H_2/Pd(C), ethanol, rt; (c) R-NH_2, $AlMe_3$, toluene, 120 ºC; (d) (i) 1*H*-tetrazole, $^{i}Pr_2NP(OBn)_2$, 25 ºC; (ii) ^{t}BuOOH aq., -20 ºC.

Scheme 4. Synthesis of compounds of series **II** (**2a**-**i** and **3a**-**c**).

Non-commercial 3-(1-naphthyl)propylamine **17** was obtained as described previously (Scheme 5).[91]

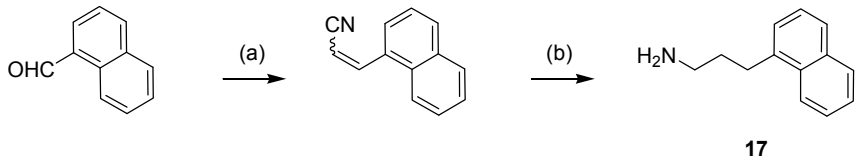

Reagents: (a) $NC(CH_2)P(O)(OC_2H_5)_2$, 6 M K_2CO_3 aq., rt; (b) H_2 /Ni-Ra, ethanol, rt.

Scheme 5. Synthesis of 3-(1-naphthyl)propylamine (**17**).

Unfortunately, none of the synthesized compounds, **2a**-**i** and **3a**-**c**, were able to bind Grb2-SH2 domain in a significant manner (IC_{50} > 1 mM). This result could be due to an excessive flexibility of these structures or to the lack of some of the interactions with the key residues of Grb2-SH2 (according to the initial design, series **II** lacked one of the interactions with Arg67 and the interaction with His107, Figure 25).

In order to distinguish between these two possibilities, a rigid analogue (**18**) was designed. Compound **18** contains the common phenylphosphate group and a benzimidazole ring separated by a single methylene unit. According to the computational model, it should be capable of interacting with both the backbone N–H and/or C=O groups of Lys109 (βD6) mimicking the $N–H^{K109}\cdots O=C^{pY+2}$ and/or the $C=O^{K109}\cdots H_2N^{pY+2}$ interactions of the pentapeptide (Figure 29).

[91] See citation 65.

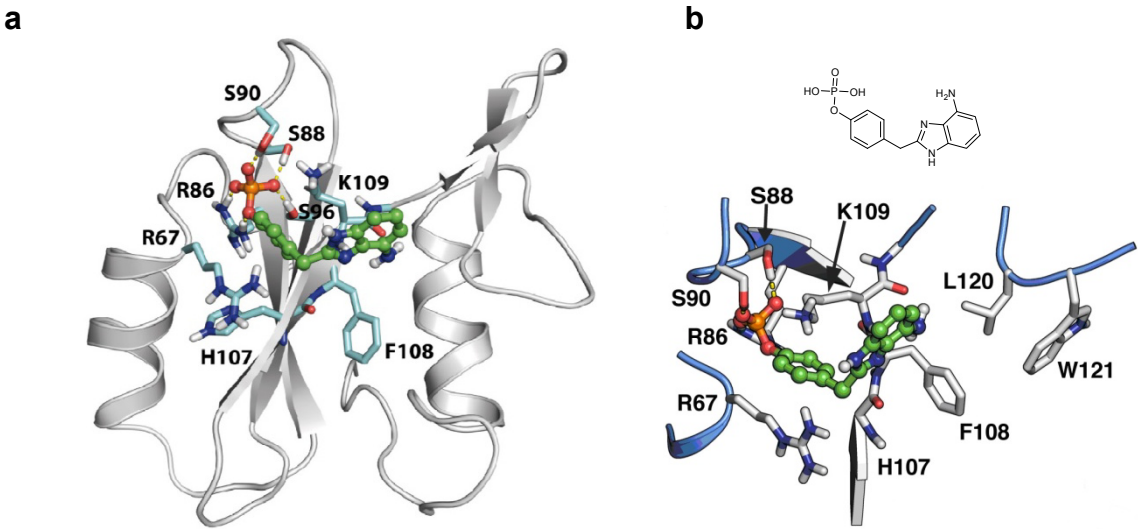

Figure 29. Representative structure obtained in the MD simulations of Grb2-SH2 in complex with **18**. **a.** Entire SH2 domain shown. **b.** Zoom-in detail of interacting amino acids.

Compound **18** was prepared by cyclization of commercially available 3-nitrobenzene-1,2-diamine with (4-hydroxyphenyl)acetic acid. Subsequent phosphorylation of the phenol group and simultaneous deprotection of the benzyl groups and reduction of the nitro substituent by hydrogenation yielded target compound **18** (Scheme 6).

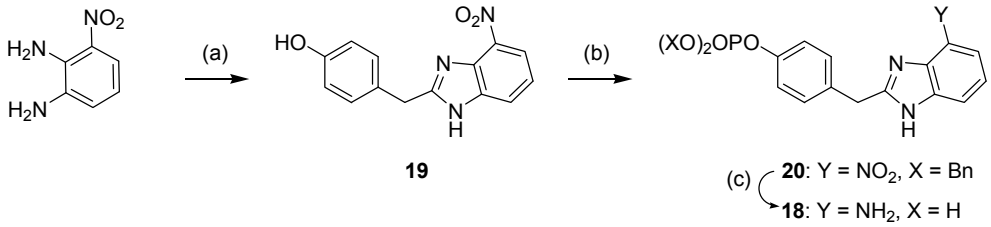

Reagents: (a) 4-OH-C_6H_4-CH_2COOH, 6 M HCl, Δ; (b) (i) 1*H*-tetrazole, $^{i}Pr_2NP(OBn)_2$, 25 ºC; (ii) $^{t}BuOOH$ aq., rt; (c) H_2/Pd(C), ethanol, rt.

Scheme 6. Synthesis of compound **18**.

Derivative **18** resulted inactive in the ELISA test (IC_{50} > 1 mM), which suggests that interactions with Arg67 (αA2) and His107 (βD4), are crucial for binding to Grb2-SH2. Therefore, compound **(*S*)-1k**, from series **I**, was selected as the most promising hit for further optimization.

3.3. Optimization of the hit compound (*S*)-1k

Hit optimization was addressed by NMR chemical shift perturbation experiments and computational models.

In order to carry out a rational optimization of **(*S*)-1k**, it was necessary to experimentally identify the amino acids involved in the binding of the compound to the Grb2-SH2 domain. Then, this information could be subsequently used in computational models that would guide

the design of new compounds with either additional or optimized interactions with the target protein.

The amino acids involved in a protein-ligand interaction can be identified using NMR chemical shift perturbation experiments with the N^{15}-labelled protein; these experiments were carried out in collaboration with Dr. Pedro Serrano and Prof. Kurt Wüthrich at The Scripps Research Institute (La Jolla, California, USA).

The NMR experiments were performed using the 98-residue Grb2-SH2 construct described by Waugh and colleagues, which comprises the polypeptide segment 55–153.[92] The assignments of the backbone amide resonances were taken from the work by Thanabal and colleagues.[93] The resonance assignments of Grb2-SH2 in the complex with **(*S*)-1k** were obtained by analyzing a series of [^{15}N,^{1}H]-Heteronuclear Single Quantum Coherence (HSQC) spectra of samples containing ^{15}N-labeled Grb2-SH2 and different ratios of compound **(*S*)-1k** (5:1→1:5). Figure 30 shows a superposition of two 2D [^{15}N,^{1}H]-HSQC spectra of Grb2-SH2 acquired in the absence and presence (1:1 molar protein:compound ratio) of **(*S*)-1k**, from which the residues with large chemical shift changes were identified.

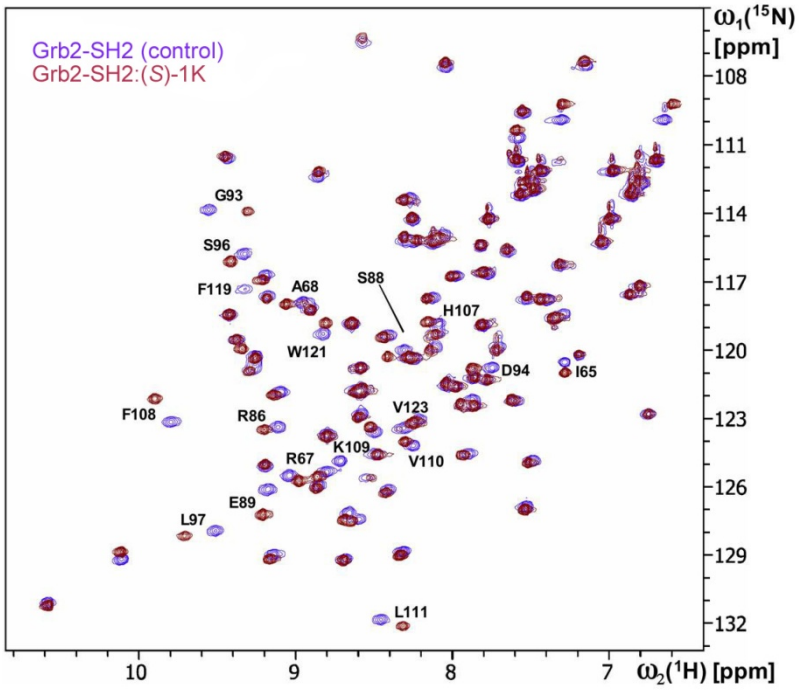

Figure 30. 2D [^{15}N,^{1}H]-HSQC spectra of the Grb2-SH2 domain free (blue) and in complex with **(*S*)-1k** (red) (molar ratio protein:compound 1:1).

[92] See citation 76d.

[93] See citation 53.

To rule out that these shifts arise solely from interactions due to the presence of pTyr, which is a common moiety in all the Grb2-SH2 inhibitors reported so far, [^{15}N,^{1}H]- HSQC spectrum of the protein in the presence of a two-fold excess of *N*-acetylphosphotyrosine was obtained under identical experimental conditions. It was found that this compound induces chemical shifts exclusively in a small number of Grb2 amino acid residues, which are all located in the pTyr binding pocket (Figure 31).

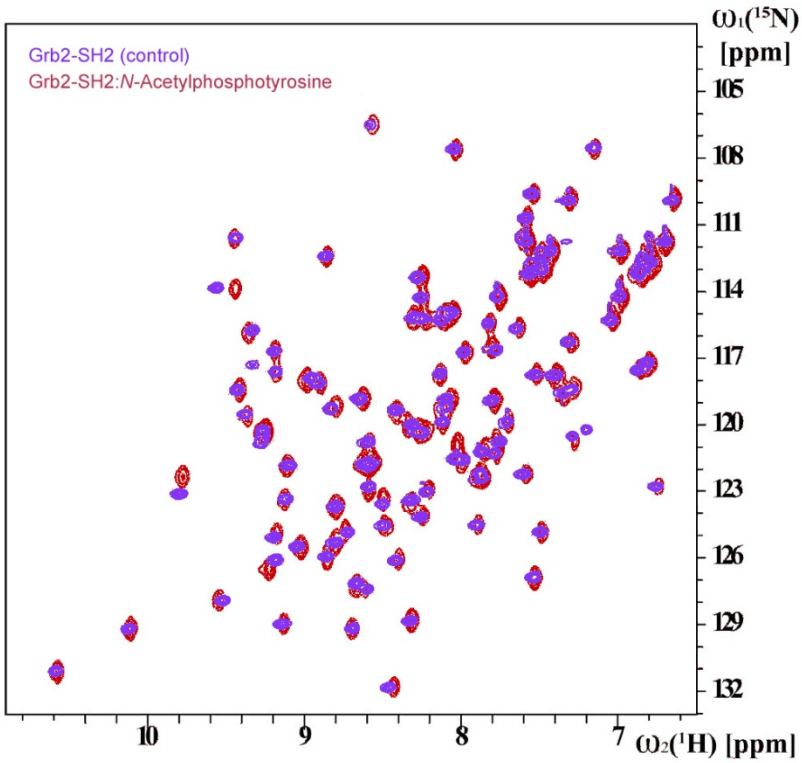

Figure 31. 2D [^{15}N,^{1}H]-HSQC spectra of the Grb2-SH2 domain free (blue) and in complex with *N*-acetylphosphotyrosine (red) (molar ratio protein:compound 1:2).

A plot of the combined ^{1}H and ^{15}N chemical shifts for each residue, $\Delta\delta$av, *versus* the Grb2-SH2 amino acid sequence shows five regions, I–V, that undergo significant chemical shift differences, which are indicative of structural rearrangements upon binding of **(*S*)-1k** (Figure 32). The most strongly affected residue in region I is Arg67 (αA2), which interacts with the N-terminal carbonyl and phosphate groups of **(*S*)-1k**, similarly to previous observations with different ligands.[94] Sequence regions II and III correspond to a hydrophilic, positively charged surface area involved in the stabilization of the phosphate group by means of electrostatic and hydrogen bond interactions. The chemical shift differences observed for Arg86 (βB5), Ser88 (βB7) and Ser96 (βC3) are particularly relevant, since these residues have previously been reported to be fundamental for the interaction with pTyr. In regions IV and V, large chemical

[94] (a) Vu, C. B. *Curr. Med. Chem.* **2000**, *7*, 1081-1100. (b) See citation 57. (c) Ogura, K.; Shiga, T.; Yokochi, M.; Yuzawa, S.; Burke, T. R. Jr.; Inagaki, F. *J. Biomol. NMR* **2008**, *42*, 197-207. (d) Nioche, P.; Liu, W.-Q.; Broutin, I.; Charbonnier, F.; Latreille, M.-T.; Vidal, M.; Roques, B.; Garbay, C.; Ducruix, A. *J. Mol. Biol*. **2002**, *315*, 1167-1177.

shift differences are seen for His107 (βD4) and Lys109 (βD6), which are engaged in hydrogen bond interactions with **(*S*)-1k** through their backbone amide groups. The neighboring residues Phe108, Val110, Leu111 and Trp121 (EF1) form a lipophilic pocket that stabilizes the protein-inhibitor complex by van der Waals interactions with the C-terminal segment of **(*S*)-1k**. The strong effect on Trp121 (EF1, region V) is of special interest, since this residue is responsible for the specificity of ligand binding to Grb2 when compared to other SH2 domain-containing proteins.[95]

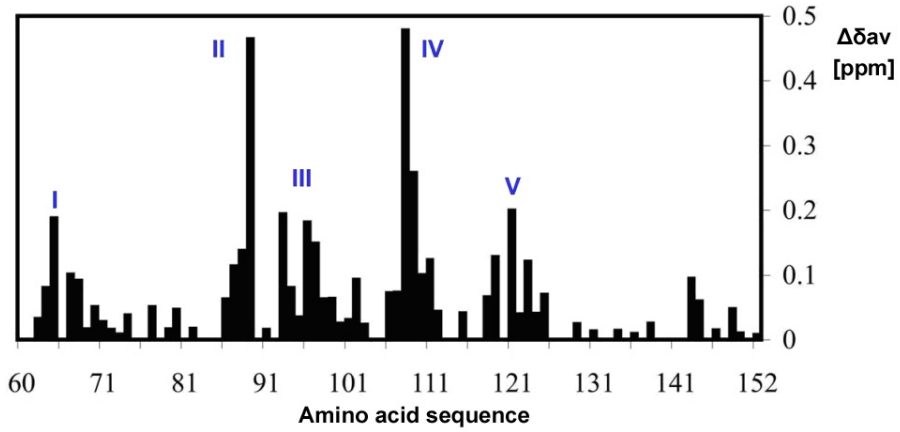

Figure 32. Plot of the $^{1}H–^{15}N$ chemical shift changes in the backbone of the Grb2–SH2 domain *versus* amino acid sequence. $\Delta\delta av$ is a weighted average of the ^{1}H and ^{15}N chemical shift differences, $\Delta\delta = \{0.5[\Delta\delta\ (^{1}H^{N})^{2} + (0.2\Delta\delta\ (^{15}N))^{2}]\}^{1/2}$, determined from comparison of the two [^{15}N,^{1}H]-HSQC spectra that are superimposed in Figure 30.

Overall, these results indicate that the residues with significant chemical shift perturbations due to the presence of bound **(*S*)-1k** (Figure 33) coincide with those found to form a binding pocket in several crystal or solution structures of Grb2-SH2,[96] and validate the assumptions used to design this new family of HER2-Grb2 interaction blockers.

[95] See citation 76d.

[96] See citation 76d.

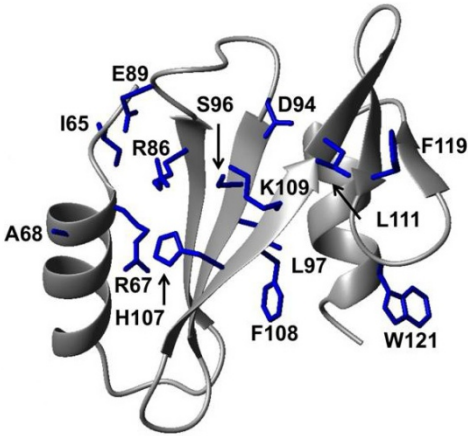

Figure 33. Ribbon representation of the Grb2-SH2 domain. The side chains of the residues that exhibit chemical shift differences ($\Delta\delta$av, as represented in Figure 32) larger than 0.1 ppm are identified.

Hence, the moderate affinity of **(*S*)-1k** (IC_{50} = 174±22 μM; Table 3) could be due to the high degree of conformational freedom associated to the methylene spacer, so that improved binding might be achieved by introducing conformational restrictions in this part of the molecule. Thus, a new compound, **(*S*)-1l**, was designed introducing in the spacer a cyclohexyl ring (see Figure 35b for the structure of **(*S*)-1l**). MD simulations in an explicit water environment with **(*S*)-1l**, and **(*S*)-1k** for comparison, were performed to evaluate the rigidity introduced by the cyclohexyl group in terms of the χ_1 and χ_2 angles (Figure 34).

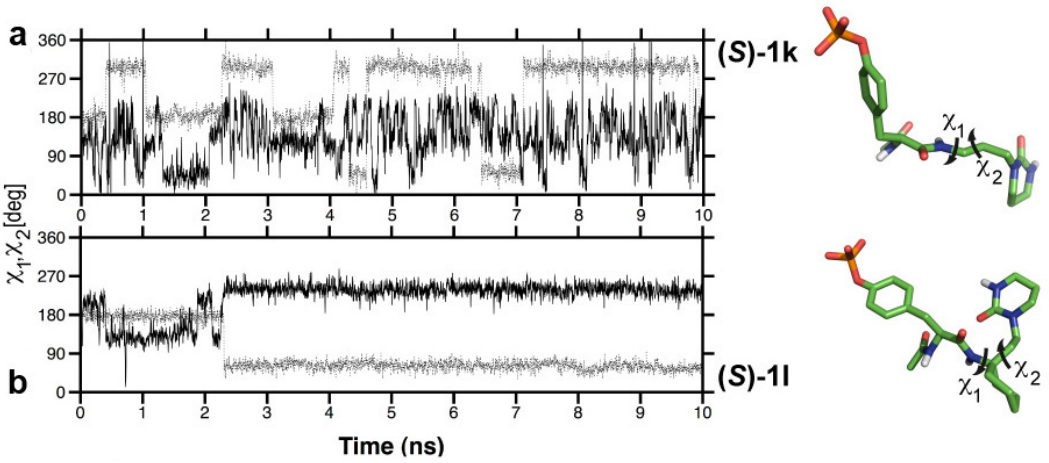

Figure 34. Evolution of dihedral angles χ_1 (black line) and χ_2 (grey line) in the vicinity of the cyclohexyl ring of **(*S*)-1k** (**a**) and the analogous angles in **(*S*)-1l** (**b**) obtained during the MD simulations of the ligands in bulk water. Representative structures of **(*S*)-1k** and **(*S*)-1l** obtained during the simulations in water are shown.

The molecule **(*S*)-1k** is highly flexible, adopting different conformations during the simulation time, while the cyclohexyl ring of **(*S*)-1l** constrains the backbone, thus favoring the β-

turn conformation required for Grb2 binding and the interactions with Phe108 (βD5) and Trp121 (EF1) (Figure 35).

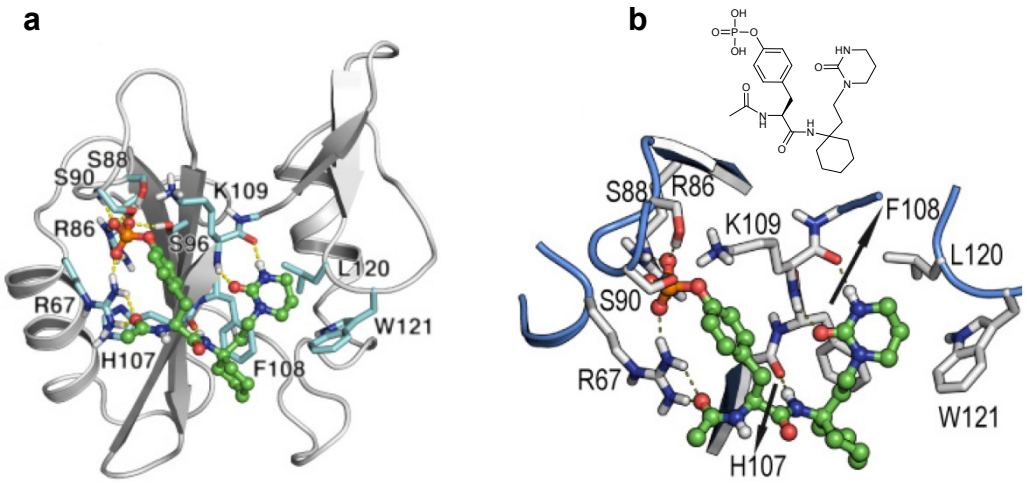

Figure 35. a. Representative structures obtained in the molecular dynamics (MD) simulations of Grb2-SH2 in complex with **(*S*)-1l**. **a.** Entire SH2 domain shown. **b.** Zoom-in detail of interacting amino acids.

The stability of **(*S*)-1l** in complex with Grb2-SH2 was also evaluated using the MM-GBSA methodology[97] and compared with the results obtained previously for the pentapeptide 2-Abz-Glu-pTyr-Ile-Asn-Gln-NH_2 and **(*S*)-1k**. The binding free energy decomposition on a per-residue basis is shown for the three complexes in Figure 36, where compounds **(*S*)-1k** and **(*S*)-1l** exhibit similar interaction profiles to 2-Abz-Glu-pTyr-Ile-Asn-Gln-NH_2, with the exceptions of Ser90 (βC2) and Leu120 (βE4). The absence of the anthranyl moiety of the peptide in **(*S*)-1k** and **(*S*)-1l** seems to facilitate the interaction between Ser90 and pTyr, whereas the terminal groups of **(*S*)-1k** and **(*S*)-1l** cannot interact with the backbone amide of Leu120 (βE4).

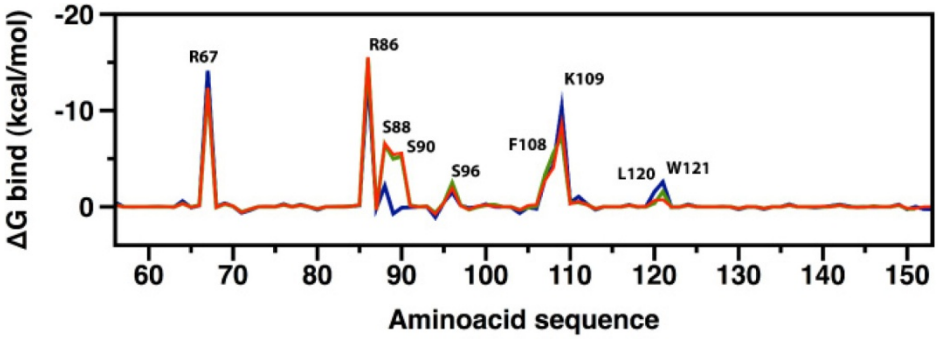

Figure 36. a. Binding free energy decomposition on a per residue basis for Grb2-SH2 in the complexes with 2-Abz-Glu-pTyr-Ile-Asn-Gln-NH_2 (blue), **(*S*)-1k** (red) and **(*S*)-1l** (green) calculated from the MD ensembles of structures (1250 structures per simulation collected every 4 ps during the last 5 ns), using the MM-GBSA methodology.

[97] See citation 84.

In order to experimentally evaluate the effect of the introduction of a cyclohexyl group in the spacer, compound **(*S*)-1l** was synthesized following the previously described methodology (Scheme 7).

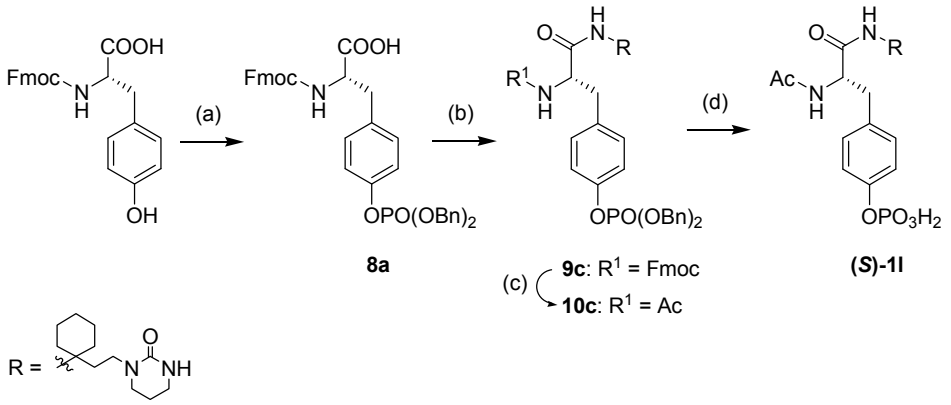

Reagents: (a) (i) NMM, ^{t}BuMe$_2$SiCl, CH$_3$CN, rt; (ii) 1*H*-tetrazole, ^{i}Pr$_2$NP(OBn)$_2$, rt; (iii) ^{t}BuOOH aq., -20 ºC; (b) DIC, HOBt, THF, **21**, rt; (c) (i) piperidine, acetonitrile, 0 ºC; (ii) ^{i}Pr$_2$NEt, Ac$_2$O, DMF, rt; (d) H$_2$/Pd(C), ethanol, rt.

Scheme 7. Synthesis of derivative **(*S*)-1l**.

Non-commercial amine **21** was prepared starting from 1-(2-aminoethyl)-*N*-Boc-cyclohexylamine and 3-[(benzyloxycarbonyl)amino]propionaldehyde (Scheme 8). They were coupled under reductive amination conditions to yield intermediate **22**. After removal of its Cbz protecting group by catalytic hydrogenation, resulting amine **23** was cyclized in the presence of 1,1'-carbonyldiimidazole (CDI) and 1,8-diazabicyclo[5.4.0]undec-7-ene (DBU) as base. Boc removal of the tetrahydropyrimidinone **24** under acid conditions followed by treatment with base afforded desired amine **21** (Scheme 8).

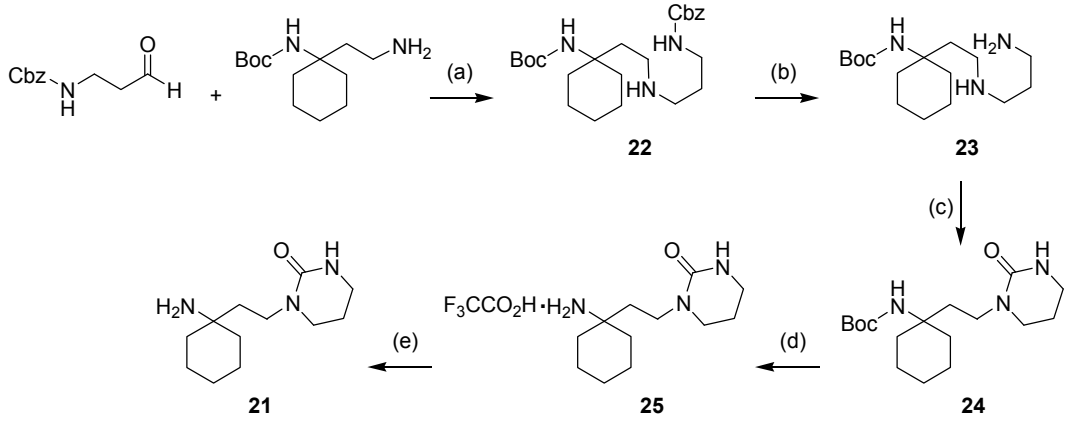

Reagents: (a) 4 A Molecular sieves, NaCNBH$_3$, methanol, AcOH, 35 ºC; (b) H$_2$, Pd(OH)$_2$(C), methanol, rt; (c) CDI, DBU, THF, 70 ºC; (d) F$_3$CCO$_2$H, CH$_2$Cl$_2$, rt; (e) 0.05 M K$_2$CO$_3$ aq., CH$_2$Cl$_2$, rt.

Scheme 8. Synthesis of 1-[2-(1-aminocyclohexyl)ethyl]tetrahydropyrimidin-2(1*H*)-one (**21**).

In the ELISA test, constrained compound **(*S*)-1l** showed an affinity for the Grb2-SH2 domain three-fold higher than the initial hit **(*S*)-1k** (IC_{50} [**(*S*)-1k**] = 174 μM, IC_{50} [**(*S*)-1l**] = 56 μM). This result indicates that iterative application of NMR and computational models has enabled optimization of **(*S*)-1k** leading to the identification of compound **(*S*)-1l** as a new small molecule with affinity for the Grb2-SH2 domain. This compound could represent a new scaffold for the development of efficient HER2-Grb2 binding blockers.

In order to attest its worthiness as a compound for future development, it is critical to start to validate its biological potential. This validation involves at least two fundamental aspects:

a) To determine whether the compound shows an interesting inhibitory profile in terms of *in vitro* cellular assays that can be ascribed to the blockade of the HER2-Grb2 molecular pathways.

b) To study whether the compound actually affects the MAPKs pathway as expected from a molecule that blocks the Grb2-associated transduction pathway.

The following sections provide a detailed description of these two approaches aimed at outlining the biological potential of **(*S*)-1l**.

3.4. *In vitro* profile of (*S*)-1l

Compound **(*S*)-1l** binds the Grb2-SH2 domain with an IC_{50} value of 56 μM. However, the interest on this scaffold for future structural modifications that eventually allow for optimized affinities is directly linked to its activity in cell systems. Therefore, its cytotoxic effect on a HER2-overexpressing breast cancer line (MCF7-HER2+) has been assessed using a standard 3-(4,5-dimethyl-1,3-thiazol-2-yl)-2,5-diphenyl-2*H*-tetrazol-3-ium bromide (MTT) cytotoxicity assay.

To measure cell viability, inhibitor-treated and non-treated cells were incubated in the presence of MTT. Those cells still viable after treatment with **(*S*)-1l** were able to metabolize the MTT reagent to formazan, a compound of bright purple colour. Determination of the absorbance at 450 nm at different concentrations of the compound under study enabled the determination of cell viability expressed as percentage of the control. To rule out general toxicity of the compound, parallel experiments were performed with N1 fibroblasts, a non-tumour cell line. The obtained results (Figure 37) indicate that **(*S*)-1l** is selectively cytotoxic towards MCF7-HER2+ *vs* fibroblasts with an EC_{50} value of 100 μM.

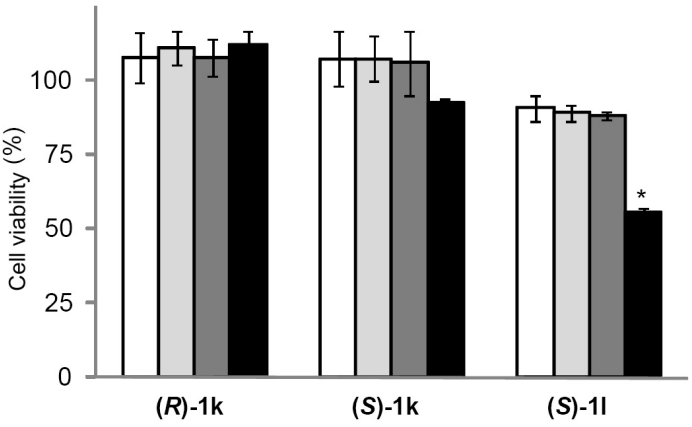

Figure 37. a. *In vitro* cytotoxic activity of **(*R*)-1k**, **(*S*)-1k** and **(*S*)-1l** towards N1 fibroblasts at concentrations of 50 μM (white) and 100 μM (light grey), and towards MCF7-HER2+ human breast cancer cells at concentrations of 50 μM (dark grey) and 100 μM (black). Results represent averages ± SEM of at least two experiments carried out in triplicate.* $p < 0.01$ *vs* control.

These results support that **(*S*)-1l** is cytotoxic in tumour cells that overexpress HER2, while not significantly affecting the non-tumour fibroblasts. If this effect is due to a direct blockade of the HER2-Grb2 interaction, the cytotoxic effect should disappear in tumour cells that do not overexpress HER2 (MCF7-HER2- and MDA-231). In line with this, an additional experiment of cell cytotoxicity in MCF7-HER2- and MDA-231 breast tumour cells was carried out (Figure 38a).

The lack of activity of **(*S*)-1l** in these cells further supported the fact that this compound is actually interfering with the HER2-Grb2 interaction. Final proof of this mechanism was addressed by immunoprecipitation. In this experiment MCF7-HER2+ cells were treated with **(*S*)-1l** or vehicle, washed, and lysed. HER2 was immunoprecipitated and both HER2 and Grb2 immunoblotted using specific antibodies (Figure 38b), and the bands were densitometered.

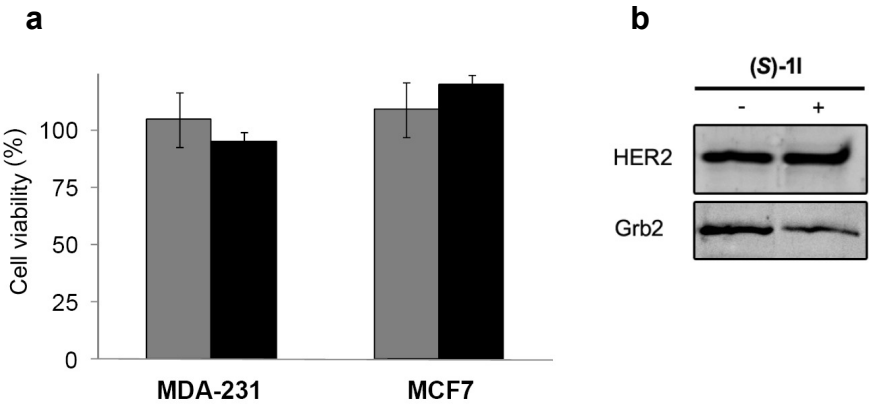

Figure 38. a. *In vitro* cytotoxic activity of **(*S*)-1l** towards HER2 negative MDA-231 and MCF7-HER2- human breast cancer cells at 50 μM (gray) and 100 μM (black). **b.** Inhibition of the HER2-Grb2 interaction by **(S)-1l**. MCF7-HER2+ cells were treated with **(*S*)-1l** or vehicle as in (**a**), washed, and lysed. HER2 was immunoprecipitated, and HER2 and Grb2 were immunoblotted using specific antibodies.

Our results showed a 30% decrease of the interaction between HER2 and Grb2 in the presence of **(*S*)-1l**. Taken together, these results clearly support that the cytotoxic effect of **(S)-1l** can be at least partially ascribed to its binding to the Grb2-SH2 domain and the concomitant inhibition of the HER2-Grb2 interaction.

In conclusion, **(*S*)-1l** can be considered as a new compound in the development of small-molecule inhibitors capable of blocking the HER2-Grb2 interaction, currently understood as one of the most critical steps downstream the HER2 oncogenic signalling.

Up to this point, it seemed logical to probe what signal transduction pathways were really affected by the **(*S*)-1l**-induced HER2-Grb2 blockade. In order to attain this objective, a proteomic platform was set up as explained hereunder.

3.5. Development of a proteomic platform to study the effect of a compound in transduction pathways

This strategy was conceived to generate information in an efficient throughput manner about expression and/or activation of downstream proteins being directly affected by the HER2-Grb2 interaction blockade.

Mass spectrometry (MS) of proteins is nowadays the best suited methodology for this objective. Therefore, we have designed a proteomic platform based on protein enrichment via affinity purification (AP) and further analysis by MS. In the last years, the growing development of AP-MS proteomic platforms has greatly contributed to advance our current understanding of protein interaction networks and their dynamic behaviour as a function of time and cell state. Various large-scale efforts have successfully enabled definition of protein interactomes in several organisms, including humans.[98] Some of the advantages of AP-MS include that analyses can be performed under near physiological conditions with no further modifications or restrictions on the cell type. It can search for multiple interactions among protein assemblies in one single run without perturbing relevant post-translational modifications. Furthermore, it can be used to probe dynamic changes in the composition of protein complexes, especially when used in combination with quantitative proteomic techniques.[99]

AP, also called affinity chromatography, makes use of specific binding interactions between molecules. A particular ligand is chemically immobilized or “coupled” to a solid support, a resin (e.g. sepharose), so that when a complex mixture is passed through the column, those molecules having specific binding affinity to the ligand become bound. In a second step, the bound molecule is stripped from the support, resulting in its purification from the original sample. In its simplest version, the ligand, also called “the bait”, is a small molecule holding specific binding properties for a given protein or set of proteins, “the prey(s)”. In this type of

[98] Choudhary, C.; Mann, M. *Nat. Rev. Mol. Cell Biol.* **2010**, *11*, 427-439.

[99] (a) Kratchmarova, I.; Blagoev, B.; Haack-Sorensen, M.; Kassem, M.; Mann, M. *Science* **2005**, *308*, 1472-1477. (b) Xu, X.; Song, Y; Li, Y; Chang, J; Zhang, H; An, L. *Protein Expr. Purif.* **2010**, *72*, 149-156.

chromatography, the proteins “fished out” with the bait are eluted by a molar excess of the same ligand in solution and identified by MS (Figure 39).

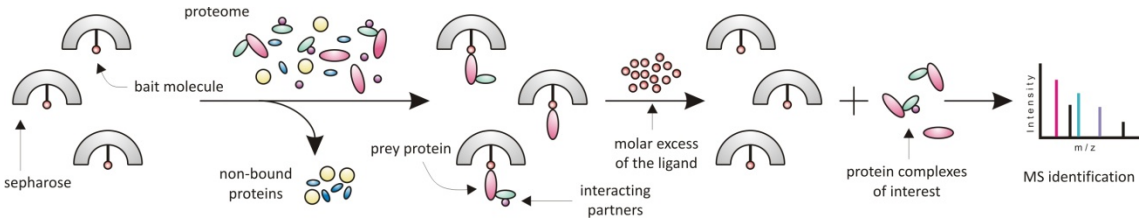

Figure 39. General scheme of AP-MS strategy.

In order to collect a reliable deal of information about proteins related to the MAPKs pathway, or, more generally, about proteins involved in cell proliferation and/or differentiation, three nucleotides extensively implicated in this type of molecular processes where chosen as bait molecules: 7-methylguanosine triphosphate (m^7GTP), adenosine-5'-triphosphate (ATP), and cyclic adenosine monophosphate (cAMP).

A second optional approach would deal with direct pulldown of Grb2 and its interacting partner proteins by means of chemically modifying the most potent inhibitor. This could be done by attaching to the inhibitor an alkyl-elongated biotin moiety not supposed to disrupt interactions of the former with the Grb2-SH2 domain, and then fixing this chain to streptavidin-sepharose beads in order to fish out and identify the bound protein complexes.

Recent experiments carried out by Bottaro *et al.*, have made use of an open-chain biotinylated version of one of their most potent Grb2-SH2 peptide ligand in order to explore its selectivity through immobilization on streptavidin-coated beads and subsequent MS analysis. They detected Grb2, Sos and other related proteins, thus confirming this technique as a powerful tool for identifying target proteins along with their associated partners.[100]

Any of these two options could be used to track the overall effect of a Grb2-SH2 ligand in the physiology of the downstream signalling proteins.[101,102]

The general strategy followed in this work can be outlined into eight main steps (Figure 40). Firstly, the proteome is pre-cleared by incubation with sepharose beads in order to remove non-specific binding proteins randomly adhered (Figure 40a). The supernatant is then incubated with the corresponding nucleotide-sepharose beads (the bait) to allow for the specific nucleotide-binding proteins (the prey) to attach to the resin. This stage is followed by washes

[100] Giubellino, A.; Shi, Z. D.; Jenkins, L. M.; Worthy, K. M.; Bindu, L. K.; Athauda, G.; Peruzzi, B.; Fisher, R. J.; Appella, E.; Burke, T. R.; Bottaro, D. P. *J. Med. Chem.* **2008**, *51*, 7459-7468.

[101] Kumar, R.; Gururaj, A. E.; Barnes, C. J. *Nat. Rev. Cancer.* **2006**, *6*, 459-471.

[102] (a) McLean, G. W.; Carragher, N. O.; Avizienyte, E.; Evans, J; Brunton, V. G.; Frame, M. C. *Nat. Rev. Cancer.* **2005**, *5*, 505-515. (b) Mitra, S. K.; Mikolon, D.; Molina, J. E.; Hsia, D. A.; Hanson, D. A.; Chi, A.; Lim, S. T.; Bernard-Trifilo, J. A.; Ilic, D.; Stupack, D. G.; Cheresh, D. A.; Schlaepfer, D. D. *Oncogene* **2006**, *25*, 5969-5984.

containing an analogue (the corresponding diphosphate version) of the assayed nucleotide. At this point, proteins forming complexes with the actual prey proteins are also expected to be captured (Figure 40b). The specific proteins are finally eluted with a molar excess of the nucleotide under study (Figure 40c). This mixture is separated by sodium dodecylsulphate-polyacrylamide gel electrophoresis (SDS-PAGE), followed by staining with coomassie blue and band slicing (Figure 40d). Afterwards, in-gel digestion of the extracted proteins is carried out using trypsin (Figure 40e). Peptides are separated in a nano-high performance liquid chromatography (nano-HPLC) system, eluted, and analyzed by MS. In a routine analysis, two MS events are automatically performed: in the first scan, the mass/charge ratio (m/z) of the intact peptides is measured. The most abundant peptides are then specifically selected and subjected to fragmentation, yielding a tandem MS (MS/MS) spectrum (Figure 40f). Finally, database searching powered by the MASCOT algorithm is used to interpret the MS data to yield a list of proteins present in the initial sample (Figure 40g).

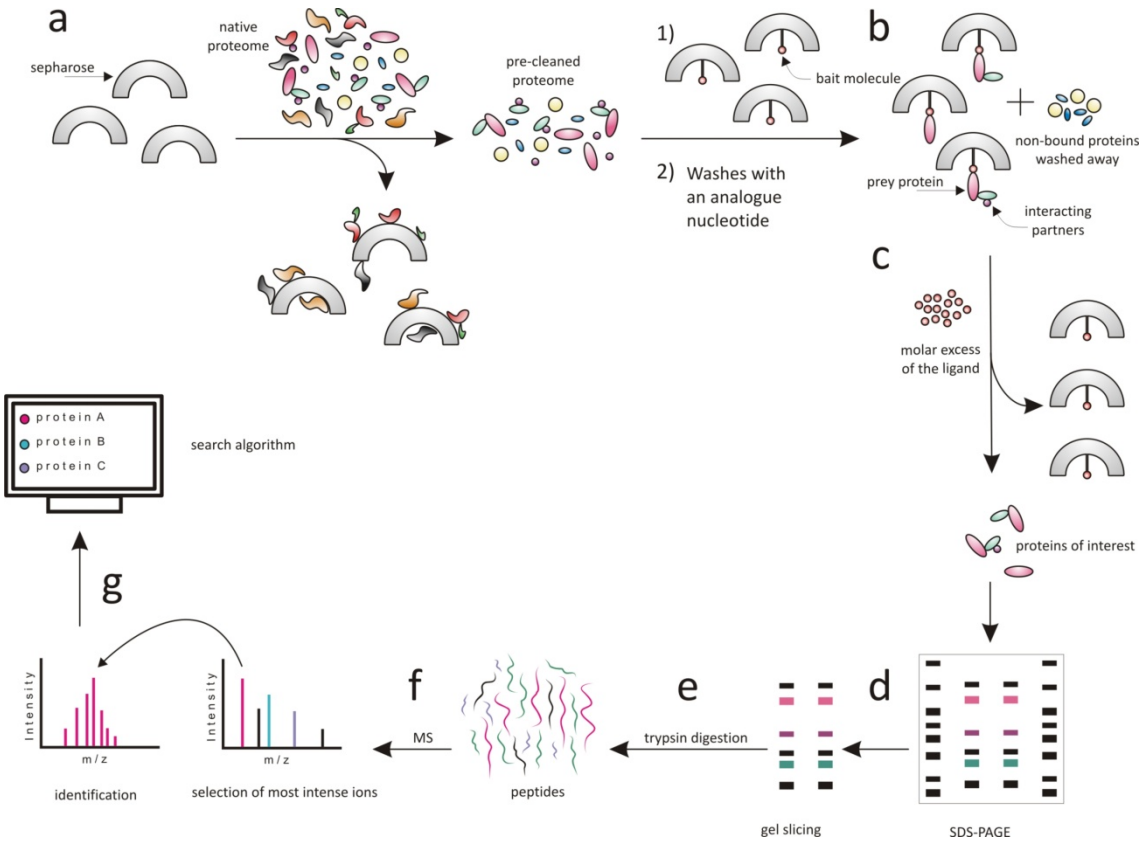

Figure 40. Schematic representation of the nucleotide AP-MS strategy. **a.** Pre-clearing step. **b.** Capture of target proteins. **c.** Elution of target protein complexes. **d.** SDS-PAGE separation of the eluted proteins and gel slicing. **e.** Trypsin digestion. **f.** Tandem MS analysis. **g.** MASCOT output.

The classification of the pulled-down hits has been done using the specialized software ProteinCenter© (Proxeon Bioinformatics A/S) according to the guidelines and annotations set

forth by the Gene Ontology Consortium (GO).[103] The GO project provides an ontology of defined terms representing gene product properties. The ontology covers three domains: cellular component, molecular function, and biological process. Given that the aim of this proteomic platform has been the identification of proteins which act as sensitive biomarkers related to a dysfunctional signalling process, both -molecular function- and -biological process- domains were considered the significant features when analysing the identified proteins. The results obtained from the above protocol applied to the study of the three selected nucleotides (m^7GTP, ATP and cAMP) are described below. In all cases pooled cytosolic human liver lysate was used as the proteome.

3.5.1. AP using m^7GTP

The m^7GTP is a specially modified nucleotide (Figure 41a) that is normally found covalently linked to the 5' end of the majority of precursor messenger RNAs (pre-mRNAs) via an unusual 5' to 5' triphosphate linkage (Figure 41b). This m^7GTP is also called the 5' cap and contributes to the mRNA stability.

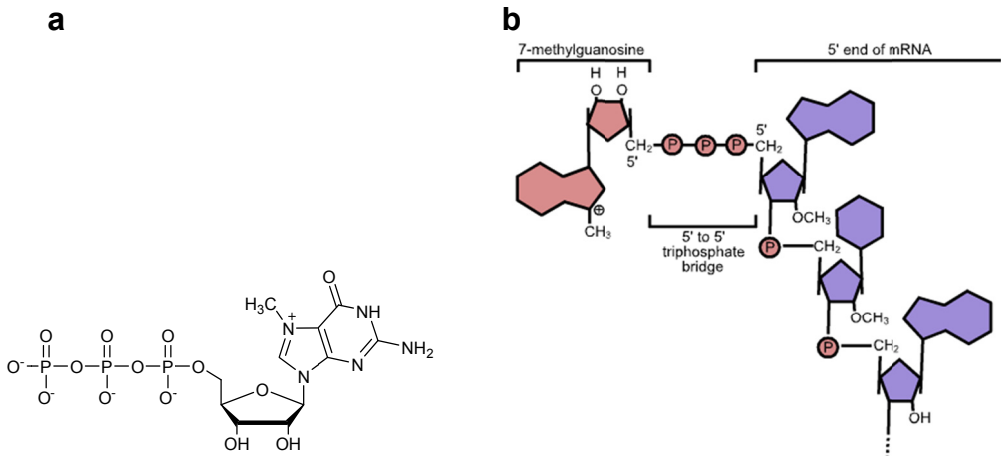

Figure 41. a. Structure of m^7GTP **b.** Schematic diagram of a m^7GTP (5' cap) attached to a mRNA.

The 5' cap is specifically recognized and bound by one of the best studied translation factors, the eukaryotic initiation factor 4E (eIF4E), which facilitates the mRNA nuclear export and regulates protein translation in the cytoplasm. This is important because overexpression of most known translation factors is currently associated with cancer progression or decreased free survival (Figure 42); but among them, eIF4E stands out as a focal point in understanding the aetiology of many malignancies. Accordingly, eIF4E overexpression correlates with poor clinical outcome and decreased survival in breast, head and neck, colorectal, lung, prostate, bladder, skin, and cervical cancers as well as lymphomas.[104,105]

[103] http://www.geneontology.org/

[104] Coleman, L. J.; Peter, M. B.; Teall, T. J.; Brannan, R. A.; Hanby, A. M.; Honarpisheh, H.; Shaaban, A. M.; Smith, L.; Speirs, V.; Verghese, E. T.; McElwaine, J. N.; Hughes, T. A. *Br. J. Cancer* **2009**, *100*, 1393-1399.

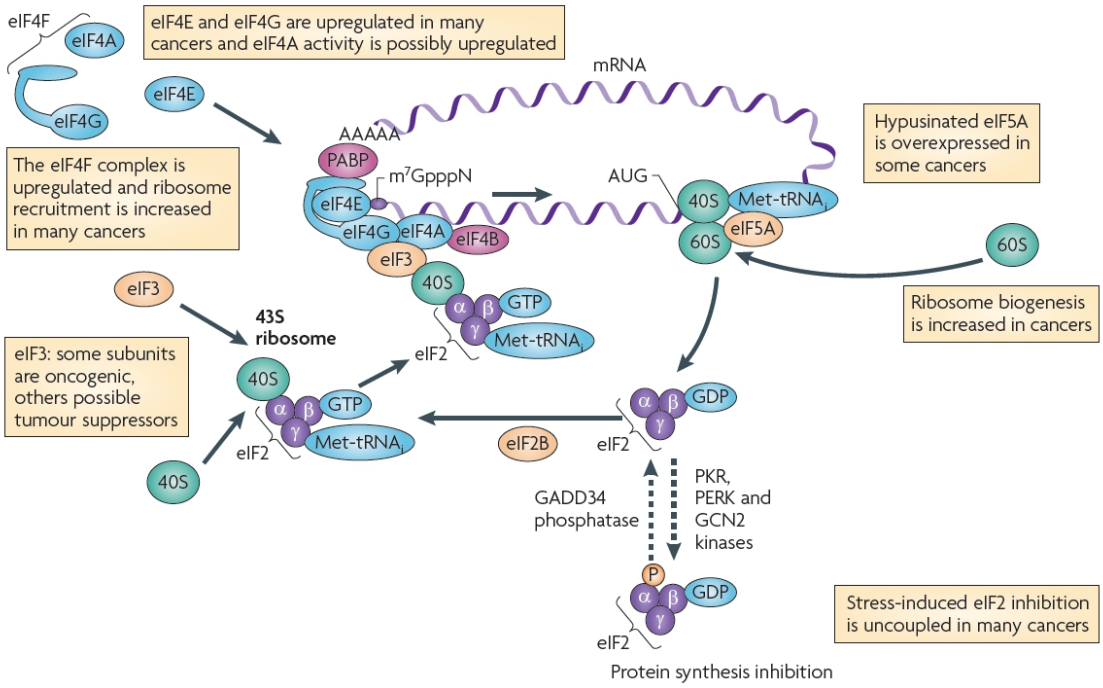

Figure 42. Schematic representation of the eukaryotic 5' cap-dependent mRNA translation and how the alterations of its components could contribute to a malignant phenoptype. (Source: See citation 106)

Although still under revision, several highly compelling data suggest that the increased phosphorylation of eIF4E at serine 209 may also be a key factor contributing to cancer development and progression.[106] Interestingly, sorafenib (Nexavar®; Bayer), an approved TKI for the treatment of advanced renal and liver cancers that targets the MAPKs pathway,[107] also promotes dephosphorylation of p-eIF4E. It is clear that the translation initiation apparatus serves as a critical site of integration and amplification of oncogenic signals. This makes eIF4E and the rest of eIFs interesting tumour biomarkers, and gives an idea about expected protein hits using m^7GTP as bait. m^7GTP-sepharose beads were used following the general protocol (Figure 40).

A representative SDS-PAGE (Figure 43) shows the selective isolation of m^7GTP-binding proteins (lane E). MS identification of the proteins in this lane yielded a total of 85 hits and the most relevant are compiled in Table 4.

[105] Silvera, D.; Formenti, S. C.; Schneider, R. J. *Nat. Rev. Cancer* **2010**, *10*, 254-266.

[106] Silva, R. L.; Wendel, H. G. *Cell Cycle* **2008**, *7*, 553-555. (b) Graff, J. R.; Konicek, B. W.; Lynch, R. L.; Dumstorf, C. A.; Dowless, M. S.; McNulty, A. M.; Parsons, S. H.; Brail, L. H.; Colligan, B. M.; Koop, J. W.; Hurst, B. M.; Deddens, J. A.; Neubauer, B. L.; Stancato, L. F.; Carter, H. W.; Douglass, L. E.; Carter, J. H. *Cancer Res.* **2009**, *69*, 3866-3873.

[107] Liu, L.; Cao, Y.; Chen, C.; Zhang, X.; McNabola, A.; Wilkie, D.; Wilhelm, S.; Lynch, M.; Carter, C. *Cancer Res*. **2006**, *66*, 11851-11858.

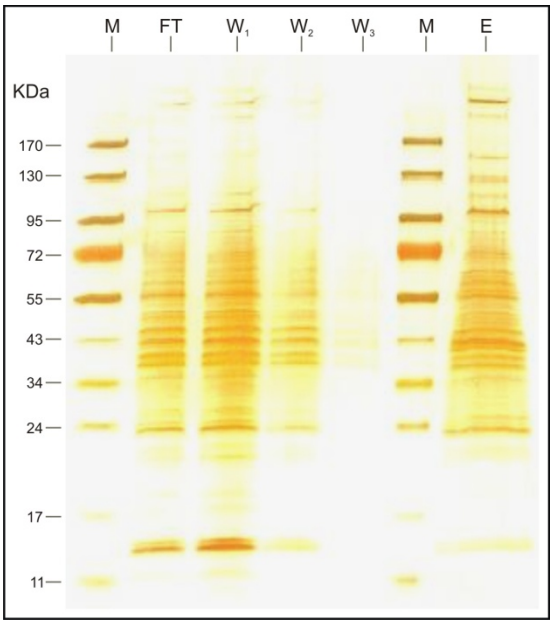

Figure 43. Silver stained 4-20% SDS-PAGE of a representative m^7GTP-AP experiment showing the following lanes: M: marker, FT: flow-through, W_i: sequential washes, and E: elution.

Table 4. Most relevant m^7GTP-related proteins.

Acc. No. [a]	Protein Name	Gene Code
P60842	Eukaryotic translation initiation factor 4A-I	EIF4A1
P06730	Eukaryotic translation initiation factor 4E	EIF4E
P68104	Eukaryotic translation elongation factor-1-alpha	EEF1A1
P24534	Eukaryotic translation elongation factor-1-beta	EEF1B2
38522	Eukaryotic translation elongation factor-1-delta	EEF1D
P13639	Eukaryotic translation elongation factor-2	EEF2
P62249	40S ribosomal protein S16	RPS16
189306	Nucleolin	NCL
P22626-2	Heterogenous nuclear ribonucleoproteins A2-B1	HNRNPA2-B1
P16930	Fumarylacetoacetase	FAH
P00326	Alcohol dehydrogenase 1C	ADH1C
157834561	Aldehyde reductase (chain A)	AKR1A1
1065362	GDP-complexed human ADP-ribosylation factor (chain B)	ARF1
1403050	Phosphoenolpyruvate carboxykinase (GTP)	PCK2
P43490	Nicotinamide phosphoribosyltransferase	PBEF1
Q9BYF0	Aldehyde oxidase	AOX1
179987	Chlordecone reductase	AKR1C4
IPI00219953.5	Cytidylate kinase	CMPK
P78417	Glutathione transferase omega-1	GSTO1
P99024	Tubulin beta-5 chain	Tubb5
P10809	60 kDa heat shock protein	HSPD1
Q16715	Pyruvate kinase	PKLR
P30047	GTP cyclohydrolase 1 feedback regulatory protein	GCHFR

[a] Accession numbers (Acc. No.) listed in this table are those used by the UniProt database (http://www.uniprot.org).

In order to assess the biological significance of the identified proteins, they were classified according to the main molecular functions and their binding preferences using data available in the GO catalogue (Figure 44).

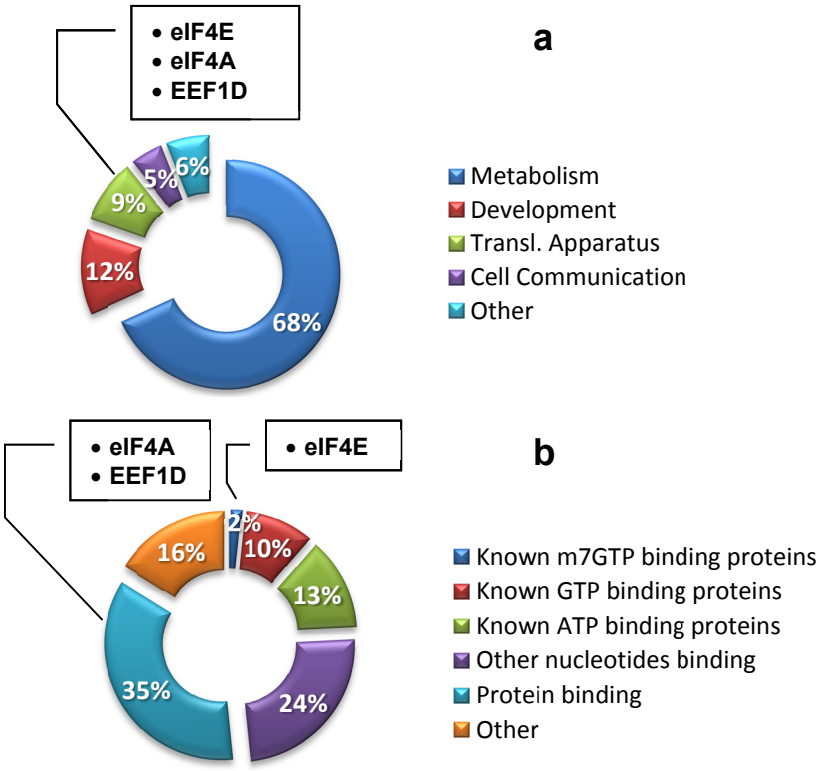

Figure 44. a. Pie chart representation of the m^7GTP pulled-down proteins according to the GO domains "Molecular Function" and "Biological Process". **b.** Pie chart representation of the m^7GTP pulled-down proteins according to their preferential binding to nucleotides or other proteins.

Supporting the significance of the results, among the identified hit proteins there are some known binders of m^7GTP, either directly or in complexes. It is also worth mentioning that in spite of not being included in the above list (as identified with lower reliability threshold), and together with the EIFs and EEFs included in Table 4, other interesting components of the translation machinery were isolated such as several eukaryotic translation initiation factors (EIF3A, 3B, 4B, 4G, 5A, and 6), as well as eIF4E binding protein 1 (EIF4EBP1), and the elongation factor 1-gamma (EEF1G).

From the above results it comes out clear that the prevailing majority of the pulled-down proteins is, in addition to translation-related, metabolism-dedicated; something which makes sense considering the native proteome studied came from human liver, by far the most important metabolic organ in mammals.

Nevertheless, the most important finding was the unequivocal identification of several translation factors. This result supports that this methodology could be used for the profiling of these factors, which have been proposed as biomarkers of multiple types of cancer.

3.5.2. AP using ATP

ATP (Figure 45) is a multifunctional nucleotide primarily used in cells as a coenzyme. It is often called the "molecular unit of currency" of intracellular energy transfer, as the hydrolysis of

one or two of its anhydride bonds provides the energy needed for the cellular function. More importantly from the cellular signalling point of view, ATP is also used as a substrate by kinases that phosphorylate proteins and lipids, as well as by adenylyl cyclase, which uses ATP to produce the second messenger molecule cAMP.

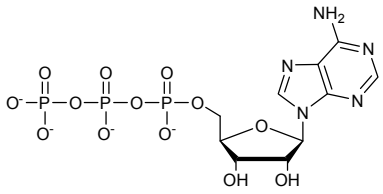

Figure 45. Adenosine-5'-triphosphate (ATP).

Therefore, the use of ATP as a bait molecule should enable the identification of a number of kinases and their associated proteins. In this case, the assay was carried out following our previously described methodology using ATP-sepharose beads (Figure 40) but in the presence of 30 mM $MgCl_2$ during the AP step, since $MgCl_2$ is required to decrease the dissociation constant of ATP from its target protein(s).[108]

A representative SDS-PAGE (Figure 46) shows the selective isolation of ATP-binding proteins (lane E). MS identification of the proteins in this lane yielded a total of 23 hits and the most relevant are compiled in Table 5.

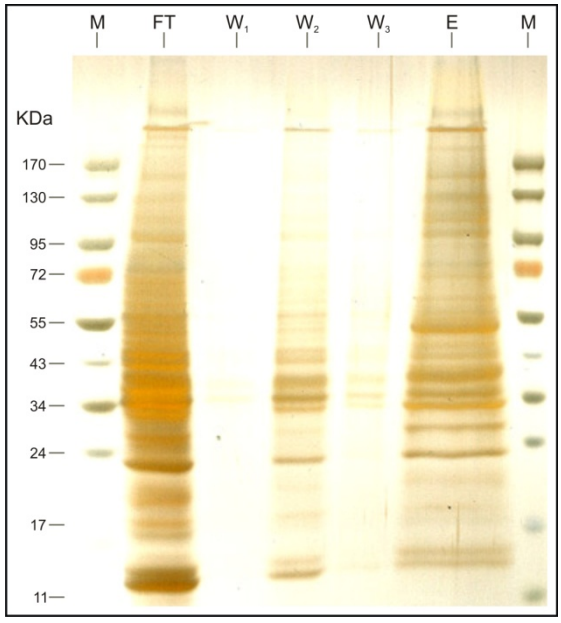

Figure 46. Silver stained 4-20% SDS-PAGE of a representative ATP-AP experiment showing the following lanes: M: marker, FT: flow-through, W_i: sequential washes, and E: elution.

[108] Lin, X.; Ayrapetov, M. K.; Sun, G. *BMC Biochem.* **2005**, *6*, 1-8.

Table 5. Most relevant ATP-related proteins.

Acc. No.[a]	Protein Name	Gene Code
20149621	Dihydroxyacetone kinase 2	DAK
P54819	Adenylate kinase isoenzyme 2, mitochondrial	AK2
O00764	Pyridoxal kinase	PDXK
6491737	*N*-Acetylglucosamine kinase	NAGK
Q9H479	Fructosamine-3-kinase	FN3K
P05165	Propionyl-CoA carboxylase (chain A)	PCCA
3860238	4-Hydroxyphenylpyruvate dioxygenase	HPD
P38117	Electron transfer flavoprotein subunit beta	ETFB
12804999	3-Hydroxybutyrate dehydrogenase, type 2	BDH2
P68133	Actin, alpha skeletal muscle	ACTA1
1336765	Glucose phosphate isomerase	GPI

[a] Accession numbers (Acc. No.) listed in this table are those used by the UniProt database (http://www.uniprot.org).

The graphical assortment according to the indicated GO standards and the binding preferences of the identified proteins are represented in Figure 47.

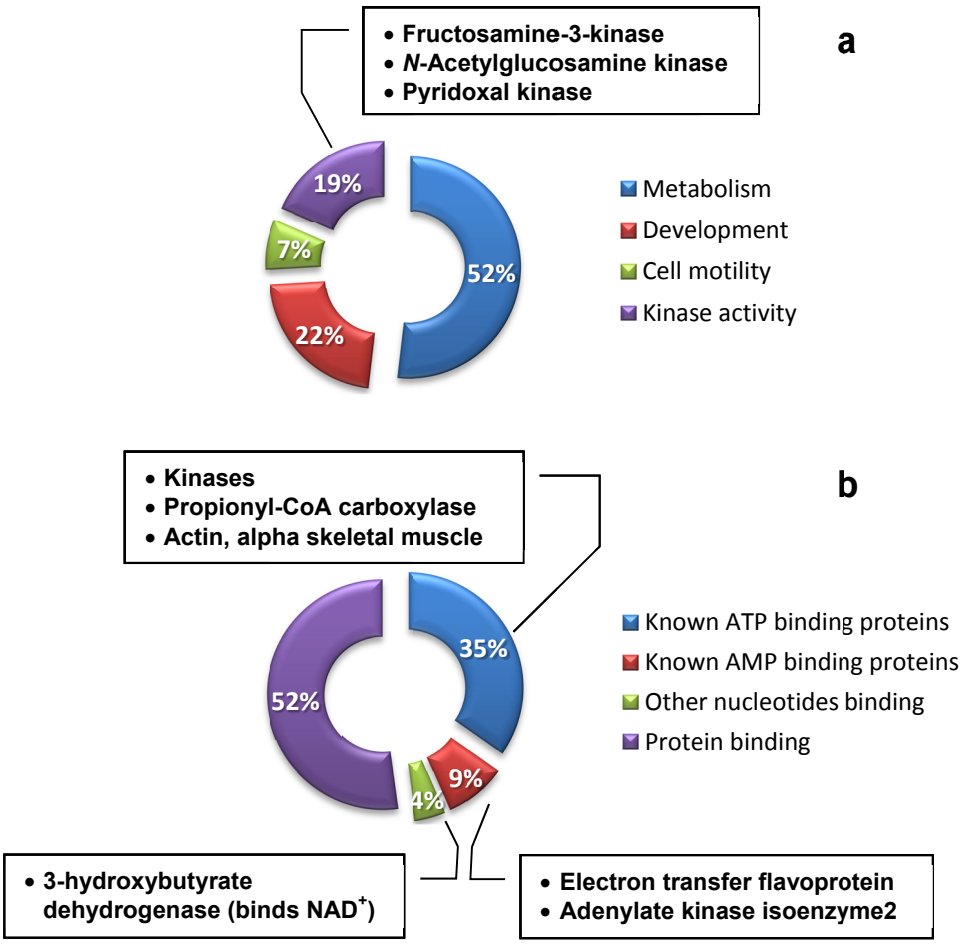

Figure 47. a. Pie chart representation of the ATP pulled-down proteins according to the GO domains "Molecular Function" and "Biological Process". **b.** Pie chart representation of the ATP pulled-down proteins according to their preferential nucleotide binding or other proteins.

Confirming the significance of the methodology, hits are mostly representative of kinases and other proteins involved in metabolic or developmental processes. Though not included in the above summary because of their low frequency of identification, very likely related to their low real cell concentration, there are several MAPK representatives.

It is conceivable that another proteome different from human liver used here to set up the methodology, would result in an increase in this class of hit proteins. For instance, the analysis of tumour cells had probably yielded a higher number of signalling kinases, as the intrinsic nature of constantly growing and dividing of such cells imposes.

3.5.3. AP using cAMP

cAMP is an important second messenger in the signal transduction of many biological processes (Figure 48). It is synthesised from ATP by adenylyl cyclase. One of the most important functions of cAMP is the activation of the protein kinase A (PKA) which will lead to phosphorylation of its downstream substrates, including other proteins as well as the cAMP response element-binding (CREB) transcription factor, which binds to certain DNA sequences increasing or decreasing gene transcription. The cAMP/PKA pathway has been reported to stimulate cell growth in many cell types while inhibiting it in others.[109] Data collected from literature about some PKA-related genes indicate an involvement of PKA in neoplastic transformation and tumour growth, especially in the onset and maintenance of endocrine tumours (hormone-responsive tissues).[110] Genes regulated by CREB are in most cases implicated in cell proliferation, differentiation and survival. Therefrom, CREB-increased expression and phosphorylation can correlate with some types of neoplasias, being the best studied the non-small cell lung cancer (NSCLC), where the patient survival is inversely proportional to CREB expression and phosphorylation.[111]

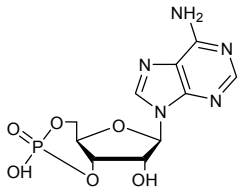

Figure 48. Cyclic adenosine monophosphate (cAMP)

In general, it is assumed that the proliferative features of PKA, besides the already mentioned possible deregulation of CREB phosphorylation, are related to its crosstalk with the

[109] Dumaz, N.; Marais, R. *FEBS J.* **2005**, *272*, 3491-3504

[110] (a) Rosenberg, D.; Groussin, L.; Jullian, E.; Perlemoine, K.; Bertagna, X.; Bertherat, J. *Ann. N. Y. Acad. Sci.* **2002**, *968*, 65-74. (b) Rivas, M.; Santisteban, P. *Mol. Cell. Endocrinol*. **2003**, *213*, 31-45.

[111] Seo, H. S.; Liu, D. D.; Bekele, B. N.; Kim, M. K.; Pisters, K.; Lippman, S. M.; Wistuba, I. I.; Koo, J. S. *Cancer Res.* **2008**, *68*, 6065-6073.

MAPKs such as B-Raf,[112] C-Raf,[113] Rap1,[114] Rap1GAP,[115] or Src.[116] Therefore, the use of cAMP as a bait would conceivably enable the identification of an important number of signalling kinases belonging to the MAPKs family (Figure 49).

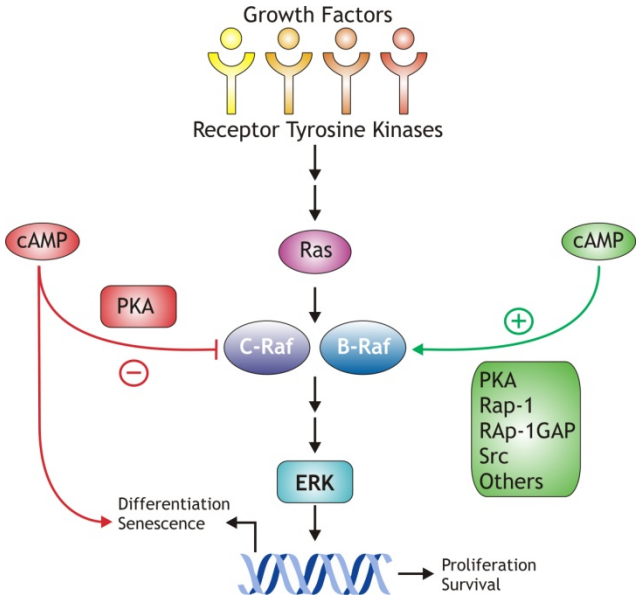

Figure 49. Crosstalk between the cAMP-PKA and the MAPK pathways.

cAMP-sepharose beads were used following the general protocol (Figure 40). In Figure 50 a representative SDS-PAGE shows the selective enrichement of cAMP-interacting proteins (lane E). Their MS identification resulted in 21 hits and the most relevant are compiled in Table 6.

[112] (a) Peraldi, P.; Frödin, M.; Barnier, J.V.; Calleja, V.; Scimeca, J. C.; Filloux, C.; Calothy, G.; Van Obberghen, E. *FEBS Lett.* **1995**, 357, 290-296. (b) Konig, S.; Guibert, B.; Morice, C.; Vernier, P.; Barnier, J. V. *C. R. Acad. Sci. III* **2001**, 324, 673-68.

[113] See citation 34.

[114] Lerosey, I.; Pizon, V.; Tavitian, A.; de Gunzburg, J. *Biochem. Biophys. Res. Commun*. **1991**,*175*, 430-436.

[115] Polakis, P.; Rubinfeld, B.; McCormick, F *J. Biol. Chem*. **1992**, *267*, 10780-10785.

[116] Schmitt, J. M. Stork, P. J. *Mol. Cell* **2002**, *9*, 85-94.

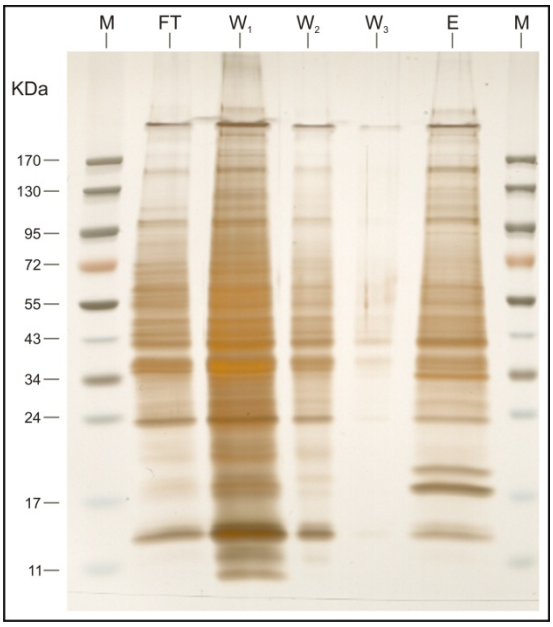

Figure 50. Silver stained 4-20% SDS-PAGE of a representative cAMP-AP experiment showing the following lanes: M: marker, FT: flow-through, W_i: sequential washes, and E: elution.

Table 6. Most relevant cAMP-related proteins.

Acc. No.[a]	Protein Name	Gene Code
P10644	cAMP-dependent protein kinase type I-alpha regulatory subunit	PRKAR1A
P13861	cAMP-dependent protein kinase type II-alpha regulatory subunit	PRKAR2A
915392	Fatty acid synthase	FASN
P07741	Adenine phosphoribosyltransferase	APRT
1093492	4-aminobutyrate aminotransferase	GABA
Q06278	Aldehyde oxidase	AOX1
3860238	4-hydroxyphenylpyruvate-dioxygenase	HPD
226527	Nucleoside diphosphate kinase	NDK
P26038	Moesin	MSN
178027	Alpha-actin	ACTA2
37492	Alpha-tubulin	TUBA1A
338695	Beta-tubulin	TUBB

[a] Accession numbers (Acc. No.) listed in this table are those used by the UniProt database (http://www.uniprot.org).

The graphical assortment according to the indicated GO standards and the binding preferences of the identified proteins are represented in Figure 51.

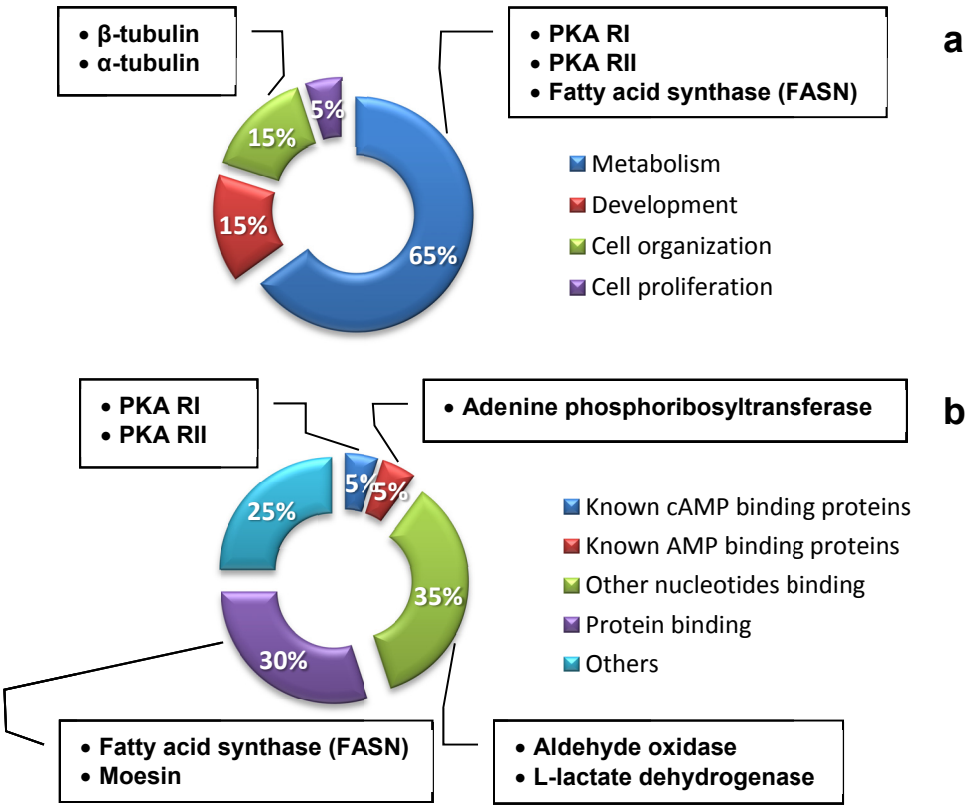

Figure 51. a. Pie chart representation of the cAMP pulled-down proteins according to the GO domains "Molecular Function" and "Biological Process". **b.** Pie chart representation of the cAMP pulled-down proteins according to their preferential binding to nucleotides, other proteins or other entities (e.g. cofactors).

Remarkably, PKA regulatory domains (RI and RII) stand out among the identified hits (accession numbers P10644 and P13861 respectively, Table 6). The rest of the proteins identified with the cAMP-pulldown experiments have metabolic functions, as expected from the use of human liver as native proteome.

As it was concluded from the isolation of eIF4E and other translation factors in the m^7GTP-based runs, the metabolic kinases in the ATP-based runs, and the unequivocal identification of PKA regulatory subunits in this set of experiments with cAMP, this methodology could be extended to other biomarkers related to the aggressiveness of tumours using the adequate proteome. This platform could be used to compare a cancer-relevant proteome (e.g. HER2+ breast cancer cells) previously treated or not with an anti-tumour compound. Then, the proteomic signature would reveal the identity and extent to which the treatment with the targeted agent effectively disrupted that cancer-relying transduction pathway.

Once we have successfully set up this type of proteomic platform, it can be used to compare the proteomes signature of tumour cell lines treated *vs* non-treated with a Grb2-SH2 ligand. These experiments are currently being carried out with **(*S*)-1l**.

Experimental Section

4. Experimental Section

4.1. Molecular dynamics simulations

Molecular dynamics (MD) simulations of Grb2-SH2 in complex with the high-affinity 2-Abz-Glu-pTyr-Ile-Asn-Gln-NH_2 pentapeptide (PDB code 1ZFP)[117] and with the designed compound **(*S*)-1k** were performed with the Sander module of AMBER 9.[118] To generate an electro-neutral system, a chloride ion was added to the system formed by Grb2 and the compound **(*S*)-1k**. These structures were placed in a rectangular box (~70 Å x 65 Å x 73 Å in size) containing ~9200 Monte Carlo-equilibrated TIP3P water molecules. The general Amber force field (GAFF)[119] was used with the parameters proposed for phosphorylated amino acids[120] and HF/6-31G*-derived RESP atomic charges. The simulations were carried out with a 2-fs integration time step during 10 ns at constant pressure, at constant temperature coupled to a heat bath, using the particle mesh Ewald method to evaluate electrostatic interactions, and the ff03 force field for peptides. Structures were collected every 4 ps during the last 5 ns (1250 structures per simulation). These structures were then used to evaluate free energies of binding using the MM-GBSA methodology.[121]

4.2. Synthetic procedures, analytical and spectral characterization

Melting points (uncorrected) were determined on a Stuart Scientific electrothermal apparatus. Infrared (IR) spectra were measured on a Bruker Tensor 27 instrument equipped with a Specac ATR accessory of 5200-650 cm^{-1} transmission range. Frequencies (ν) are expressed in cm^{-1}. NMR spectra were recorded on a Bruker Avance 300-AM (^1H, 300 MHz; ^{13}C, 75 MHz; ^{19}F, 235 MHz) or Bruker 200-AC spectrometer (^1H, 200 MHz; ^{13}C, 50 MHz) at the UCM's facility. Chemical shifts (δ) are expressed in parts per million (ppm) relative to internal tetramethylsilane used as internal reference; coupling constants (*J*) are expressed in hertz (Hz). The following abbreviations are used to describe peak patterns when appropriate: s (singlet), d (doublet), t (triplet), q (quadruplet), qt (quintuplet), sx (sextuplet), sp (septuplet), m (multiplet), and br (broad). Mass spectrometry (MS) was carried out on a Bruker LC-Esquire in electrospray mode (ESI) at the UCM's facility. Optical rotations were recorded with a Perkin Elmer 781 polarimeter. Elemental analyses (C, H, N) were performed on a LECO CHNS-932 apparatus at the UCM's facility and are within 0.5% of the theoretical values, confirming a purity of at least

---

[117] See citation 52.

[118] Case, D. A.; Darden, T. A.; Cheatham III, T. E.; Simmerling, C. L.; Wang, J.; Duke, R. E.; Luo, R.; Merz, K. M.; Pearlman, D. A.; Crowley, M.; Walker, R. C.; Zhang, W.; Wang, B.; Hayik, S.; Roitberg, A.; Seabra, G.; Wong, K. F.; Paesani, F.; Wu, X.; Brozell, S.; Tsui, V.; Gohlke, H.; Yang, L.; Tan, C.; Mongan, J.; Hornak, V.; Cui, G.; Beroza, P.; Mathews, D. H.; Schafmeister, C.; Ross, W. S.; Kollman, P. A. AMBER 9, University of California, San Francisco.

[119] Wang, J.; Wolf, R. M.; Caldwell, J. W.; Kollman, P. A.; Case, D. A. *J. Comput. Chem.* **2004**, *25*, 1157-1174.

[120] Homeyer, N.; Horn, A. H.; Lanig, H.; Sticht, H. *J. Mol. Model.* **2006**, *12*, 281-289.

[121] See citation 85.

95% for all tested compounds. Hydrogenation reactions were carried out in a 3900 Parr hydrogenation apparatus. Analytical thin-layer chromatography (TLC) was run on silica gel plates (Merck, Kieselgel 60 F-254) with detection by UV light, iodine, 10% phosphomolybdic acid solution in ethanol or 10% ninhydrine in ethanol. Flash chromatography was performed on glass column using silica gel 60 (Merck, particle size 230-400 mesh). Starting materials, reagents, and solvents were purchased as high-grade commercial products from Sigma-Aldrich, Fluka, Panreac, SDS, Lancaster, Bachem, Cymit, Novabiochem or Scharlab, and were used without further purification unless otherwise noted. Toluene, methylene chloride, and tetrahydrofuran were used freshly distilled over P_2O_5, CaH_2, and Na turnings respectively. Methanol was used after immediate drying with activated molecular sieves.

4.2.1. Synthesis of compounds of series I (1a-l)

4.2.1.1. Synthesis of intermediate amines 7a,b and 21.

Amines **7a**,**b** were synthesized according to previously described procedures and their ^{1}H NMR spectroscopic data coincide with those previously reported.[122]

1-(3-Aminopropyl)tetrahydropyrimidin-2(1*H*)-one (7a). Yield: 41%. Yellowish oil.
IR (CH_2Cl_2, cm^{-1}): 3293 (NH), 1639 (C=O), 1522 (NH), 1451 (C–N–H), 1273.
^{1}H-NMR ($CDCl_3$, δ): 1.67 (qt, *J* = 6.7 Hz, 2H, CH_2), 1.89 (qt, *J* = 5.9 Hz, 2H, CH_2), 2.07 (s, 2H, NH_2), 2.67 (t, *J* = 6.6 Hz, 2H, $C\underline{H}_2NH_2$), 3.21-3.30 (m, 4H, CH_2N, $C\underline{H}_2NH$), 3.38 (t, *J* = 6.8 Hz, 2H, NCH_2), 5.09 (s, 1H, NH).
^{13}C-NMR ($CDCl_3$, δ): 22.3, 31.0, 38.9, 40.5, 44.4, 45.2 (6 x CH_2), 156.6 (CO).

1-(2-Aminoethyl)imidazolin-2-one (7b). Yield: 50%. Yellowish oil.
IR (CH_2Cl_2, cm^{-1}): 3294 (NH), 1678 (C=O), 1498 (NH), 1452 (C–N–H), 1273.
^{1}H-NMR ($CDCl_3$, δ): 1.66 (s, 2H, NH_2), 2.78 (t, *J* = 6.1 Hz, 2H, $C\underline{H}_2NH_2$), 3.18 (t, *J* = 6.1 Hz, 2H, NCH_2), 3.39-3.40 (m, 4H, 2 x CH_2), 4.58 (s, 1H, NH).
^{13}C-NMR ($CDCl_3$, δ): 38.3, 39.6, 45.1, 46.5 (4 x CH_2), 163.7 (CO).

Benzyl 3-[(2-{1-[(*tert*-butoxycarbonyl)amino]cyclohexyl}ethyl)amino]propylcarbamate (22).

To a stirred solution of 1-(2-aminoethyl)-*N*-Boc-cyclohexylamine (1.65 mmol, 1.25 equiv) over 4 Å molecular sieves (~4 g) in freshly distilled anhydrous methanol (25 mL) were successively added 3-[(benzyloxycarbonyl)amino]propionaldehyde (1.32 mmol, 1 equiv) acidified with acetic acid (0.15 mL) and $NaCNBH_3$ (1.98 mmol, 1.5 equiv) under argon atmosphere. After being stirred at 35 ºC for 24 h, the mixture was filtered over a celite bed, thoroughly washed out with ethyl acetate, concentrated under reduced pressure and purified by flash column chromatography to afford the pure protected triamine **22** as a colourless oil.

[122] See citation 88.

Chromatography: dichloromethane:ethyl acetate:ammonia, 8:1.5:0.5 → 5:4.5:0.5. **Yield:** 86%.
IR (CH_2Cl_2, cm^{-1}): 3402 (NH), 1693 (C=O), 1525 (C_{Ar}-C_{Ar}), 1256, 1164 (O-CO-N).
^{1}H-NMR ($CDCl_3$, δ): 1.26-1.57 (m, 18H, 3 x CH_3, 4 x CH_2, CH_{2a}), 1.92-2.11 (m, 5H, 2 x CH_2, CH_{2b}), 2.97-3.01 (m, 4H, 2 x C$\underline{H_2}$NH), 3.31-3.33 (m, 2H, C$\underline{H_2}$NH), 3.81 (br s, 1H, NH), 4.55 (br s, 1H, NH), 5.11 (s, 2H, CH_2O), 5.59 (br s, 1H, NH), 7.27-7.37 (m, 5H, Ar).
^{13}C-NMR ($CDCl_3$, δ): 21.6 (2 x CH_2), 25.6, 28.2 (2 x CH_2), 28.5 (3 x CH_3), 35.2 (2 x CH_2), 36.9, 38.8, 44.6, 46.8 (4 x CH_2), 53.7 (C), 66.9 (CH_2), 80.1 (C), 128.1 (CH Ar), 128.2 (2 x CH Ar), 128.6 (2 x CH Ar), 136.5 (C Ar), 156.2, 157.4 (2 x CO).

***tert*-Butyl 1-{2-[(3-aminopropyl)amino]ethyl}cyclohexylcarbamate (23).**

Protected triamine **22** (0.92 mmol, 1 equiv) was dissolved in methanol (~15 mL), Pearlman's catalyst (20% $Pd(OH)_2$ on carbon, 500 mg x mmol) was added, and the suspension was hydrogenated with shaking at rt for 48 h under an initial pressure of 45-50 psi. The catalyst was filtered through a celite bed and the filtrate concentrated under reduced pressure to obtain the amine **23** as a colourless oil, which was set to cyclize immediately with no further purification.

Yield: 97%.
IR (CH_2Cl_2, cm^1): 3377 (NH), 1689 (C=O).
^{1}H-NMR (CH_3OD, δ): 1.29-1.49 (m, 13H, 3 x CH_3, 2 x CH_2), 1.69-2.04 (m, 10H, 5 x CH_2), 2.58-2.75 (m, 6H, 3 x CH_2N).
^{13}C-NMR (CH_3OD, δ): 14.5, 21.5, 21.7 (3 x CH_2), 25.9 (2 x CH_2), 27.9 (3 x CH_3), 29.8, 31.5, 35.1, 39.5, 44.5 (5 x CH_2), 53.7, 78.4 (2 x C), 155.7 (CO).

***tert*-Butyl 1-[2-(2-oxotetrahydropyrimidin-1(2*H*)-yl)ethyl]cyclohexylcarbamate (24).**

To a solution of CDI (0.44 mmol, 2 equiv) in THF (10 mL/mmol CDI) under argon atmosphere at 70 ºC, a mixture of the previously prepared triamine **23** (0.29 mmol, 1 equiv) and DBU (1 equiv) in THF (50 mL/mmol triamine) was added dropwise and stirred for 24 h. Afterwards, an identical amount of CDI was added, and the mixture was left to react for additional 24 h. The crude was then concentrated under reduced pressure, resuspended in ethyl acetate and successively washed with saturated NH_4Cl (3 x 40 mL) and brine (2 x 30 mL). The organic extract was dried over anhydrous Na_2SO_4, the solvent evaporated under reduced pressure and purified by flash column chromatography to yield the cyclic urea derivative **24** as a colourless oil.

Chromatography: dichloromethane:ethyl acetate, 1:1 → ethyl acetate:ethanol 9:1.

Yield: 38%.

IR (CH_2Cl_2, cm^{-1}): 3323 (NH), 1707, 1647 (C=O), 1522, 1450 (N-CO-N).

^{1}H-NMR ($CDCl_3$, δ): 1.36-1.49 (m, 17H, 3 x CH_3, 4 x CH_2), 1.91-1.93 (m, 6H, 3 x CH_2), 3.24-3.34 (m, 6H, 3 x CH_2N), 4.49 (br s, 1H, NH), 5.25 (br s, 1H, NH).

^{13}C-NMR ($CDCl_3$, δ): 21.9 (2 x CH_2), 22.6, 26.1 (2 x CH_2), 29.3 (3 x CH_3), 30.1 (2 x CH_2), 32.3, 35.4, 40.9, 45.5 (4 x CH_2), 54.0, 79.0 (2 x C), 155.0, 156.6 (2 x CO).

1-[2-(2-Oxotetrahydropyrimidin-1(2*H*)-yl)ethyl]cyclohexanaminium trifluoroacetate (25).

Cyclic Boc-protected amine **24** (0.28 mmol, 1 equiv) was treated with TFA (20 equiv) in dichloromethane (30 mL x mmol Boc-amine) and stirred under argon atmosphere for 1.5 h. The crude was concentrated under reduced pressure and washed with diethyl ether (6 x 5 mL) to yield the amine **21** as its TFA salt.

Yield: 77%. Amorphous solid.

IR ($(CH_3)_2CO$, cm^{-1}): 3326 (NH), 1677 (C=O), 1625, 1536 (N-CO-N).

^{19}F-NMR ($(CD_3)_2CO$, δ): -76 (s, 3F).

^{1}H-NMR ($(CD_3)_2CO$, δ): 1.29-1.97 (m, 14H, 7 x CH_2), 3.28 (t, *J* = 5.2 Hz, 2H, CH_2N), 3.39 (t, *J* = 5.7 Hz, 2H, CH_2N), 3.54 (t, *J* = 5.9 Hz, 2H, CH_2N), 6.34 (br s, 1H, NH), 8.58 (br s, 3H, NH_3^+).

^{13}C-NMR ($(CD_3)_2CO$, δ): 21.5 (2 x CH_2), 22.1, 25.2, 33.2 (3 x CH_2), 35.0 (2 x CH_2), 40.0, 42.9, 45.7 (3 x CH_2), 55.2 (C), 158.0 (CO).

1-[2-(1-Aminocyclohexyl)ethyl]tetrahydropyrimidin-2(1*H*)-one (21).

Free amine **21** was obtained after addition of 2 equiv of K_2CO_3 (15 mL of a 0.050 M K_2CO_3 solution in water) to its TFA salt **25** (0.19 mmol, 1 equiv) in dichloromethane (15 mL). This binary phase was stirred for 12 h at 25 ºC, extracted with dichloromethane (3 x 10 mL), dried over Na_2SO_4, and concentrated under reduced pressure to yield free amine **21** as a yellowish oil.

Yield: quantitaitive.

IR (CH_2Cl_2, cm^{-1}): 3325 (NH), 1678 (C=O), 1621, 1533 (N-CO-N).

^{1}H-NMR ($CDCl_3$, δ): 1.39-1.96 (m, 14H, 7 x CH_2), 2.39-2.43 (m, 2H, NH_2), 3.30 (t, *J* = 5.7 Hz, 2H, $C\underline{H_2}NH$), 3.44 (t, *J* = 6.0 Hz, 2H, CH_2N), 3.65 (m, 2H, CH_2N), 5.48 (br s, 1H, NH).

^{13}C-NMR ($CDCl_3$, δ): 22.1 (2 x CH_2), 23.1, 25.8 (2 x CH_2), 30.1 (2 x CH_2), 37.0, 40.6, 43.1, 45.9 (4 x CH_2), 55.9 (C), 157.4 (CO).

4.2.1.2. Synthesis of *N*-butyryl-L-tyrosine (4)

Compound **4** was synthesized according to previously described procedures and its ^{1}H-NMR spectroscopic data coincide with those previously reported.[123]

IR (CH_3OH, cm^{-1}): 3296 (NH), 1736, 1647 (C=O), 1531 (N–C=O), 1516 (NH), 1222 (ArC–O).
^{1}H-RMN (CH_3OD, δ): 0.82 (t, *J* = 7.3, 3H, CH_3), 1.53 (sx, *J* = 7.4, 2H, CH_2), 2.12 (t, *J* = 7.4, 2H, CH_2), 2.82 (dd, *J* = 14.0, 9.3, 1H, CH_2 Tyr), 3.09 (dd, *J* = 14.0, 4.9, 1H, CH_2 Tyr), 4.58 (dd, *J* = 9.1; 5.0, 1H, CH Tyr), 6.67 (d, *J* = 8.5, 2H, Ar Tyr), 7.02 (d, *J* = 8.5, 2H, Ar Tyr).
^{13}C-RMN (CH_3OD, δ): 13.9 (CH_3), 20.2 (CH_2), 37.6 (CH_2 Tyr), 38.6 (CH_2), 55.1 (CH Tyr), 116.1 (2 x CH Ar), 129.1 (C Ar), 131.2 (2 x CH Ar), 157.1 (C Ar), 175.0, 175.9 (2 x CO).

4.2.1.3. General procedure for the synthesis of *N*-acyl-*O*-(dibenzylphosphono)-L-tyrosines (5a-c) and *O*-(dibenzylphosphono)-*N*-Fmoc-L- and D-tyrosines (8a,b).

N-methylmorpholine (4.48 mmol, 1 equiv) in dry acetonitrile (0.25 mL x mmol) and *tert*-butyldimethylsilyl chloride (1 equiv) were successively added to a solution of **4**, or of the commercially available *N*-acetyl-L-tyrosine, *N*-benzoyl-L-tyrosine, *N*-Fmoc-L-tyrosine or *N*-Fmoc-D-tyrosine (1 equiv) in dry acetonitrile (2.5 mL x mmol). After 10 min at rt, dibenzyl diisopropylphosphoramidite (1.1 equiv) and a solution of 1*H*-tetrazole (3 equiv) in dry acetonitrile were added. After 3 h, the solution was cooled to -20 ºC and 70% aqueous *tert*-butyl hydroperoxide (1 equiv) was added. After 10 min, an aqueous solution of 10% $Na_2S_2O_3$ (2 mL x mmol) was added at -20 ºC. The mixture was subsequently transferred to a separating funnel, extracted with dichloromethane (6 mL x mmol), and washed again with aqueous 10% $Na_2S_2O_3$ (3 mL x mmol). The solvent was removed under reduced pressure, and the residue was dissolved in a mixture of acetic acid/THF/H_2O (2:1:1.6) and stirred for 60 min at rt. The organic solvent was evaporated under reduced pressure, and the resultant oil was redissolved in diethyl ether (40 mL) and extracted with a saturated solution of $NaHCO_3$ (3 x 10 mL). The combined aqueous layers were acidified to pH 2 with concentrated HCl, and extracted with dichloromethane (3 x 10 mL). The organic extract was dried over anhydrous Na_2SO_4, and the solvent was evaporated under reduced pressure to yield compounds **5a-c, 8a**,**b** as colourless oils.

***N*-Acetyl-*O*-[bis(benzyloxy)phosphoryl]-L-tyrosine (5a).**
Chromatography: dichloromethane → dichloromethane:methanol, 8:2. **Yield:** 77%.
Spectroscopic data coincide with those previously reported.[124]

[123] See citation 86.

[124] Llinás-Brunet, M.; Beaulieu, P. L.; Cameron, D. R.; Ferland, J.-M.; Gauthier, J.; Ghiro, E.; Gillard, J.; Gorys, V.; Poirier, M.; Rancourt, J.; Wernic, D.; Betageri, R.; Cardozo, M.; Jakes, S.; Lukas, S.; Patel, U.; Proudfoot, J.; Moss, N. *J. Med. Chem.* **1999**, *42*, 722-729.

IR (CH_2Cl_2, cm^{-1}): 3289 (NH), 1733 (OC=O), 1655 (NC=O), 1547 (N–CO), 1507 (NH), 1268, 1215 (P–OC), 1015, 960 (C–OP).

^{1}H-NMR ($CDCl_3$, δ): 1.83 (s, 3H, CH_3), 2.97 (dd, *J* = 13.9, 5.8 Hz, 1H, CH_2 Tyr), 3.16 (dd, *J* = 13.6, 3.8 Hz, 1H, CH_2 Tyr), 4.80-4.95 (m, 1H, CH Tyr), 5.05 (s, 2H, OCH_2), 5.09 (s, 2H, OCH_2), 6.64 (d, *J* = 8.3 Hz, 1H, NH), 6.92 (s, 4H, Ar Tyr), 7.28 (m, 10H, Ar), 10.50 (s, 1H, OH).

^{13}C-NMR ($CDCl_3$, δ): 22.7 (CH_3), 36.5 (CH_2 Tyr), 53.2 (CH Tyr), 70.4, 70.5 (2 x OCH_2), 120.1, 120.2 (2 x CH Ar), 128.1 (2 x CH Ar), 128.2 (2 x CH Ar), 128.7 (2 x CH Ar), 128.9 (2 x CH Ar), 130.8 (2 x CH Ar), 133.4 (2 x CH Ar), 135.0, 135.1, 149.3, 149.4 (4 x C Ar), 171.3, 173.9 (2 x CO).

***O*-[Bis(benzyloxy)phosphoryl]-*N*-butyryl-L-tyrosine (5b).**

Chromatography: dichloromethane:ethanol, 9.6:0.4 → 9:1. **Yield:** 78%.

IR (CH_2Cl_2, cm^{-1}): 3290 (NH), 1735 (OC=O), 1650 (NC=O), 1545 (N–CO), 1507 (NH), 1267, 1214 (P–OC), 1014, 1000 (C–OP).

^{1}H-NMR ($CDCl_3$, δ): 0.87 (t, *J* = 7.3 Hz, 3H, CH_3), 1.58 (sx, *J* = 7.3 Hz, 2H, CH_2), 2.13 (t, *J* = 7.3 Hz, 2H, CH_2), 3.14 (d, *J* = 4.9 Hz, 2H, CH_2 Tyr), 4.83-4.92 (m, 1H, CH Tyr), 5.09 (s, 2H, OCH_2), 5.13 (s, 2H, OCH_2), 6.43 (d, *J* = 7.0 Hz, 1H, NH), 6.98-7.09 (m, 4H, Ar Tyr), 7.32 (m, 10H, CH Ar).

^{13}C-NMR ($CDCl_3$, δ): 13.8 (CH_3), 19.1 (CH_2), 36.6 (CH_2 Tyr), 38.3 (CH_2), 53.0 (CH Tyr), 70.3, 70.4 (2 x OCH_2), 120.0, 120.1 (2 x CH Ar), 128.2 (4 x CH Ar), 128.7 (4 x CH Ar), 128.9 (2 x CH Ar), 130.9 (2 x CH Ar), 133.5, 135.2, 135.3, 149.4 (4 x C Ar), 173.0, 173.6 (2 x CO).

***N*-Benzoyl-*O*-[bis(benzyloxy)phosphoryl)-L-tyrosine (5c).**

Chromatography: dichloromethane → dichloromethane:ethanol, 9:1. **Yield:** 66%.

IR (CH_2Cl_2, cm^{-1}): 3291 (NH), 1733 (OC=O), 1640 (NC=O), 1514 (NH), 1215 (P–OC), 1016, 962 (C–OP).

^{1}H-NMR ($CDCl_3$, δ): 3.00-3.22 (m, 2H, CH_2 Tyr), 4.83-4.88 (m, 1H, CH Tyr), 4.92 (s, *2*H, OCH_2), 4.97 (s, 2H, OCH_2), 6.86 (d, *J* = 8.5 Hz, 2H, Ar Tyr), 6.95 (d, *J* = 8.4 Hz, 2H, Ar Tyr), 7.14-7.34 (m, 12H, Ar), 7.50-7.54 (m, 3H, Ar).

^{13}C-NMR ($CDCl_3$, δ): 36.5 (CH_2 Tyr), 53.9 (CH Tyr), 70.4 (2 x OCH_2), 115.7 (2 x CH Ar), 120.1 (2 x CH Ar), 126.9 (C Ar), 127.2 (4 x CH Ar), 128.2 (4 x CH Ar), 128.9 (2 x CH Ar), 130.5 (2 x CH Ar), 130.9 (2 x CH Ar), 132.1 (CH Ar), 133.4 (C Ar), 135.1 (2 x C Ar), 155.8 (C Ar), 167.9, 173.7 (2 x CO).

***O*-[Bis(benzyloxy)phosphoryl]-*N*-[(9*H*-fluoren-9-ylmethoxy)carbonyl]-L-tyrosine (8a).**

Chromatography: dichloromethane:ethanol, 9.9:0.1 → 9.6:0.4. **Yield:** 63%. **$[\alpha]_D$** -5.0 (*c* 0.5, methanol).

IR (CH_2Cl_2, cm^{-1}): 3300 (COO–H), 1720 (OC=O), 1607 (NC=O), 1507, 1451 (C_{Ar}-C_{Ar}), 1259, 1214 (P–OC), 1016, 962 (C–OP).

^{1}H-NMR ($CDCl_3$, δ): 3.06-3.07 (m, 2H, CH_2 Tyr), 3.99-4.16 (m, 1H, CH Fmoc), 4.22-4.44 (m, 2H, CH_2 Fmoc), 4.63-4.64 (m, 1H, CH Tyr), 5.01 (s, 2H, OCH_2), 5.05 (s, 2H, OCH_2), 5.42 (d, *J* = 7.8 Hz, 1H, NH), 6.96 (s, 4H, Ar Tyr), 7.19-7.35 (m, 14H, CH Ar), 7.49 (d, *J* = 7.1 Hz, 2H, CH Ar), 7.67 (d, *J* = 7.2 Hz, 2H, CH Ar).

^{13}C-NMR ($CDCl_3$, δ): 37.1 (CH_2 Tyr), 47.2 (CH Fmoc), 54.5 (CH Tyr), 66.8 (CH_2 Fmoc), 70.1, 70.3 (2 x OCH_2), 119.9 (2 x CH Ar), 125.1 (C Ar), 127.1 (2 x CH Ar), 127.7 (2 x CH Ar), 128.1 (4 x CH Ar), 128.4 (4 x CH Ar), 128.6 (2 x CH Ar), 128.7 (2 x CH Ar), 130.8 (2 x CH Ar), 133.1 (2 x C Ar), 135.1, 135.3 (2 x C Ar), 141.3 (2 x CH Ar), 143.7 (2 x C Ar), 149.4 (C Ar), 155.8, 173.4 (2 x CO).

***O*-[Bis(benzyloxy)phosphoryl]-*N*-[(9*H*-fluoren-9-ylmethoxy)carbonyl]-D-tyrosine (8b).**

Yield: 67%.

Data of this compound were identical to those reported for its enantiomer **8a** except for the specific rotation. **$[\alpha]_D$** +5.0 (*c* 0.5, methanol).

4.2.1.4. General procedure for the synthesis of *N*-acyl-*O*-(dibenzylphosphono)-L-tyrosinamides (6a-j) and *O*-(dibenzylphosphono)-*N*-Fmoc-L- and D-tyrosinamides (9a-c).

To a solution of the corresponding compound **5a-c**, **8a,b** (1 equiv) in dry dichloromethane (5 mL x mmol), were added HOBt (1.0-1.5 equiv) and EDC (1.0-1.5 equiv) and the mixture was vigorously stirred at rt for 30 min under argon atmosphere. The temperature was then lowered to 0 ºC and a solution of the appropriate amine (0.9-1.2 equiv) in dichloromethane (2 mL x mmol) was added. After 10 min the temperature was raised to rt and stirring was continued for 2 h. Then, the reaction mixture was washed with water (3 x 10 mL x mmol) and brine (3 x 10 mL x mmol), dried over anhydrous Na_2SO_4, and the solvent was removed under reduced pressure.

Alternatively, for **9c**, to a solution of amine **21** (0.20 mmol, 1 equiv) in anhydrous THF (30 mL x mmol) under argon atmosphere and vigorous stirring, a previously activated mixture of **8a** (0.23 mmol, 1.15 equiv), DIC (0.25 mmol, 1.3 equiv) and HOBt (0.25 mmol, 1.3 equiv) in anhydrous THF (10 mL x mmol **8a**) was added and left to react for 24 h at 25 ºC. The crude was then successively washed with 1 M HCl (3 x 30 mL) and brine (3 x 30 mL), dried over anhydrous Na_2SO_4, and the solvent was removed under reduced pressure.

In all cases the resultant crudes were purified by flash column chromatography to afford pure amides **6a-j** and **9a-c** as colourless oils.

***N*-Acetyl-*O*-[bis(benzyloxy)phosphoryl)-*N*-[3-(2-oxotetrahydropyrimidin-1(2*H*)-yl)propyl]-L-tyrosinamide (6a).**

Chromatography: ethyl acetate → ethyl acetate:ethanol, 9:1. **Yield:** 51%.

IR (CH_2Cl_2, cm^{-1}): 3292 (NH), 1639 (C=O), 1524 (N–CO), 1508 (NH), 1278, 1215 (P–OC), 1015, 955 (C–OP).

^{1}H-NMR ($CDCl_3$, δ): 1.45-1.54 (m, 2H, CH_2), 1.86 (qt, *J* = 5.8 Hz, 2H, CH_2), 1.97 (s, 3H, CH_3), 2.92-3.25 (m, 10H, 4 x CH_2N, CH_2 Tyr), 4.65 (dd, *J* = 14.6, 6.5 Hz, 1H, CH Tyr), 4.88 (br s, 1H, NH), 5.01 (s, 2H, OCH_2), 5.12 (s, 2H, OCH_2), 6.38 (d, *J* = 8.3 Hz, 1H, NH), 7.04 (d, *J* = 8.7 Hz, 2H, Ar Tyr), 7.13 (d, *J* = 8.5 Hz, 2H, Ar Tyr), 7.29-7.33 (m, 10H, Ar), 7.61 (t, *J* = 5.9 Hz, 1H, NH).
^{13}C-NMR ($CDCl_3$, δ): 22.1 (CH_3), 23.4, 26.6, 35.1, 37.9, 40.4, 43.6, 45.1 (7 x CH_2), 54.6 (CH Tyr), 70.0, 70.1 (2 x OCH_2), 120.0 (2 x CH Ar), 120.1 (2 x CH Ar), 128.1 (4 x CH Ar), 128.7 (4 x CH Ar), 130.8 (2 x CH Ar), 133.9, 135.5, 149.5, 149.7 (4 x C Ar), 157.0, 170.0, 170.5 (3 x CO).

***N*-Acetyl-*O*-[bis(benzyloxy)phosphoryl]-*N*-[2-(2-oxoimidazolidin-1-yl)ethyl]-L-tyrosinamide (6b).**

Chromatography: ethyl acetate:methanol, 9:1 → 7:3. **Yield:** 56%.
IR (CH_2Cl_2, cm^{-1}): 2934 (NH), 1772, 1711 (C=O), 1488, 1434 (C_{Ar}–C_{Ar}), 1509 (NH), 1213 (P–OC), 1097 (C–OP).

^{1}H-NMR ($CDCl_3$, δ): 1.73 (s, 3H, CH_3), 2.84-2.94 (m, 2H, CH_2 Tyr), 3.14-3.32 (m, 8H, 4 x CH_2N), 4.60-4.67 (m, 1H, CH Tyr), 5.01 (s, 2H, OCH_2), 5.05 (s, 2H, OCH_2), 6.50 (d, *J* = 8.4 Hz, 1H, NH), 6.96 (d, *J* = 8.4 Hz, 2H, Ar Tyr), 7.05 (d, *J* = 8.4 Hz, 2H, Ar Tyr), 7.26-7.27 (m, 10H, Ar).
^{13}C-NMR ($CDCl_3$, δ): 22.9 (CH_3), 36.9, 37.8, 38.1, 42.6, 45.1 (5 x CH_2), 53.9 (CH Tyr), 69.7, 69.9 (2 x OCH_2), 119.6 (2 x CH Ar), 119.7 (2 x CH Ar), 127.8 (4 x CH Ar), 128.4 (4 x CH Ar), 130.5 (2 x CH Ar), 133.7, 135.1, 149.5, 149.7 (4 x C Ar), 165.0, 170.0, 170.5 (3 x CO).

***N*-Acetyl-*O*-[bis(benzyloxy)phosphoryl]-*N*-[2-(1*H*-imidazol-5-yl)ethyl]-L-tyrosinamide (6c).**

Chromatography: dichloromethane → dichloromethane:methanol 9:1. **Yield:** 25%.
IR (CH_2Cl_2, cm^{-1}): 3282 (NH), 1644 (C=O), 1526 (N–CO), 1509 (NH), 1229 (P–OC), 1090 (C–OP).

^{1}H-NMR ($CDCl_3$, δ): 1.61 (s, 3H, CH_3), 2.57 (t, *J* = 6.4 Hz, 2H, CH_2), 2.87-2.91 (m, 2H, CH_2 Tyr), 3.29-3.32 (m, 2H, CH_2NH), 4.45-4.52 (m, 1H, CH Tyr), 5.02 (s, 2H, OCH_2), 5.06 (s, 2H, OCH_2), 6.35 (s, 1H, imid), 6.78-6.84 (m, 1H, NH), 6.90 (d, *J* = 7.9 Hz, 2H, Ar Tyr), 7.03 (d, *J* = 8.5 Hz, 2H, Ar Tyr), 7.26-7.27 (m, 10H, Ar), 7.39 (s, 1H, imid).
^{13}C-NMR ($CDCl_3$, δ): 21.9 (CH_3), 25.9, 37.5, 39.0 (3 x CH_2), 54.8 (CH Tyr), 69.9, 70.1 (2 x OCH_2), 116.7, 119.8, 120.0, 127.1 (4 x CH Ar), 127.4 (2 x CH Ar), 128.0 (2 x CH Ar), 128.7 (2 x CH Ar), 130.3, 132.2, 133.7, 134.3 (4 x CH Ar), 135.0 (2 x CH Ar), 135.5, 136.7, 139.9, 149.1, 149.3 (5 x C Ar), 170.1, 171.3 (2 x CO).

***N*-Acetyl-*O*-[bis(benzyloxy)phosphoryl]-*N*-[3-(2-oxopyrrolidin-1-yl)propyl]-L-tyrosinamide (6d).**

Chromatography: dichloromethane → dichloromethane:methanol, 9.5:0.5. **Yield:** 65%.

IR (CH_2Cl_2, cm^{-1}): 3278 (NH), 1660 (C=O), 1548 (N–CO), 1508 (NH), 1283, 1216 (P–OC), 1016, 956 (C–OP).

^{1}H-NMR ($CDCl_3$, δ): 1.51-1.52 (m, 2H, CH_2), 1.90-1.95 (m, 2H, CH_2), 1.93 (s, 3H, CH_3), 2.27 (t, *J* = 8.1 Hz, 2H, CH_2CO), 2.97-3.27 (m, 8H, 3 x CH_2N, CH_2 Tyr), 4.61-4.64 (m, 1H, CH Tyr), 5.05 (s, 2H, OCH_2), 5.08 (s, 2H, OCH_2), 6.76-6.78 (m, 1H, NH), 7.02 (d, *J* = 8.5 Hz, 2H, Ar Tyr), 7.12 (d, *J* = 8.5 Hz, 2H, Ar Tyr), 7.28-7.34 (m, 10H, Ar).

^{13}C-NMR ($CDCl_3$, δ): 17.8 (CH_2), 23.1 (CH_3), 26.4, 30.8, 35.6, 37.5, 39.3, 47.2 (6 x CH_2), 54.6 (CH Tyr), 69.9, 70.0 (2 x OCH_2), 119.9 (2 x CH Ar), 128.0 (4 x CH Ar), 128.6 (6 x CH Ar), 130.6 (2 x CH Ar), 134.0, 135.3, 149.3, 149.5 (4 x C Ar), 170.3, 170.9, 175.7 (3 x CO).

***O*-[Bis(benzyloxy)phosphoryl]-*N*-butyryl-*N*-[3-(2-oxotetrahydropyrimidin-1(2*H*)-yl)propyl]-L-tyrosinamide (6e).**

Chromatography: dichloromethane → dichloromethane:ethanol, 9.5:0.5. **Yield:** 80%.

IR (CH_2Cl_2, cm^{-1}): 3289 (NH), 1644 (C=O), 1508 (NH), 1277, 1215 (P–OC), 1015, 953 (C–OP).

^{1}H-NMR ($CDCl_3$, δ): 0.71 (t, *J* = 7.6 Hz, 3H, CH_3), 1.34-1.48 (m, 4H, 2 x CH_2), 1.70-1.73 (m, 2H, CH_2), 2.00 (t, *J* = 7.01 Hz, 2H, CH_2), 2.77-3.11 (m, 10H, 4 x CH_2N, CH_2 Tyr), 4.46-4.47 (m, 1H, CH Tyr), 4.91 (s, 2H, OCH_2), 4.95 (s, 2H, OCH_2), 6.21 (d, *J* = 7.9 Hz, 1H, NH), 6.88 (d, *J* = 8.5 Hz, 2H, Ar Tyr), 6.97 (d, *J* = 8.6 Hz, 2H, Ar Tyr), 7.12-7.16 (m, 10H, Ar), 7.30 (br s, 1H, NH).

^{13}C-NMR ($CDCl_3$, δ): 13.8 (CH_3), 19.0, 21.8, 26.6, 35.3, 37.9, 38.4, 40.2, 44.0, 45.0 (9 x CH_2), 54.5 (CH Tyr), 70.1 (2 x OCH_2), 120.0 (2 x CH Ar), 127.6 (2 x CH Ar), 128.1 (2 x CH Ar), 128.5 (2 x CH Ar), 128.6 (2 x CH Ar), 128.7 (2 x CH Ar), 129.5 (2 x CH Ar), 134.0, 135.5 (2 x C Ar), 149.4 (2 x C Ar), 157.0, 170.8, 173.0 (3 x CO).

***O*-[Bis(benzyloxy)phosphoryl]-*N*-butyryl-*N*-[2-(2-oxoimidazolidin-1-yl)ethyl]-L-tyrosinamide (6f).**

Chromatography: dichloromethane:ethanol, 9.7:0.3 → 9.5:0.5. **Yield:** 40%.

IR (CH_2Cl_2, cm^{-1}): 3287 (NH), 1647 (C=O), 1545 (N–CO), 1506 (NH), 1273, 1214 (P–OC), 1015, 955 (C–OP).

^{1}H-NMR ($CDCl_3$, δ): 0.78 (t, *J* = 7.3 Hz, 3H, CH_3), 1.50 (sx, *J* = 7.4 Hz, 2H, CH_2), 2.08 (t, *J* = 7.2 Hz, 2H, CH_2CO), 2.96 (d, *J* = 6.6 Hz, 2H, CH_2 Tyr), 3.15-3.40 (m, 8H, 4 x CH_2N), 4.58-4.66 (m, 1H, CH Tyr), 5.01 (s, 2H, OCH_2), 5.05 (s, 2H, OCH_2), 6.36 (d, *J* = 8.2 Hz, 1H, NH), 6.93 (d, *J* = 8.3 Hz, 2H, Ar Tyr), 7.06 (d, *J* = 8.6 Hz, 2H, Ar Tyr), 7.21-7.30 (m, 10H, Ar).

^{13}C-NMR ($CDCl_3$, δ): 13.5 (CH_3), 18.8, 29.5, 37.1, 37.8, 38.1, 42.7, 45.1 (7 x CH_2), 53.7 (CH Tyr), 69.7, 69.8 (2 x OCH_2), 119.6 (2 x CH Ar), 119.7 (2 x CH Ar), 127.8 (4 x CH Ar), 128.4 (4 x CH Ar), 130.5 (2 x CH Ar), 133.7 (C Ar), 135.3 (2 x C Ar), 149.2 (C Ar), 163.2, 171.2, 172.9 (3 x CO).

***O*-[Bis(benzyloxy)phosphoryl]-*N*-butyryl-*N*-[3-(2-oxopyrrolidin-1-yl)propyl]-L-tyrosinamide (6g).**

Chromatography: ethyl acetate:ethanol, 9.7:0.3 → 9.4:0.6. **Yield:** 68%.

IR (CH_2Cl_2, cm^{-1}): 3292 (NH), 1650 (C=O), 1542 (N–CO), 1507 (NH), 1277, 1214 (P–OC), 1015, 955 (C–OP).

^{1}H-NMR ($CDCl_3$, δ): 0.71 (t, *J* = 7.4 Hz, 3H, CH_3), 1.34-1.53 (m, 4H, 2 x CH_2), 1.87 (sx, *J* = 7.4 Hz, 2H, CH_2), 2.01 (td, *J* = 7.5, 2.5 Hz, 2H, CH_2NH), 2.17 (t, *J* = 8.1 Hz, 2H, CH_2CO), 2.79-3.16 (m, 8H, 2 x CH_2N, CH_2 Tyr, CH_2CO), 4.50-4.51 (m, 1H, CH Tyr), 4.91 (s, 2H, OCH_2), 4.95 (s, 2H, OCH_2), 6.07 (d, *J* = 8.0 Hz, 1H, NH), 6.88 (d, *J* = 8.6 Hz, 2H, Ar Tyr), 6.98 (d, *J* = 8.8 Hz, 2H, Ar Tyr), 7.11-7.19 (m, 10H, Ar).

^{13}C-NMR ($CDCl_3$, δ): 13.5 (CH_3), 17.7, 18.7, 26.2, 30.6, 35.2, 37.5, 38.2, 39.0, 47.0 (9 x CH_2), 54.1 (CH Tyr), 69.7, 69.8 (2 x OCH_2), 119.8, 119.9 (2 x CH Ar), 127.8 (4 x CH Ar), 128.4 (2 x CH Ar), 128.5 (4 x CH Ar), 130.4 (2 x CH Ar), 133.6, 135.2, 135.3, 149.3 (4 x C Ar), 170.6, 172.7, 175.6 (3 x CO).

***N*-Benzoyl-*O*-[bis(benzyloxy)phosphoryl]-*N*-[3-(2-oxotetrahydropyrimidin-1(2*H*)-yl)propyl]-L-tyrosinamide (6h).**

Chromatography: ethyl acetate:ethanol, 9.8:0.2 → 9:1. **Yield:** 30%.

IR (CH_2Cl_2, cm^{-1}): 3292 (NH), 1639 (C=O), 1524 (N–CO), 1508 (NH), 1278, 1215 (P–OC), 1015, 955 (C–OP).

^{1}H-NMR ($CDCl_3$, δ): 1.42-1.64 (m, 2H, CH_2), 1.83 (qt, *J* = 5.5 Hz, 2H, CH_2), 3.05-3.30 (m, 10H, 4 x CH_2N, CH_2 Tyr), 4.82-4.92 (m, 1H, CH Tyr), 5.05 (s, 2H, OCH_2), 5.09 (s, 2H, OCH_2), 7.04 (d, *J* = 8.5 Hz, 2H, Ar Tyr), 7.17 (d, *J* = 8.3 Hz, 2H, Ar Tyr), 7.27-7.49 (m, 13H, Ar), 7.64 (br t, *J* = 5.7 Hz, 1H, NH), 7.77 (dd, *J* = 6.3, 1.6 Hz, 2H, Ar).

^{13}C-NMR ($CDCl_3$, δ): 21.8, 26.5, 35.3, 38.0, 40.1, 43.7, 44.9 (7 x CH_2), 54.9 (CH Tyr), 69.8, 69.9 (2 x OCH_2), 119.8 (2 x CH Ar), 127.1 (2 x CH Ar), 127.9 (4 x CH Ar), 128.4 (2 x CH Ar), 128.5 (6 x CH Ar), 130.7 (2 x CH Ar), 131.4 (CH Ar), 133.8, 134.1, 135.3, 135.5, 149.2 (5 x C Ar), 166.8 (CO), 170.3 (2 x CO).

***N*-Benzoyl-*O*-[bis(benzyloxy)phosphoryl]-*N*-[2-(2-oxoimidazolidin-1-yl)ethyl]-L-tyrosinamide (6i).**

Chromatography: dichloromethane:ethanol, 9.8:0.2 → 9.5:0.5. **Yield:** 35%.

IR (CH_2Cl_2, cm^{-1}): 3295 (NH), 1688, 1655 (C=O), 1540 (N–CO), 1509 (NH), 1276, 1217 (P–OC), 1017, 958 (C–OP).

^{1}H-NMR ($CDCl_3$, δ): 3.14-3.45 (m, 10H, 4 x CH_2N, CH_2 Tyr), 4.17 (br s, 1H, NH), 4.80-5.00 (m, 1H, CH Tyr), 5.06 (s, 2H, OCH_2), 5.10 (s, 2H, OCH_2), 7.02 (d, *J* = 7.8 Hz, 2H, Ar Tyr), 7.16 (d, *J* = 8.3 Hz, 2H, Ar Tyr), 7.24-7.35 (m, 13H Ar), 7.78 (d, *J* = 6.8 Hz, 2H, Ar).

^{13}C-NMR ($CDCl_3$, δ): 37.2, 37.9, 38.2, 42.8, 45.2 (5 x CH_2), 54.5 (CH Tyr), 69.8, 70.0 (2 x OCH_2), 119.7, 119.8 (2 x CH Ar), 127.1 (2 x CH Ar), 127.9 (4 x CH Ar), 128.4 (2 x CH Ar), 128.5

(2 x CH Ar), 128.6 (4 x CH Ar), 130.7 (2 x CH Ar), 131.6 (CH Ar), 133.8 (2 x C Ar), 135.3 (2 x C Ar), 149.2 (C Ar), 167.1 (CO), 171.1 (2 x CO).

***N*-Benzoyl-*O*-[bis(benzyloxy)phosphoryl]-*N*-[3-(2-oxopyrrolidin-1-yl)propyl]-L-tyrosinamide (6j).**

Chromatography: ethyl acetate → ethyl acetate:ethanol, 9:1. **Yield:** 42%.

IR (CH_2Cl_2, cm^{-1}): 3290 (NH), 1654 (C=O), 1537 (N–CO), 1508 (NH), 1276, 1215 (P–OC), 1015, 956 (C–OP).

^{1}H-NMR ($CDCl_3$, δ): 1.57 (qt, *J* = 6.6 Hz, 2H, CH_2), 1.98 (qt, *J* = 6.6 Hz, 2H, CH_2), 2.34 (t, *J* = 7.8 Hz, 2H, CH_2), 3.05-3.19 (m, 6H, 3 x CH_2), 3.30 (t, *J* = 6.6 Hz, 2H, CH_2), 4.86-4.88 (m, 1H, CH Tyr), 5.07 (s, 2H, OCH_2), 5.11 (s, 2H, OCH_2), 7.06 (d, *J* = 8.5 Hz, 2H, Ar Tyr), 7.11 (br s, 1H, NH), 7.20 (d, *J* = 8.3 Hz, 2H, Ar Tyr), 7.32-7.52 (m, 13H, Ar), 7.78 (m, 2H, Ar).

^{13}C-NMR ($CDCl_3$, δ): 17.9, 26.4, 30.8, 35.6, 37.9, 39.3, 47.3 (7 x CH_2), 55.0 (CH Tyr), 69.9, 70.0 (OCH_2), 120.0, 120.1 (2 x CH Ar), 127.2 (2 x CH Ar), 128.0 (4 x CH Ar), 128.5 (2 x CH Ar), 128.6 (4 x CH Ar), 128.7 (2 x CH Ar), 130.7 (2 x CH Ar), 131.7 (CH Ar), 133.7, 133.9, 135.3, 135.6, 149.5 (5 x C Ar), 167.0, 170.7, 175.9 (3 x CO).

***O*-[Bis(benzyloxy)phosphoryl]-*N*-[(9*H*-fluoren-9-ylmethoxy)carbonyl]-*N*-[3-(2-oxotetrahydropyrimidin-1(2*H*)-yl)propyl]-L-tyrosinamide (9a).**

Chromatography: dichloromethane → dichloromethane:ethanol, 9.8:0.2. **Yield:** 55%.

$[\alpha]_D$ -11.2 (*c* 1.0, methanol).

IR (CH_2Cl_2, cm^{-1}): 3361 (NH), 1737 (C=O), 1260 (P–OC), 1030 (C–OP).

^{1}H-NMR ($CDCl_3$, δ): 1.48-1.51 (m, 2H, CH_2), 1.80-1.86 (m, 2H, CH_2), 2.95-3.18 (m, 10H, 4 x CH_2N, CH_2 Tyr), 4.14 (t, *J* = 7.1 Hz, 1H, CH Fmoc), 4.27-4.31 (m, 3H, CH_2 Fmoc, CH Tyr), 4.65 (br s, 1H, NH), 5.01 (s, 2H, OCH_2), 5.06 (s, 2H, OCH_2), 5.53 (d, *J* = 8.5 Hz, 1H, NH), 6.99 (d, *J* = 8.2 Hz, 2H, Ar Tyr), 7.13 (d, *J* = 7.8 Hz, 2H, Ar Tyr), 7.19-7.32 (m, 14H, Ar), 7.50-7.56 (m, 3H, Ar, NH), 7.68 (d, *J* = 7.3 Hz, 2H, Ar).

^{13}C-NMR ($CDCl_3$, δ): 22.1, 26.6, 35.4, 38.5, 40.5, 43.9, 45.1 (7 x CH_2), 47.2 (CH Fmoc), 56.5 (CH Tyr), 67.1 (CH_2 Fmoc), 70.5 (2 x OCH_2), 120.0 (2 x CH Ar), 121.0 (2 x CH Ar), 125.3 (2 x CH Ar), 127.2 (2 x CH Ar), 127.8 (2 x CH Ar), 128.3 (4 x CH Ar), 128.7 (6 x CH Ar), 130.7 (2 x CH Ar), 133.9 (C Ar), 135.6 (2 x C Ar), 141.1 (2 x C Ar), 143.9 (2 x C Ar), 149.5 (C Ar), 155.8 (CO), 170.4 (2 x CO).

***O*-[Bis(benzyloxy)phosphoryl]-*N*-[(9*H*-fluoren-9-ylmethoxy)carbonyl]-*N*-[3-(2-oxotetrahydropyrimidin-1(2*H*)-yl)propyl]-D-tyrosinamide (9b).**

Yield: 81%. Data of this compound were identical to those reported for its enantiomer **9a** except for the specific rotation. **$[\alpha]_D$** +11.2 (*c* 1.0, methanol).

***O*-[Bis(benzyloxy)phosphoryl]-*N*-[(9*H*-fluoren-9-ylmethoxy)carbonyl]-*N*-{1-[2-(2-oxotetrahydropyrimidin-1(2*H*)-yl)ethyl]cyclohexyl}-L-tyrosinamide (9c).**

Chromatography: dichloromethane → dichloromethane:ethanol, 9.5:0.5. **Yield:** 50%.

IR (CH_2Cl_2, cm^{-1}): 3295 (NH), 1709, 1664, 1632 (C=O), 1525 (N–CO), 1261 (P–OC), 1017 (C–OP).

^{1}H-NMR ($CDCl_3$, δ): 1.44-1.69 (m, 14H, 7 x CH_2), 2.34-3.23 (m, 8H, 3 x CH_2N, CH_2 Tyr), 3.64 (br s, 1H, NH), 4.14-4.41 (m, 4H, CH Fmoc, CH_2 Fmoc, CH Tyr), 5.09 (s, 2H, OCH_2), 5.31 (s, 2H, OCH_2), 5.37 (br s, 1H, NH), 7.07-7.26 (m, 4H, Ar Tyr), 7.33-7.36 (m, 14H, Ar), 7.38-7.74 (m, 5H, 4 x Ar, NH).

^{13}C-NMR ($CDCl_3$, δ): 21.7, 21.9, 22.8, 25.6 (4 x CH_2), 29.8 (2 x CH_2), 35.0, 37.9, 40.3, 43.0, 45.2 (5 x CH_2), 47.2 (CH Fmoc), 53.6 (C), 55.7 (CH Tyr), 67.2 (CH_2 Fmoc), 70.0, 70.1 (2 x OCH_2), 120.1 (2 x CH Ar), 120.2 (2 x CH Ar), 125.2 (C Ar), 127.2 (2 x CH Ar), 127.8 (2 x CH Ar), 128.1 (4 x CH Ar), 128.5 (6 x CH Ar), 130.8 (2 x CH Ar), 134.1 (2 x C Ar), 135.5 (2 x C Ar), 141.4 (2 x CH Ar), 143.9 (2 x C Ar), 149.5 (C Ar), 156.3 (CO), 171.9 (2 x CO).

4.2.1.5. General procedure for the synthesis of *N*-Acetyl-*O*-[bis(benzyloxy)phosphoryl]-*N*-[3-(2-oxotetrahydropyrimidin-1(2*H*)-yl)propyl]tyrosinamides (10a-c).

To a solution containing the corresponding amide **9a-c** (1 equiv) in dry acetonitrile at 0 ºC, piperidine (13.5 equiv) was added dropwise under argon atmosphere. The solution was stirred for 2 h at rt. The reaction mixture was evaporated to dryness, the residue redissolved in dimethylformamide (7.5 mL x mmol) and *N*,*N*-diisopropylethylamine (DIPEA, 2 equiv) and acetic anhydride (2 equiv) were added. The reaction was stirred for 3 h at rt. Finally, the solvent was removed under reduced pressure and the resulting crude mixture was resuspended in ethyl acetate and sequentially washed with 1 M HCl (3 x 30 mL) and brine (3 x 30 mL). The organic extract was dried over anhydrous Na_2SO_4 and the solvent evaporated under reduced pressure. The crudes were purified by flash column chromatography to afford pure target compunds **10a-c** as oils.

***N*-Acetyl-*O*-[bis(benzyloxy)phosphoryl]-*N*-[3-(2-oxotetrahydropyrimidin-1(2*H*)-yl)propyl]-L-tyrosinamide (10a).**

Chromatography: dichloromethane:ethanol, 9.7:0.3 → 9.3:0.7. **Yield:** 47%. Data of this compound were identical to those reported for **6a** except for the specific rotation. **$[\alpha]_D$** +1.2 (*c* 1.0, methanol).

***N*-Acetyl-*O*-[bis(benzyloxy)phosphoryl]-*N*-[3-(2-oxotetrahydropyrimidin-1(2*H*)-yl)propyl]-D-tyrosinamide (10b).**

Chromatography: dichloromethane:ethanol, 9.7:0.3 → 9.3:0.7. **Yield:** 75%. Data of this compound were identical to those reported for its enantiomer **6a** except for the specific rotation. **$[\alpha]_D$** -1.1 (*c* 1.0, methanol).

***N*-Acetyl-*O*-[bis(benzyloxy)phosphoryl]-*N*-{1-[2-(2-oxotetrahydropyrimidin-1(2*H*)-yl)ethyl]cyclohexyl}-L-tyrosinamide (10c).**

Chromatography: dichloromethane:ethanol, 9.9:0.1→ 9.2:0.8. **Yield:** 66%.

IR (CH_2Cl_2, cm^{-1}): 3315 (NH), 1728, 1653 (C=O), 1539 (N–CO), 1234 (P–OC), 1088 (P=O).

^{1}H-NMR ($CDCl_3$, δ): 1.40-2.22 (m, 17H, 7 x CH_2, CH_3), 2.97-3.37 (m, 8H, 3 x CH_2N, CH_2 Tyr), 4.61-4.69 (m, 2H, CH Tyr, NH), 5.07 (s, 2H, OCH_2), 5.10 (s, 2H, OCH_2), 6.12 (br s, 1H, NH), 6.79 (d, *J* = 8.1 Hz, 1H, NH), 7.05 (d, *J* = 6.0 Hz, 2H, Ar Tyr), 7.18 (d, *J* = 6.0 Hz, 2H, Ar Tyr), 7.27-7.32 (m, 10H, Ar).

^{13}C-NMR ($CDCl_3$, δ): 21.6 (2 x CH_2), 22.1 (CH_2), 23.2 (CH_3), 25.5, 34.4, 34.9 (3 x CH_2), 37.3 (2 x CH_2), 40.4, 42.6, 45.2 (3 x CH_2), 54.8 (CH Tyr), 55.6 (C), 69.9, 70.0 (2 x OCH_2), 119.9 (2 x CH Ar), 128.0 (4 x CH Ar), 128.6 (6 x CH Ar), 130.7 (2 x CH Ar), 134.2, 135.4, 135.5, 149.4 (4 x C Ar), 156.0, 170.2, 170.3 (3 x CO).

4.2.1.6. General procedure for the synthesis of *N*-acyl-*O*-phosphonotyrosinamides (1a-l).

To a solution of the corresponding amide **6a-j** or **10a-c** (1 equiv) in absolute ethanol (10 mL x mmol), 10% Pd(C) was added (200 mg x mmol), and the suspension was hydrogenated at rt at an initial pressure of 45 psi, until disappearance of the starting benzylated amide (TLC). The reaction mixture was filtered over celite and the solvent was removed under reduced pressure to yield the pure debenzylated amides **1a-l**, which were then recrystallized from the appropriate solvent(s).

***N*-Acetyl-*N*-[3-(2-oxotetrahydropyrimidin-1(2*H*)-yl)propyl]-*O*-phosphono-L-tyrosinamide (1a).**

Yield: 71%; **mp:** 141-143 ºC (dichloromethane/methanol); **$[\alpha]_D$** +0.5 (*c* 1.0, methanol).

IR (CH_3OH, cm^{-1}): 3275 (NH), 1644 (C=O), 1535 (N–CO), 1509 (NH), 1221 (P–OC), 1025, 956 (C–OP).

^{1}H-NMR (CD_3OD, δ): 1.59 (t, *J* = 7.0 Hz, 2H, CH_2), 1.86-1.93 (m, 2H, CH_2), 1.92 (s, 3H, CH_3), 2.78-3.35 (m, 10H, 4 x CH_2N, CH_2 Tyr), 4.46 (t, *J* = 6.5 Hz, 1H, CH Tyr), 7.14-7.15 (m, 4H, Ar Tyr).

^{13}C-NMR (CD_3OD, δ): 22.5 (CH_3), 23.0, 28.2, 37.5, 38.3, 41.1, 45.7, 46.5 (7 x CH_2), 56.8 (CH Tyr), 121.4 (2 x CH Ar), 131.0 (2 x CH Ar), 133.1, 158.8 (2 x C Ar), 173.3 (CO), 173.6 (2 x CO).

MS (ESI) 441.9 $(M-H)^-$. **Anal**. **Calcd. for** $C_{18}H_{27}N_4O_7P$: C, 48.87; H, 6.15; N, 12.66. **Found**: C, 48.23; H, 5.99; N, 12.17.

***N*-Acetyl-*N*-[2-(2-oxoimidazolidin-1-yl)ethyl]-*O*-phosphono-L-tyrosinamide (1b).**

Yield: 91%; **mp:** 105-108 ºC (dichloromethane/methanol); **$[\alpha]_D$** +1.5 (*c* 1.0, methanol).

IR (CH_3OH, cm^{-1}): 3261 (NH), 1654 (C=O), 1542 (N–CO), 1508 (NH), 1271, 1228 (P–OC), 1080, 1025 (C–OP).

^{1}H-NMR (CD_3OD, δ): 1.90 (s, 3H, CH_3), 2.83-3.10 (m, 2H, CH_2), 3.21-3.42 (m, 8H, 4 x CH_2N), 4.47-4.55 (m, 1H, CH Tyr), 7.11 (d, *J* = 8.4 Hz, 2H, Ar Tyr), 7.35 (d, *J* = 8.4 Hz, 2H, Ar Tyr).

^{13}C-NMR (CD_3OD, δ): 22.3 (CH_3), 38.1, 38.6, 39.2, 43.9, 46.4 (5 x CH_2), 56.4 (CH Tyr), 121.5 (2 x CH Ar), 131.0 (2 x CH Ar), 133.1, 153.3 (2 x C Ar), 165.4, 173.2, 173.8 (3 x CO).

MS (ESI) 413.3 $(M-H)^-$. **Anal. Calcd. for** $C_{16}H_{23}N_4O_7P$: C, 46.38; H, 5.59; N, 13.52. **Found**: C, 45.97; H, 5.99; N, 13.21.

***N*-Acetyl-*N*-[2-(1*H*-imidazol-5-yl)ethyl]-*O*-phosphono-L-tyrosinamide (1c).**

Yield: 34%; **mp:** 81-83 ºC (ethanol/water); **$[\alpha]_D$** -0.5 (*c* 0.6, methanol)

IR (CH_3OH, cm^{-1}): 3282 (NH), 1644 (C=O), 1526 (N–CO), 1509 (NH), 1229 (P–OC), 1090 (C–OP).

^{1}H-NMR (D_2O, δ): 1.82 (s, 3H, CH_3), 2.56 (t, *J* = 6.4 Hz, 2H, CH_2), 2.70-2.87 (m, 2H, CH_2N), 3.13-3.18 (m, 1H, ½ CH_2 Tyr), 3.28-3.35 (m, 1H, ½ CH_2 Tyr), 4.23-4.25 (m, 1H, CH Tyr), 6.82 (s, 1H, imid), 6.93 (d, *J* = 9.6 Hz, 2H, Ar Tyr), 7.03 (d, *J* = 8.0 Hz, 2H, Ar Tyr), 7.22-7.31 (m, 1H, imid), 8.56 (s, 1H, NH).

^{13}C-NMR (CD_3OD, δ): 21.9 (CH_3), 23.9, 36.6, 37.7 (3 x CH_2), 55.8 (CH Tyr), 116.1 (CH Ar), 120.7 (2 x CH Ar), 130.5 (2 x CH Ar), 130.8, 132.0 (2 x C Ar), 133.3 (CH Ar), 151.1 (C Ar), 173.5, 174.2 (2 x CO).

MS (ESI) 577.1 $(M+H)^+$. **Anal. Calcd. for** $C_{16}H_{21}N_4O_6P$: C, 48.49; H, 5.34; N, 14.14. **Found**: C, 47.98; H, 5.62; N, 13.97.

***N*-Acetyl-*N*-[3-(2-oxopyrrolidin-1-yl)propyl]-*O*-phosphono-L-tyrosinamide (1d).**

Yield: 93%; **mp:** 77-79 ºC (dichloromethane/ethanol); **$[\alpha]_D$** +2.7 (*c* 1.0, methanol).

IR (CH_3OH, cm^{-1}): 3279 (NH), 1650 (C=O), 1549 (N–CO), 1508 (NH), 1294, 1219 (P–OC), 1025, 960 (C–OP).

^{1}H-NMR (CD_3OD, δ): 1.46-1.49 (m, 2H, CH_2), 1.75 (s, 3H, CH_3), 1.89-1.92 (m, 2H, CH_2), 2.21 (t, *J* = 8.0 Hz, 2H, CH_2CO), 2.64-3.15 (m, 8H, 3 x CH_2N, CH_2 Tyr), 4.32-4.35 (m, 1H, CH Tyr), 6.95 (d, *J* = 8.5 Hz, 2H, Ar Tyr), 7.05 (d, *J* = 8.4 Hz, 2H, Ar Tyr).

^{13}C-NMR (CD_3OD, δ): 19.0 (CH_2), 22.7 (CH_3), 27.8, 32.2, 37.7, 38.4, 41.2, 48.8 (6 x CH_2), 56.8 (CH Tyr), 121.4 (2 x CH Ar), 131.6 (2 x CH Ar), 135.0, 152.0 (2 x C Ar), 173.4, 173.6, 178.2 (3 x CO).

MS (ESI) 370.1 $(M-CH_3CONH)$, 426.4 $(M-H)^-$. **Anal. Calcd. for** $C_{18}H_{26}N_3O_7P$: C, 50.58; H, 6.13; N, 9.83. **Found**: C, 50.93; H, 6.46; N, 9.84.

***N*-Butyryl-*N*-[3-(2-oxotetrahydropyrimidin-1(2*H*)-yl)propyl]-*O*-phosphono-L-tyrosinamide (1e).**

Yield: 90%; **mp:** 87-89 ºC (dichloromethane/ethanol); **$[\alpha]_D$** -0.7 (*c* 1.0, methanol).

IR (CH_3OH, cm^{-1}): 3299 (NH), 1641 (C=O), 1536 (N–CO), 1508 (NH), 1220 (P–OC), 1024 (C–OP).

^{1}H-NMR (CD_3OD, δ): 0.85 (t, *J* = 7.5 Hz, 3H, CH_3), 1.44-1.66 (m, 4H, 2 x CH_2), 1.83-1.93 (m, 2H, CH_2), 2.16 (t, *J* = 7.2 Hz, 2H, CH_2), 2.61-2.92 (m, 2H, CH_2 Tyr), 3.00-3.25 (m, 8H, 4 x CH_2N), 4.51 (t, *J* = 7.6 Hz, 1H, CH Tyr), 7.13 (d, *J* = 9.0 Hz, 2H, Ar Tyr), 7.21 (d, *J* = 8.8 Hz, 2H, Ar Tyr).

^{13}C-NMR (CD_3OD, δ): 12.5 (CH_3), 18.5, 21.5, 26.8, 35.8, 36.5, 36.9, 39.0, 44.0, 45.3 (9 x CH_2), 54.9 (CH Tyr), 120.0 (2 x CH Ar), 129.7 (2 x CH Ar), 133.0, 151.0 (2 x C Ar), 172.4, 173.6, 177.1 (3 x CO).

MS (ESI) 469.6 $(M-H)^-$. **Anal. Calcd. for** $C_{20}H_{31}N_4O_7P$: C, 51.06; H, 6.64; N, 11.91. **Found**: C, 51.64; H, 6.96; N, 11.55.

***N*-Butyryl-*N*-[2-(2-oxoimidazolidin-1-yl)ethyl]-*O*-phosphono-L-tyrosinamide (1f).**

Yield: 90%; **mp:** 143-145 ºC (dichloromethane/ethanol); **$[\alpha]_D$** -0.4 (*c* 0.5, methanol).

IR (CH_3OH, cm^{-1}): 3281 (NH), 1654 (C=O), 1541 (N–CO), 1507 (NH), 1273, 1227 (P–OC), 1080 (C–OP).

^{1}H-NMR (CD_3OD, δ): 0.39 (t, *J* = 7.3 Hz, 3H, CH_3), 1.47-1.59 (m, 2H, CH_2), 2.15 (t, *J* = 7.3 Hz, 2H, CH_2), 2.76-3.65 (m, 10H, 4 x CH_2N, CH_2 Tyr), 4.49-4.57 (m, 1H, CH Tyr), 7.13 (d, *J* = 9.0 Hz, 2H, Ar Tyr), 7.19 (d, *J* = 8.8 Hz, 2H, Ar Tyr).

^{13}C-NMR (CD_3OD, δ): 13.3 (CH_3), 20.0, 37.7, 38.2, 38.3, 38.8, 43.4, 46.0 (7 x CH_2), 55.8 (CH Tyr), 121.0 (2 x CH Ar), 130.6 (2 x CH Ar), 133.0, 152.0 (2 x C Ar), 165.0, 173.5, 175.5 (3 x CO).

MS (ESI) 441.7 $(M-H)^-$. **Anal. Calcd. for** $C_{18}H_{27}N_4O_7P$: C, 48.87; H, 6.15; N, 12.66. **Found**: C, 48.32; H, 6.40; N, 12.22.

***N*-Butyryl-*N*-[3-(2-oxopyrrolidin-1-yl)propyl]-*O*-phosphono-L-tyrosinamide (1g).**

Yield: 90%; **mp:** 99-102 ºC (dichloromethane/ethanol); **$[\alpha]_D$** -1.2 (*c* 1.0, methanol).

IR (CH_3OH, cm^{-1}): 3272 (NH), 1649 (C=O), 1544 (N–CO), 1508 (NH), 1292, 1220 (P–OC), 1017, 957 (C–OP).

^{1}H-NMR (CD_3OD, δ): 0.85 (t, *J* = 6.7 Hz, 3H, CH_3), 1.45-1.67 (m, 4H, 2 x CH_2), 2.04 (t, *J* = 6.8 Hz, 2H, CH_2CO), 2.17 (t, *J* = 6.4 Hz, 2H, CH_2CO), 2.38 (t, *J* = 7.6 Hz, 2H, CH_2), 2.81-3.21 (m, 6H, 2 x CH_2, CH_2 Tyr), 3.42 (t, *J* = 5.7 Hz, 2H, CH_2), 4.52 (t, *J* = 6.8 Hz, 1H, CH Tyr), 7.13 (d, *J* = 7.8 Hz, 2H, Ar Tyr), 7.21 (d, *J* = 7.8 Hz, 2H, Ar Tyr).

^{13}C-NMR (CD_3OD, δ): 12.3 (CH_3), 17.0, 18.6, 26.0, 30.8, 36.0, 37.0, 37.2, 39.8, 48.0 (9 x CH_2), 54.9 (CH Tyr), 120.0 (2 x CH Ar), 130.0 (2 x CH Ar), 131.0, 150.9 (2 x C Ar), 172.0, 174.5, 176.2 (3 x CO).

MS (ESI) 454.5 $(M-H)^-$. **Anal. Calcd. for** $C_{20}H_{30}N_3O_7P$: C, 52.74; H, 6.64; N, 9.23. **Found**: C, 52.35; H, 6.44; N, 9.13.

***N*-Benzoyl-*N*-[3-(2-oxotetrahydropyrimidin-1(2*H*)-yl)propyl]-*O*-phosphono-L-tyrosinamide (1h).**

Yield: 80%; **mp:** 174-177 ºC (dichloromethane/methanol); **$[\alpha]_D$** -0.4 (*c* 0.8, methanol).

IR (CH_3OH, cm^{-1}): 3293 (NH), 1636 (C=O), 1535 (N–CO), 1509 (NH), 1224 (P–OC), 956 (C–OP).

^{1}H-NMR (CD_3OD, δ): 1.63 (qt, *J* = 6.3 Hz, 2H, CH_2), 1.90 (qt, *J* = 5.6 Hz, 2H, CH_2), 2.98-3.27 (m, 10H, 4 x CH_2N, CH_2 Tyr), 4.71 (t, *J* = 7.7 Hz, 1H, CH Tyr), 7.14 (d, *J* = 8.5 Hz, 2H, Ar Tyr), 7.26 (d, *J* = 7.8 Hz, 2H, Ar Tyr), 7.40-7.52 (m, 3H, Ar), 7.76 (d, *J* = 6.8 Hz, 2H, Ar).

^{13}C-NMR ($(CD_3)_2SO$, δ): 22.0, 27.3, 36.2, 36.6, 41.1, 44.2, 45.0 (7 x CH_2), 55.3 (CH Tyr), 119.5 (2 x CH Ar), 127.5 (2 x CH Ar), 128.2 (2 x CH Ar), 130.0 (2 x CH Ar), 131.3 (CH Ar), 133.4, 134.2, 150.5 (3 x C Ar), 155.6, 166.4, 171.1 (3 x CO).

MS (ESI) 503.4 $(M-H)^-$. **Anal. Calcd. for** $C_{23}H_{29}N_4O_7P$: C, 54.76; H, 5.79; N, 11.11. **Found**: C, 54.42; H, 5.84; N, 10.95.

***N*-Benzoyl-*N*-[2-(2-oxoimidazolidin-1-yl)ethyl]-*O*-phosphono-L-tyrosinamide (1i).**

Yield: 78%; **mp:** 137-139 ºC (dichloromethane/methanol); **$[\alpha]_D$** +0.6 (*c* 1.0, methanol).

IR (CH_3OH, cm^{-1}): 3304 (NH), 1646 (C=O), 1508 (NH), 1270, 1221 (P–OC), 1019, 959 (C–OP).

^{1}H-NMR (CD_3OD, δ): 2.51-3.39 (m, 10H, 4 x CH_2N, CH_2 Tyr), 4.57-4.60 (m, 1H, CH Tyr), 7.03 (d, *J* = 7.8 Hz, 2H, Ar Tyr), 7.24 (d, *J* = 7.7 Hz, 2H, Ar Tyr), 7.42 (m, 3H, Ar), 7.83 (d, *J* = 7.5 Hz, 2H, Ar), 8.17 (br s, 1H, NH), 8.54 (d, *J* = 8.2 Hz, 1H, NH).

^{13}C-NMR ($(CD_3)_2SO$, δ): 39.0, 42.5, 43.3, 44.1, 45.7 (5 x CH_2), 56.1 (CH Tyr), 120.4 (2 x CH Ar), 128.3 (2 x CH Ar), 128.9 (2 x CH Ar), 130.7 (2 x CH Ar), 132.1 (CH Ar), 135.0, 136.0, 152.9 (3 x C Ar), 161.3, 167.2, 172.3 (3 x CO).

MS (ESI) 475.2 $(M-H)^-$. **Anal. Calcd. for** $C_{21}H_{25}N_4O_7P$: C, 52.94; H, 5.29; N, 11.76. **Found**: C, 52.73; H, 5.68; N, 11.95.

***N*-Benzoyl-*N*-[3-(2-oxopyrrolidin-1-yl)propyl]-*O*-phosphono-L-tyrosinamide (1j).**

Yield: 90%; **mp:** 124-126 ºC (dichloromethane/methanol); **$[\alpha]_D$** -0.2 (*c* 1.5, methanol).

IR (CH_3OH, cm^{-1}): 3290 (NH), 1644 (C=O), 1539 (N–CO), 1508 (NH), 1294 (P–OC), 1025 (C–OP).

^{1}H-NMR (CD_3OD, δ): 1.63 (qt, *J* = 6.9 Hz, 2H, CH_2), 2.03 (qt, *J* = 7.7 Hz, 2H, CH_2), 2.36 (t, *J* = 8.0 Hz, 2H, CH_2CO), 3.00-3.23 (m, 6H, 3 x CH_2N), 3.43-3.44 (m, 2H, CH_2 Tyr), 4.70-4.71 (m, 1H, CH Tyr), 7.13 (d, *J* = 7.6 Hz, 2H, Ar Tyr), 7.26 (d, *J* = 8.2 Hz, 2H, Ar Tyr), 7.40-7.56 (m, 3H, Ar), 7.76 (d, *J* = 6.6 Hz, 2H, Ar).

^{13}C-NMR (CD_3OD, δ): 17.3, 26.2, 30.5, 36.2, 36.7, 39.6, 47.2 (7 x CH_2), 55.6 (CH Tyr), 119.8 (2 x CH Ar), 127.0 (2 x CH Ar), 128.0 (2 x CH Ar), 129.8 (2 x CH Ar), 131.3 (CH Ar), 132.8, 133.7, 150.9 (3 x C Ar), 168.6, 171.1, 172.1 (3 x CO).

MS (ESI) 488.6 $(M-H)^-$. **Anal. Calcd. for** $C_{23}H_{28}N_3O_7P$: C, 56.44; H, 5.77; N, 8.59. **Found**: C, 56.15; H, 5.57; N, 8.07.

***N*-Acetyl-*N*-[3-(2-oxotetrahydropyrimidin-1(2*H*)-yl)propyl]-*O*-phosphono-L-tyrosinamide ((*S*)-1k).**

Yield: 47%. Data of this compound were identical to those reported for **1a** except for the specific rotation. **$[\alpha]_D$** +3.2 (*c* 1.0, methanol).

Anal. Calcd. for $C_{18}H_{27}N_4O_7P$: C, 48.87; H, 6.15; N, 12.66. **Found**: C, 48.45; H, 6.20; N, 12.33.

***N*-Acetyl-*N*-[3-(2-oxotetrahydropyrimidin-1(2*H*)-yl)propyl]-*O*-phosphono-D-tyrosinamide ((*R*)-1k).**

Yield: 51%. Data of this compound were identical to those reported for **(*S*)-1k** except for the specific rotation. **$[\alpha]_D$** -3.0 (*c* 1.0, methanol).

Anal. Calcd. for $C_{18}H_{27}N_4O_7P$: C, 48.87; H, 6.15; N, 12.66. **Found**: C, 48.46; H, 5.99; N, 12.29.

***N*-Acetyl-*N*-[3-(2-oxotetrahydropyrimidin-1(2*H*)-yl)propyl]-*O*-phosphono-D,L-tyrosinamide ((*R,S*)-1k).**

Yield: 35%. Data of this compound were identical to those reported for enantiomers **(*R*)-** and **(*S*)-1k** except for the specific rotation.

Anal. Calcd. for $C_{18}H_{27}N_4O_7P$: C, 48.87; H, 6.15; N, 12.66. **Found**: C, 48.70; H, 6.20; N, 12.53.

***N*-Acetyl-*N*-{1-[2-(2-oxotetrahydropyrimidin-1(2*H*)-yl)ethyl]cyclohexyl}-*O*-phosphono-L-tyrosinamide (1l).**

Yield: 88%; **mp:** 166-167 ºC (diethyl ether); **$[\alpha]_D$** +0.7 (*c* 1.0, methanol).

IR (CH_3OH, cm^{-1}): 3291 (NH), 1642 (C=O), 1548 (N–CO), 1517 (NH), 1234 (P–OC), 1106 (P=O), 1030 (C–OP).

^{1}H-NMR (CD_3OD, δ): 1.17-2.11 (m, 17H, 7 x CH_2, CH_3), 2.81 (dd, *J* = 15.0, 9.0 Hz, 1H, ½ CH_2 Tyr), 3.03 (dd, *J* = 15.0, 6.3 Hz, 1H, ½ CH_2 Tyr), 3.12-3.27 (m, 6H, 3 x CH_2N), 4.54 (dd, *J* = 8.8, 6.4 Hz, 1H, CH Tyr), 7.18-7.21 (m, 4H, Ar Tyr).

^{13}C-NMR (CD_3OD, δ): 22.4 (CH_3), 22.7 (2 x CH_2), 23.1, 26.8, 35.5, 35.7, 36.3, 38.1, 41.1, 43.9, 46.5 (9 x CH_2), 56.6 (CH Tyr), 57.0 (C), 121.3 (CH Ar), 121.4 (CH Ar), 130.7 (2 x CH Ar), 131.8, 154.6 (2 x C Ar), 158.6, 173.1, 173.5 (3 x CO).

MS (ESI) 509.1 $(M-H)^-$. **Anal. Calcd. for** $C_{23}H_{35}N_4O_7P$: C, 54.11; H 6.91; N, 10.97. **Found**: C, 53.88; H, 6.25; N, 10.35.

4.2.2. Synthesis of compounds of series II (2a-i, 3a-c)

4.2.2.1. Synthesis of 3-(1-naphthyl)propylamine (17)

Amine **17** was prepared as previously reported and ^{1}H- and ^{13}C-NMR data are consistent with those described.[125]

3-(1-naphthyl)propylamine (17).

Yield: 70%. Yellowish oil.

^{1}H-NMR ($CDCl_3$, δ): 1.80 (qt, *J* = 7.5 Hz, 2H, CH_2), 2.65 (t, *J* = 7.3 Hz, 2H, CH_2), 3.00 (t, *J* = 7.7 Hz, 2H, CH_2N), 7.20-7.43 (m, 4H, 4 x CH Ar), 7.60-7.61 (m, 1H, CH Ar), 7.70-7.80 (m, 1H, CH Ar), 7.95 (d, *J* = 7.6 Hz, 1H, CH Ar).

^{13}C-RMN (CD_3OD, δ): 33.6, 36.0 (2 x CH_2), 44.4 (CH_2N), 127.2, 129.0, 129.3, 129.5, 130.3, 132.2 (7 x CH Ar), 135.6, 137.9, 141.4 (3 x C Ar).

4.2.2.2. General procedure for the synthesis of ethyl ω-[4-(benzyloxy)phenoxy]alkanoates (11a,b)

Ethyl 4-bromobutyrate or ethyl 5-bromovalerate (1.5 equiv), K_2CO_3 (2 equiv) and 18-crown ether (0.1 equiv) were added to a solution of 4-benzyloxyphenol (1 equiv) in acetone (3 mL x mmol). The mixture was refluxed overnight, then cooled to rt and the solvent was evaporated under reduced pressure. The residue was resuspended in water and extracted with diethyl ether. The organic layer was washed with 1 M NaOH and brine, dried over anhydrous Na_2SO_4 and the solvent was eliminated under reduced pressure to afford **11a,b** as white solids that were purified by column chromatography.

Ethyl 4-[4-(benzyloxy)phenoxy]butanoate (11a).

^{1}H-NMR data coincide with those previously described.[126]

Chromatography: hexane → hexane:ethyl acetate, 9.5:0.5. **Yield:** 92%; **mp:** 53-55 ºC.

IR (neat, cm^{-1}): 1731 (C=O), 1507 (C_{Ar}-C_{Ar}), 1228, 1178 (C-O).

^{1}H-NMR ($CDCl_3$, δ): 1.18 (t, *J* = 7.1 Hz, 3H, CH_3), 2.00 (qt, *J* = 6.7 Hz, 2H, CH_2), 2.43 (t, *J* = 7.3 Hz, 2H, CH_2CO), 3.87 (t, *J* = 6.1 Hz, 2H, CH_2O), 4.06 (q, *J* = 7.1 Hz, 2H, CH_2O), 4.93 (s, 2H, CH_2O), 6.65-6.86 (m, 4H, 4 x CH Ar), 7.19-7.36 (m, 5H, 5 x CH Ar).

^{13}C-NMR ($CDCl_3$, δ): 14.4 (CH_3), 24.9 (CH_2CO), 31.0 (CH_2), 60.6, 67.5, 70.9 (3 x CH_2O), 115.6, 116.0, 127.6, 128.0, 128.7 (9 x CH Ar), 137.2, 152.9, 153.1 (3 x C Ar), 173.1 (CO).

---

[125] See citation 65.

[126] Zhang, W. X.; Fan, C. Q.; Tu, B.; Zhao, X.; Jiang, X. K.; Li, Z. T. *Chinese J. Chem.* **2003**, *21*, 739-745.

Ethyl 5-[4-(benzyloxy)phenoxy]pentanoate (11b).

^{1}H-NMR data coincide with those previously described.[127]

Chromatography: hexane → hexane:ethyl acetate, 9.5:0.5. **Yield:** 95%; **mp:** 55-57 ºC.

IR (neat, cm^{-1}): 1724 (C=O), 1512 (C_{Ar}-C_{Ar}), 1255, 1188 (C-O).

^{1}H-NMR ($CDCl_3$, δ): 1.17 (t, *J* = 7.1 Hz, 3H, CH_3), 1.65-1.85 (m, 4H, 2 x CH_2), 2.30 (t, *J* = 7.1 Hz, 2H, CH_2CO), 3.83 (t, *J* = 5.8 Hz, 2H, CH_2O), 4.04 (q, *J* = 7.1 Hz, 2H, CH_2O), 4.92 (s, 2H, CH_2O), 6.70-7.00 (m, 4H, 4 x CH Ar), 7.20-7.40 (m, 5H, 5 x CH Ar).

^{13}C-NMR ($CDCl_3$, δ): 14.3 (CH_3), 21.7, 28.8 (2 x CH_2), 34.0 (CH_2CO), 60.4, 68.0, 70.8 (3 x CH_2O), 115.4, 116.0, 127.5, 128.0, 128.6 (9 x CH Ar), 137.5, 153.0, 153.5 (3 x C Ar), 173.6 (CO).

4.2.2.3. General procedure for the synthesis of ethyl ω-(4-hydroxyphenoxy)alkanoates (12a,b).

To a solution of **11a** or **11b** (1 equiv) in absolute ethanol (20 mL x mmol), 10% Pd(C) was added (50 mg x mmol), and the suspension was hydrogenated at rt at an initial pressure of 50 psi, until disappearance of starting material. The reaction mixture was filtered over celite and the solvent was removed under vacuum to afford pure debenzylated **12a,b** as amorphous solids which were purified by column chromatography.

Ethyl 4-(4-hydroxyphenoxy)butanoate (12a).

Chromatography: dichloromethane → dichloromethane:ethanol, 9.8:0.2. **Yield:** 92%.

IR (neat, cm^{-1}): 3390 (OH), 1731, 1707 (C=O), 1510 (C_{Ar}-C_{Ar}), 1230, 1211 (C–O).

^{1}H-NMR ($CDCl_3$, δ): 1.17 (t, *J* = 7.1 Hz, 3H, CH_3), 1.98 (qt, *J* = 6.7 Hz, 2H, CH_2), 2.43 (t, *J* = 7.3 Hz, 2H, CH_2CO), 3.83 (t, *J* = 6.1 Hz, 2H, CH_2O), 4.07 (q, *J* = 7.1 Hz, 2H, CH_2O), 6.60-6.76 (m, 4H, 4 x CH Ar).

^{13}C-NMR ($CDCl_3$, δ): 14.2 (CH_3), 24.7 (CH_2), 31.0 (CH_2CO), 60.8, 67.5 (2 x CH_2O), 115.7, 116.1 (4 x CH Ar), 150.0, 152.5 (2 x C Ar), 173.8 (CO).

Ethyl 5-(4-hydroxyphenoxy)pentanoate (12b).

^{1}H-NMR data coincide with those previously described.[128]

Chromatography: dichloromethane → dichloromethane:ethanol, 9.9:0.1. **Yield:** 80%.

IR (neat, cm^{-1}): 3393 (OH), 1731, 1707 (C=O), 1510 (C_{Ar}-C_{Ar}), 1230, 1212 (C–O).

^{1}H-NMR ($CDCl_3$, δ): 1.05 (t, *J* = 7.1 Hz, 3H, CH_3), 1.51-1.69 (m, 4H, 2 x CH_2), 2.19 (t, *J* = 7.1 Hz, 2H, CH_2CO), 3.67 (t, *J* = 5.8 Hz, 2H, CH_2O), 3.94 (q, *J* = 7.1 Hz, 2H, CH_2O), 6.51-6.66 (m, 4H, 4 x CH Ar).

---

[127] Ikura, M.; Nakatani, S.; Yamamoto, S.; Habashita, H.; Sugiura, T.; Takahashi, K.; Ogawa, K.; Ohno, H.; Nakai, H.; Toda, M. *Bioorg. Med. Chem.* **2006**,*14*, 4241-4252.

[128] See citation 129.

^{13}C-NMR ($CDCl_3$, δ): 14.3 (CH_3), 21.5, 28.6 (2 x CH_2), 33.9, (CH_2CO) 60.6, 68.0 (2 x CH_2O), 115.6, 116.0 (4 x CH Ar), 150.0, 152.5 (2 x C Ar), 174.3 (CO).

4.2.2.4. General procedure for the synthesis of *N*-substituted 4-(4-hydroxyphenoxy)butanamides (13a-h) and 5-(4-hydroxyphenoxy)pentanamides (14a-c).

A solution of appropriate freshly distilled amine (2 equiv) and $AlMe_3$ (2 equiv) was ice-cooled and stirred for 1 h under argon atmosphere. Then a solution of **12a** or **12b** (1 equiv) in dry toluene (0.5 mL x mmol) was added and the reaction refluxed for 4 h. After evaporating the solvent to dryness, the crude oil was purified by column chromatography.

4-(4-Hydroxyphenoxy)-*N*-(2-phenylethyl)butanamide (13a).

Chromatography: hexane:ethyl acetate, 9:1 → 7:3. **Yield:** 51%.

IR (neat, cm^{-1}): 3296 (OH), 1644 (C=O), 1543 (N–CO), 1509 (NH), 1229 (C–OH).

^{1}H-NMR ($CDCl_3$, δ): 2.07 (qt, *J* = 6.7 Hz, 2H, CH_2), 2.34 (t, *J* = 7.2 Hz, 2H, CH_2CO), 2.80 (t, *J* = 6.9 Hz, 2H, CH_2), 3.50-3.57 (m, 2H, $C\underline{H}_2NH$), 3.91 (t, *J* = 5.9 Hz, 2H, CH_2O), 5.59 (br s, 1H, NH), 6.70-6.79 (m, 4H, 4 x CH Ar), 7.15-7.31 (m, 5H, 5 x CH Ar).

^{13}C-NMR ($CDCl_3$, δ): 26.1 (CH_2), 33.1 (CH_2CO), 35.8 (CH_2), 40.7 (CH_2NH), 67.1 (CH_2O), 115.7 (2 x CH Ar), 116.2, 126.6, 128.8 (7 x CH Ar), 141.5, 150.3, 152.8 (3 x C Ar), 172.7 (CO).

4-(4-Hydroxyphenoxy)-*N*-(3-phenylpropyl)butanamide (13b).

Chromatography: hexane:ethyl acetate, 9:1 → 7:3. **Yield:** 71%.

IR (neat, cm^{-1}): 3294 (OH), 1642 (C=O), 1548 (N–CO), 1509 (NH), 1229 (C–OH).

^{1}H-NMR ($CDCl_3$, δ): 1.81 (qt, *J* = 7.3 Hz, 2H, CH_2), 2.05 (qt, *J* = 6.3 Hz, 2H, CH_2), 2.34 (t, *J* = 7.2 Hz, 2H, CH_2CO), 2.62 (t, *J* = 7.7 Hz, 2H, CH_2), 3.29 (q, *J* = 6.7 Hz, 2H, $C\underline{H}_2NH$), 3.90 (t, *J* = 5.9 Hz, 2H, CH_2O), 5.70 (br s, 1H, NH), 6.73-6.80 (m, 4H, CH Ar), 7.12-7.38 (m, 5H, CH Ar).

^{13}C-NMR ($CDCl_3$, δ): 25.4, 31.2 (2 x CH_2), 33.2, 33.4 (CH_2, CH_2CO), 39.4 (CH_2NH), 67.6 (CH_2O), 115.5, 116.2, 126.0, 128.4, 128.6 (9 x CH Ar), 141.3, 150.2, 152.6 (3 x C Ar), 172.7 (CO).

4-(4-Hydroxyphenoxy)-*N*-(*iso*butyl)butanamide (13c).

Chromatography: dichlromethane:ethyl acetate, 9:1 → 8:2. **Yield:** 76%.

IR (neat, cm^{-1}): 3217 (OH), 1643 (C=O), 1551 (N–CO), 1510 (NH), 1217 (C–OH).

^{1}H-NMR ($CDCl_3$, δ): 0.80 (d, *J* = 6.6 Hz, 2 x CH_3), 1.65 (sp, *J* = 6.7 Hz, 1H, CH), 1.98 (qt, *J* = 6.6, 2H, CH_2), 2.31 (t, *J* = 7.2 Hz, 2H, CH_2CO), 3.00 (t, *J* = 6.4 Hz, 2H, $C\underline{H}_2NH$), 3.80 (t, *J* = 5.9 Hz, 2H, CH_2O), 5.90 (t, *J* = 5.7 Hz, 1H, NH), 6.60-6.70 (m, 4H, 4 x CH Ar), 7.50-7.70 (s, 1H, OH).

^{13}C-NMR ($CDCl_3$, δ): 20.1 (2 x CH_3), 27.1 (CH_2), 28.5 (CH), 33.2 (CH_2CO), 45.3 (CH_2NH), 67.6 (CH_2O), 115.6, 116.1 (4 x CH Ar), 150.0, 152.0 (2 x C Ar), 173.0 (CO).

4-(4-Hydroxyphenoxy)-*N*-(3-methylbutyl)butanamide (13d).

Chromatography: hexane:ethyl acetate, 1:1. **Yield:** 46%.

IR (neat, cm^{-1}): 3297 (OH), 1643 (C=O), 1550 (N–CO), 1509 (NH), 1228 (C–OH).

^{1}H-NMR ($CDCl_3$, δ): 0.80 (d, *J* = 6.5 Hz, 6H, 2 x CH_3), 1.26 (q, *J* = 7.4 Hz, 2H, CH_2), 1.50 (sp, *J* = 6.7 Hz, 1H, CH), 1.94-2.11 (m, 2H, CH_2), 2.31 (t, *J* = 7.2 Hz, 2H, CH_2CO), 3.14-3.24 (m, 2H, $C\underline{H}_2NH$), 3.83 (t, *J* = 5.9 Hz, 2H, CH_2O), 5.64 (br s, 1H, NH), 6.61-6.73 (m, 4H, 4 x CH Ar).

^{13}C-NMR ($CDCl_3$, δ): 22.3 (2 x CH_3), 25.4 (CH_2), 25.7 (CH), 33.1 (CH_2CO), 37.9, 38.3 (CH_2NH, CH_2), 67.5 (CH_2O), 115.5, 116.0 (4 x CH Ar), 150.5, 152.5 (2 x C Ar), 172.9 (CO).

***N*-(2-Ethylhexyl)-4-(4-hydroxyphenoxy)butanamide (13e).**

Chromatography: hexane:ethyl acetate, 8:2 → 6:4. **Yield:** 49%.

IR (neat, cm^{-1}): 3305 (OH), 1646 (C=O), 1552 (N–CO), 1511 (NH), 1231 (C–OH).

^{1}H-NMR ($CDCl_3$, δ): 0.74-0.81 (m, 6H, 2 x CH_3), 1.15-1.23 (m, 9H, 4 x CH_2, CH), 2.00 (qt, *J* = 6.5, 2H, CH_2), 2.32 (t, *J* = 7.2 Hz, 2H, CH_2CO), 3.12 (t, *J* = 5.9 Hz, 2H, $C\underline{H}_2NH$), 3.80 (t, *J* = 5.9 Hz, 2H, CH_2O), 5.70 (t, *J* = 5.5 Hz, 1H, NH), 6.60-6.73 (m, 4H, 4 x CH Ar), 7.30 (br s, 1H, OH).

^{13}C-NMR ($CDCl_3$, δ): 10.6, 14.0 (2 x CH_3), 23.0, 24.1, 25.5, 28.2, 30.9 (5 x CH_2), 33.2 (CH_2CO), 39.2 (CH), 42.5 (CH_2NH), 67.5 (CH_2O), 115.5, 116.1 (4 x CH Ar), 150.6, 152.2 (2 x C Ar), 173.2 (CO).

4-(4-Hydroxyphenoxy)-*N*-[2-[(1-naphthyl)amino]ethyl]butanamide (13f).

Chromatography: hexane:ethyl acetate, 9:1 → 6:4. **Yield:** 82%.

IR (neat, cm^{-1}): 3267 (OH), 1640 (C=O), 1584 (C_{Ar}-C_{Ar}), 1533 (N–CO), 1509 (NH), 1227 (C–OH).

^{1}H-NMR ($CDCl_3$, δ): 1.89-2.01 (m, 2H, CH_2), 2.26 (t, *J* = 7.1 Hz, 2H, CH_2CO), 3.20 (t, *J* = 5.5 Hz, 2H, $C\underline{H}_2NH$), 3.50 (q, *J* = 5.7 Hz, 2H, $C\underline{H}_2NH$), 3.70 (t, *J* = 5.8 Hz, 2H, CH_2O), 4.93 (br s, 1H, OH), 6.10 (t, *J* = 6.0 Hz, NH), 6.39 (d, *J* = 8.0 Hz, 1H, CH Ar), 6.48-6.60 (m, 4H, 4 x CH Ar), 7.01-7.37 (m, 4H, 4 x CH Ar), 7.64-7.70 (m, 2H, 2 x CH Ar).

^{13}C-NMR ($CDCl_3$, δ): 25.4 (CH_2), 33.1 (CH_2CO), 39.0, 45.0 (2 x CH_2NH), 67.3 (CH_2O), 103.7, 115.5, 116.1, 117.4, 120.2, 124.9, 125.8, 126.5, 128.5 (11 x CH Ar), 134.2, 143.2, 150.1, 152.4 (5 x C Ar), 174.4 (CO).

4-(4-Hydroxyphenoxy)-*N*-[2-(dimethylamino)ethyl]butanamide (13g).

Chromatography: ethyl acetate:ethanol, 8:2 → 7:3. **Yield:** 63%.

IR (neat, cm^{-1}): 3261 (OH), 1655 (C=O), 1552 (N–CO), 1510 (NH), 1222 (C–OH), 1053 (C-N).

^{1}H-NMR ($CDCl_3$, δ): 1.94 (qt, *J* = 6.7 Hz, 2H, CH_2), 2.24 (m, 6H, 2 x CH_3), 2.45 (t, *J* = 6.2 Hz, 2H, CH_2CO), 3.30-3.40 (m, 4H, $C\underline{H}_2NH$, CH_2N), 3.75 (t, *J* = 6.1 Hz, 2H, CH_2O), 6.40 (br s, 1H, NH), 6.64 (m, 4H, 4 x CH Ar).

^{13}C-NMR ($CDCl_3$, δ): 25.2 (CH_2), 32.7 (CH_2CO), 36.3 (NCH_2), 44.7 (2 x CH_3), 58.0 (CH_2NH), 67.5 (CH_2O), 115.5, 116.0 (4 x CH Ar), 150.4, 152.4 (2 x C Ar), 172.9 (CO).

4-(4-Hydroxyphenoxy)-*N*-[3-(1-naphthyl)propyl]butanamide (13h).

Chromatography: dichloromethane → dichloromethane:ethyl acetate; 8:2. **Yield:** 76%.

IR (neat, cm^{-1}): 3294 (OH), 1643 (C=O), 1536 (N–CO), 1509 (NH), 1229 (C–OH).

^{1}H-NMR ($CDCl_3$, δ): 1.94 (qt, *J* = 7.4 Hz, 2H, CH_2), 2.03 (qt, *J* = 6.7 Hz, 2H, CH_2), 2.32 (t, *J* = 7.2 Hz, 2H, CH_2CO), 3.08 (t, *J* = 7.6 Hz, 2H, CH_2), 3.36 (q, *J* = 7.6 Hz, 2H, $C\underline{H}_2NH$), 3.88 (t, *J* = 6.0 Hz, 2H, CH_2O), 5.64 (br s, 1H, NH), 6.68-6.76 (m, 4H, 4 x CH Ar), 7.27 (d, *J* = 6.7 Hz, 1H, CH Ar), 7.38 (t, *J* = 7.6 Hz, 1H, CH Ar), 7.44-7.52 (m, 2H, 2 x CH Ar), 7.70 (d, *J* = 8.2 Hz, 1H, CH Ar), 7.85 (m, 1H, CH Ar), 7.98 (m, 1H, CH Ar).

^{13}C-NMR ($CDCl_3$, δ): 25.8 (CH_2), 30.7 (2 x CH_2), 33.5 (CH_2CO), 40.0 (CH_2NH), 67.9 (CH_2O), 115.9, 116.5 (4 x CH Ar), 124.0 (CH Ar), 126.0 (2 x CH Ar), 126.4 (2 x CH Ar), 127.3, 129.2 (2 x CH Ar), 132.1, 134.3, 137.8, 150.9, 152.8 (5 x C Ar), 173.4 (CO).

5-(4-Hydroxyphenoxy)-*N*-(2-phenylethyl)pentanamide (14a).

Chromatography: hexane:ethyl acetate, 8:2 → 6:4. **Yield:** 95%.

IR (neat, cm^{-1}): 3292 (OH), 1643 (C=O), 1544 (N–CO), 1509 (NH), 1230 (C–OH).

^{1}H-NMR ($CDCl_3$, δ): 1.61-1.70 (m, 4H, 2 x CH_2), 2.12 (t, *J* = 6.9 Hz, 2H, CH_2CO), 2.72 (t, *J* = 6.9 Hz, 2H, CH_2), 3.44 (q, *J* = 6.6 Hz, 2H, $C\underline{H}_2NH$), 3.72 (t, *J* = 5.6 Hz, 2H, CH_2O), 5.70 (br s, 1H, NH), 6.59-6.71 (m, 4H, 4 x CH Ar), 7.08-7.23 (m, 5H, 5 x CH Ar).

^{13}C-NMR ($CDCl_3$, δ): 22.5, 28.8 (2 x CH_2), 35.6, 36.3 (CH_2CO, CH_2), 40.7 (CH_2NH), 68.2 (CH_2O), 115.6, 116.2, 126.5, 128.5, 128.7 (9 x CH Ar), 138.6, 150.4, 152.4 (3 x C Ar), 173.3 (CO).

5-(4-Hydroxyphenoxy)-*N*-[2-[(1-naphthyl)amino]ethyl]pentanamide (14b).

Chromatography: hexane:ethyl acetate, 8:2 → 6:4. **Yield:** 81%.

IR (neat, cm^{-1}): 3308 (OH), 1639 (C=O), 1581 (C_{Ar}-C_{Ar}), 1531 (N–CO), 1509 (NH), 1229 (C–OH).

^{1}H-NMR ($CDCl_3$, δ): 1.55-1.72 (m, 4H, 2 x CH_2), 2.15 (t, *J* = 7.0 Hz, 2H, CH_2CO), 3.20-3.28 (m, 2H, $C\underline{H}_2NH$), 3.45-3.54 (m, 2H, $C\underline{H}_2NH$), 3.70 (t, *J* = 5.9 Hz, 2H, CH_2O), 4.93 (br s, 1H, OH), 6.06 (t, *J* = 6.0 Hz, 1H, NH), 6.42 (d, *J* = 7.5 Hz, 1H, CH Ar), 6.53-6.68 (m, 4H, 4 x CH Ar), 7.10-7.37 (m, 4H, 4 x CH Ar), 7.64-7.70 (m, 2H, 2 x CH Ar).

^{13}C-NMR ($CDCl_3$, δ): 23.0, 29.5, (2 x CH_2), 36.2 (CH_2CO), 39.0, 45.7 (2 x CH_2NH), 68.6 (CH_2O), 103.6, 116.1, 116.4, 116.7, 121.6, 124.9, 126.2, 127.5, 128.9, (11 x CH Ar) 135.2, 145.0, 151.1, 153.4 (5 x C Ar), 174.4 (CO).

5-(4-Hydroxyphenoxy)-*N*-[3-(1-naphthyl)propyl]pentanamide (14c).

Chromatography: hexane:ethyl acetate, 8:2 → 6:4. **Yield:** 42%.

IR (neat, cm^{-1}): 3274 (OH), 1640 (C=O), 1598 (N–CO), 1509 (NH), 1229 (C–OH).

^{1}H-NMR ($CDCl_3$, δ): 1.60-1.80 (m, 4H, 2 x CH_2), 1.90 (qt, *J* = 7.5 Hz, 2H, CH_2), 2.02-2.20 (m, 2H, CH_2CO), 2.98-3.10 (m, 2H, CH_2), 3.30 (q, *J* = 6.9 Hz, 2H, $C\underline{H}_2NH$), 3.71-3.90 (m, 2H,

OCH_2), 5.50 (br s, 1H, NH), 6.66 (m, 4H, 4 x CH Ar), 7.23-7.47 (m, 4H, 4 x CH Ar), 7.60 (d, *J* = 7.9 Hz, 1H, CH Ar), 7.76-7.80 (m, 1H, CH Ar), 7.90-7.95 (m, 1H, CH Ar).

^{13}C-NMR ($CDCl_3$, δ): 22.6, 28.9, 30.4 (4 x CH_2), 36.2 (CH_2CO), 39.5 (CH_2NH), 68.2 (CH_2O), 115.5, 116.0, 123.5, 125.5, 125.9, 126.8, 127.0, 128.8 (11 x CH Ar), 137.2, 150.0, 152.3 (5 x C Ar), 173.0 (CO).

4.2.2.5. General procedure for the synthesis of dibenzyl 4-{[ω-(alkylamino)-ω-oxoalkyl]oxy}phenyl phosphates 15a-h and 16a-c.

To a solution of the corresponding compound **13a-h** or **14a-c** (1 equiv) in acetonitrile (1 mL x mmol), dibenzyl diisopropylphosphoramidite (1.5 equiv) and a solution of 1*H*-tetrazole in acetonitrile (2 equiv) were added. After vigorously stirring for 3 h under an argon atmosphere, the reaction was cooled to 0 ºC and 70% aqueous *tert*-butyl hydroperoxide (1 equiv) was added. After 1 h an aqueous solution of 10% $Na_2S_2O_3$ (1 mL x mmol) was added, stirring was continued for 10 min, and the solution was then transferred to a separating funnel, extracted with dichloromethane and washed with 10% $Na_2S_2O_3$ (10 mL x mmol) and brine. The organic layer was dried under anhydrous Na_2SO_4, the solvent removed by evaporation under reduced pressure, and the residue purified by column chromatography to obtain pure target compunds **15a-h** and **16a-c**.

Dibenzyl 4-{4-oxo-4-[(2-phenylethyl)amino]butoxy}phenyl phosphate (15a).

Chromatography: dichloromethane:ethyl acetate, 9:1 → 6:4. **Yield:** 60%. Oil.

IR (neat, cm^{-1}): 3287 (NH), 1647 (C=O), 1547 (N–CO), 1505 (NH), 1211 (P–OC), 1081, 1020 (C–OP).

^{1}H-NMR ($CDCl_3$, δ): 1.90-2.20 (m, 2H, CH_2), 2.25 (t, *J* = 7.0 Hz, 2H, CH_2CO), 2.73 (t, *J* = 6.9 Hz, 2H, CH_2), 3.31-3.56 (m, 2H, $C\underline{H}_2NH$), 3.95 (t, *J* = 6.0 Hz, 2H, CH_2O), 5.01 (s, 2H, CH_2O), 5.05 (s, 2H, CH_2O), 5.50 (s, 1H, NH), 6.63 (d, *J* = 9.0 Hz, 2H, 2 x CH Ar), 6.93 (d, *J* = 9.0 Hz, 2H, 2 x CH Ar), 7.07-7.29 (m, 15H, 15 x CH Ar).

^{13}C-NMR ($CDCl_3$, δ): 31.0 (CH_2), 32.6, 33.2 (CH_2, CH_2CO), 39.1 (CH_2NH), 67.4 (CH_2O), 69.7 (2 x CH_2O), 115.4, 120.8, 125.8, 127.5, 127.8, 128.2 (19 x CH Ar), 135.2, 141.4, 144.1, 155.9 (5 x C Ar), 172.3 (CO).

Dibenzyl 4-{4-oxo-4-[(3-phenylpropyl)amino]butoxy}phenyl phosphate (15b).

Chromatography: dichloromethane:ethyl acetate, 7:3. **Yield:** 40%. Oil.

IR (neat, cm^{-1}): 3304 (NH), 1649 (C=O), 1549 (N–CO), 1504 (NH), 1269, 1200 (P–OC), 1009, 956 (C–OP).

^{1}H-NMR ($CDCl_3$, δ): 1.80 (qt, *J* = 7.4 Hz, 2H, CH_2), 2.07 (qt, *J* = 6.5 Hz, 2H, CH_2), 2.34 (t, *J* = 7.2 Hz, 2H, CH_2CO), 2.61 (t, *J* = 7.7 Hz, 2H, CH_2), 3.25 (q, *J* = 6.6 Hz, 2H, CH_2NH), 3.89 (t, *J* = 6.1 Hz, 2H, CH_2O), 5.07 (s, 2H, CH_2O), 5.11 (s, 2H, CH_2O), 6.63 (t, *J* = 5.6 Hz, 1H, NH), 6.75 (d, *J* = 9.0 Hz, 2H, 2 x CH Ar), 7.04 (d, *J* = 9.0 Hz, 2H, 2 x CH Ar), 7.12-7.34 (m, 15H, 15 x CH Ar).

^{13}C-NMR ($CDCl_3$, δ): 31.0 (2 x CH_2), 32.6, 33.2 (CH_2, CH_2CO), 39.1 (CH_2NH), 67.4 (CH_2O), 69.7 (2 x CH_2O), 115.4, 120.8, 125.8, 127.5, 127.8, 128.2 (19 x CH Ar), 135.2, 141.4, 144.1, 155.9 (5 x C Ar), 172.3 (CO).

Dibenzyl 4-[4-(*iso*butylamino)-4-oxobutoxy]phenyl phosphate (15c).

Chromatography: dichloromethane:ethyl acetate, 9:1 → 7:3. **Yield:** 75%. Amorphous solid.

IR (neat, cm^{-1}): 3320 (NH), 1650 (C=O), 1551 (N–CO), 1506 (NH), 1273, 1202 (P–OC), 1011, 957 (C–OP).

^{1}H-NMR ($CDCl_3$, δ): 0.80 (d, *J* = 6.6, 6H, 2 x CH_3), 1.73 (sp, *J* = 6.0 Hz, 1H, CH), 2.1 (qt, *J* = 6.0, 2H, CH_2), 2.37 (t, *J* = 6.5 Hz, 2H, CH_2CO), 3.06 (t, *J* = 6.0 Hz, 2H, C$\underline{H_2}$NH), 3.94 (t, *J* = 6.0 Hz, 2H, CH_2O), 5.07 (s, 2H, CH_2O), 5.11 (s, 2H, CH_2O), 5.82 (br s, 1H, NH), 6.76 (d, *J* = 9.0 Hz, 2H, 2 x CH Ar), 7.03 (d, *J* = 9.0 Hz, 2H, 2 x CH Ar), 7.33 (m, 10H, 10 x CH Ar).

^{13}C-NMR ($CDCl_3$, δ): 20.1 (2 x CH_3), 25.3 (CH_2), 28.5 (CH), 33.0 (CH_2CO), 46.9 (CH_2NH), 67.4 (CH_2O), 70.0 (2 x CH_2O), 115.2, 121.0, 128.0, 128.6 (14 x CH Ar), 135.4, 144.1, 156.0 (4 x C Ar), 172.3 (CO).

Dibenzyl 4-{4-[(3-methylbutyl)amino]-4-oxobutoxy}phenyl phosphate (15d).

Chromatography: dichloromethane:ethyl acetate, 9:1 → 7:3. **Yield:** 41%. Amorphous solid.

IR (neat, cm^{-1}): 3297 (NH), 1644 (C=O), 1558 (N–CO), 1504 (NH), 1202 (P–OC), 1009, 963 (C–OP).

^{1}H-NMR ($CDCl_3$, δ): 0.76 (d, *J* = 6.5, 6H, 2 x CH_3), 1.23 (q, *J* = 7.0 Hz, 2H, CH_2), 1.46 (sp, *J* = 6.7 Hz, 1H, CH), 1.94-2.02 (m, 2H, CH_2), 2.30 (t, *J* = 7.2 Hz, 2H, CH_2CO), 3.11 (q, *J* = 6.9 Hz, 2H, C$\underline{H_2}$NH), 3.83 (t, *J* = 6.1 Hz, 2H, CH_2O), 4.95 (s, 2H, CH_2O), 5.00 (s, 2H, CH_2O), 6.40 (br s, 1H, NH), 6.64 (d, *J* = 9.0 Hz, 2H, 2 x CH Ar), 6.92 (d, *J* = 9.0 Hz, 2H, 2 x CH Ar), 7.19 (m, 10H, 10 x CH Ar).

^{13}C-NMR ($CDCl_3$, δ): 22.3 (2 x CH_3), 25.1 (CH_2), 25.5 (CH), 32.5 (CH_2CO), 37.8, 38.5 (CH_2NH, CH_2), 67.7 (CH_2O), 70.0 (2 x CH_2O), 115.1, 120.7, 127.8, 128.5 (14 x CH Ar), 135.5, 144.1, 156.2 (4 x C Ar), 172.5 (CO).

Dibenzyl 4-{4-[(2-ethylhexyl)amino]-4-oxobutoxy}phenyl phosphate (15e).

Chromatography: dichloromethane:ethyl acetate, 9:1 → 8:2. **Yield:** 65%. Oil.

IR (neat, cm^{-1}): 3325 (NH), 1649 (C=O), 1549 (N–CO), 1504 (NH), 1270, 1200 (P–OC), 1009, 955 (C–OP).

^{1}H-NMR ($CDCl_3$, δ): 0.82-0.88 (m, 6H, 2 x CH_3), 1.21-1.32 (m, 9H, 4 x CH_2, CH), 2.08 (qt, *J* = 6.0 Hz, 2H, CH_2), 2.35 (t, *J* = 7.2 Hz, 2H, CH_2CO), 3.14-3.19 (m, 2H, C$\underline{H_2}$NH), 3.91 (t, *J* = 5.9 Hz, 2H, CH_2O), 5.07 (s, 2H, CH_2O), 5.09 (s, 2H, CH_2O), 5.98 (t, *J* = 6.3 Hz, 1H, NH), 6.75 (d, *J* = 9.0 Hz, 2H, 2 x CH Ar), 7.02 (d, *J* = 9.0 Hz, 2H, 2 x CH Ar), 7.31 (m, 10H, 10 x CH Ar).

^{13}C-NMR ($CDCl_3$, δ): 11.2, 14.5 (2 x CH_3), 23.4, 24.5, 25.6, 29.2, 31.3 (5 x CH_2), 33.2 (CH_2CO), 39.7 (CH), 42.7 (CH_2NH), 67.8, 70.2, 70.3 (3 x CH_2O), 115.6, 121.3, 128.3, 129.0 (14 x CH Ar), 135.8, 144.5, 156.5 (4 x C Ar), 172.7 (CO).

Dibenzyl 4-(4-{[2-[(1-naphthyl)amino]ethyl]amino}-4-oxobutoxy)phenyl phosphate (15f).

Chromatography: dichloromethane:ethyl acetate, 8:2 → 1:1. **Yield:** 30%; **mp:** 91-92 ºC.

IR (neat, cm^{-1}): 3266 (NH), 1652 (C=O), 1551 (N–CO), 1504 (NH), 1246, 1205 (P–OC), 1081, 935 (C–OP).

^{1}H-NMR ($CDCl_3$, δ): 1.90-2.04 (m, 2H, CH_2), 2.31 (t, *J* = 7.2 Hz, 2H, CH_2CO), 3.22 (t, *J* = 5.4 Hz, 2H, $C\underline{H}_2NH$), 3.53 (q, *J* = 5.6 Hz, 2H, $C\underline{H}_2NH$), 3.78 (t, *J* = 6.0 Hz, 2H, CH_2O), 5.10 (s, 2H, CH_2O), 5.12 (s, 2H, CH_2O), 6.26 (br s, 1H, NH), 6.42 (m, 1H, NH), 6.61 (d, *J* = 9.0 Hz, 2H, 2 x CH Ar), 6.91 (d, *J* = 9.0 Hz, 2H, 2 x CH Ar), 7.14-7.41 (m, 15H, 15 x CH Ar), 7.69-7.95 (m, 2H, 2 x CH Ar).

^{13}C-NMR ($CDCl_3$, δ): 25.3 (CH_2), 32.8 (CH_2CO), 37.7 (CH_2NH), 44.0 (CH_2NH), 67.3 (CH_2O), 70.0 (2 x CH_2O), 115.4, 120.6, 121.0, 126.0, 126.7, 128.1, 128.7 (21 x CH Ar), 134.4, 135.4, 143.2, 156.1 (7 x C Ar), 173.8 (CO).

Dibenzyl 4-(4-{[2-(dimethylamino)ethyl]amino}-4-oxobutoxy)phenyl phosphate (15g).

Chromatography: ethyl acetate:ethanol, 9:1 → 6:4. **Yield:** 36%. Oil.

IR (neat, cm^{-1}): 3320 (NH), 1655 (C=O), 1552 (N–CO), 1510 (NH), 1270, 1900 (P–OC), 1011, 955 (C–OP).

^{1}H-NMR ($CDCl_3$, δ): 1.90-2.30 (m, 2H, CH_2), 2.32 (s, 6H, 2 x CH_3), 2.62 (t, *J* = 5.7 Hz, 2H, CH_2CO), 3.29-3.43 (m, 4H, $C\underline{H}_2NH$, CH_2N), 3.80 (t, *J* = 6.2 Hz, 2H, CH_2O), 5.0 (s, 2H, CH_2O), 5.04 (s, 2H, CH_2O), 6.59-6.73 (m, 2H, 2 x CH Ar), 6.90-6.94 (m, 2H, 2 x CH Ar), 6.97-7.03 (m, 10H, 10 x CH Ar).

^{13}C-NMR ($CDCl_3$, δ): 24.8 (CH_2), 29.8 (CH_2CO), 42.9 (NCH_2), 49.5 (2 x CH_3), 50.2 (NCH_2), 67.5 (CH_2O), 70.3 (2 x CH_2O), 114.9, 120.8, 126.7, 127.4, 128.3, 129.0, 132.7 (14 x CH Ar), 137.9, 146.0, 154.5 (4 x C Ar), 173.7 (CO).

Dibenzyl 4-(4-{[3-(1-naphthyl)propyl]amino}-4-oxobutoxy)phenyl phosphate (15h).

Chromatography: dichloromethane:ethyl acetate; 9:1 → 8.5:1.5. **Yield:** 58%. Oil.

IR (neat, cm^{-1}): 3314 (NH), 1647 (C=O), 1649 (N–CO), 1506 (N–H), 1202 (P–OC), 1011, 958 (C–OP).

^{1}H-NMR ($CDCl_3$, δ): 1.95 (qt, *J* = 7.4 Hz, 2H, CH_2), 2.05 (qt, *J* = 6.7 Hz, 2H, CH_2), 2.29 (t, *J* = 7.3 Hz, 2H, CH_2CO), 3.10 (t, *J* = 7.6 Hz, 2H, CH_2), 3.36 (q, *J* = 6.7 Hz, 2H, $C\underline{H}_2NH$), 3.90 (t, *J* = 6.0 Hz, 2H, OCH_2), 5,08 (s, 2H, CH_2O), 5,10 (s, 2H, CH_2O), 5.68 (t, *J* = 5.3 Hz, 1H, NH), 6.75 (m, 2H, 2 x CH Ar), 7.03 (m, 2H, 2 x CH Ar), 7.28-7.52 (m, 14H, 14 x CH Ar), 7.71 (d, *J* = 8.1 Hz, 1H, CH Ar), 7.82-7.85 (m, 1H, CH Ar), 7.97-8.00 (m, 1H, CH Ar).

^{13}C-NMR ($CDCl_3$, δ): 25.6 (CH_2), 30.8 (2 x CH_2), 33.3 (CH_2CO), 39.5 (CH_2NH), 67.7 (CH_2O), 70.2 (2 x CH_2O), 115.6 (2 x CH Ar), 121.3 (2 x CH Ar), 123.9 (CH Ar), 125.9 (2 x CH Ar), 126.4 (2 x CH Ar), 127.3 (CH Ar), 128.4 (4 x CH Ar), 129.0 (6 x CH Ar), 129.3 (CH Ar), 132.1, 134.3, 135.8, 135.9, 137.8, 142.5, 156.4 (7 x C Ar), 172.7 (CO).

Dibenzyl 4-({5-oxo-5-[(2-phenylethyl)amino]pentyl}oxy)phenyl phosphate (16a).

Chromatography: hexane:ethyl acetate, 9:1 → 6:4. **Yield:** 51%. Amorphous solid.

IR (neat, cm^{-1}): 3311 (NH), 1646 (C=O), 1547 (N–CO), 1504 (NH), 1274, 1200 (P–OC), 1009, 955 (C–OP).

^{1}H-NMR ($CDCl_3$, δ): 1.62-1.71 (m, 4H, 2 x CH_2), 2.11 (t, *J* = 6.0 Hz, 2H, CH_2CO), 2.73 (t, *J* = 6.0 Hz, 2H, CH_2), 3.41-3.47 (m, 2H, $C\underline{H}_2NH$), 3.81 (t, *J* = 6.0 Hz, 2H, CH_2O), 5,01 (s, 2H, CH_2O), 5.04 (s, 2H, CH_2O), 5.50 (br s, 1H, NH), 6.68 (d, *J* = 9.0 Hz, 2H, 2 x CH Ar), 6.68 (d, *J* = 9.0 Hz, 2H, 2 x CH Ar), 7.09-7.25 (m, 15H, 15 x CH Ar).

^{13}C-NMR ($CDCl_3$, δ): 22.4, 28.7 (2 x CH_2), 35.8, 36.3 (CH_2, CH_2CO), 41.0 (CH_2NH), 68.0 (CH_2O), 70.0 (2 x CH_2O), 115.3, 121.0, 126.5, 128.5, 129.0 (19 x CH Ar), 135.5, 138.9, 144.1, 156.1 (5 x C Ar), 173.3 (CO).

Dibenzyl 4-[(5-{[2-[(1-naphthyl)amino]ethyl]amino}-5-oxopentyl)oxy]phenyl phosphate (16b).

Chromatography: hexane:ethyl acetate, 8:2 → 6:4. **Yield:** 37%; **mp:** 94-95 ºC.

IR (neat, cm^{-1}): 3278 (NH), 1652 (C=O), 1548 (N–CO), 1504 (NH), 1246, 1205 (P–OC), 1023, 936 (C–OP).

^{1}H-NMR ($CDCl_3$, δ): 1.61-1.77 (m, 4H, 2 x CH_2), 2.19 (t, *J* = 7.0 Hz, 2H, CH_2CO), 3.31 (t, *J* = 5.4 Hz, 2H, $C\underline{H}_2NH$), 3.50-3.70 (m, 2H, $C\underline{H}_2NH$), 3.74 (t, *J* = 5.9 Hz, 2H, CH_2O), 5.00 (s, 2H, CH_2O), 5.04 (s, 2H, CH_2O), 6.18 (br s, 1H, NH), 6.50 (d, *J* = 7.2 Hz, 1H, CH Ar), 6.62 (d, *J* = 7.5 Hz, 2H, 2 x CH Ar), 6.93 (d, *J* = 7.5 Hz, 2H, 2 x CH Ar), 7.12-7.38 (m, 14H, 14 x CH Ar), 7.70-7.82 (m, 2H, 2 x CH Ar).

^{13}C-NMR ($CDCl_3$, δ): 23.0, 29.5 (2 x CH_2), 36.2 (CH_2CO), 39.0, 45.7 (2 x CH_2NH), 68.0, 70.0 (3 x CH_2O), 115.2, 120.9, 123.6, 125.6, 126.0, 126.9, 128.0, 128.6, 128.8 (21 x CH Ar), 131.7, 133.9, 135.4, 137.5, 142.5, 156.1 (7 x C Ar), 172,5 (CO).

Dibenzyl 4-[(5-{[3-(1-naphthyl)propyl]amino}-5-oxopentyl)oxy]phenyl phosphate (16c).

Chromatography: hexane:ethyl acetate, 9:1 → 6:4. **Yield:** 56%. Oil.

IR (neat, cm^{-1}): 3305 (NH), 1647 (C=O), 1547 (N–CO), 1504 (NH), 1267, 1200 (P–OC), 1009, 956 (C–OP).

^{1}H-NMR ($CDCl_3$, δ): 1.60-1.80 (m, 4H, 2 x CH_2), 1.90 (qt, *J* = 7.5 Hz, 2H, CH_2), 2.02-2.20 (m, 2H, CH_2CO), 2.98-3.10 (m, 2H, CH_2), 3.30 (q, *J* = 6.9 Hz, 2H, $C\underline{H}_2NH$), 3.71-3.90 (m, 2H, OCH_2), 5,00 (s, 2H, CH_2O), 5,03 (s, 2H, CH_2O), 5.50 (br s, 1H, NH), 6.67 (d, *J* =9.0 Hz, 2H, 2 x CH Ar), 6.95 (d, *J* =9.0 Hz, 2H, 2 x CH Ar), 7.23-7.47 (m, 14H, 14 x CH Ar), 7.60 (d, *J* = 7.9 Hz, 1H, CH Ar), 7.76-7.80 (m, 1H, CH Ar), 7.90-7.95 (m, 1H, CH Ar).

^{13}C-NMR ($CDCl_3$, δ): 22.6, 28.7, 30.5 (4 x CH_2), 36.2 (CH_2CO), 39.5 (CH_2NH), 68.0, 70.0 (3 x CH_2O), 115.2, 120.9, 123.6, 125.6, 126.0, 126.9, 128.0, 128.6 128.8 (21 x CH Ar), 131.7, 133.9, 135.4, 137.5, 142.5, 156.1 (7 x C Ar), 172.5 (CO).

4.2.2.6. General procedure for the synthesis of 4-{[ω-(alkylamino)-ω-oxoalkyl]oxy}phenyl dihydrogen phosphates 2a-i and 3a-c.

Final compounds **2a-i** and **3a-c** were obtained from their corresponding benzylated precursors **15a-h** and **16a-c** (1 equiv) following the general procedure previously described in **5.2.1.6.** Derivative **2i** was obtained after 48 h of hydrogenation of its precursor **15h**.

4-{4-Oxo-4-[(2-phenylethyl)amino]butoxy}phenyl dihydrogen phosphate (2a).

Yield: 72%; **mp:** 169-173 ºC (methanol/chloroform).

IR (neat, cm^{-1}): 3300 (OH), 1641 (C=O), 1553 (N–CO), 1505 (NH), 1202 (P–OC), 1028, 968 (C–OP).

^{1}H-NMR (CD_3OD, δ): 1.86-1.93 (m, 2H, CH_2), 2.23 (t, *J* = 7.3 Hz, 2H, CH_2CO), 2.67 (t, *J* = 7.2 Hz, 2H, CH_2), 3.30 (t, *J* = 7.2 Hz, 2H, $C\underline{H_2}NH$), 3.79 (t, *J* = 6.0 Hz, 2H, CH_2O), 6.70 (d, *J* = 7.8 Hz, 2H, 2 x CH Ar), 7.01-7.18 (m, 7H, 7 x CH Ar).

^{13}C-NMR (CD_3OD, δ): 26.6 (CH_2), 33.4 (CH_2CO), 36.4 (CH_2), 41.8 (CH_2NH), 68.4 (CH_2O), 115.9, 122.2, 127.2, 129.3, 129.6 (9 x CH Ar), 142.3, 156.5 (3 x C Ar), 174.3 (CO).

MS (ESI): 378.2 $(M-H)^-$. **Anal. Calcd. for $C_{18}H_{22}NO_6P$:** C, 56.99; H, 5.85; N, 3.69. **Found:** C, 56.64; H, 5.60; N, 3.70.

4-{4-Oxo-4-[(3-phenylpropyl)amino]butoxy}phenyl dihydrogen phosphate (2b).

Yield: 52%; **mp:** 145-147 ºC (methanol/chloroform).

IR (neat, cm^{-1}): 3278 (OH), 1643 (C=O), 1572 (N–CO), 1504 (NH), 1202 (P–OC), 966 (C–OP).

^{1}H-NMR (CD_3OD, δ): 1.77 (qt, *J* = 7.2 Hz, 2H, CH_2), 1.90-2.15 (m, 2H, CH_2), 2.36 (t, *J* = 7.2 Hz, 2H, CH_2CO), 2.55 (t, *J* = 7.2 Hz, 2H, CH_2), 3.18 (t, *J* = 7.0 Hz, 2H, $C\underline{H_2}NH$), 3.93 (t, *J* = 6.1 Hz, 2H, CH_2O), 6.84 (m, 2H, 2 x CH Ar), 7.00-7.30 (m, 7H, 7 x CH Ar).

^{13}C-NMR (CD_3OD, δ): 26.8, 32.3 (2 x CH_2), 33.7, 34.2 (CH_2, CH_2CO), 40.1 (CH_2NH), 68.7 (CH_2O), 116.1, 116.6, 116.8, 122.4, 127.0, 127.9, 129.4, 130.4, 135.5 (9 CH Ar), 143.5, 157.0 (3 C Ar), 173.2 (CO).

MS (ESI): 392.0 $(M-H)^-$. **Anal. Calcd. for $C_{19}H_{24}NO_6P$:** C, 58.01; H, 6.15; N, 3.56. **Found:** C, 57.95; H, 5.85; N, 3.75.

4-[4-(*Iso*butylamino)-4-oxobutoxy]phenyl dihydrogen phosphate (2c).

Yield: 65%; **mp:** 167-170 ºC (methanol/chloroform).

IR (neat, cm^{-1}): 3299 (OH), 1642 (C=O), 1553 (N–CO), 1506 (NH), 1208 (P–OC), 969 (C–OP).

^{1}H-NMR (CD_3OD, δ): 0.96 (d, *J* = 6.7 Hz, 6H, 2 x CH_3), 1.83 (sp, *J* = 6.7 Hz, 1H, CH), 2.12 (qt, *J* = 6.6 Hz, 2H, CH_2), 2.46 (t, *J* = 7.3 Hz, 2H, CH_2CO), 3.06 (d, *J* = 6.9 Hz, 2H, $C\underline{H_2}NH$), 4.02 (t, *J* = 6.1 Hz, 2H, CH_2O), 6.90 (d, *J* = 8.2 Hz, 2H, 2 x CH Ar), 7.20 (d, *J* = 8.2 Hz, 2H, 2 x CH Ar).

^{13}C-NMR (CD_3OD, δ): 20.3 (2 x CH_3), 26.7 (CH_2), 29.5 (CH), 33.5 (CH_2CO), 47.8 (CH_2NH), 68.4 (CH_2O), 115.9, 122.2 (4 x CH Ar), 147.0, 157.0 (2 x C Ar), 176.0 (CO).

MS (ESI): 330.0 $(M-H)^-$. **Anal. Calcd. for $C_{14}H_{22}NO_6P$:** C, 50.75; H, 6.69; N, 4.23. **Found:** C, 51.08; H, 6.98; N, 4.23.

4-{4-[(3-Methylbutyl)amino]-4-oxobutoxy}phenyl dihydrogen phosphate (2d).

Yield: 63%; **mp:** 167-168 ºC (ethanol/chloroform).

IR (neat, cm^{-1}): 3298 (OH), 1640 (C=O), 1594 (N–CO), 1511 (NH), 1217, 1166 (P–OC), 1032, 996 (C–OP).

^{1}H-NMR (CD_3OD, δ): 0.80 (d, *J* = 7.0, 6H, 2 x CH_3), 1.18-1.31 (m, 2H, CH_2), 1.40-1.60 (m, 1H, CH), 1.80-2.05 (m, 2H, CH_2), 2.15-2.38 (m, 2H, CH_2CO), 3.10 (t, *J* = 7.0 Hz, 2H, $C\underline{H_2}NH$), 3.70-3.92 (m, 2H, CH_2O), 6.60-7.20 (m, 4H, 4 x CH Ar).

^{13}C-NMR (CD_3OD, δ): 22.9 (2 x CH_3), 26.8 (CH_2), 27.0 (CH), 33.7 (CH_2CO), 38.7, 39.4 (CH_2NH, CH_2), 68.7 (CH_2O), 116.4, 122.5 (4 x CH Ar), 152.5, 157.1 (2 x C Ar), 173.6 (CO).

MS (ESI): 344.0 $(M-H)^-$. **Anal. Calcd. for $C_{15}H_{24}NO_6P$:** C, 52.17; H, 7.01; N, 4.06. **Found:** C, 52.13; H, 6.80; N, 4.12.

4-{4-[(2-Ethylhexyl)amino]-4-oxobutoxy}phenyl dihydrogen phosphate (2e).

Yield: 62%; **mp:** 177-179 ºC (methanol/chloroform).

IR (neat, cm^{-1}): 3296 (OH), 1656 (C=O), 1591 (N–CO), 1511 (NH), 1217, 1166 (P–OC), 997 (C–OP).

^{1}H-NMR (CD_3OD, δ): 0.69-0.95 (m, 6H, 2 x CH_3), 1.13-1.39 (m, 9H, 4 x CH_2, CH), 1.90 (qt, *J* = 6.6 Hz, 2H, CH_2), 2.23 (t, *J* = 7.2 Hz, 2H, CH_2CO), 2.97 (d, *J* = 6.0 Hz, 2H, $C\underline{H_2}NH$), 3.80 (t, *J* = 6.1 Hz, 2H, CH_2O), 6.72 (d, *J* = 8.9 Hz, 2H, 2 x CH Ar), 6.98 (d, *J* = 8.5 Hz, 2H, 2 x CH Ar).

^{13}C-NMR (CD_3OD, δ): 11.2, 14.4 (2 x CH_3), 24.1, 25.2, 26.8, 30.0, 32.0 (5 x CH_2), 33.5 (CH_2CO), 40.6 (CH), 43.4 (CH_2NH), 68.6 (CH_2O), 116.2, 122.2 (4 x CH Ar), 147.8, 158.8 (2 x C Ar), 175.6 (CO).

MS (ESI): 386.1 $(M-H)^-$. **Anal. Calcd. for $C_{18}H_{30}NO_6P$:** C, 55.80; H, 7.81; N, 3.62. **Found:** C, 55.46; H, 7.55; N, 3.74.

4-(4-{[2-[(1-Naphthyl)amino]ethyl]amino}-4-oxobutoxy)phenyl dihydrogen phosphate (2f).

Yield: 47%; **mp:** 82-84 ºC (methanol/chloroform).

IR (neat, cm^{-1}): 3286 (OH), 1641 (C=O), 1581 (C_{Ar}-C_{Ar}), 1535 (N–CO), 1504 (NH), 1207 (P–OC), 1046, 943 (C–OP).

^{1}H-NMR (CD_3OD, δ): 1.95 (qt, *J* = 6.0 Hz, 2H, CH_2), 2.31 (t, *J* = 7.1 Hz, 2H, CH_2CO), 3.20-3.30 (m, 2H, $C\underline{H_2}NH$), 3.41-3.45 (m, 2H, $C\underline{H_2}NH$), 3.77 (t, *J* = 6.1 Hz, 2H, CH_2O), 6.60-6.75 (m, 3H, 3 x CH Ar), 6.95-7.34 (m, 6H, 6 x CH Ar), 7.64-7.68 (m, 1H, CH Ar), 7.85-7.89 (m, 1H, CH Ar).

^{13}C-NMR (CD_3OD, δ): 26.6 (CH_2), 33.6 (CH_2CO), 39.5, 45.8 (2 x CH_2NH), 68.4 (CH_2O), 116.0, 121.7, 122.2, 125.6, 126.6, 127.3, 129.3 (11 x CH Ar) 135.8, 144.1, 146.8, 156.7 (5 x C Ar), 174.4 (CO).

MS (ESI): 443.3 $(M-H)^-$. **Anal. Calcd. for $C_{22}H_{25}N_2O_6P$:** C, 59.46; H, 5.67; N, 6.30. **Found:** C, 59.11; H, 5.33; N, 5.87.

4-(4-{[2-(Dimethylamino)ethyl]amino}-4-oxobutoxy)phenyl dihydrogen phosphate (2g).

Yield: 82%; **mp:** 175-176 ºC (methanol/chloroform).

IR (neat, cm^{-1}): 3247 (OH), 1656(C=O), 1556 (N–CO), 1505 (NH), 1215 (P–OC), 1099, 1049 (C–OP).

^{1}H-NMR (CD_3OD, δ): 2.10 (qt, *J* = 6.5 Hz, 2H, CH_2), 2.48 (t, *J* = 7.1 Hz, 2H, CH_2CO), 2.90 (s, 6H, 2 x CH_3), 3.25 (t, *J* = 6.2 Hz, 2H, $C\underline{H}_2NH$), 3.58 (t, *J* = 6.1 Hz, 2H, NCH_2), 4.09 (t, *J* = 5.9 Hz, 2H, CH_2O), 7.00 (d, *J* = 9.1 Hz, 2H, 2 x CH Ar), 7.20 (d, *J* = 8.5 Hz, 2H, 2 x CH Ar).

^{13}C-NMR (CD_3OD, δ): 24.7 (CH_2), 32.5 (CH_2CO), 34.6 (NCH_2), 43.0 (2 x CH_3), 56.6 (CH_2N), 68.0 (CH_2O), 115.8, 121.6 (4 x CH Ar), 146.3, 154.2 (2 x C Ar), 177.1 (CO).

MS (ESI): 345.0 $(M-H)^-$. **Anal. Calcd. for $C_{14}H_{23}N_2O_6P$:** C, 48.55; H, 6.69; N, 8.09. **Found:** C, 48.67; H, 6.98; N, 7.86.

4-(4-{[3-(1-Naphthyl)propyl]amino}-4-oxobutoxy)phenyl dihydrogen phosphate (2h).

Yield: 47%; **mp:** 169-171 ºC (diethyl ether).

IR (DCM, cm^{-1}): 3294 (O–H), 1641 (C=O), 1505 (N–H), 1205 (P–OC), 958 (C–OP).

^{1}H-NMR (CD_3OD, δ): 1.92 (qt, *J* = 7.4 Hz, 2H, CH_2), 2.05 (qt, *J* = 6.7 Hz, 2H, CH_2), 2.39 (t, *J* = 7.4 Hz, 2H, CH_2CO), 3.09 (t, *J* = 7.8 Hz, 2H, CH_2), 3.27 (m, 2H, $C\underline{H}_2NH$), 3.95 (t, *J* = 5.9 Hz, 2H, OCH_2), 6.83 (m, 2H, 2 x CH Ar), 7.10 (m, 2H, 2 x CH Ar), 7.30-7.51 (m, 4H, 4 x CH Ar), 7.69 (d, *J* = 7.9 Hz, 1H, CH Ar), 7.82-7.85 (m, 1H, CH Ar), 8.02-8.05 (m, 1H, CH Ar).

^{13}C-NMR (CD_3OD, δ): 25.7, 30.3, 30.6 (3 x CH_2), 32.7 (CH_2CO), 39.4 (CH_2NH), 67.6 (CH_2O), 115.1 (2 x CH Ar), 121.3 (2 x CH Ar), 123.7, 125.5, 125.6, 125.9, 126.1, 126.7, 128.8 (7 x CH Ar), 132.1, 134.5, 138.3, 146.5, 155.9 (5 x C Ar), 174.9 (CO).

MS (ESI): 442.0 $(M-H)^-$. **Anal. Calcd. for $C_{23}H_{26}NO_6P$:** C, 62.30; H, 5.91; N, 3.16. **Found:** C, 61.85; H, 5.73; N, 3.24.

4-(4-Oxo-4-{[3-(5,6,7,8-tetrahydronaphthalen-1-yl)propyl]amino}butoxy)phenyl dihydrogen phosphate (2i).

Yield: 71%; **mp:** 157-159 ºC (diethyl ether).

IR (neat, cm^{-1}): 3293 (O–H), 1642 (C=O), 1507 (N–H), 1211 (P–OC), 956 (C–OP).

^{1}H-NMR (CD_3OD, δ): 1.53-1.81 (m, 7H, 3 x CH_2, ½ CH_2), 2.05 (qt, *J* = 6.5 Hz, 2H, CH_2), 2.37 (t, *J* = 7.1 Hz, 2H, CH_2CO), 2.54-2.59 (m, 1H, ½ CH_2), 2.65-2.76 (m, 4H, 2 x CH_2), 3.30-3.33 (m, 2H, $C\underline{H}_2NH$), 3.91-3.97 (m, 2H, OCH_2), 6.81-7.13 (m, 7H, 7 x CH Ar).

^{13}C-NMR (CD_3OD, δ): 24.1, 24.7, 26.8, 27.1, 31.0, 31.2, 33.7, 35.2 (8 x CH_2), 40.4 (CH_2NH), 68.6 (CH_2O), 115.9 (2 x CH Ar), 122.3 (CH Ar), 126.3 (2 x CH Ar), 127.2, 128.2 (2 x CH Ar), 135.7, 138.3, 140.8, 142.1, 156.6 (5 x C Ar), 175.5 (CO).

MS (ESI): 446.5 $(M-1)^-$. **Anal. Calcd. for $C_{23}H_{30}NO_6P$:** C, 61.74; H, 6.76; N, 3.13. **Found:** C, 61.50; H, 6.75; N, 3.09.

4-({5-Oxo-5-[(2-phenylethyl)amino]pentyl}oxy)phenyl dihydrogen phosphate (3a).

Yield: 58%; **mp:** 187-189 ºC (methanol/chloroform).

IR (neat, cm^{-1}): 3282 (OH), 1643 (C=O), 1555 (N–CO), 1504 (NH), 1246, 1203 (P–OC), 1021, 964 (C–OP).

^{1}H-NMR (CD_3OD, δ): 1.50-1.75 (m, 4H, 2 x CH_2), 2.00-2.20 (m, 2H, CH_2CO), 2.70 (t, *J* = 7.3 Hz, 2H, CH_2), 3.31 (t, *J* = 7.3 Hz, 2H, $C\underline{H}_2NH$), 3.70-3.90 (m, 2H, CH_2O), 6.75 (d, *J* = 9.0 Hz, 2H, 2 x CH Ar), 7.00-7.20 (m, 7H, 7 x CH Ar).

^{13}C-NMR (CD_3OD, δ): 23.6, 29.7 (2 x CH_2), 36.5, 36.7 (CH_2CO, CH_2), 41.8 (CH_2NH), 69.0 (CH_2O), 116.1, 122.5, 127.5, 129.6, 130.0 (9 x CH Ar), 140.7, 157.4 (3 x C Ar), 176.0 (CO).

MS (ESI): 392.0 $(M-H)^-$. **Anal. Calcd. for $C_{19}H_{24}NO_6P$:** C, 58.01; H, 6.15; N, 3.56. **Found:** C, 57.98; H, 6.24; N, 3.64.

4-[(5-{[2-[(1-Naphthyl)amino]ethyl]amino}-5-oxopentyl)oxy]phenyl dihydrogen phosphate (3b).

Yield: 43%; **mp:** 65-67 ºC (methanol/chloroform).

IR (neat, cm^{-1}): 3297 (OH), 1641 (C=O), 1581 (C_{Ar}-C_{Ar}), 1530 (N–CO), 1509 (NH), 1230 (P–OC), 1059, 935 (C–OP).

^{1}H-NMR (CD_3OD, δ): 1.60-1.77 (m, 4H, 2 x CH_2), 2.25 (t, *J* = 7.0 Hz, 2H, CH_2CO), 3.30 (t, *J* = 6.0 Hz, 2H, $C\underline{H}_2NH$), 3.55-3.64 (m, 2H, $C\underline{H}_2NH$), 3.80 (t, *J* = 6.0 Hz, 2H, CH_2O), 6.52 (d, *J* = 7.0 Hz, 1H, CH Ar), 6.60-6.71 (m, 4H, 4 x CH Ar), 7.09 (d, *J* = 8.0 Hz, 1H, CH Ar), 7.23 (d, *J* = 7.7 Hz, 1H, CH Ar), 7.31-7.41 (m, 2H, CH Ar), 7.62-7.74 (m, 1H, CH Ar), 7.96-8.01 (m, 1H, CH Ar).

^{13}C-NMR (CD_3OD, δ): 23.7, 29.9 (2 x CH_2), 36.8 (CH_2CO), 39.7, 45.2 (2 x CH_2NH), 68.2 (CH_2O), 104.6, 116.7, 117.8, 121.8, 125.4, 126.6, 127.6, 129.3 (11 x CH Ar), 135.9, 140.8, 145.1, 157.3 (5 x C Ar), 176.9 (CO).

MS (ESI): 457.2 $(M-H)^-$. **Anal. Calcd. for $C_{23}H_{27}N_2O_6P$:** C, 60.26; H, 5.94; N, 6.11. **Found:** C, 60.03; H, 6.02; N, 6.41.

4-[(5-{[3-(1-Naphthyl)propyl]amino}-5-oxopentyl)oxy]phenyl dihydrogen phosphate (3c).

Yield: 45%; **mp:** 135-137 ºC (methanol/chloroform).

IR (neat, cm^{-1}): 3274 (OH), 1644 (C=O), 1557 (N–CO), 1504 (NH), 1203 (P–OC), 964 (C–OP).

^{1}H-NMR (CD_3OD, δ): 1.60-1.80 (m, 4H, 2 x CH_2), 1.87-1.93 (m, 2H, CH_2), 2.04-2.24 (m, 2H, CH_2CO), 2.99-3.12 (m, 2H, CH_2), 3.25-3.35 (m, 2H, $C\underline{H}_2NH$), 3.75-3.85 (m, 2H, OCH_2), 6.73 (d, *J* = 9.0 Hz, 2H, 2 x CH Ar), 7.10 (d, *J* = 9.0 Hz, 2H, 2 x CH Ar), 7.23-7.47 (m, 4H, 4 x CH Ar), 7.56-7.62 (m, 1H, CH Ar), 7.66-7.80 (m, 1H, CH Ar), 7.90-7.95 (m, 1H, CH Ar).

^{13}C-NMR (CD_3OD, δ): 23.6, 29.8, 31.2, 31.6 (4 x CH_2), 36.7 (CH_2CO), 40.3 (CH_2NH), 68.9 (CH_2O), 116.0, 116.6, 122.2, 124.6, 126.4, 126.5, 126.8, 127.7, 129.7 (11 x CH Ar), 131.5, 133.7, 137.2, 148.5, 156.2 (5 x C Ar), 176.0 (CO).

MS (ESI): 456.3 $(M-H)^-$. **Anal. Calcd. for $C_{24}H_{28}NO_6P$:** C, 63.01; H, 6.17; N, 3.06. **Found:** C, 63.02; H, 6.03; N, 2.96.

4.2.3. Synthesis of 4-[(4-amino-1*H*-benzimidazol-2-yl)methyl]phenyl dihydrogen phosphate (18)

4-[(4-Nitro-1H-benzimidazol-2-yl)methyl]phenol (19).

To a stirred suspension of 3-nitrobenzene-1,2-diamine (1 equiv) and 4-hydroxyphenyl acetic acid, an aqueous solution of 6 M HCl (1 mL x mmol) was added, and the reaction refluxed overnight. After cooled to rt, the mixture was neutralized with saturated $NaHCO_3$ and extracted with ethyl acetate (3 x 15 mL x mmol). The organic layer was dried over anhydrous Na_2SO_4 and the solvent was eliminated under reduced pressure to afford **19** as a solid that was purified by column chromatography.

Chromatography: dichloromethane → dichloromethane:ethyl acetate, 1:1. **Yield:** 58%; **mp:** 228-230 ºC.

IR (neat, cm^{-1}): 1640, 1613, 1596 (NC=N), 1509 (N=O), 1341 (C_{Ar}-NO_2).

^{1}H-NMR (CD_3OD, δ): 4.13 (s, 2H, CH_2), 6.63 (d, *J* = 8.6 Hz, 2H, CH Ar), 7.07 (d, *J* = 8.6 Hz, 2H, CH Ar), 7.27 (t, *J* = 8.09 Hz, 1H, CH Ar), 7.85 (d, *J* = 7.9 Hz, 1H, CH Ar), 8.03 (d, *J* = 8.2 Hz, 1H, CH Ar).

^{13}C-NMR (CD_3OD, δ): 33.8 (CH_2), 115.5 (3 x CH Ar), 118.7 (CH Ar), 121.6 (CH Ar), 127.5 (C Ar), 129.8 (2 x CH Ar), 133.8, 134.9, 146.0, 156.6, 158.7 (5 x C Ar).

Dibenzyl 4-[(4-nitro-1H-benzimidazol-2-yl)methyl]phenyl phosphate (20).

Derivative **20** was obtained following the general procedure described in **5.2.2.5.** starting from 0.37 mmol of **19**.

Chromatography: dichloromethane:ethyl acetate, 9:1 → 7:3. **Yield:** 58%. Oil.

IR (neat, cm^{-1}): 1637, 1607, 1586 (N-C=N), 1507 (N=O), 1372 (C_{Ar}-NO_2), 1267 (P-OC), 1015 (C-OP).

^{1}H-NMR ($CDCl_3$, δ): 4.15 (s, 2H, CH_2), 5.04 (s, 2H, CH_2O), 5.06 (s, 2H, CH_2O), 6.98 (d, *J* = 8.7 Hz, 2H, CH Ar), 7.07 (d, *J* = 8.5 Hz, 2H, CH Ar), 7.27 (m, 11H, CH Ar), 7.95 (d, *J* = 8.0 Hz, 1H, CH Ar), 8.03 (d, *J* = 8.2 Hz, 1H, CH Ar).

^{13}C-NMR ($CDCl_3$, δ): 30.1 (CH_2), 70.5, 70.6 (2 x CH_2O), 119.4 (CH Ar), 120.9, 121.0, 121.9, 127.1 (4 x CH Ar), 128.5 (4 x CH Ar), 129.0 (4 x CH Ar), 129.1 (2 x CH Ar), 130.6 (2 x CH Ar), 133.1, 133.5, 135.6, 135.7, 146.4, 150.1, 150.2, 156.4 (8 x C Ar).

4-[(4-Amino-1H-benzimidazol-2-yl)methyl]phenyl dihydrogen phosphate (18).

Derivative **18** was obtained following the general procedure described in **5.2.1.6.** starting from 0.13 mmol of its benzylated precursor **20**.

Yield: 80%. Oil.

IR (neat, cm^{-1}): 3366 (N-H), 1610 (C=N), 1237 (P-OC), 1103 (C-OP).

^{1}H-NMR (CD_3OD, δ): 4.02 (s, 2H, CH_2), 6.39 (d, *J* = 7.6 Hz, 1H, CH Ar), 6.68 (d, *J* = 7.2 Hz, 1H, CH Ar), 6.83 (t, *J* = 7.8 Hz, 1H, CH Ar), 7.05 (d, *J* = 8.6 Hz, 2H, CH Ar), 7.16 (d, *J* = 8.4 Hz, 2H, CH Ar).

^{13}C-NMR (CD_3OD, δ): 33.7 (CH_2), 106.1, 119.5, 119.6, 122.4 (4 x CH Ar), 128.2 (2 x CH Ar), 128.6 (CH Ar), 127.9, 133.5, 135.2, 147.0, 152.17, 153.8 (6 x C Ar).

MS (ESI) 318.1 $(M-H)^-$. **Anal. Calcd. for $C_{14}H_{14}N_3O_4P$:** C, 52.67; H, 4.42; N, 13.16. Found: C, 52.23; H, 4.69; N, 13.37.

4.3. Determination of the binding affinity by competition assays.

Precoated streptavidin 96-well plates (Sigma-Aldrich, Spain) were incubated overnight at 4 ºC with 100 μL/well of biotin-Ahx-PSpYVNVQN peptide (Sigma-Aldrich, Spain) at 200 nM in PBS. After four treatments with washing buffer (PBS containing 0.1% Tween-20), non-specific binding was blocked with PBS containing 5% skimmed powdered milk for 1 h at rt and washed three times with washing buffer. Reaction mixtures contained competitors, and 200 nM glutathione *S*-transferase fusion protein (GST)-Grb2(54-164) (Santa Cruz Biotechnology) in PBS containing 3% BSA, which had previously been preincubated by shaking for 2 h at rt. The components were added to the plate and the mixture was incubated for 2 h at rt without shaking. Unbound GST-Grb2(54-164) was removed by three washes with washing buffer. Bound GST-Grb2(54-164) was revealed after a sequence of incubation with a mouse anti-GST antibody (BD Biosciences; used for 1 h at rt at 1 μg/mL in PBS containing 3% BSA), three washes, incubation with HRP-conjugated goat anti-mouse (Biorad; used for 1 h at rt at 1/500 in PBS containing 5% skimmed powdered milk), three washes, and final addition of *3*,*3′*,*5*,*5′*-Tetramethylbenzidine (TMB, Sigma-Aldrich, Spain). The reaction was stopped with 0.5 M H_2SO_4, and absorbance at 450 nm was read in a microplate reader (UVM-340, ASYS Hitech GmbH). Controls were done by omitting each reagent separately, and no significant absorbance was observed in any of the incomplete assays. For each experiment, non-specific binding was measured and subtracted for each experimental point. Dose-response curves were constructed by nonlinear regression of the competition curves, using Prism. IC_{50} values are expressed as mean±SEM, and they correspond to at least three independent experiments carried out in duplicate. Compound 1224-130, kindly donated by Prof. T. R. Burke, was used as control of the ELISA test. This compound shows an IC_{50} value of 0.0148 μM in our assay, comparable to the value previously reported.[129]

[129] See citation 90.

4.4. NMR Protein Spectroscopy sample preparation.

These experiments were carried out as described previously.[130]

4.5. HER2-Grb2 interaction

HER2-positive MCF7 cells were exposed to the compound or to vehicle as described above for cell cytotoxicity experiments in 150 mm dishes. Cells were washed twice with ice-cold PBS and then scraped off the plates in cell-lysis buffer (1% NP-40, 20 mM Tris-HCl, pH = 7.4, 0.14 M NaCl, 1 mM EDTA, 1 mM EGTA) containing protease inhibitor cocktail (Roche) and phosphatase inhibitor cocktail I and II (Sigma). Lysates were prepared by glass-douncer homogenization in ice and followed by centrifugation in a microfuge (12000*g* for 10 min at 4 ºC). Supernatants were saved and protein concentration quantified by the Lowry-based DC protein assay (Biorad). For coimmunoprecipitation, 2 mg protein were incubated with 60 µL of an anti-HER2 agarose immobilized antibody (Affibody AB, Sweden) in a final volume of 300 µL for 3 h with rotation at 4 ºC. Beads were washed five times with lysis buffer, eluted with 200 µL of electrophoresis sample (Laemmli) buffer and heated at 95 ºC for 10min. Thereafter, proteins were separated on a 10% SDS-polyacrylamide gel and transferred onto nitrocellulose membranes. Membranes were washed once with Tris-buffered solution (TBS, 10 mM Tris, 150 mM NaCl, pH = 8.0), once with TBS-T (TBS with 0.1% Tween-20) and incubated for 1 h at rt in blocking buffer (1% BSA in TBS-T) to prevent non-specific antibody binding. Then, membranes were incubated with the corresponding primary antibodies anti-HER2 and anti-Grb2 (Santa Cruz Biotechnology) diluted in blocking buffer overnight at 4 ºC (1:500, 0.4 µg/mL). After three 5-min washes in TBS-T, membranes were incubated for 1 h with the corresponding HRP-conjugated secondary antibody (1:5000, Biorad), washed again three times with TBS-T and developed using a commercial kit (Amersham ECL western blotting detection reagents, GE Healthcare). Bands were densitometered to calculate the ratio of HER2-associated Grb2 in the presence or absence of the compound under study.

4.6. Cell cytotoxicity

Non-malignant fibroblasts N1 and breast tumor cell lines (HER2-positive and HER2-negative MCF7 cells and MDA-231 cells) were kindly donated by Drs. R. Colomer (MD Anderson International Spain) and T. Puig (Institut Català d'Oncologia, Institut d'Investigació Biomèdica de Girona, and Universitat de Girona, Spain). Cells were routinely incubated in a humidified atmosphere at 37 ºC with 5% CO_2 and passaged in DMEM medium (Invitrogen) containing 10% FBS (Gibco), 1% L-glutamine (Gibco), 1% sodium pyruvate (Gibco), 1% Penicillin-Streptomycin solution (Gibco). Cell cytotoxicity was determined using a standard colorimetric MTT assay (Sigma) following manufacturer´s instructions. Briefly, N1 or MCF7 cells were plated out at a density of 5 x 10^3 cells/100 µL/well in 96-well microtitre plates and

[130] See citation 84.

incubated for 24 h. Then the medium was removed and cells were incubated for 24 h with fresh medium containing different concentrations of the compounds under study. Afterwards, fresh medium (100 μL/well) and 10 μL of a 5 mg/mL MTT solution were added and cells were incubated for 3 h at 37 ºC. After careful removal of the supernatants, the MTT-formazan crystals formed by metabolically viable cells were dissolved in DMSO (100 μL/well) and absorbance was measured at 570 nm in a UVM-340, ASYS Hitech GmbH multi-well plate reader. Absorbance at 620 nm was used as background correction and substracted from each experimental point. Viability values are expressed as percentage of the control as mean±SEM, and they correspond to two independent experiments carried out in duplicate.

4.7. Proteomic studies.

4.7.1. m^7GTP-binding proteins

m^7GTP-binding proteins were pulled-down using a procedure previously described.[131] Briefly 250 μL (5 mg of protein content approx.) of pooled cytosolic human liver lysates (Sigma-Aldrich, Denmark) were added protease inhibitor cocktail (Sigma-Aldrich, Denmark) and pre-cleared after incubation (under gentle toss) in 2 separate eppendorf tubes (100 μL beads + 125 μL lysates each) at 4 ºC for 30 min with sepharose beads (20% in ethanol, Jena Bioscience) which had been previously washed with 50 mM HEPES buffer pH 7.6 (3 x 100 μL). After spinning down the beads, the non-bound supernatant was transferred to a new pair of previously HEPES-washed (3 x 100 μL) tubes (50 μL beads + 115 μL precleared extract approx.) containing γ-amino-hexyl-m^7GTP-sepharose (20% in ethanol, Jena Bioscience). The tubes were again incubated at 4 ºC for 2 h and, once spun, the flow-through (FT) removed. Beads were then washed with buffer 1 (W1, 3 x 100 μL/ tube; 50 μM GDP, 250 mM KCl, 1 mM DTT, and 50 mM HEPES pH 7.6; spun dry and supernatant (W1) saved. Beads were washed twice (1 x 200 μL/ tube; 250 mM KCl, 1 mM DTT, and 50 mM HEPES pH 7.6) and, after spinning, washes were saved as W2 and W3. Finally, spun dry beads were eluted (1 x 30 μL/ tube) with elution buffer (E, 1 mM m^7GTP, 200 mM KCl, 1 mM DTT, and 50 mM HEPES pH 7.6). Eluted proteins were stored at -80 ºC for further processing, saving 15 μL, however, to be run with equivalent quantities of FT, W1, W2, and W3 in SDS-PAGE silver stained.

4.7.2. cAMP-binding proteins

A similar procedure to the one described in **5.7.1.** was followed except for the use of 8-amino-hexyl-cAMP-sepharose (50 μL beads + 115 μL precleared extract approx. per tube) and for the composition of washing and elution buffers: W1 (3 x 100 μL/ tube; 50 μM ADP, 500 mM KCl, 1mM DTT, and 50 mM HEPES pH 7.6); W2 and W3 (1 x 200 μL/ tube; 500 mM KCl, 1mM DTT, and 50 mM HEPES pH 7.6); E (1 x 30 μL/ tube; 10mM cAMP, 200 mM KCl, 1mM DTT, and 50 mM HEPES pH 7.6).

[131] Webb, N. R.; Chari, R. V.; DePillis, G.; Kozarich, J. W.; Rhoads, R.E. *Biochemistry* **1984**, *23*, 177-181.

4.7.3. ATP-binding proteins

The procedure was similar to the one described in **5.7.1.** although with some minor modifications as detailed. Protease inhibited human cytosolic liver lysates were dialysed for 6 h at 4 ºC (Thermo Scientific Slide-A-Lyzer Dialysis Cassettes, 3.5K MWCO) to remove salts and small molecules. Then, 1 M $MgCl_2$ solution was added to the dialysed lysates to a final concentration of 30 mM. Sepharose pre-clearing step was carried out as in the previous procedures and affinity purification was done employing γ-amino-hexyl-ATP-sepharose (50 µL beads + 115 µL precleared extract approx. per tube). After incubation for 2 h at 4 ºC, beads were washed an eluted using the following buffers composition: W1: (3 x 200 µL/ tube; 100 µM ADP, 500 mM KCl, 1mM DTT, and 50 mM HEPES pH 7.6). W2 and W3 (1 x 200 µL/ tube; 500 mM KCl, 1mM DTT, and 50 mM HEPES pH 7.6). And E (1 x 30 µL/ tube; 10 mM ATP, 200 mM KCl, 1mM DTT, and 50 mM HEPES pH 7.6).

4.7.4. Sample preparation for LC-MS.

Eluates from the m^7GTP, cAMP and ATP-sepharose columns were precipitated by incubation overnight at 4 ºC with two volumes of 50% solution of trichloroacetic acid (TCA). Precipitated proteins were isolated by centrifugation in a microfuge (12000*g* for 10 min at 4 ºC), the supernatant was removed and the pellets were further washed (2 x 200 µL) with a 1:1 mixture of ethanol:ethyl ether. Pellets were dried for 15 min in an speed-vacuum system, resuspended in 13.5 µL of water and 4.5 µL of 4x reducing buffer, and loaded in a 4-20% polyacrylamide gel (PAGEr® Gold Precast Gel, Lonza USA). The gel was further stained for 1 h with ethanolic coomassie blue.

Slices of gel were excised according to the silver pattern observed in the control gel of the corresponding experiments and introduced in pre-lubricated commercial eppendorf tubes. Alternative washes of acetonitrile and water (3 x 100 µL each) and spinning cycles (12000*g* for 15 min) were carried until no coomassie blue came out of the gel pieces. After the last acetonitrile wash and spinning cycle, gel pieces were completely covered and incubated for 20 min (on ice) with trypsin solution (6.66 ng/µL in NH_4HCO_3). Then, supernatant excess of trypsin was removed, substituted for ~30 µL of 50 mM NH_4HCO_3 and the tubes incubated at 37 ºC overnight.

Digested peptides were desalted and filtered on in-house made C18-Oligo R3 microcolumns. The peptide mixtures (~100 µL) were loaded, washed with 100 µL of 5% formic acid, and eluted with 30 µL of a 70% acetonitrile and 5% formic acid solution by applying air pressure with a small syringe. Eluates were collected in 1.5 mL eppendorf tubes, concentrated in a speed-vacuum system and analysed by nanoLC-MS/MS.

4.7.5. NanoLC-MS/MS

All digested peptide mixtures were separated by an on-line nano-LC system and analyzed by ESI tandem mass spectrometry on a LTQ/Orbitrap system (ThermoFisher

Scientific). Peptide mixtures were loaded onto a 40 mm trap column, packed with 25 mm Poros 10R2 (10 µm) and 15 mm C18 (5 µm), at 10 µL/min flow. Separation was performed with a flow of 0.3 µl/min on a 20 cm reverse-phase column (Biosphere C18, 5 µm, Nanoseparations, The Netherlands). Peptides were separated using a 25 min-gradient and subsequently eluted with a flow of 0.3 µl/min with a gradient 5 to 60% B (acetonitrile with 0.1% formic acid [v/v]) in A (water with 0.1% formic acid [v/v]). ESI was performed with nano-LC spray tips, Nanoseparations, The Netherlands). General mass spectrometric conditions were: electrospray voltage, 1.8-2.0 kV; no sheath and auxiliary gas flow; ion transfer tube temperature, 125 °C; collision gas pressure, normalised collision energy, 30-32% for MS^2. Ion selection threshold was 500 counts for MS^2.

Conclusions

5. Conclusions

1. Based on the crystal structure of the Grb2-SH2 domain in complex with the high-affinity pentapeptide 2-Abz-Glu-pTyr-Ile-Asn-Gln-NH_2 ligand, we have designed and synthesized two series of novel non-peptide compounds that maintain all (series **I**) or some (series **II**) of the key interactions with the Grb2-SH2 domain.

2. An ELISA-type competition assay was set up in order to determine the ability of all final compounds to bind the Grb2-SH2 domain. Among the tested compounds, derivative **(*S*)-1k** of series **I** showed the highest affinity (IC_{50} = 174 μM). The fact that none of the compounds of series **II** was able to bind the Grb2-SH2 domain in a significant manner is consistent with the importance of the interactions with Arg67 and His107.

3. The binding mode of **(*S*)-1k** to the Grb2-SH2 domain has been experimentally validated using NMR chemical shift perturbation studies. Based on these data, optimization of **(*S*)-1k** by the introduction of conformational restriction in its structure has yielded **(*S*)-1l**. This compound, with an IC_{50} value of 56 μM, stands out as one of the highest affinity non-peptide compounds described so far.

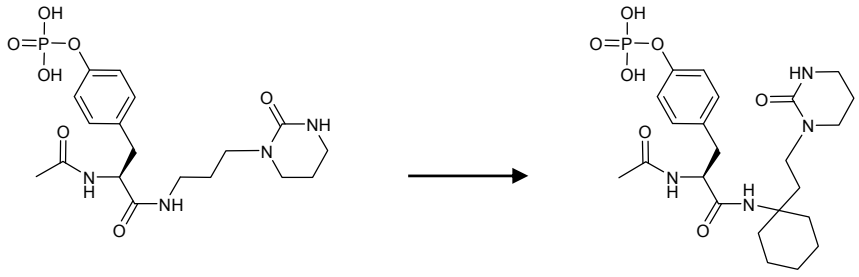

(*S*)-1k **(*S*)-1l**

4. Compound **(*S*)-1l** was further assessed for its cytotoxic *in vitro* potential in HER2-positive and negative human breast cancer cell lines, as well as in N1 fibroblasts. Importantly, **(*S*)-1l** exclusively affected proliferation of HER2-positive MCF7 cells (IC_{50} = 100 μM). This result supports that **(*S*)-1l** is devoid of general cytotoxicity towards non-tumour cells, and that it interferes specifically with the HER2 downstream pathway. Accordingly, using immunoprecipitation experiments, it has been demonstrated that **(*S*)-1l** directly impairs the interaction between HER2 and Grb2.

5. Considering the promising profile of **(*S*)-1l** and the interest on the delineation of all the molecular pathways affected by the compound, a throughput proteomic platform has been designed and validated using different nucleotides. Currently, this platform is being used to compare a relevant proteome (HER2+ breast cancer cells) previously treated or not with **(*S*)-1l**. Then, the proteomic signature should reveal the identity and extent of the transduction pathway(s) affected.

UNIVERSIDAD COMPLUTENSE DE MADRID

FACULTAD DE CIENCIAS QUÍMICAS

Departamento de Química Orgánica I

DESARROLLO DE NUEVOS INHIBIDORES DE LA INTERACCIÓN ENTRE EL RECEPTOR HER2 Y LA PROTEÍNA ADAPTADORA Grb2

Memoria que para optar al

Título de Doctor

presenta

Ángel Lorenzo Orcajo Rincón

Directoras:

Prof. Dra. María Luz López Rodríguez

Prof. Dra. Bellinda Benhamú Salama

Prof. Dra. Silvia Ortega Gutiérrez

MADRID, 2012

Introducción General

1. Introducción General

Cáncer es el término genérico con el que se describe a un grupo de más de cien enfermedades con un denominador común, la generación rápida de células anormales que crecen más allá de sus límites naturales. Siendo éstas capaces en muchos casos de invadir tejidos adyacentes o migrar a otras zonas del organismo, el resultado es casi siempre el mismo: disfunción orgánica progresiva y probablemente letal.

Valoraciones recientes de la Organización Mundial de la Salud[1] sitúan al cáncer como una de las principales causas de muerte a nivel mundial, y estiman su incidencia en 13,1 millones de fallecimientos para el 2030.

El cáncer es un proceso multi-etapas, y la visión más clásica sitúa su punto de partida en el daño al ADN de una célula, que resulta de mutaciones provocadas por diversos agentes externos (carcinógenos físicos, químicos o biológicos) sobre uno o varios genes. Procesos tan determinantes como la proliferación celular, crecimiento, diferenciación y apoptosis, pueden verse severamente afectados por estas mutaciones. La pérdida total de función de estos genes normalmente conlleva una rápida y permanente expansión clónica completamente alterada e independiente de estimulación externa (ej. factores de crecimiento, hormonas, etc), que desencadena la aparición del fenotipo de la enfermedad.[2] En este punto, la masa celular se ha convertido en una neoplasia maligna cada vez más descontrolada, capaz de inducir la generación de nuevos vasos sanguíneos en su periferia (angiogénesis) y de iniciar un proceso de digestión de las capas celulares o endotelio en el que está contenido, para finalmente acceder al torrente sanguíneo y colonizar nuevos tejidos (metástasis).[3]

Los genes cuya mutación implica la aparición de cáncer se denominan oncogenes, dentro de los cuales se cuentan muchos de los receptores de membrana implicados en los procesos de división y crecimiento celular. Tales receptores son activados por sus ligandos, los cuales pueden ser producidos por células vecinas (estimulación paracrina), o por ella misma (estimulación autocrina). La mayor parte de los receptores implicados en procesos de división y diferenciación celular son receptores con actividad proteína quinasa; es decir, son capaces de transferir grupos fosfato desde la molécula donadora, trifosfato de adenosina (*adenosine triphosphate*, ATP), a residuos de serina, treonina o tirosina de una proteína sustrato.[4] La fosforilación de proteínas tiene dos funciones fundamentales: (i) cambiar la conformación de una proteína y como consecuencia modificar su actividad enzimática, y (ii) generar sitios de

---

[1] http://www.who.int/mediacentre/factsheets/fs297/en/index.html.

[2] (a) Fukasawa, K. *Nat. Rev. Cancer* **2007**, *7*, 911-924. (b) Haber, D. A.; Gray, N. S.; Baselga, J. *Cell* **2011**, *145*, 19-24.

[3] (a) McSherry, E. A.; Donatello, S.; Hopkins, A. M.; McDonnell, S. *Cell. Mol. Life Sci.* **2007**, *64*, 3201-3218. (b) Brennan, K.; Offiah, G.; McSherry, E. A.; Hopkins, A. M. *J. Biomed. Biotechnol.,* Hindawi Publishing Corporation, doi:10.1155/2010/460607 **2010**. (c) Arteaga, C. L.; Baselga, J. *Clin. Cancer Res.* **2012**, *18*, 612-618.

[4] (a) Alberts, B.; Johnson, A.; Lewis, J.; Raff, M.; Roberts, K.; Walter, P. *Molecular Biology of the Cell*, Taylor & Francis Inc., 5th Ed., **2007**. (b) DeVita Jr., V. T.; Lawrence T. S.; Rosenberg, S. A.; DePinho, R. A.; Weinberg, R. A. *Cancer: Principles and Practice of Oncology*, Wolters Kluwer - Lippincott Williams & Wilkins, 9th Ed., **2011**.

reconocimiento para otras proteínas señalizadoras. En general puede decirse que la fosforilación contribuye a la transmisión y amplificación de la señal mitogénica. Usualmente, este proceso de transmisión y amplificación tiene como consecuencia la activación secuencial de la proteína Ras y de la vía de las proteínas quinasas activadas por mitógenos (*mitogen-activated protein kinases,* MAPKs).[5] Son ellas las responsables últimas de la activación de los genes comprometidos en la división celular.[6]

Los receptores con actividad tirosina quinasa (*tyrosine kinase receptors,* TKRs) se clasifican en cuatro familias en función de su similitud estructural. En particular, la subclase I, fundamental en los procesos tumorales, comprende los diferentes receptores de factor de crecimiento epidérmico (*epidermal growth factor receptors,* EGFRs). Este grupo de proteínas se compone de cuatro miembros bien diferenciados: HER1 (también llamado EGFR o ErbB1), HER2 (neu o ErbB2), HER3 (ErbB3) y HER4 (ErbB4).[7] Los HERs se expresan en varios tipos de tejidos, siendo los más comunes del tipo epitelial, mesenquimal y neuronal. Estructuralmente los cuatro receptores de esta familia están constituidos por un dominio extracelular de unión a ligando, una hélice transmembrana de carácter hidrofóbico y un dominio intracelular con actividad tirosina quinasa (Figura 1a).[8]

El dominio intracelular con actividad tirosina quinasa de los receptores HERs se encuentra altamente conservado dentro de la familia, excepto en el caso de HER3, que carece de actividad quinasa (Figura 1a). Por otra parte, los dominios extracelulares se encuentran poco conservados, lo que sugiere un alto grado de especialización en cuanto a la unión con sus respectivos ligandos.[9] Tras la unión a su ligando específico (vía subdominios I y III), estos receptores sufren un importante cambio conformacional que deja expuesto el brazo de dimerización ubicado en el subdominio II y que permite su interacción con otro receptor vecino. Esta situación no es posible en HER2 dada la extensiva interacción entre los subdominios I y III, por lo que adopta una conformación constitutivamente activa y dispuesta a la dimerización (Figura 1b).[10] Esta característica podría explicar la importante capacidad que tiene HER2 para inducir transformación celular en situación de sobreexpresión.

---

[5] (a) Sebolt-Leopold, J. S. *Oncogene* **2000**, *19*, 6594-6599. (b) Chapman, M. S.; Miner, J. N. *Expert Opin. Investig. Drugs* **2011**, *20*, 209-220.

[6] (a) Barbacid, M. *Ann. Rev. Biochem*. **1987**, *56*, 779-827. (b) Young, A.; Lyons, J.; Miller, A. L.; Phan, V. T.; Alarcón, I. R.; McCormick, F. *Adv. Cancer Res.* **2009**, *102*, 1-17.

[7] Baselga, J.; Swain, S. M. *Nat. Rev. Cancer* **2009**, *9*, 463-475.

[8] (a) Olayioye, M. A.; Neve, R. M.; Lane, H. A.; Hynes, N. E. *EMBO J.* **2000**, *19*, 3159-3167. (b) Ferguson, K. M.; Berger, M. B.; Mendrola, J. M.; Cho, H. S.; Leahy, D. J.; Lemmon, M. A. *Mol. Cell* **2003**, *11*, 507-517. (c) Lurje, G.; Lenz, H. J. *Oncology* **2009**, *77*, 400-410.

[9] (a) Yarden, Y.; Sliwkowski, M. X. *Nat. Rev. Mol. Cell Biol.* **2001**, *2*, 127-137. (b) Burgess, A. W. *Growth Factors* **2008**, *26*, 263-274.

[10] (a) Burgess, A. W.; Cho, H. S.; Eigenbrot, C; Ferguson, K. M.; Garrett, T. P. J.; Leahy, D. J.; Lemmon M. A.; Sliwkowski, M. X.; Ward, C. W.; Yokoyama, S. *Mol. Cell* **2003**, *12*, 541-552. (b) Lemmon, M. A. *Exp. Cell Res.* **2009**, *315*, 638-648.

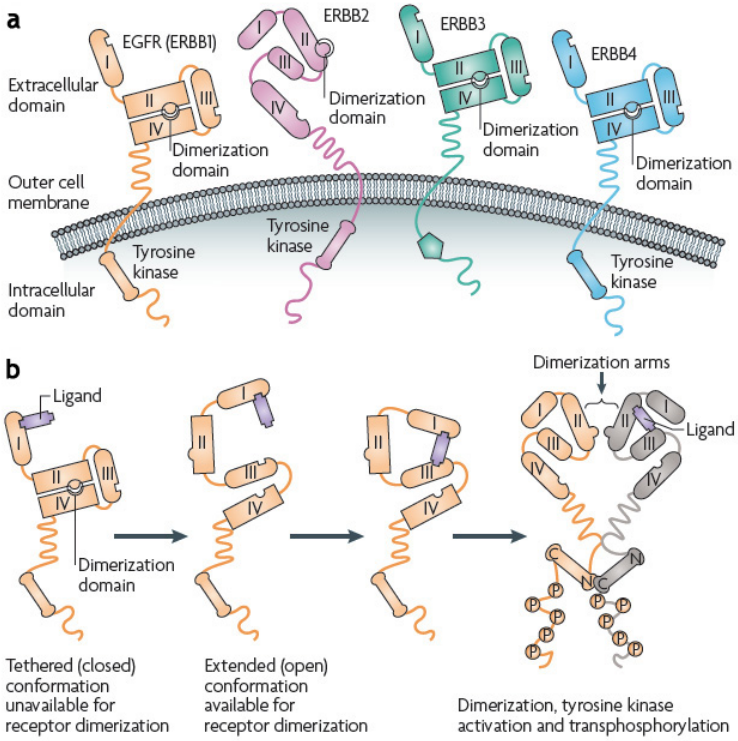

Figura 1. a. Representación esquemática de los cuatro receptores miembros de la familia ErbB (ErbB1-4). **b.** Cambio de la conformación plegada a la extendida tras la unión a su respectivo ligando; modificación imprescindible para que se produzca la dimerización receptor-receptor. (Reproducido de la cita 7)

En condiciones fisiológicas normales la activación de los HERs es controlada por la expresión tanto espacial como temporal de sus ligandos endógenos, proteínas de la familia de los factores de crecimiento epidérmico (*epidermal growth factors*, EGFs). Este grupo está compuesto por trece miembros que en muchos casos solapan su acción sobre un mismo receptor (Figura 2a).[11]

Así, cada receptor puede ser activado por más de un ligando, exceptuando HER2, del que aún no se conoce su ligando endógeno. A pesar de ello, es el que más interés ha atraído dentro de la oncología clínica y molecular por ser el receptor de heterodimerización preferido del resto de los miembros de esta familia.[12]

En resumen, la unión específica de un ligando a su receptor induce la formación de homo- y heterodímeros, lo que conlleva la activación del dominio con actividad tirosina quinasa, resultando finalmente en la fosforilación de residuos específicos de tirosina en el dominio intracelular del receptor.[13] Estos residuos fosforilados sirven como puntos de reconocimiento

[11] (a) Citri, A.; Yarden, Y. *Nat. Rev. Mol. Cell Biol*. **2006**, *7*, 505-516. (b) Avraham, R.; Yarden, Y. *Nat. Rev. Mol. Cell Biol*. **2011**, *12*, 104-117.

[12] (a) Hynes, N. E.; Lane, H. A. *Nat. Rev. Cancer* **2005**, *5*, 341-354. (b) Zhang, H.; Berezov, A.; Wang, Q.; Zhang, G.; Drebin, J.; Murali, R.; Greene, M. I. *J. Clin. Invest.* **2007**, *117*, 2051-2058. (c) Hynes, N. E.; MacDonald, G. *Curr. Opin. Cell Biol.* **2009**, *21*,177-184.

[13] (a) Zhang, X.; Gureasko, J.; Shen, K.; Cole, P. A.; Kuriyan, J. *Cell* **2006**, *125*, 1137-1149. (b) Bose, R.; Zhang, X. *Exp. Cell Res.* **2009**, *315*, 649-658.

para una gran variedad de proteínas adaptadoras (como por ejemplo Shc, Grb7, Grb2, Nck, PLCγ, Figura 2b), cuya activación desencadena una cascada de fosforilaciones consecutivas de moléculas que forman parte de las rutas de transmisión de la señal mitogénica o vía de las MAPKs.[14]

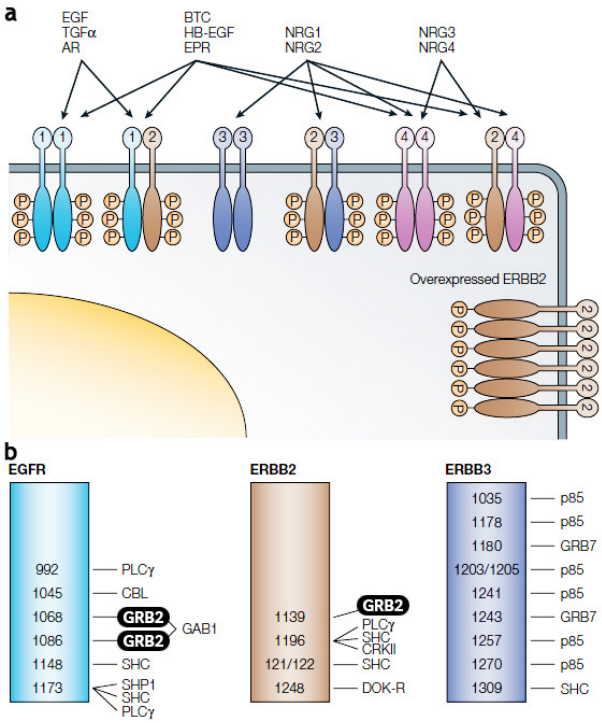

Figura 2. a. Miembros de la familia EGF y sus respectivos receptores. **b.** Representación esquemática de los sitios de autofosforilación mejor estudiados en HER1-3 y sus proteínas adaptadoras relacionadas. (Reproducido de la cita 12a)

La activación de la vía de las MAPKs[15,16] se produce fundamentalmente a través de la proteína adaptadora Grb2,[17] la cual reconoce los residuos de tirosina fosforilados en HER2 a través de su dominio SH2 (*Src homology 2*). Una vez unida a HER2, a través de otro dominio, SH3, se acopla a la proteína Sos, la cual finalmente activa Ras (Figura 3).[18,19]

---

[14] (a) Mendelsohn, J.; Baselga, J. *J. Clin. Oncol.* **2003**, *21*, 2787-2799. (b) Cargnello, M.; Roux, P. P. *Microbiol. Mol. Biol. Rev.* **2011**, *75*, 50-83.

[15] Kolch, W. *Biochem. J.* **2000**, *351*, 289-305.

[16] Sebolt-Leopold, J. S.; Herrera, R. *Nat. Rev. Cancer* **2004**, *4*, 937-947.

[17] (a) Gale, N. W.; Kaplan, S.; Lowenstein, E. J.; Schlessinger, J.; Bar-Sagi, D. *Nature* **1993**, *363*, 88-92. (b) Tari, A. M.; Lopez-Berestein, G. *Semin. Oncol.* **2001**, *28*, 142-147. (c) Giubellino, A.; Burke, T. R. Jr.; Bottaro, D. P. *Expert Opin. Ther. Targets* **2008**, *12*, 1021-1033.

[18] McCormick, F. *Nature* **1993**, *363*, 15-16.

[19] (a) Downward, J. *Nat. Rev. Cancer* **2003**, *3*, 11-22. (b) Matallanas, D.; Crespo, P. *Curr. Opin. Mol. Ther.* **2010**, *12*, 674-683.

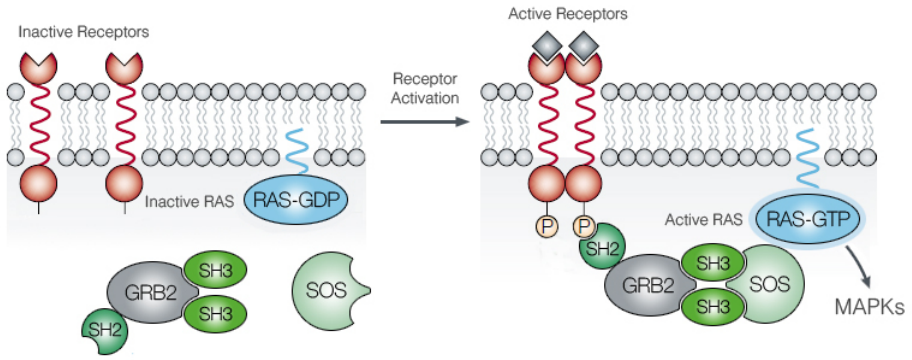

Figura 3. Representación esquemática de la activación de Ras-MAPKs iniciada por la unión ligando-receptor y mediada a través de Grb2.

Una vez activa, Ras fosforila y, de esta manera, moviliza el primer nivel de las MAPKs compuesto por la famila de Raf (o MAPKKK), que a su vez fosforila a MEK1/2 (o MAPKK) y éstas a ERK1/2 (o MAPK). Esta cascada de fosforilaciones consecutivas termina en la activación de numerosos factores de transcripción implicados en procesos celulares tan vitales como la inflamación, mecanismos de reparación, crecimiento, proliferación, migración celular y angiogénesis.[20]

Por esta razón el desarrollo de inhibidores de la interacción entre el receptor HER2 y la proteína adaptadora Grb2 podría constituir una nueva terapia para el tratamiento del cáncer,[21] sobre todo de aquellos tipos caracterizados por una elevada expresión de HER2. Así, se ha descrito que aproximadamente el 30% de los tumores de mama sobreexpresan HER2, condición que también se presenta en otros tipos de neoplasias (tales como ovario, pulmón, páncreas, colon, esófago, endometrio, cuello uterino o glándulas salivales).[22]

1.1. Inhibidores de la interacción HER2-Grb2

El desarrollo de compuestos capaces de inhibir la interacción entre el receptor HER2 y la proteína adaptadora Grb2 es un área de investigación que ha recibido una enorme atención en los últimos años. Esto se ha visto favorecido por la determinación de la estructura tridimensional de diferentes dominios SH2, en particular, del de la proteína Grb2.

Grb2 es una proteína de 25 KDa compuesta por un dominio SH2 rodeado por dos dominios SH3 (Figura 4).[23] El dominio SH3 se une específicamente a regiones ricas en

[20] Chang, F.; Steelman, L. S.; Lee, J. T.; Shelton, J. G.; Navalonic, P. M.; Blalock, W. L.; Franklin, R. A.; McCubrey, J. A. *Leukemia* **2003**, *17*, 1263-1293.

[21] (a) Schubbert, S.; Shannon, K.; Bollag, G. *Nat. Rev. Cancer* **2007**, *7*, 295-308. (b) Lee-Hoeflich, S. T.; Crocker, L.; Yao, E.; Pham, T.; Munroe, X.; Hoeflich, K. P.; Sliwkowski, M. X.; Stern, H. M. *Cancer Res.* **2008**, *68*, 5878-5887. (c) Baselga, J. *Ann. Oncol.* **2010**, *21*, Suppl. 7:vii36-40.

[22] (a) Slamon, D. J.; Clark, G. M.; Wong, S. G.; Levin, W. J.; Ullrich, A.; McGuire, W. L. *Science* **1987**, *235*, 177-182. (b) Holbro, T.; Hynes, N. E. *Annu. Rev. Pharmacol. Toxicol.* **2004**, *44*, 195-217. (c) Higgins, M. J.; Baselga, J. *J. Clin. Invest.* **2011**, *121*, 3797-3803.

[23] Maignan, S.; Guilloteau, J. P.; Fromage, N.; Arnoux, B.; Becquart, J.; Ducruix, A. *Science* **1995**, *268*, 291-293.

prolina,[24] mientras que el dominio SH2 de Grb2 reconoce secuencias peptídicas específicas que contengan pTyr (Glu-pTyr-Ile-Asn-Gln)[25] en el receptor con actividad tirosina quinasa. En 1996 se elucidó mediante resonancia magnética nuclear (RMN) heteronuclear multidimensional la estructura tridimensional (3D) del dominio SH2 de Grb2, similar a la de otros dominios SH2.[26]

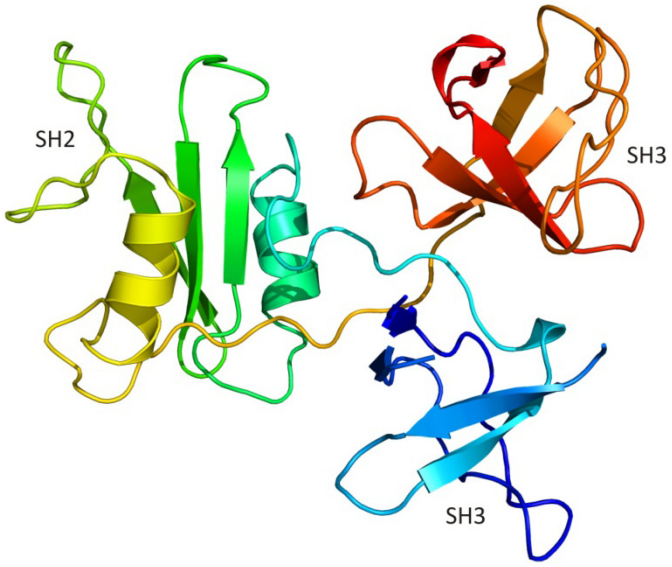

Figura 4. Estructura de rayos X de la proteína Grb2 humana obtenida a una resolución de 3,1 Á (Código PDB: 1gri).

En general, los dominios SH2 poseen dos regiones de reconocimiento principales, la primera de ellas dedicada al anclaje de la pTyr, y la segunda especializada en el reconocimiento de la secuencia que rodea al resto de pTyr. La elucidación estructural del complejo dominio SH2 de Grb2-ligando tanto mediante cristalografía de rayos X[27] como RMN[28] indica que el plegamiento óptimo del ligando en este dominio es en forma de U, a diferencia de lo descrito para otros dominios SH2 de otras proteínas donde el péptido que porta el residuo de pTyr se encuentra en una conformación extendida. Tras un extenso barrido estructural capaz de cubrir ambas regiones, han sido compuestos peptídicos con afinidad por el dominio SH2 de Grb2 los inhibidores más potentes descritos hasta la fecha. Sin embargo, es también posible encontrar algunos ejemplos aislados de pequeñas moléculas orgánicas capaces de unirse al dominio SH2 de Grb2 aunque con menor afinidad.

---

[24] Véase cita 17a.

[25] Rahuel, J.; García-Echeverría, C.; Furet, P.; Strauss, A.; Caravatti, G.; Fretz, H.; Schoepfer, J.; Gay, B. *J. Mol. Biol.* **1998**, *279*, 1013-1022.

[26] Thornton, K. H.; Mueller, W. T.; McConnell, P.; Zhu, G.; Saltiel, A. R.; Thanabal, V. *Biochemistry* **1996**, *35*, 11852-11864.

[27] Rahuel, J.; Gay, B.; Erdmann, D.; Strauss, A.; García-Echeverría, C.; Furet, P.; Caravatti, G.; Fretz, H.; Schoepfer, J.; Grütter, M. G. *Nat. Struct. Biol.* **1996**, *3*, 586-589.

[28] Ogura, K.; Tsuchiya, S.; Terasawa, H.; Yuzawa, S.; Hatanaka, H.; Mandiyan, V.; Schlessinger, J.; Inagaki, F. *J. Mol. Biol.* **1999**, *289*, 439-445.

Los inhibidores peptídicos se pueden definir como tri- y tetrapéptidos de cadena abierta,[29,30,31,32] (Figura 5), derivados tensionados (con restricción conformacional local)[33] y macrociclos (con restricción conformacional global) de mayor peso molecular[34,35,36,37] (Figura 6), todos ellos con alta afinidad por el dominio SH2 de Grb2.

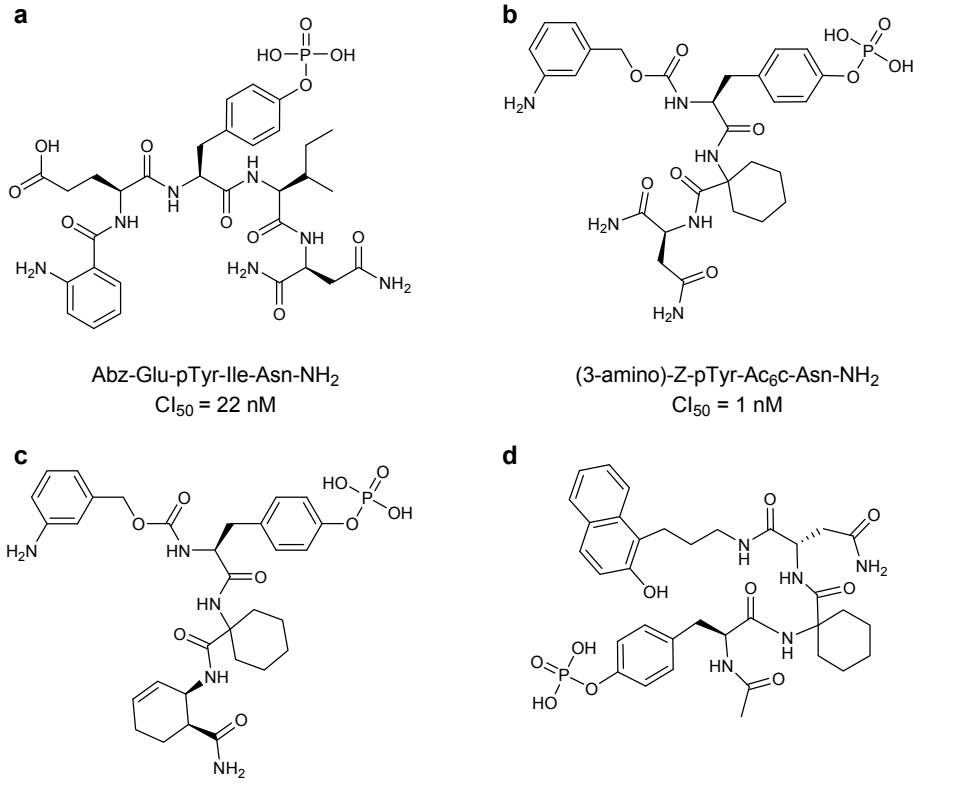

Figura 5. Inhibidores peptídicos de cadena abierta.

[29] Fretz, H.; Furet, P.; García-Echeverría, C.; Schoepfer, J.; Rahuel, J. *Curr. Pharm. Des.* **2000**, *6*, 1777-1796.

[30] García-Echeverría, C.; Furet, P.; Gay, B.; Fretz, H.; Rahuel, J.; Schoepfer, J.; Caravatti, G. *J. Med. Chem.* **1998**, *41*, 1741-1744.

[31] Furet, P.; García-Echeverría, C.; Gay, B.; Schoepfer, J.; Zeller, M.; Rahuel, J. *J. Med. Chem.* **1999**, *42*, 2358-2363.

[32] Véase cita 29.

[33] (a) Liu, D. G.; Wang, X. Z.; Gao, Y.; Li, B.; Yang, D.; Burke, T. R. Jr. *Tetrahedron* **2002**, *58*, 10423–10428. (b) Oishi, S.; Kang, S. U.; Liu, H.; Zhang, M.; Yang, D.; Deschamps, J. R.; Burke, T. R. Jr. *Tetrahedron* **2004**, *60*, 2971-2977.

[34] Song, Y. L.; Roller, P. P.; Long, Y. Q. *Bioorg. Med. Chem. Lett.* **2004**, *14*, 3205-3208.

[35] Li, P.; Zhang, M.; Long, Y. Q.; Peach, M. L.; Liu, H.; Yang, D.; Nicklaus, M.; Roller, P. P. *Bioorg. Med. Chem. Lett.* **2003**, *13*, 2173-2177.

[36] Shi, Z. D.; Lee, K.; Wei, C. Q.; Roberts, L. R.; Worthy, K. M.; Fisher, R. J.; Burke, T. R. Jr. *J. Med. Chem.* **2004**, *47*, 788-791.

[37] Jian, S.; Liao, C.; Bindu, L.; Yin, B.; Worthy, K. W.; Fisher, R. J.; Burke, T. R. Jr.; Nicklaus, M. C.; Roller, P. P. *Bioorg. Med. Chem. Lett.* **2009**, *19*, 2693-2698.

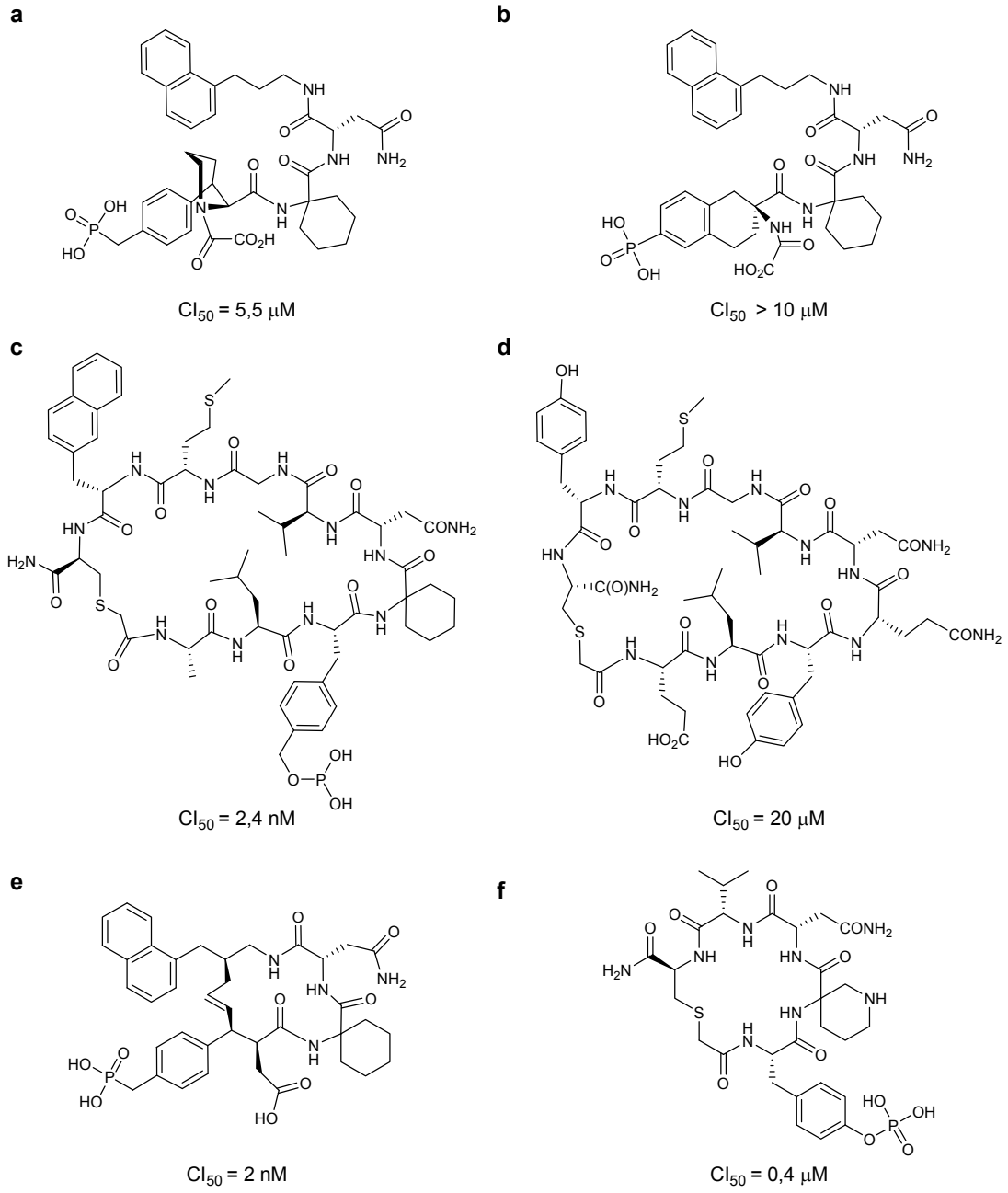

Figura 6. Inhibidores con restricción conformacional local (**a**, **b**) y macrocíclicos (**c**-**f**).

Dentro de las moléculas pequeñas se encuentran tanto inhibidores que aún contienen el residuo de pTyr[38] como compuestos en los que se ha eliminado totalmente[39,40,41] (Figura 7).

[38] Schoepfer, J.; Gay, B.; Caravatti, G.; García-Echeverría, C.; Fretz, H.; Rahuel, J.; Furet, P. *Bioorg. Med. Chem. Lett.* **1998**, *8*, 2865-2870.

[39] Caravatti, G.; Rahuel, J.; Gay, B.; Furet, P. *Bioorg. Med. Chem. Lett.* **1999**, *9*, 1973-1978.

[40] Harris, G. D.; Nguyen, A.; App, H.; Hirth, P.; McMahon, G.; Tang, C. *Org. Lett.* **1999**, *1*, 431-433.

[41] Nam, J. Y.; Kim, H. K.; Kwon, J. Y.; Han, M. Y.; Son, K. H.; Lee, U. C.; Choi, J. D.; Kwon, B. M. *J. Nat. Prod.* **2000**, *63*, 1303-1305.

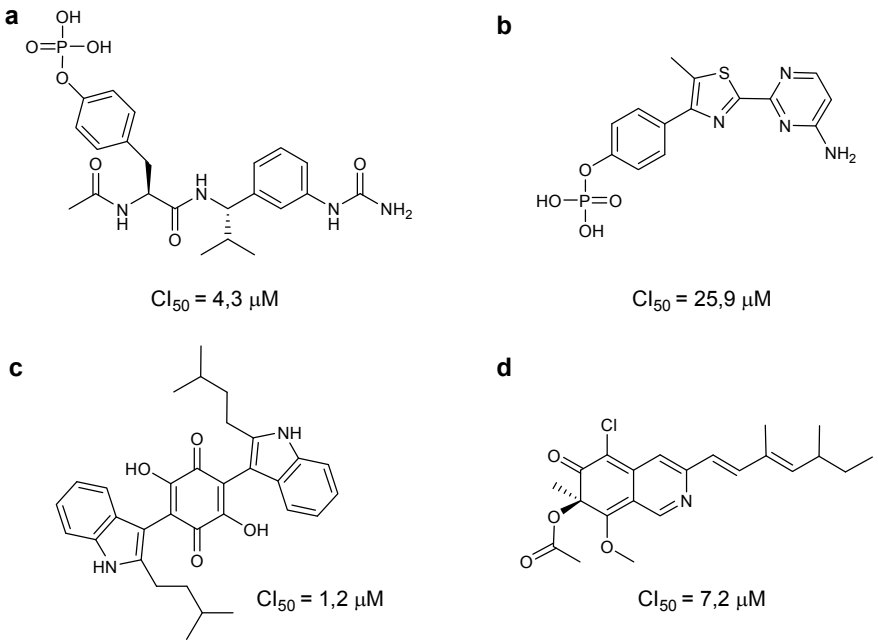

Figura 7. Inhibidor no peptídico en el que aún se conserva el residuo de pTyr (**a**) y estructuras no relacionadas (**b**-**d**).

De lo expuesto resulta evidente que el bloqueo de la interacción HER2-Grb2 mediante el empleo de ligandos del dominio SH2 de Grb2 representa una prometedora estrategia de terapia dirigida contra el cáncer.

Sin embargo, esta aproximación terapéutica aún no ha podido ser validada, ya que la mayoría de ligandos disponibles capaces de unirse eficientemente al dominio SH2 de Grb2 son de naturaleza peptídica y con limitaciones de biodisponibilidad, lo que ha dificultado su desarrollo farmacéutico. Por lo tanto, la identificación de pequeñas moléculas se presenta como una opción muy interesante dentro de este campo. En este sentido, en nuestro grupo de investigación hemos comenzado un proyecto dirigido al desarrollo de compuestos de carácter no peptídico capaces de unirse al dominio SH2 de Grb2 y bloquear su vía de señalización.

Objetivos

2. Objetivos

El objetivo principal de este proyecto es el desarrollo de moléculas pequeñas de naturaleza no peptídica con afinidad por el dominio Grb2-SH2. La consecución de este objetivo implica las siguientes etapas:

1. Diseño de compuestos empleando como punto de partida la estructura cristalográfica del complejo formado por el dominio SH2 de Grb2 y el pentapéptido de alta afinidad 2-Abz-Glu-pTyr-Ile-Asn-Gln-NH_2.

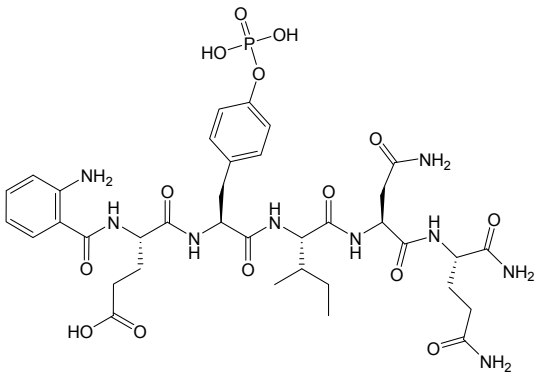

2-Abz-Glu-pTyr-Ile-Asn-Gln-NH_2

2. Síntesis y determinación de la afinidad de los compuestos sintetizados por el dominio SH2 de Grb2.

3. Proceso de optimización.

4. Validación del potencial biológico del/los compuesto(s) optimizado(s).

Resultados y Discusión

3. Resultados y Discusión

3.1. Diseño de compuestos con afinidad por el dominio SH2 de Grb2

Empleando como punto de partida la estructura cristalográfica del dominio SH2 de Grb2 unido al pentapéptido de alta afinidad 2-Abz-Glu-pTyr-Ile-Asn-Gln-NH_2[42] se diseñaron dos series de compuestos que mantienen todas las interacciones clave de dicho pentapéptido con el dominio Grb2-SH2 (serie **I**) o bien solo algunas de ellas (serie **II**) (Figura 8).[43]

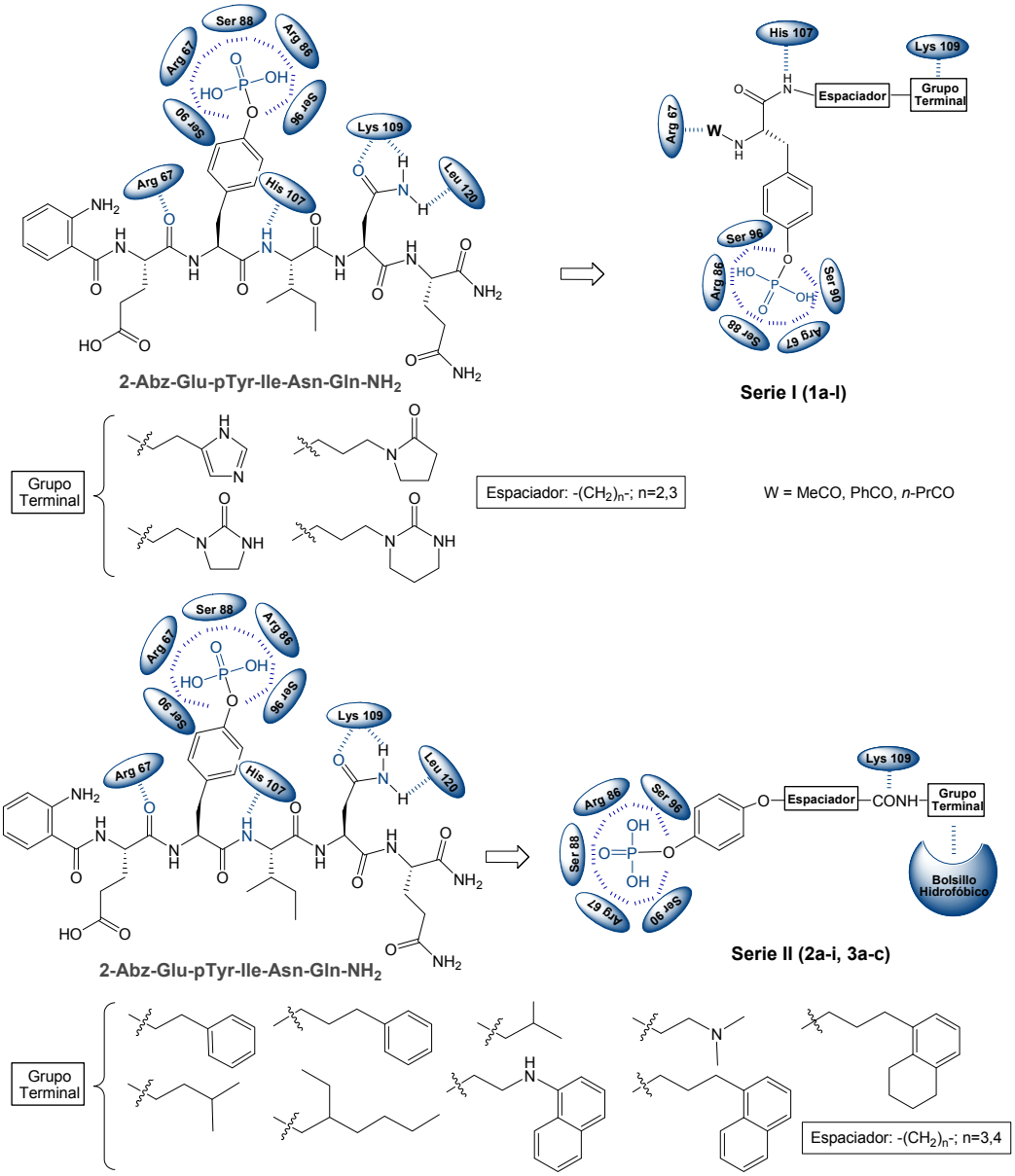

Figura 8. Diseño de las estructuras generales **I** y **II**.

[42] Véase cita 25.

[43] Orcajo-Rincón, Á. L.; Ortega-Gutiérrez, S.; Serrano, P.; Torrecillas, I. R.; Wüthrich, K.; Campillo, M.; Pardo, L.; Viso, A.; Benhamú, B.; López-Rodríguez, M. L. *J. Med. Chem.* **2011**, *54*, 1096-1100.

Las Figuras 9 y 10 muestran los modelos computacionales obtenidos para algunos de los compuestos representativos de dichas series:

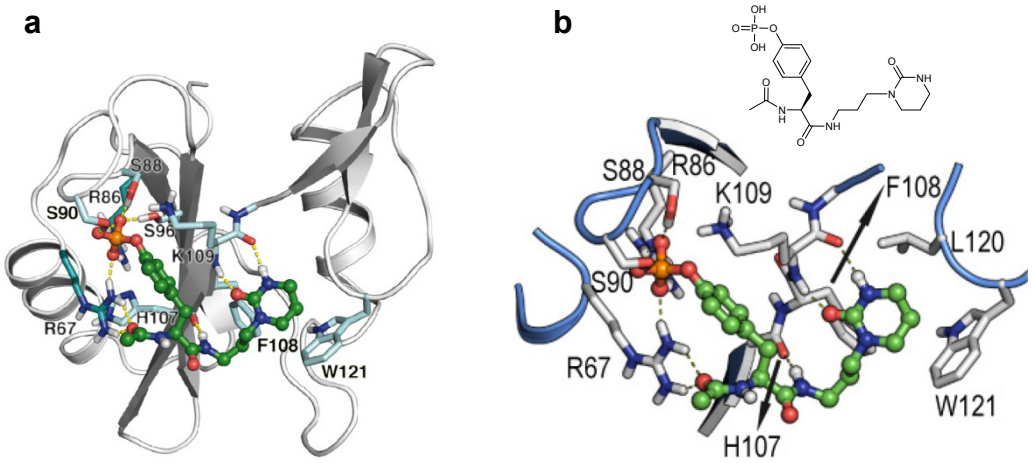

Figura 9. Modelos computacionales del complejo formado por el compuesto **(*S*)-1k**, perteneciente a la serie **I**, y el dominio SH2 de Grb2. **a.** Dominio SH2 completo. **b.** Sección ampliada con los aminoácidos de interacción.

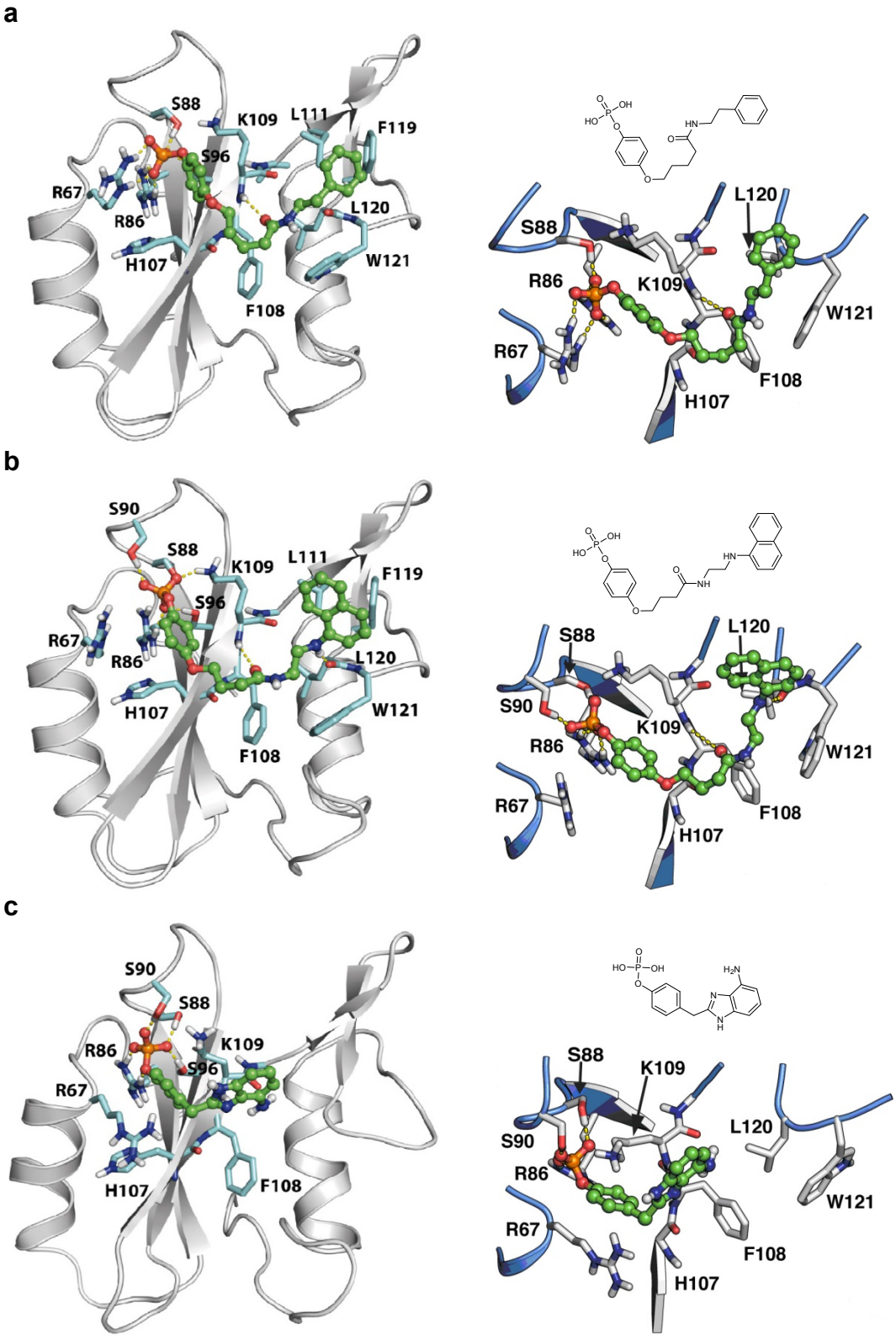

Figura 10. Modelos computacionales de los complejos formados por el dominio SH2 de Grb2 con el compuesto **3a** (panel **a**), el compuesto **2f** (panel **b**) y el compuesto **18** (panel **c**). Las imágenes muestran el dominio SH2 completo (paneles izquierdos) así como las correspondientes secciones ampliadas con los aminoácidos de interacción (paneles derechos).

3.2. Síntesis de los compuestos de las series I-II y determinación de su afinidad por Grb2-SH2

La síntesis de los compuestos de las diferentes series **1a**-**j** (serie **I**), **2a**-**i**, **3a**-**c** y **18** (serie **II**), así como la determinación de su afinidad por el dominio Grb2-SH2 se llevó a cabo de forma iterativa. Los Esquemas 1-5 describen la metodología sintética empleada en cada caso.

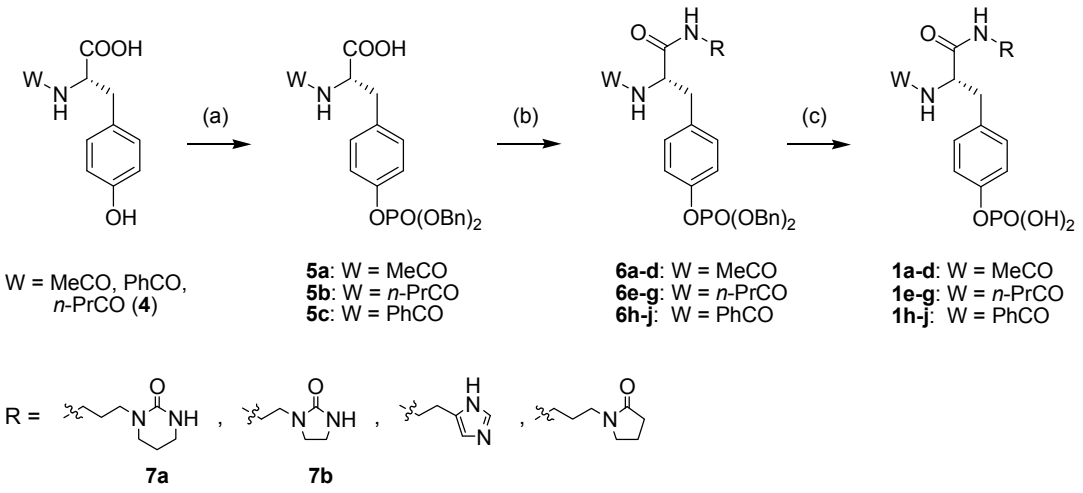

Reactivos: (a) (i) NMM, $^{t}BuMe_2SiCl$, CH_3CN, ta; (ii) 1*H*-tetrazol, $^{i}Pr_2NP(OBn)_2$, ta; (iii) $^{t}BuOOH$ ac., -20 ºC; (b) EDC, HOBt, CH_2Cl_2, R-NH_2, ta; (c) H_2/Pd(C)/etanol, ta.

Esquema 1. Síntesis de los compuestos **1a**-**j**.

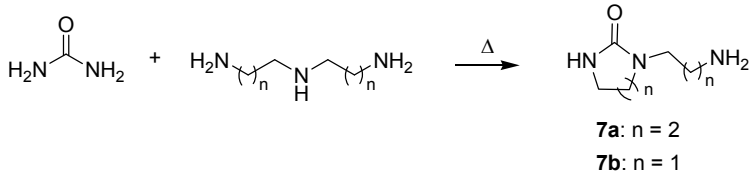

Esquema 2. Síntesis de las aminas **7a**,**b**.

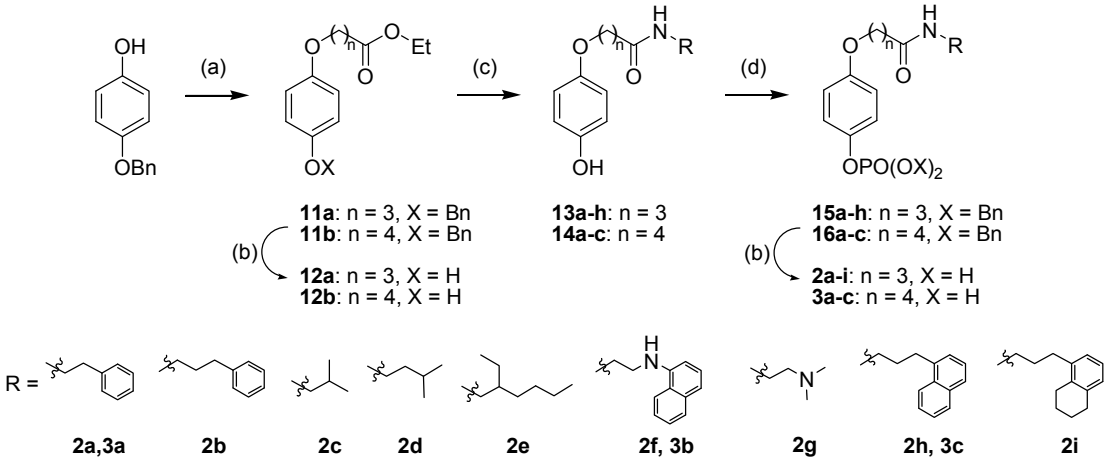

Reactivos: (a) $Br(CH_2)_nCOOEt$, K_2CO_3, éter corona, acetona, 60 ºC; (b) H_2/Pd(C), etanol, ta; (c) R-NH_2, $AlMe_3$, tolueno, 120 ºC; (d) (i) 1*H*-tetrazol, $^{i}Pr_2NP(OBn)_2$, 25 ºC; (ii) ^{t}BuOOH ac., -20 ºC.

Esquema 3. Síntesis de los compuestos de la serie **II** (**2a**-**i** y **3a**-**c**).

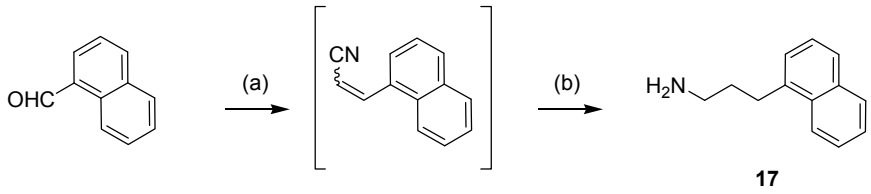

Reactivos: (a) $NC(CH_2)P(O)(OC_2H_5)_2$, K_2CO_3 ac. 6 M, ta; (b) H_2 /Ni-Ra, etanol, ta.

Esquema 4. Síntesis de la 3-(1-naftil)propilamina (**17**).

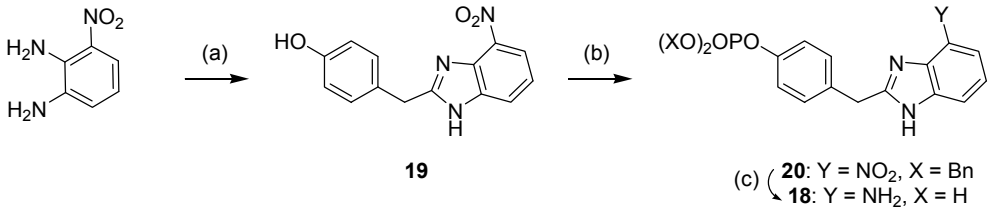

Reactivos: (a) 4-OH-C_6H_4-CH_2COOH, HCl 6 M, Δ; (b) (i) 1*H*-tetrazol, $^{i}Pr_2NP(OBn)_2$, 25 ºC; (ii) ^{t}BuOOH ac., ta; (c) H_2/Pd(C), etanol, ta.

Esquema 5. Síntesis del compuesto **18**.

La evaluación biológica de todos los compuestos sintetizados requirió la puesta a punto de un ensayo tipo ELISA. Los valores obtenidos para los compuestos de la serie **I** se recogen en la Tabla 1, destacando el derivado **1a** que, con un valor de CI_{50} = 190 ± 25 μM, es el que presenta mayor afinidad por el dominio SH2 de Grb2. Ninguno de los compuestos de la serie **II** mostró afinidad por la proteína (CI_{50} > 1 mM).

Tabla 1. Afinidades de los compuestos **1a**-**j** por el dominio SH2 de Grb2.

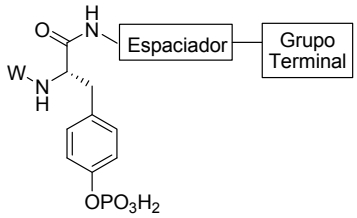

Compuesto	W	Espaciador	Grupo T.	CI_{50} (μM)[a,b]
1a	Me-CO-	-$(CH_2)_3$-		190±25
1b	Me-CO-	-$(CH_2)_2$-		Inactivo[c]
1c	Me-CO-	-$(CH_2)_2$-		Inactivo[c]
1d	Me-CO-	-$(CH_2)_3$-		Inactivo[c]
1e	*n*Pr-CO-	-$(CH_2)_3$-		314±5
1f	*n*Pr-CO-	-$(CH_2)_2$-		1330±98
1g	*n*Pr-CO-	-$(CH_2)_3$-		Inactivo[c]
1h	Ph-CO-	-$(CH_2)_3$-		Inactivo[c]
1i	Ph-CO-	-$(CH_2)_2$-		Inactivo[c]
1j	Ph-CO-	-$(CH_2)_3$-		Inactivo[c]

[a] Los ensayos de unión competitivos entre el dominio SH2 de Grb2 expresado como proteína de fusión a GST y el fosfopéptido biotina-Ahx-PSpYVNVQN fueron llevados a cabo tal como se detalla en la Parte Experimental (*Experimental Section* de la versión en lengua inglesa) de esta memoria. Las curvas dosis-respuesta fueron generadas empleando el programa Prisma. Los datos se expresan como la media±EE de al menos dos experimentos independientes realizados por duplicado. [b] Para el compuesto 1224-130, cedido por el Prof. T. R. Burke y usado como control en el test ELISA, los valores de CI_{50} obtenidos en nuestro laboratorio se corresponden con el descrito previamente.[44] [c] Los compuestos inactivos desplazan menos del 10% del fosfopéptido a la máxima concentración empleada (5 mM).

[44] Wei, C.-Q.; Li, B.; Guo, R.; Yang, D.; Burke, T. R. Jr. *Bioorg. Med. Chem. Lett.* **2002**, *12*, 2781-2784.

Puesto que la síntesis empleada para los derivados de la serie **I** (Esquema 1) conlleva un cierto grado de racemización (Figuras 11 y 12), se puso a punto una ruta para acceder a los enantiómeros de **1a**, el compuesto que hasta el momento había mostrado la mayor afinidad (CI_{50} = 190 μM, Tabla 1). Así, se sintetizaron los derivados enantiopuros **(*R*)-** y **(*S*)-1k** (Esquema 6) y el racémico **(*R*,*S*)-1k** (en este caso empleando condiciones análogas a las indicadas en el Esquema 1, pero partiendo de N-acetiltirosina racémica) y se determinó la afinidad de estos tres compuestos por el dominio SH2 de Grb2 (Tabla 2).

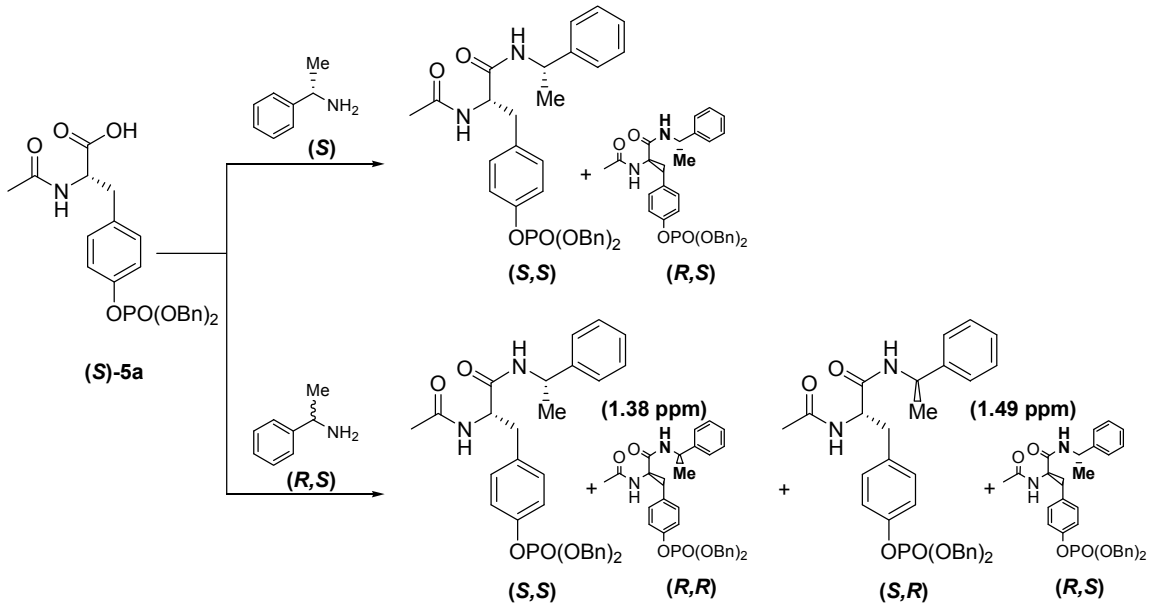

Figura 11. Evaluación del grado de racemización asociado a la síntesis de los compuestos **1a**-**j**.

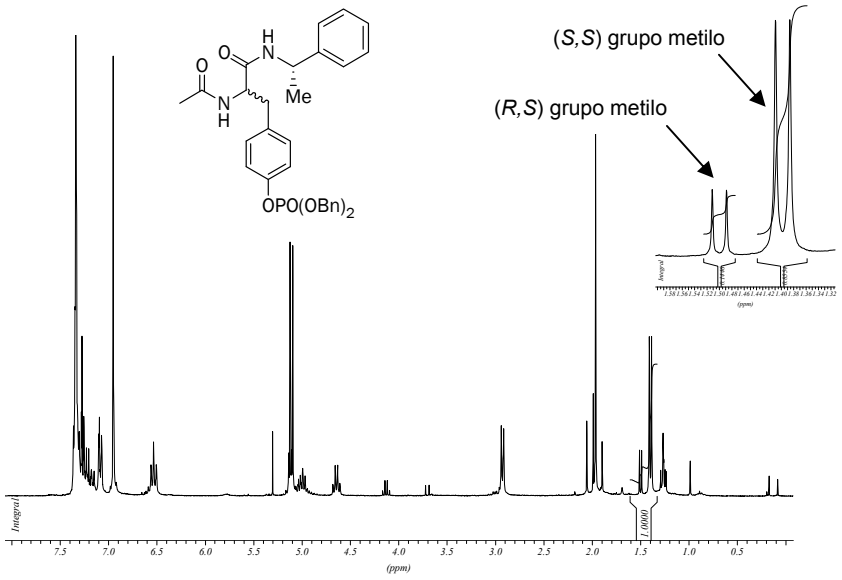

Figura 12. Espectro de ^{1}H-RMN de la mezcla diastereomérica resultante de la condensación del ácido **(*S*)-5a** con (1*S*)-1-feniletilamina.

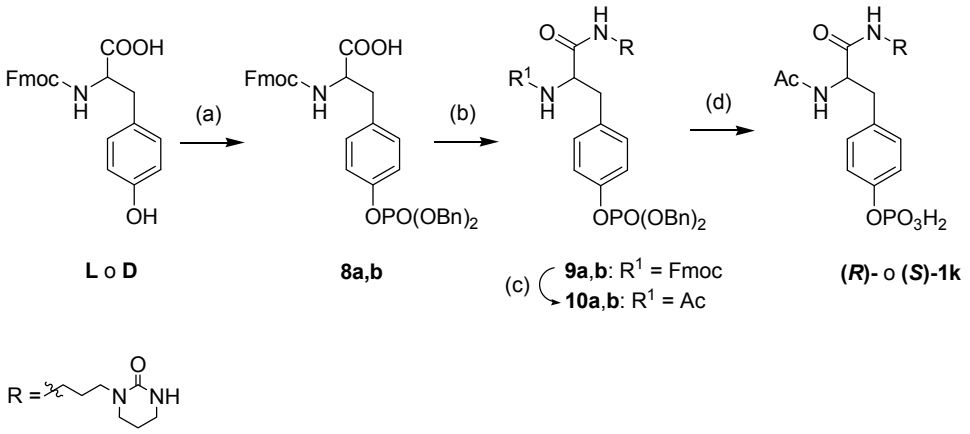

Reactivos: (a) (i) NMM, $^{t}BuMe_2SiCl$, CH_3CN, ta; (ii) 1*H*-tetrazol, $^{i}Pr_2NP(OBn)_2$, ta; (iii) $^{t}BuOOH$ ac., -20 ºC; (b) EDC, HOBt, CH_2Cl_2, **7a**, ta; (c) piperidina, CH_3CN, 0 ºC; (ii) $^{i}Pr_2NEt$, Ac_2O, DMF, ta; (d) H_2/Pd(C), etanol, ta.

Esquema 6. Síntesis de los derivados enantiopuros **(*R*)-** y **(*S*)-1k**.

Tabla 2. Afinidades de los compuestos **(*R*)-**, **(*S*)-**, y **(*R*,*S*)-1k** por el dominio SH2 de Grb2.

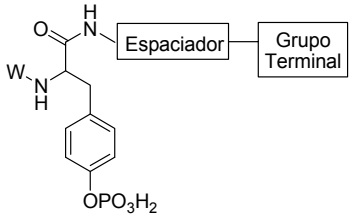

Compuesto	W	Espaciador	Grupo T.	CI_{50} (μM)[a,b]
1a	Me-CO-	-$(CH_2)_3$-	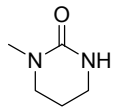	190±25
(*S*)-1k				174±22
(*R*)-1k				Inactivo[c]
(*R,S*)-1k				2307±644

[a-c] Para una explicación detallada véase nota al pie de la Tabla 1.

Estos resultados permitieron seleccionar el compuesto **(*S*)-1k** como *hit* inicial para su optimización.

3.3. Optimización del *hit* (*S*)-1k

Con el fin de optimizar el compuesto **(*S*)-1k**, se determinó en primer lugar, de forma experimental, los aminoácidos del dominio Grb2-SH2 con los que **(*S*)-1k** interacciona. Para ello se llevaron a cabo experimentos de RMN (*Heteronuclear Single Quantum Coherence*, HSQC) empleando proteína marcada con ^{15}N (Figuras 13 y 14).

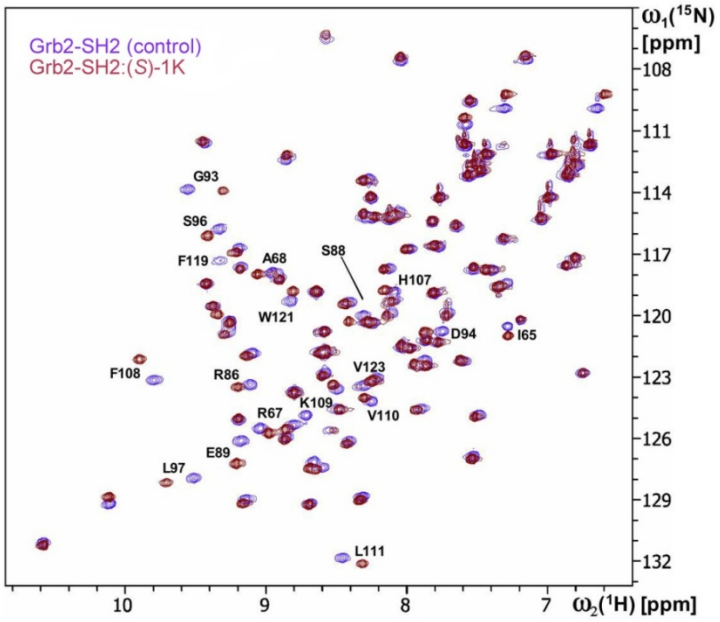

Figura 13. Espectro 2D [^{15}N,^{1}H]-HSQC del dominio Grb2-SH2 en ausencia (azul) y en presencia de **(*S*)-1k** (rojo) (relación molar compuesto:proteína 1:1).

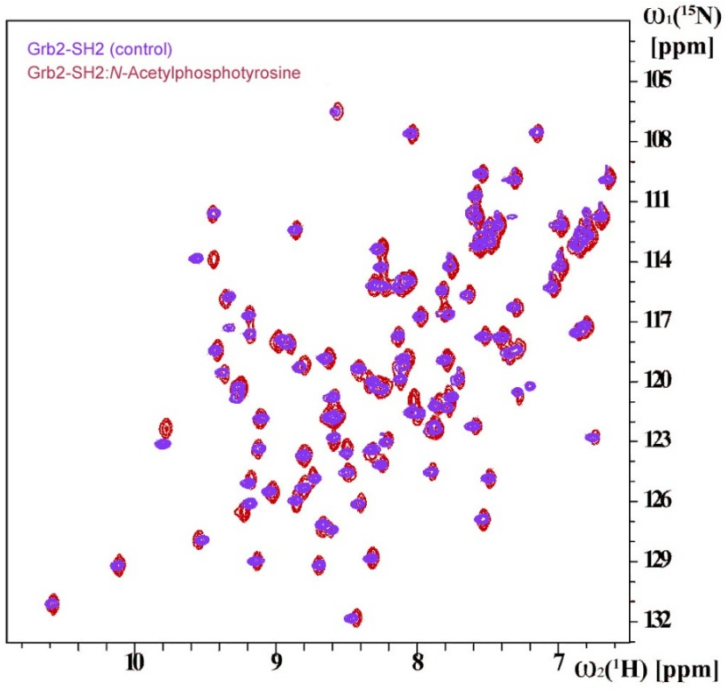

Figura 14. Espectro 2D [^{15}N,^{1}H]-HSQC del dominio Grb2-SH2 en ausencia (azul) y en presencia de *N*-acetilfosfotirosina (rojo) (relación molar compuesto:proteína 2:1).

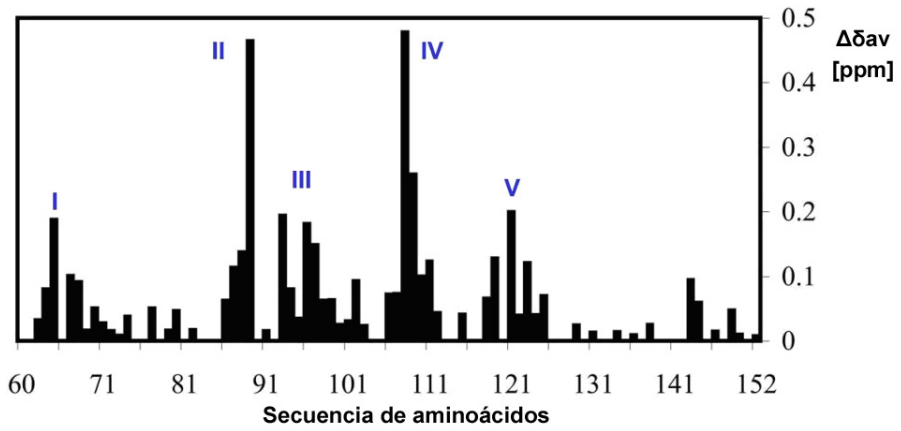

Figura 15. Modificación de los desplazamientos químicos combinados $^{1}H–^{15}N$ ($\Delta\delta av$) del dominio Grb2-SH2 frente a su secuencia primaria de aminoácidos. $\Delta\delta av$ es el promedio ponderado de las diferencias en desplazamiento químico de ^{1}H y ^{15}N, $\Delta\delta = \{0.5[\Delta\delta\ (^{1}H^{N})^{2} + (0.2\Delta\delta\ (^{15}N))^{2}]\}^{1/2}$, determinado a partir de la comparación de los dos espectros [^{15}N,^{1}H]-HSQC superpuestos en la Figura 13.

El gráfico de la Figura 15 indica los residuos con los que **(*S*)-1k** interacciona, es decir, aquéllos cuyo desplazamiento químico se modifica en presencia del compuesto [zona I (Arg67); zonas II y III (Arg86, Ser88 y Ser96); zona IV (His107 y Lys109); y zona V (Trp121)]. Estos resultados validan claramente el diseño realizado.

Teniendo en cuenta estos resultados, parece razonable suponer que la moderada actividad de **(*S*)-1k** (CI_{50} = 174±22 μM; Tabla 2) podría ser debida al alto grado de libertad conformacional asociado a su espaciador metilénico, por lo que la introducción de restricciones conformacionales en esta parte de la molécula quizá permitiría aumentar la afinidad. Con este objetivo, se diseñó un nuevo compuesto, **(*S*)-1l**, en cuyo espaciador se incorporó un anillo de ciclohexilo como elemento restrictivo (Figura 16).

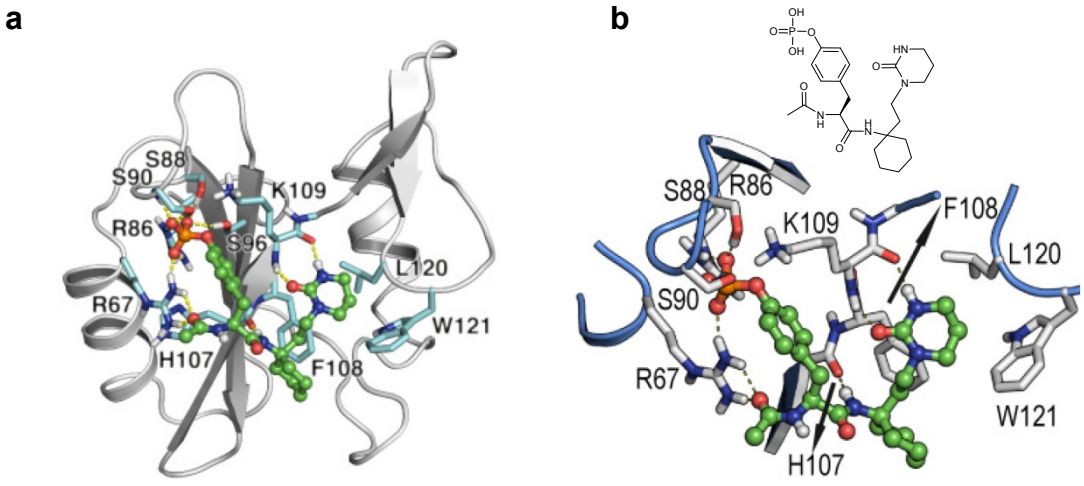

Figura 16. a. Modelo computacional del complejo formado por el compuesto **(*S*)-1l** y el dominio SH2 de Grb2. **a.** Dominio SH2 completo. **b.** Sección ampliada con los aminoácidos de interacción.

La síntesis del compuesto **(*S*)-1l** (Esquema 7) hizo necesaria la obtención previa de la amina intermedia **21** (Esquema 8).

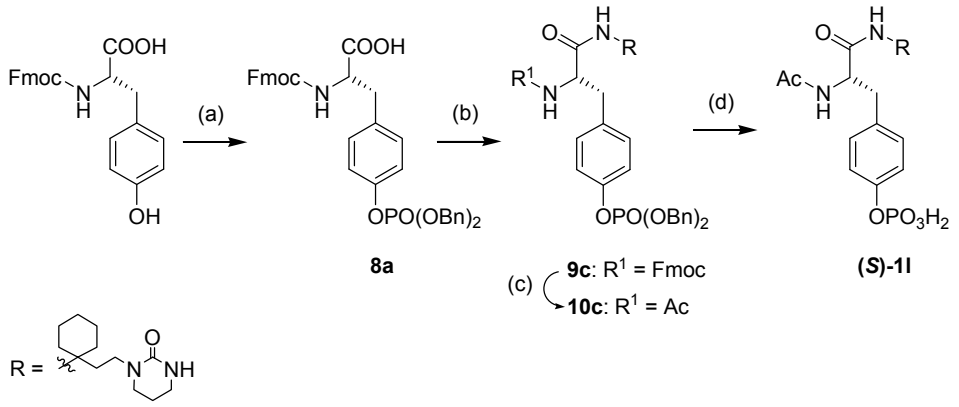

Reactivos: (a) (i) NMM, ^{t}BuMe$_2$SiCl, CH$_3$CN, ta; (ii) 1*H*-tetrazol, ^{i}Pr$_2$NP(OBn)$_2$, ta; (iii) ^{t}BuOOH ac., -20 ºC; (b) DIC, HOBt, THF, R-NH$_2$ (**21**), ta; (c) (i) piperidina, acetonitrilo, 0 ºC; (ii) ^{i}Pr$_2$NEt, Ac$_2$O, DMF, ta; (d) H$_2$/Pd(C), etanol, ta.

Esquema 7. Síntesis del derivado **(*S*)-1l**.

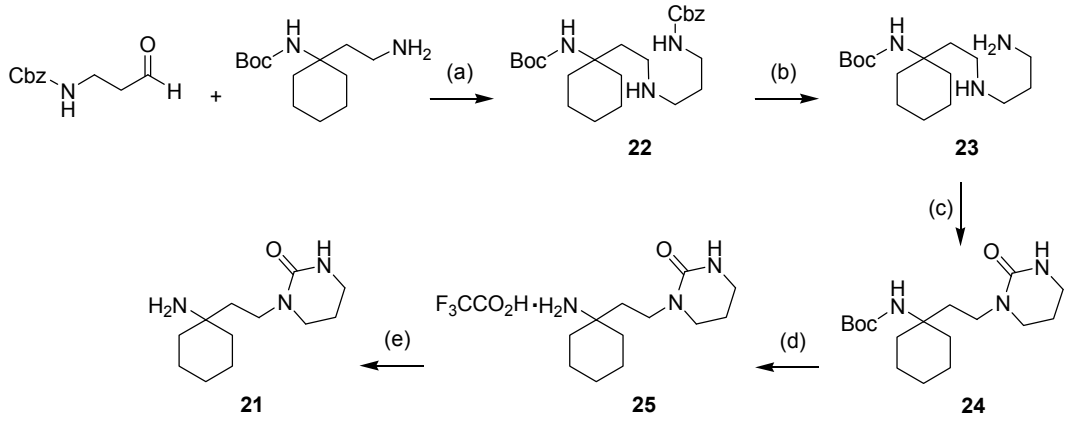

Reactivos: (a) Tamiz molecular 4 A, NaCNBH$_3$, metanol, AcOH, 35 ºC; (b) H$_2$, Pd(OH)$_2$(C), metanol, ta; (c) CDI, DBU, THF, 70 ºC; (d) F$_3$CCO$_2$H, CH$_2$Cl$_2$, ta; (e) K$_2$CO$_3$ ac. 0.05 M, CH$_2$Cl$_2$, ta.

Esquema 8. Síntesis de 1-[2-(1-aminociclohexil)etil]tetrahidropirimidin-2(1*H*)-ona (**21**).

El compuesto **(*S*)-1l** mostró una afinidad por el dominio Grb2-SH2 aproximadamente tres veces mayor que el *hit* inicial **(*S*)-1k** (CI_{50} [**(*S*)-1k**] = 174 μM, CI_{50} [**(*S*)-1l**] = 56 μM).

Este resultado muestra como la aplicación iterativa de modelos computacionales y RMN ha permitido la optimización de un *hit* inicial (**(*S*)-1k**) y la identificación de **(*S*)-1l** como un nuevo ligando del dominio Grb2-SH2. Sin embargo, con el fin de confirmar el interés de **(*S*)-1l** como candidato susceptible de desarrollo futuro, es vital conocer cuál es su potencial biológico. Para ello se consideraron dos aspectos fundamentales:

a) Determinar si el compuesto muestra actividad antitumoral en sistemas celulares debido al bloqueo de la interacción HER2-Grb2.

b) Estudiar si el compuesto **(*S*)-1l** afecta la vía de las MAPKs tal y como se esperaría de una molécula capaz de bloquear las vías de transducción mitogénicas dependientes de Grb2.

3.4. Perfil *in vitro* de (*S*)-1l

Con el fin de establecer si **(*S*)-1l** es un compuesto con actividad en sistemas celulares, se determinó su citotoxicidad en células de cáncer de mama con sobreexpresión de HER2 (MCF7-HER2+). Si **(*S*)-1l** es capaz de bloquear el crecimiento de estas células tumorales debido a su capacidad para inhibir la interacción ente HER2 y Grb2, este compuesto deberá resultar citotóxico en éstas pero no así en células no tumorales (como por ejemplo fibroblastos) o células tumorales que no expresen niveles apreciables de HER2 (como por ejemplo MCF7-HER2- o MDA-231). Por tanto se estudió la capacidad de **(*S*)-1l** para inhibir la proliferación de estas cuatro líneas celulares. Los resultados obtenidos indican que efectivamente **(*S*)-1l** es citotóxico en las células MCF7-HER2+, pero no en fibroblastos (Figura 17) ni en células MCF7-HER2- ni en MDA-231 (Figura 18a).

Asimismo se confirmó mediante experimentos de inmunoprecipitación que **(*S*)-1l** es capaz de bloquear la interacción entre HER2 y la proteína adaptadora Grb2 (Figura 18b).

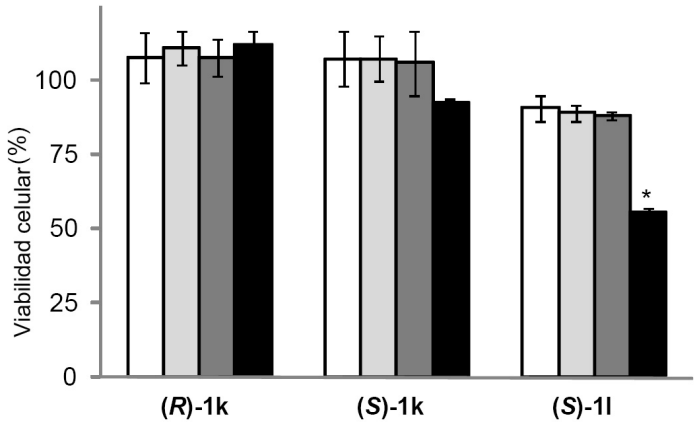

Figura 17. a. Inhibición de la proliferación celular de **(*R*)-1k**, **(*S*)-1k** y **(*S*)-1l** en fibroblastos N1 a concentraciones de 50 μM (blanco) y 100 μM (gris claro), y en células de carcinoma mamario humano MCF7-HER2+ a concentraciones de 50 μM (gris oscuro) y 100 μM (negro). Los resultados representan la media ± EE de al menos dos experimentos llevados a cabo por triplicado.* $p < 0.01$ *vs* control.

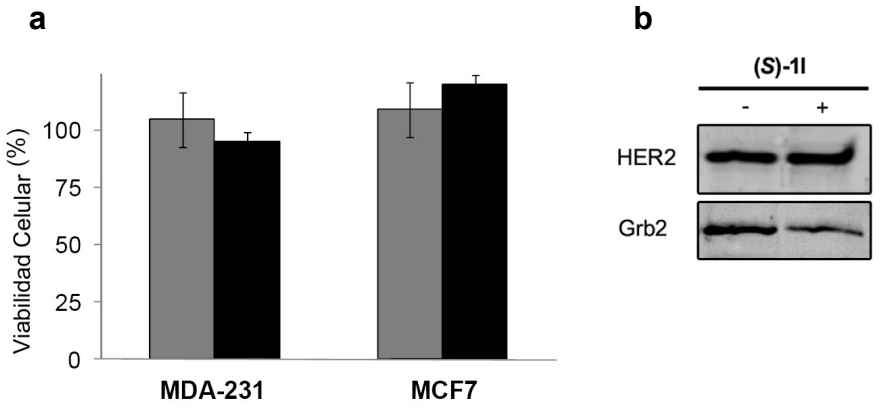

Figura 18. a. Inhibición de la proliferación celular de **(*S*)-1l** en células de carcinoma mamario humano con muy baja expresión de HER2 (MDA-231 y MCF7-HER2-) a concentraciones de 50 μM (gris) y 100 μM (negro). **b.** Inhibición de la interacción HER2-Grb2 por **(*S*)-1l**. Las células MCF7-HER2+ fueron tratadas con **(S)-1l** o vehículo como en (**a**), lavadas y lisadas. Se inmunoprecipitó HER2 y los niveles de HER2 y Grb2 se determinaron mediante anticuerpos específicos (*western blot*).

Por tanto, en conjunto, todos estos resultados confirman que **(*S*)-1l** puede considerarse como un nuevo esqueleto estructural en el desarrollo de moléculas pequeñas capaces de bloquear la interacción entre HER2 y Grb2, considerada actualmente como uno de los pasos críticos en la vía de señalización oncogénica de este receptor.

Una vez comprobada la actividad de **(*S*)-1l** en sistemas celulares, a continuación nos propusimos desarrollar una plataforma proteómica que permitiera identificar las rutas de señalización celular afectadas por este compuesto.

3.5. Desarrollo de una plataforma proteómica para la identificación de rutas de señalización celular

Esta estrategia consiste en la identificación y/o cuantificación de proteínas con el fin de establecer cuáles se expresan de forma diferencial debido a la administración de un compuesto. Considerando que un inhibidor de la interacción HER2-Grb2 deberá afectar a proteínas relacionadas con funciones de proliferación y diferenciación celular, tales como quinasas, proteínas asociadas, factores de transcripción, etc., decidimos desarrollar una plataforma basada en el empleo de tres nucleótidos (m^7GTP, ATP y AMPc) soportados en fase sólida. Estos nucleótidos se unen a multitud de proteínas que regulan las vías de señalización y que deberían ser afectadas por la administración de un inhibidor de la interacción HER2-Grb2. Así, por ejemplo, el ATP es el nucleótido al que se unen todas las quinasas, necesario para transferir el grupo fosfato de éste a la proteína sustrato.

Por tanto, se emplearon m^7GTP, ATP y AMPc soportados en fase sólida con el fin de aislar por precipitación aquellas proteínas capaces de interaccionar con ellos y así separarlas del resto del proteoma objeto de estudio. Una vez aisladas, estas proteínas son digeridas con tripsina e identificadas mediante espectrometría de masas en tándem (EM/EM) (Figura 19). Esta metodología permitirá establecer de forma inequívoca qué proteínas y qué vías,

relacionadas con estos nucleótidos, se afectan por la administración de un inhibidor de la interacción HER2-Grb2.

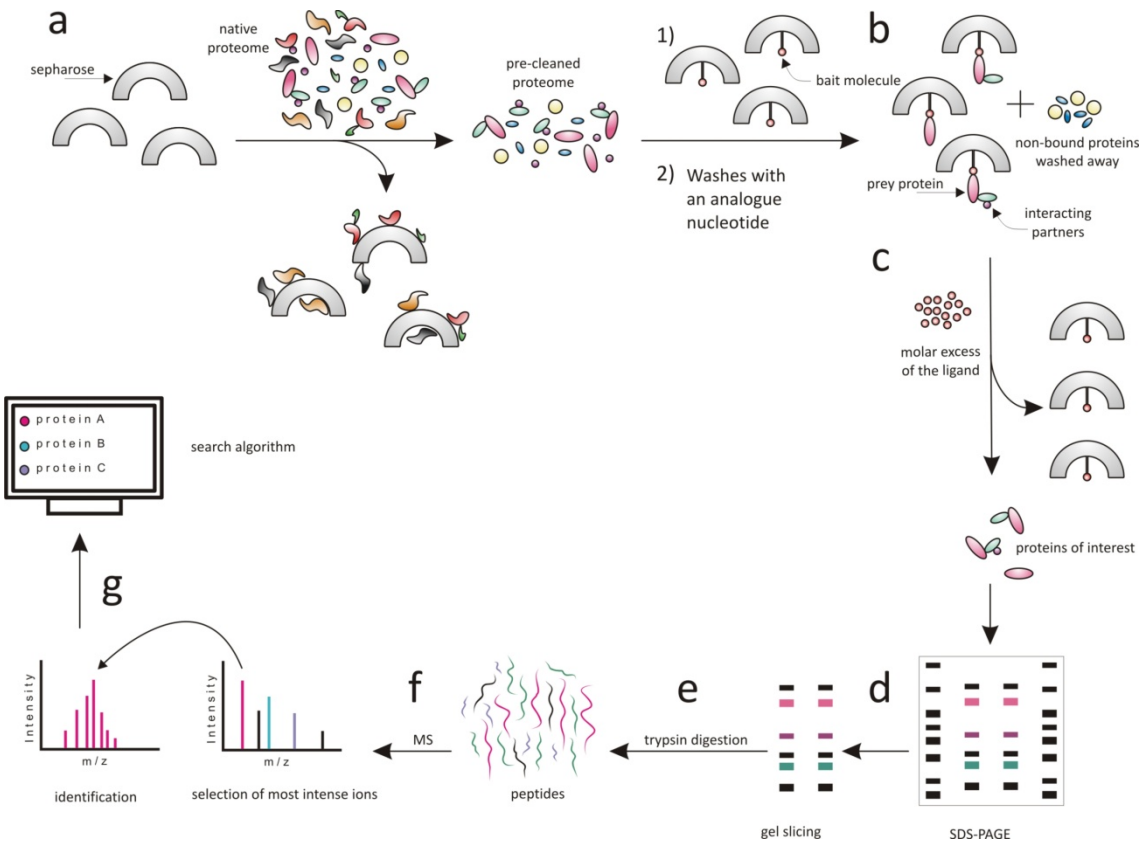

Figura 19. Representación esquemática de la estrategia de purificación por afinidad (PA) -EM basada en nucleótidos de interés. **a.** Fase de pre-lavado. **b.** Captura de proteínas diana. **c.** Elución de los complejos proteicos de interés. **d.** Separación por SDS-PAGE de las proteínas capturadas y aislamiento de las bandas de interés. **e.** Digestión con tripsina. **f.** Análisis tándem de EM. **g.** Resultados de MASCOT.

Los listados de las proteínas más relevantes halladas en los experimentos con m^7GTP, ATP y AMPc se resumen en las Tablas 3, 4 y 5, respectivamente.

Tabla 3. Listado de las proteínas más relevantes asociadas a los experimentos con m^7GTP.

No. Acc. [a]	Nombre de la Proteína	Código del Gen
P60842	Eukaryotic translation initiation factor 4A-I	EIF4A1
P06730	Eukaryotic translation initiation factor 4E	EIF4E
P68104	Eukaryotic translation elongation factor-1-alpha	EEF1A1
P24534	Eukaryotic translation elongation factor-1-beta	EEF1B2
38522	Eukaryotic translation elongation factor-1-delta	EEF1D
P13639	Eukaryotic translation elongation factor-2	EEF2
P62249	40S ribosomal protein S16	RPS16
189306	Nucleolin	NCL
P22626-2	Heterogenous nuclear ribonucleoproteins A2-B1	HNRNPA2-B1
P16930	Fumarylacetoacetase	FAH
P00326	Alcohol dehydrogenase 1C	ADH1C
157834561	Aldehyde reductase (chain A)	AKR1A1
1065362	GDP-complexed human ADP-ribosylation factor (chain B)	ARF1
1403050	Phosphoenolpyruvate carboxykinase (GTP)	PCK2
P43490	Nicotinamide phosphoribosyltransferase	PBEF1
Q9BYF0	Aldehyde oxidase	AOX1
179987	Chlordecone reductase	AKR1C4
IPI00219953.5	Cytidylate kinase	CMPK
P78417	Glutathione transferase omega-1	GSTO1
P99024	Tubulin beta-5 chain	Tubb5
P10809	60 kDa heat shock protein	HSPD1

[a] Los números de acceso (No. Acc.) listados en esta tabla son los empleados por la base de datos UniProt (http://www.uniprot.org).

Tabla 4. Listado de las proteínas más relevantes asociadas a los experimentos con ATP.

No. Acc. [a]	Nombre de la Proteína	Código del Gen
20149621	Dihydroxyacetone kinase 2	DAK
P54819	Adenylate kinase isoenzyme 2, mitochondrial	AK2
O00764	Pyridoxal kinase	PDXK
6491737	*N*-Acetylglucosamine kinase	NAGK
Q9H479	Fructosamine-3-kinase	FN3K
P05165	Propionyl-CoA carboxylase (chain A)	PCCA
3860238	4-Hydroxyphenylpyruvate dioxygenase	HPD
P38117	Electron transfer flavoprotein subunit beta	ETFB
12804999	3-Hydroxybutyrate dehydrogenase, type 2	BDH2
P68133	Actin, alpha skeletal muscle	ACTA1
1336765	Glucose phosphate isomerase	GPI

[a] Los números de acceso (No. Acc.) listados en esta tabla son los empleados por la base de datos UniProt (http://www.uniprot.org).

Tabla 5. Listado de las proteínas más relevantes asociadas a los experimentos con AMPc.

No. Acc. [a]	Nombre de la Proteína	Código del Gen
P10644	cAMP-dependent protein kinase type I-alpha regulatory subunit	PRKAR1A
P13861	cAMP-dependent protein kinase type II-alpha regulatory subunit	PRKAR2A
915392	Fatty acid synthase	FASN
P07741	Adenine phosphoribosyltransferase	APRT
1093492	4-aminobutyrate aminotransferase	GABA
Q06278	Aldehyde oxidase	AOX1
3860238	4-hydroxyphenylpyruvate-dioxygenase	HPD
226527	Nucleoside diphosphate kinase	NDK
P26038	Moesin	MSN
178027	Alpha-actin	ACTA2
37492	Alpha-tubulin	TUBA1A
338695	Beta-tubulin	TUBB

[a] Los números de acceso (No. Acc.) listados en esta tabla son los empleados por la base de datos UniProt (http://www.uniprot.org).

La clasificación de las proteínas identificadas se realizó con la ayuda de un paquete software especializado (ProteinCenter©, Proxeon Bioinformatics A/S) de acuerdo a los criterios definidos por el Consorcio *Gene Ontology* (GO)[45] y, en particular, considerando los dominios "Función Molecular" y "Proceso Biológico" para su clasificación. Los resultados de este proceso aplicado a las proteínas asociadas a m^7GTP, ATP y AMPc se ilustran en las Figuras 20, 21 y 22, respectivamente.

[45] http://www.geneontology.org/

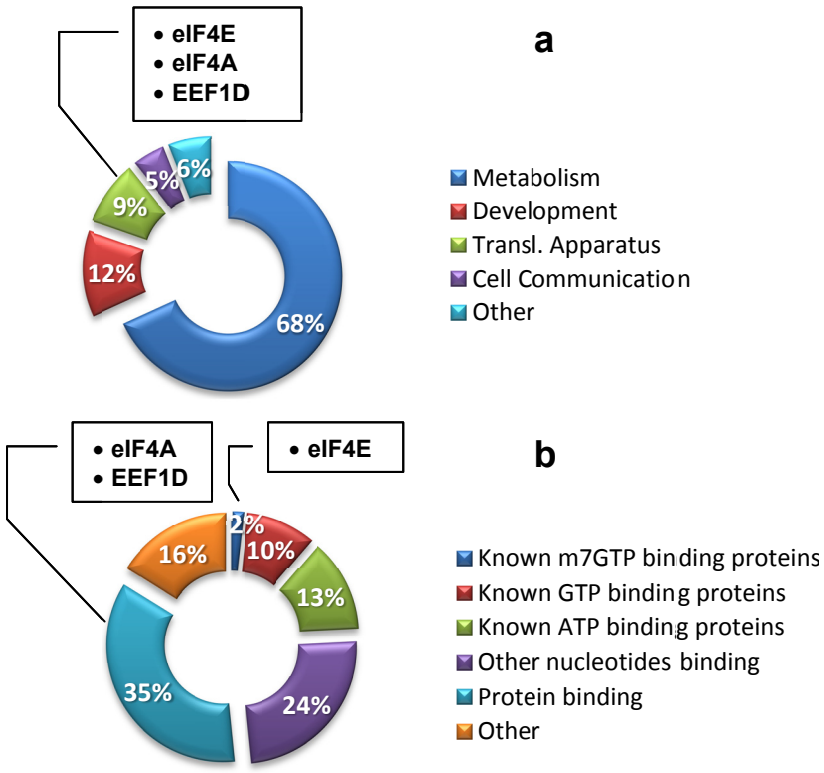

Figura 20. a. Representación en diagrama de sectores de las proteínas asociadas a m^7GTP según los dominios GO "Función Molecular" y "Proceso Biológico". **b.** Representación en diagrama de sectores de las proteínas asociadas a m^7GTP según su afinidad por nucleótidos u otras proteínas.

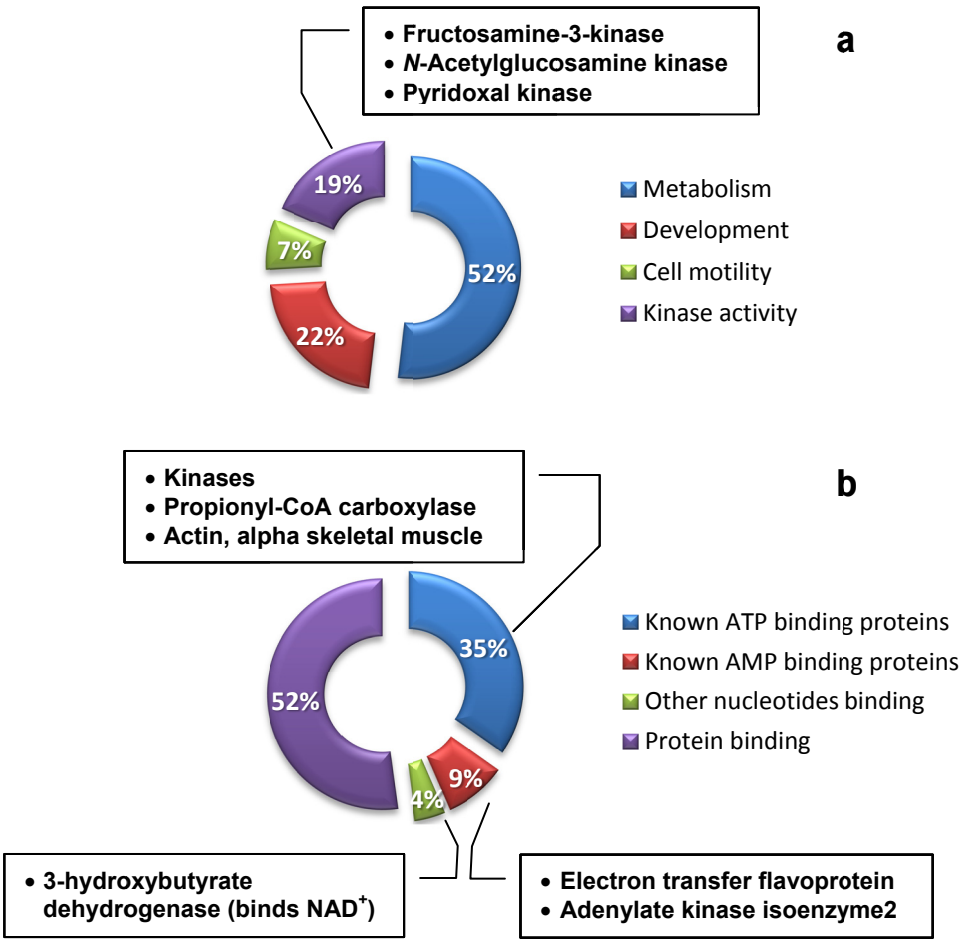

Figura 21. a. Representación en diagrama de sectores de las proteínas asociadas a ATP según los dominios GO "Función Molecular" y "Proceso Biológico". **b.** Representación en diagrama de sectores de las proteínas asociadas a ATP según su afinidad por nucleótidos u otras proteínas.

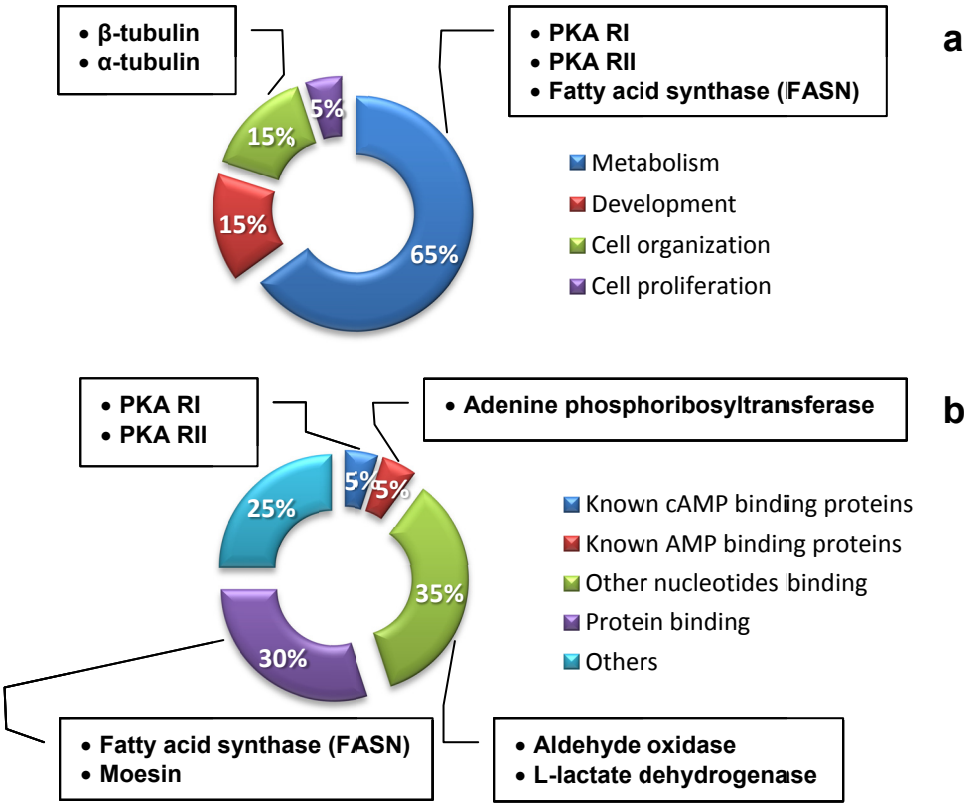

Figura 22. a. Representación en diagrama de sectores de las proteínas asociadas a AMPc según los dominios GO "Función Molecular" y "Proceso Biológico". **b.** Representación en diagrama de sectores de las proteínas asociadas a AMPc según su afinidad por nucleótidos u otras proteínas.

Estos experimentos han permitido el aislamiento de proteínas muy representativas de cada una de las vías de señalización en las que los tres nucleótidos están implicados. La purificación con m^7GTP resultó principalmente en el aislamiento de varios factores de traducción imprescindibles en el metabolismo celular. Asimismo, merece especial relevancia la identificación de quinasas y proteínas dependientes de GPCRs encontradas en los experimentos con ATP y AMPc, respectivamente.

Considerando el hecho de que el proteoma empleado en estos experimentos fue extracto citosólico de hígado humano, es lógico pensar que la mayoría las proteínas aisladas tuvieran actividad metabólica. Por lo tanto, es razonable que el uso de otros proteomas como por ejemplo provenientes de células cancerosas, resultaría en una mayor identificación de proteínas de señalización. Así pues, esta metodología está siendo actualmente aplicada al estudio comparativo de proteomas cancerosos (carcinoma mamario HER2+) tratados y no tratados con **(*S*)-1l**. Esto permitiría trazar los cambios en el perfil proteómico del tejido estudiado y el grado de afectación de una o más vías de señalización tras el tratamiento farmacológico.

Conclusiones

4. Conclusiones

1. Basándonos en la estructura cristalográfica del dominio SH2 de Grb2 en complejo con el ligando pentapeptídico de alta afinidad 2-Abz-Glu-pTyr-Ile-Asn-Gln-NH2, se han diseñado y sintetizado dos series de compuestos de naturaleza no peptídica que mantienen todas (serie **I**) o algunas (serie **II**) de las interacciones con el dominio SH2 de Grb2.

2. Con el fin de determinar la capacidad de los compuestos sintetizados para unirse al dominio SH2 de Grb2, se ha puesto a punto un ensayo competitivo tipo ELISA. De todos los compuestos estudiados, el derivado **(*S*)-1k** de la serie **I** mostró el valor más elevado de afinidad (CI_{50} = 174 μM). El hecho de que ninguno de los derivados de la serie **II** presentara una capacidad significativa para unirse a Grb2-SH2 indica que las interacciones eliminadas (Arg67 e His107) son clave para el reconocimiento de este dominio.

3. El modo de unión de **(*S*)-1k** a Grb2-SH2 ha sido validado experimentalmente empleando estudios de RMN (HSQC). Basándonos en esta información se ha llevado a cabo la optimización de **(*S*)-1k** mediante la introducción de restricciones conformacionales en su estructura, lo que permitió la obtención del derivado **(*S*)-1l**. Éste, con un valor CI_{50} de 56 μM, es actualmente uno de los compuestos no peptídicos con mayor afinidad por Grb2-SH2.

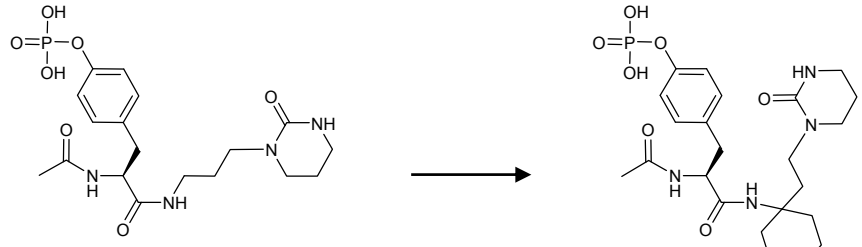

(*S*)-1k **(*S*)-1l**

4. El compuesto **(*S*)-1l** fue además estudiado *in vitro* en sistemas celulares, incluyendo células de carcinoma mamario MCF7-HER2 positivas (MCF7-HER2+) y negativas (MCF7-HER2-), así como en fibloblastos N1 de células no tumorales. Los resultados obtenidos mostraron que **(*S*)-1l** inhibe selectivamente la proliferación de las células MCF7-HER2+ (CI_{50} = 100 μM), sin afectar de forma significativa al resto. Estos resultados confirman que **(*S*)-1l** interfiere específicamente con la vía de señalización de HER2, disminuyendo significativamente la interacción entre HER2 y Grb2, efecto demostrado mediante experimentos de inmunoprecipitación.

5. Considerando el atractivo perfil de actividad de **(*S*)-1l** y el interés que supone identificar las vías de señalización a las que afecta, se diseñó y validó una plataforma proteómica basada en diferentes nucleótidos. Actualmente dicha plataforma se está empleando en células de carcinoma mamario HER2+ tratadas con **(*S*)-1l** con el fin de determinar exactamente las vías de señalización afectadas por este compuesto.